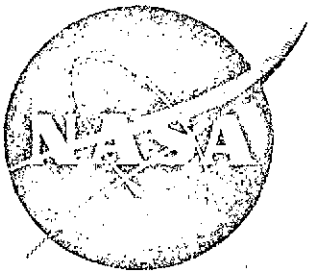

INFORMATION EXTRACTION TECHNIQUES FOR MULTISPECTRAL SCANNER DATA

by

W. A. Malila, R. B. Crane, and R. E. Turner

INFRARED AND OPTICS LABORATORY
WILLOW RUN LABORATORIES
INSTITUTE OF SCIENCE AND TECHNOLOGY
THE UNIVERSITY OF MICHIGAN

June 1972

prepared for

NATIONAL AERONAUTICS AND SPACE ADMINISTRATION

NASA Manned Spacecraft Center
Contract NAS 9-9784

NOTICES

Sponsorship. The work reported herein was conducted by the Willow Run Laboratories of the Institute of Science and Technology for the National Aeronautics and Space Administration, Earth Resources Office, under NASA Contract NAS9-9784. Contracts and grants to The University of Michigan for the support of sponsored research are administered through the Office of the Vice-President for Research.

WRL 31650-74-T

TECHNICAL REPORT

INFORMATION EXTRACTION TECHNIQUES FOR MULTISPECTRAL SCANNER DATA

by

W. A. Malila, R. B. Crane, and R. E. Turner

INFRARED AND OPTICS LABORATORY
WILLOW RUN LABORATORIES
INSTITUTE OF SCIENCE AND TECHNOLOGY
THE UNIVERSITY OF MICHIGAN

prepared for

NATIONAL AERONAUTICS AND SPACE ADMINISTRATION

June 1972

CONTRACT NAS 9-9784

NASA Manned Spacecraft Center
Houston, Texas
Earth Resources Office

FOREWORD

This report describes part of a comprehensive and continuing program of research in multispectral remote sensing of environment from aircraft and satellites. The research is being carried out for the NASA Manned Spacecraft Center, Houston, Texas, by Willow Run Laboratories, a unit of The University of Michigan's Institute of Science and Technology. The basic objective of this program is to develop remote sensing as a practical tool for obtaining extensive information quickly and economically.

Recently, many new applications for remote sensing have been developed. These include agricultural census-taking, detecting of diseased plants, urban land studies, measurment of water depth, studies of air and water pollution, and general assessment of land-use patterns. However, extension of the application of recognition techniques to areas other than those used to program the recognition processor are necessary to make operational survey systems a reality. The work reported herein was directed toward the solution of the problem of extending recognition techniques. Four aspects of the work are discussed: (1) simulation of the systematic variations in multispectral data; (2) investigation of techniques for overcoming systematic variations during recognition processing of multispectral data; (3) comparison of two different type of likelihood functions; and (4) data collection itself.

The research covered in this report was performed under NASA Contract NAS 9-9784, Task C2. The program was directed by R. R. Legault, Associate Director of Willow Run Laboratories, and J. D. Erickson, Principal Investigator and Head of the Multispectral Analysis Section of the Laboratories. The Willow Run Laboratories' number for this report is 31650-74-T.

ACKNOWLEDGMENTS

This report represents the work of several people. Mr. William A. Malila, under Dr. Jon D. Erickson Principal Investigator, had overall responsibility for the effort under Task 3.2 of NASA Contract NAS 9-9784. Dr. Robert E. Turner was the principal contributor to the work on radiative transfer modeling; he had computer programming support from Mr. Alan A. Kortesoja. Dr. Robert B. Crane was the principal contributor to the preprocessing studies, with computer programming support provided by Mr. John M. Clifford and Dr. Wyman Richardson. Drs. Crane and Richardson also collaborated on the investigation of likelihood functions for decision rules. The authors express their appreciation for the assistance received from those named above and for technical discussions with Mr. Richard J. Kauth and others in the Infrared and Optics Division of the Willow Run Laboratories.

ABSTRACT

This report addresses the problem of extending the applicability of recognition-processing procedures for multispectral scanner data from areas and conditions used for programming the recognition computers to other data from different areas viewed under different measurement conditions. The reflective spectral region (~0.3 to 3.0 μm) is considered. A potential application of such techniques is in conducting area surveys.

Work in three general areas is reported. The first is an examination, from a physical basis, of the nature of sources of systematic variation in multispectral scanner radiation signals. Calculations with an improved radiative transfer model are used to examine the dependence of radiation quantities on a variety of parameters and conditions of measurement. The second is an investigation of various techniques for overcoming systematic variations in scanner data. One technique, preprocessing with a generalized transformation, is developed and applied successfully to a set of data collected under hazy conditions to remove variations associated with scan angle and to extend signatures from one altitude to another. The final study evaluates the use of decision rules based upon empirical distributions of scanner signals rather than upon the usually assumed multivariate normal (Gaussian) signal distributions. It is concluded that the normal assumption is justified and that the time required by the increased complexity involved in implementing an empirical rule could be better utilized in other ways.

CONTENTS

Foreword iii
Acknowledgments iv
Abstract v
Figures ix
Tables xii
Summary 1
1. Introduction and Statement of Problem 3
1.1. Perspective 5
1.1.1. Signals and Measurement Parameters; Measurement Conditions and Auxiliary Information 6
1.1.2. Decision Rules 8
1.1.3. Preprocessing Transformations 10
1.1.4. System Modeling 10
1.2. Summary of Work Performed During the Year 11
1.2.1. Simulation and Examination of Systematic Variations in Data 11
1.2.2. Investigation of Techniques for Overcoming Systematic Variations 13
1.2.3. Investigation into the Suitability of the Normal Likelihood Function for Decision Rules 14
1.2.4. Data-Collection Missions Performed 14
2. Examination of Systematic Variations in Multispectral Scanner Radiation Signals by Simulation 15
2.1. The Radiative Transfer Model 16
2.1.1. Aspects of the Model 16
2.1.2. Model Improvements During the Past Year 18
2.1.3. Verification of the Model 19
2.2. Results of Calculations 22
2.2.1. Variation of Sensor Signals with Scan Angle 26
2.2.2. Variation of Sensor Signals with Visual Range 26
2.2.3. Variation of Sensor Signals with Time of Day 30
2.2.4. Variation of Sensor Signals with Season 37
2.3. Other Sources of Variation 42
2.3.1. Sensor Characteristics 42
2.3.2. Reflectance Characteristics of Element Being Viewed 42
2.3.3. Reflectance Characteristics of Elements Adjoining the Element Being Viewed 45
3. Techniques for Overcoming Systematic Variations in Scanner Data 50
3.1. Preprocessing 52
3.1.1. Potential Uses and Limitations of Preprocessing Information 53
3.1.2. Preprocessing Techniques for One-Dimensional Correction 55
3.1.3. Extension of Techniques to Two Dimensions 56
3.1.4. Technique for Removing Systematic Variations in Scanner Data with the Use of the Radiative Transfer Model 56
3.1.5. Removing the Effects of Neighboring Materials from Radiance Signals Near Boundaries 58
3.2. Adjustment of Decision-Rule Parameters 58
3.3. Supporting Analysis of Interdependencies of Radiation Quantities 59

4. Application of Preprocessing Techniques 66
4.1. Results of Using the U-V Transformation on Simulated Data 66
4.2. Results of the Use of the U-V Transformation on Real Scanner Data 68
4.3. Comparison Between Simulated and Real Data 78

5. Investigation into the Suitability of the Normal Likelihood Function for Recognition Decision Rules 81

6. Data-Collection Missions 84

7. Conclusions and Recommendations 85
7.1. Simulation and Modeling of Scanner Signals 85
7.1.1. Conclusions 85
7.1.2. Recommendations 85
7.2. Techniques for Removing Systematic Effects 86
7.2.1. Conclusions 86
7.2.2. Recommendations 87
7.3. Investigation of Decision-Rule Likelihood Functions 88

Appendix I: The Radiative Transfer Model 89

Appendix II: Derivation of an Empirical Technique for Correcting Haze Effects Near Boundaries 99

Appendix III: Investigation into the Suitability of Normal Likelihood Function for Recognition Decision Rules 103

Appendix IV: Importance of Atmospheric Scattering in Remote Sensing . . . 123

Appendix V: Preprocessing Techniques to Reduce Atmospheric and Sensor Variability in Multispectral Scanner Data 171

Appendix VI: List of Related Reports 183

References 187

Distribution List 189

FIGURES

1. Illustration of the Usefulness of Auxiliary Information, a_0, in Delimiting the Signal Space Occupied by Signals, x, from Material Class, m 9
2. Dependence of Sky Radiance on Scan Angle (in the Solar Plane); Solar Zenith Angle = 65.8° 20
3. Dependence of Sky Radiance on Scan Angle (Perpendicular to the Solar Plane); Solar Zenith Angle = 65.8° 20
4. Dependence of Sky Radiance on Azimuth Angle 20
5. Dependence of Sky Radiance on Scan Angle (in the Solar Plane); Solar Zenith Angle = 68.6° 21
6. Dependence of Sky Radiance on Scan Angle (Perpendicular to the Solar Plane); Solar Zenith Angle = 68.6° 21
7. Comparison of Reflectance Curves—from Model Calculations and ERSIS Data 23
8. Dependence of Sky Radiance on Scan Angle (in the Solar Plane); Solar Zenith Angle = 36.9° 23
9. Dependence of Sky Radiance on Scan Angle (Perpendicular to the Solar Plane); Solar Zenith Angle = 36.9° 24
10. Dependence of Sky Radiance on Scan Angle (in the Solar Plane); Solar Zenith Angle = 0° 24
11. Dependence of Sky Radiance on Scan Angle (in the Solar Plane); Solar Zenith Angle = 84.3° 25
12. Dependence of Sky Radiance on Scan Angle (Perpendicular to the Solar Plane); Solar Zenith Angle = 84.3° 25
13. Dependence of Transmittance on Wavelength and Scan Angle 27
14. Dependence of Transmittance on Visual Range and Scan Angle 27
15. Dependence of Path Radiance on Visual Range and Scan Angle 28
16. Dependence of Total Radiance from Diffuse Surface on Visual Range and Scan Angle 28
17. Dependence of Sky Radiance on Visual Range and Scan Angle 29
18. Dependence of Transmittance on Visual Range and Wavelength 29
19. Dependence of Transmittance on Visual Range and Altitude 31
20. Dependence of Diffuse Upward Irradiance on Visual Range and Altitude 31
21. Dependence of Diffuse Downward Irradiance on Visual Range and Altitude 32
22. Dependence of Diffuse Downward Irradiance on Visual Range and Wavelength 32
23. Dependence of Total Downward Irradiance on Visual Range and Altitude 33
24. Dependence of Sky Radiance on Visual Range and Wavelength 33
25. Dependence of Path Radiance on Visual Range and Wavelength 34

26. Dependence of Path Radiance on Visual Range and Altitude 34
27. Dependence of Total Radiance on Visual Range and Wavelength 35
28. Typical Flight Configuration for Airborne Scanner System 36
29. Dependence of Diffuse Downward Irradiance on Time and Visual Range 38
30. Dependence of Total Downward Irradiance on Time and Visual Range . . 38
31. Dependence of Sky Radiance on Time and Scan Angle 39
32. Dependence of Path Radiance on Time and Scan Angle 39
33. Dependence of Total Radiance on Time and Scan Angle 40
34. Variation of Diffuse Upward Irradiance with Time at an Altitude of 0 km over a Surface of Green Vegetation 41
35. Variation of Diffuse Downward Irradiance with Time at an Altitude of 0 km over a Surface of Green Vegetation 41
36. Variation of Total Downward Irradiance with Time at an Altitude of 0 km over a Surface of Green Vegetation 43
37. Variation of Direct Solar, Diffuse Downward, and Total Irradiances with Time at an Altitude of 0 km over a Surface of Green Vegetation (June 21) 43
38. Variation of Direct Solar, Diffuse Downward, and Total Irradiances with Time at an Altitude of 0 km over a Surface of Green Vegetation (December 21) 44
39. Geometry for Two-Dimensional Atmospheric Model 46
40. Block Diagram of Correction to Remove the Effect of Neighboring Materials from Radiance Signals Near Boundaries 60
41. Ratio of Total Downward Irradiance at an Altitude of 5 km to Total Downward Irradiance at Earth's Surface as a Function of Wavelength 60
42. Ratio of Diffuse Downward Irradiance to the Total Downward Irradiance as a Function of Visual Range 62
43. Ratio of Total Downward Irradiance at an Altitude of 5 km to Total Downward Irradiance at Earth's Surface as a Function of Time 62
44. Dependence of Diffuse Downward Irradiance at Altitude h on Diffuse Downward Irradiance at Earth's Surface 63
45. Ratio of Path Radiance to Total Radiance at an Altitude of 5 km as a Function of Time 63
46. Dependence of Path Radiance at an Altitude of 5 km to Total Atmospheric Transmittance 65
47. Dependence of Path Radiance on Bare Radiance at an Altitude of 5 km . . 65
48. Calculated 0.4-μm Radiance Values as a Function of Scan Angle 67
49. U for Calculated Radiance Values 67
50. V for Calculated Radiance Values 69
51. Calculated Radiance Values After Application of Quadratic Correction . . 69
52. Calculated 0.8-μm Radiance Values as a Function of Scan Angle 71

Page intentionally left blank

TABLES

1. Average Reflectance for Green Vegetation Compiled from Real Data for Several Wavelengths 31
2. Fields Selected for Testing U-V Transformation 72
3. Comparison of Recognition Results 79
4. Results of the Use of Field Mean for Recognition with an Intrafield Likelihood Decisison Rule 79
5. Summary of 1966 Data Used in Empirical Distribution Study 107
6. Summary of 1969 Data Used in Empirical Distribution Study 108
7. Summary of Non-Normality Tests on Signatures 114

INFORMATION EXTRACTION TECHNIQUES FOR MULTISPECTRAL SCANNER DATA

SUMMARY

This report describes part of a comprehensive and continuing program to investigate remote sensing of the environment from aircraft and satellites. The overall objective of this multidisciplinary program at the Willow Run Laboratories of The University of Michigan is to develop Earth resources information systems (which use remote sensing) as practical tools to provide the planner and decision maker with extensive information quickly and economically. The major problem discussed in this report is the extension of the application of recognition techniques to areas other than that have been used to program the recognition processor. This problem must be solved to make operational area-survey systems a reality. Work on four aspects of the problem is reported; the majority of our effort was directed toward the first two.

Simulation of the systematic variations in multispectral scanner data was carried out by means of our substantially improved radiative transfer model. These variations result from: (1) changes in measurement parameters such as scan angle; (2) the presence of the atmosphere and changes in its properties; and (3) changes in sun position associated with time of day, time of year, latitude, and longitude. The model has been developed to the point that close agreement is achieved between calculated and measured values of sky radiance under light haze conditions (the only reliable data available that we can use to check the models). We believe that we can model the atmospheric effects on radiance measurements under cloud-free or uniform overcast conditions, and we have developed a reliable basic model upon which we can add refinements (e.g., the effects of scattered clouds). In order to model multispectral scanner data more exactly, bidirectional reflectance functions for surface materials should be included instead of the diffuse conditions that have been assumed to date.

Techniques were also investigated for overcoming systematic variations during recognition processing of multispectral scanner data. A generalized version of earlier preprocessing methods was developed and successfully tested on a set of data collected under hazy conditions. The procedure was used to eliminate the measurable variation of the data as a function of scan angle. Although variations undoubtedly exist after correction, the intrafield and interfield variations masked the residual scan angle variations in the data set used for the testing. Bidirectional reflectance properties of ground covers did not limit the correction to any measurable extent because the correction procedure has the inherent ability to remove an average bidirectional reflectance function. This same correction procedure was used to extend signatures

between different data sets, i.e., sets collected at two different altitudes. An alternative procedure for signature extension shown to be less restrictive involves changing the likelihood function parameters rather than (or in addition to) preprocessing the data.

We compared the use of two different types of likelihood functions in a maximum likelihood decision rule. Decisions were made on data subsets from individual fields with the use of decision rules that assumed multivariate normal signal distributions and empirical histogram signal distributions, respectively. Although the normal likelihood function does not exactly describe data collected by the multispectral scanner, its use does not seriously degrade recognition performance for data sets analyzed. Our tests show that removal of systematic effects will result in greater improvements in recognition performance than those that can be obtained by use of empirical likelihood functions.

Data were collected for future analysis, development, and testing techniques for extending recognition procedures. The flight lines were chosen so that problems associated with large area surveys can be explored.

1
INTRODUCTION AND STATEMENT OF PROBLEM

Remote sensing with multichannel optical/mechanical scanners is a potential method for obtaining area-survey information more rapidly, more accurately, more economically, and/or more completely than is possible with methods currently in use. The desired information can be derived from recognition maps (or their equivalents) produced by electronic computers designed or programmed to perform recognition functions on data collected by multispectral scanners.

The essence of airborne and spaceborne remote sensing is discrimination, on the basis of radiation received by the sensor, between various surface materials of interest and their backgrounds. Because the radiation emanating from different materials has distinct spectral characteristics, multispectral remote sensing techniques can make use of observations in more than one wavelength interval to discriminate between classes of materials.

Discrimination over large areas would be much simpler if the spectral radiance received from a given class remained constant, but it does not. Throughout the day, the sun changes position; the properties of the atmospheric path change with viewing angle and position along the flight line; and clouds come and go. Furthermore, the spectral reflectance properties of the surface materials within any class are subject to variation for physical and/or biological reasons.

The major problem discussed in this report is extension of the application of recognition-processing procedures for data from areas and conditions used for programming recognition computers (i.e., to set the decision-rule parameters) to other data from different areas viewed under different measurement conditions. In other words, the problem is to develop recognition techniques that continue to obtain satisfactory recognition results when conditions change, without complete reprograming of the recognition processor and without the costly ground observations that such reprograming requires. The term signature is frequently used to describe the training-set statistics used for recognition, so the procedure of extending recognition-processing techniques is sometimes called signature extension.

The paragraphs that follow describe, generally, the problem, our approach, and the areas in which we have concentrated our efforts. Sections 1.1 and 1.2 are more detailed. The first presents and elaborates on our perspective or point of view for recognition studies. The second summarizes the work accomplished during the reporting period.

We must consider the nature of the variations present in scanner signals in order to design methods to overcome their effects. In this report, we restrict ourselves to short-wavelength signals in the spectral region of approximately 0.3 to 3.0 μm. We find variations associated with the sun position, the atmosphere, the materials being observed, and the scanner.

A multivariate probability density function describes the distribution of incoming signals from each class of material, and its shape is broadened by the presence of sources of both random and systematic variations. Statistical decision rules are usually employed in recognition processing to account for the variations found in the multispectral scanner data; such rules are most appropriate for random variations. These decision rules use approximations of the signal-probability density function (i.e., likelihood functions). Therefore, the likelihood function is a logical choice to serve as a focal point for studies of multispectral recognition.

The analysis and implementation of multispectral recognition techniques are relatively easy for samples of populations having multivariate normal (Gaussian) density functions. Optimal statistical decision rules then can be derived, based on maximum likelihood or related principles. For recognition processing of multispectral scanner data, we usually assume that the signals have multivariate normal distributions, even though our studies have shown that this is not always the case. One possible reason for the non-normality of the data is the presence of systematic variations, such as those associated with scan angle (i.e., associated with the length of the atmospheric path and the viewing geometry). Experience has shown that, when the scan angle is ignored, the probability density functions of different material classes often overlap, and poor recognition performance is achieved.

One way to improve recognition performance in such cases is to define several subclasses to represent different scan angle intervals of each class of material. This approach can lead to many training sets and increased processing requirements. An alternative approach, which we have been pursuing, is to preprocess or transform the data to remove the systematic variations before applying the recognition rules. In general, both multiplicative and additive adjustments must be made on the data as continuous functions of scan angle.

In addition to the scan angle or cross-track dimension of image data, we should also consider the along-track dimension. Slow changes may occur in the properties of the atmosphere along an extended flight path. Even if the atmosphere were to remain constant, changes in the position of the sun would result in changes in the received signal characteristics. The approaches used to make scan angle corrections in the across-track dimension can be adapted to carry out continuous along-track corrections. In addition, one might use feedback from the recognition results to modify the preprocessor characteristics to extend the initial training-set data in time and space away from the areas used for training.

Continuous flight data might not always be available for computation of along-track corrections. In that case, one must resort to a discrete or discontinuous correction, such as in a flight-to-flight or day-to-day processing situation. The generalized preprocessing transformation described here provides a mechanism for making corrections to link two data sets. The transformation can use information about the similarity of material samples observed in both data sets or can make use of auxiliary information, or both.

A preprocessing operation transforms all signals in exactly the same way, regardless of their material class. Therefore, preprocessing is an efficient operation for computation. If all materials do not have exactly the same dependence on the parameter controlling the preprocessing (e.g., the scan angle), then the correction function represents an average correction which minimizes a selected error criterion associated with the sample population used to generate the correction function.

Preprocessing might not be the most effective way to account for the variation associated with a given parameter, if distinctive information for various materials is associated with that parameter. Alternatively, then, one could adjust the statistical decision-rule parameters independently for each material, as a function of the parameter.

For processing based on the multivariate normal assumption, the mean vectors and covariance matrices of the materials are the decision-rule parameters of interest. The mean vector is the more important of the two, and its adjustment has received most of the attention to date. In the most general case, adjustments of the covariance matrices should also be considered. The relative magnitudes of system noise and radiation signal variance will affect whether or not we adjust covariances and the best method to use for the adjustment.

Insight into the physical processes that result in the observed radiation signals and the signals' dependence on various factors can be gained through the use of simulation models. The basic model required is one which describes radiative transfer processes within and through Earth's atmosphere. Other models of the sensors, the data processors, and the target materials complete the overall system model. The simulation model is particularly useful in explaining and characterizing systematic variations in scanner data.

1.1. PERSPECTIVE

In classification or recognition processing of multispectral scanner data, a decision is made regarding which of several possible classes of ground surface materials was observed in each spatial resolution element. When material class, m, is observed, the primary sensor (the multispectral scanner) produces a signal vector, x. Other signal vectors (a, b, and c) from auxiliary sources may be introduced to augment the primary signals. The decision process is best described with likelihood functions; therefore, likelihood functions are used as the focal point for our discussion of all steps in the recognition process.

At this point, we shall consider only the primary scanner signal vector, x. The likelihood function, $L(x|m)$, is mathematically identical to the probability density function, $p(x|m)$, of the n-channel signal vector, $x = x_1, \ldots, x_n$, conditional on material class, m; i.e., $L(x|m) = p(x|m)$. Conventionally, when the probability density function is considered, m is regarded as fixed and x is regarded as variable. When the likelihood function is considered, x is regarded as fixed and

m is regarded as variable. While acknowledging this distinction, we use the symbol p to preserve a single notation and use the terms likelihood and conditional density interchangeably.

1.1.1. SIGNALS AND MEASUREMENT PARAMETERS; MEASUREMENT CONDITIONS AND AUXILIARY INFORMATION

A remote sensing instrument measures the radiation field that reaches it from the scene being viewed. The intensity of the measured radiation depends on several measurement parameters (wavelength; spatial dimensions, polarization; and time), over which the operator has control, and on the prevailing measurement conditions (surface weather; atmosphere constituent distribution; sun position; and cloud distribution), over which he has little or no control.

Of necessity, the measuring instrument samples the continuous domain of the measurement parameters. For example, every sensor has a specific wavelength passband(s), a restricted field of view, a direction of view, a definite polarization characteristic, and a definite interval of time over which a measurement is made. One general problem in remote sensing is choice of the proper sampling scheme (i.e., designing the sensor and the data collection procedures) to allow the desired discrimination between signals from different scene materials to be carried out most effectively.

In multispectral remote sensing, both with cameras and optical/mechanical scanners, sampling in the spectral parameter domain has been implemented in discrete wavelength passbands, i.e., spectral channels. Ideally, these passbands should be chosen to maximize the differences between the signals received from various materials on the ground.

In the spatial domain, the scanner has an optical aperture function and electrical filters which limit the spatial frequencies represented by the signals. Furthermore, each scanner scene is imaged from a fixed line in space, so that the observation geometry varies continuously as a function of scan angle. The direction of scan relative to the sun's azimuth position and to the sensor altitude also is an important spatial measurement parameter.

The polarization parameter usually has been ignored in remote sensing applications, but might be used more in the future to minimize the effects of specular reflections or to take advantage of certain physical effects.

Time is a measurement parameter insofar as the starting time, and thus, the initial measurement conditions, of a collection mission can be selected. However, once a mission has begun, changes in measurement conditions linked to time are uncontrollable even though they might be predictable (e.g., the position of the sun).

Two conditions of measurement which effect the amount, spectrum, and spatial distribution of the radiation that reaches the ground surface are the distribution of atmospheric constituents (e.g., haze particles) and the distribution of clouds. The reflecting properties of surface ma-

terials depend in part on the surface weather conditions (e.g., temperature, humidity, wind speed and direction, and recent precipitation history).

If information about the conditions of measurement is to be used in recognition processing, it must be received through auxiliary information channels. This auxiliary information might come from special processing of signals received from the prime sensor, from an auxiliary sensor aboard the sensor platform, or from ground-based instrumentation and observations.

We have identified the likelihood function as the key to an understanding of recognition processing. Likelihood functions may be made simple or complex, according to the number and combination of channels considered. These channels may include both the primary signal channels (the multispectral scanner outputs) and the auxiliary signal channels, or their subsets.

When no auxiliary information is being used, $p(x|m)$ is the likelihood function. In most recognition-processing operations, training sets of data are used to obtain empirical estimates of the likelihood function for each class of material. If the conditions which prevailed during the collection period were relatively constant, the estimated density functions will be concentrated in relatively small regions in signal space (i.e., x space), and decision rules based on them can be successfully applied to data observed under similar conditions. The density function estimated under these relatively constant conditions is not actually $p(x|m)$, the density function over all measurement conditions. Rather, it is the density of x, given both m and the specific conditions of measurement, $p(x|m$ plus the specific measurement conditions). The overall density function would be more spread out in signal space and, if applied in recognition processing, would result in increased numbers of errors.

When auxiliary information is used, the definition of the likelihood function is expanded to include the additional signal channels. For example, the likelihood function might become

$$p(x, a, b, c|m)$$

where x = the signal vector from the multispectral scanner, a function of wavelength, space, polarization, and time

a = a signal vector from auxiliary radiation sensors carried on the aircraft (e.g., sun sensor)

b = a vector to describe the measurement conditions, i.e., information from sources other than those on the aircraft (e.g., weather observations and ground-based measurements) and/or from estimates based on airborne measurements

c = a vector of measurements (or calculated estimates) of the solar geometry and the viewing geometry

m = the class of material present

The expanded signal space now has dimensions equal to the sum of the dimensions of the vectors x, a, b, and c. When the data from training sets are taken over the expected variety of measurement conditions, the projection or marginal distribution of the cluster of observations from any particular class of material onto the x-signal space will be spread out, as illustrated by the x-axis projection of Fig. 1. In the expanded signal space, the cluster of observation occupies a much smaller fraction of the total volume, thereby improving chances of discrimination. For example, joint use of the auxiliary input, a, permits one to narrow the region in x space, where the projected observations cluster for any given measurement condition, a_0.

The choice of auxiliary inputs for use in recognition processing will depend upon how easily the inputs can be measured and upon how well they represent those measurement conditions which produce the greatest variability in the primary scanner signals. The chance of making good choices for auxiliary inputs will be improved by development of a better understanding of the dependencies of both the multispectral scanner signals and the possible auxiliary signals on the variation of the measurement conditions.

In summary, the problem is to extend the application of recognition-processing rules over a variety of measurement parameters and conditions. The empirical use of auxiliary information for this purpose consists of adding information related to the conditions of measurement to the signal space and estimating the parameters of the likelihood function. Estimations are based on training data drawn from a variety of measurement conditions. Relationships developed through theoretical modeling and analyses can be used to augment, structure, or replace the empirical procedures.

1.1.2. DECISION RULES

Without discussing the details of decision rules, it is sufficient to say that optimum rules are rules that depend on the likelihood function of the original or a transformed version of the signals. We can implement a practical recognition processor by: (1) choosing a convenient mathematical form with which to approximate the true likelihood function for each material class; (2) using a training set of the signal data, and corresponding data on measurement conditions, to estimate the parameters of this mathematical form for each material class; (3) calculating the likelihood of each input sample for each material class, using the approximate form with its estimated parameters; and (4) deciding to which class the point should be assigned based on a criterion function of the likelihoods. A practical processor must accept and process signals with statistics described by the true likelihood function, even though the processor classifies signals based on some approximation to the true likelihood function.

The multivariate normal density function is commonly chosen to approximate the likelihood function. The parameters of this form are the mean vector and covariance matrix, and its implementation in recognition processing requires only the calculation of a quadratic form. In

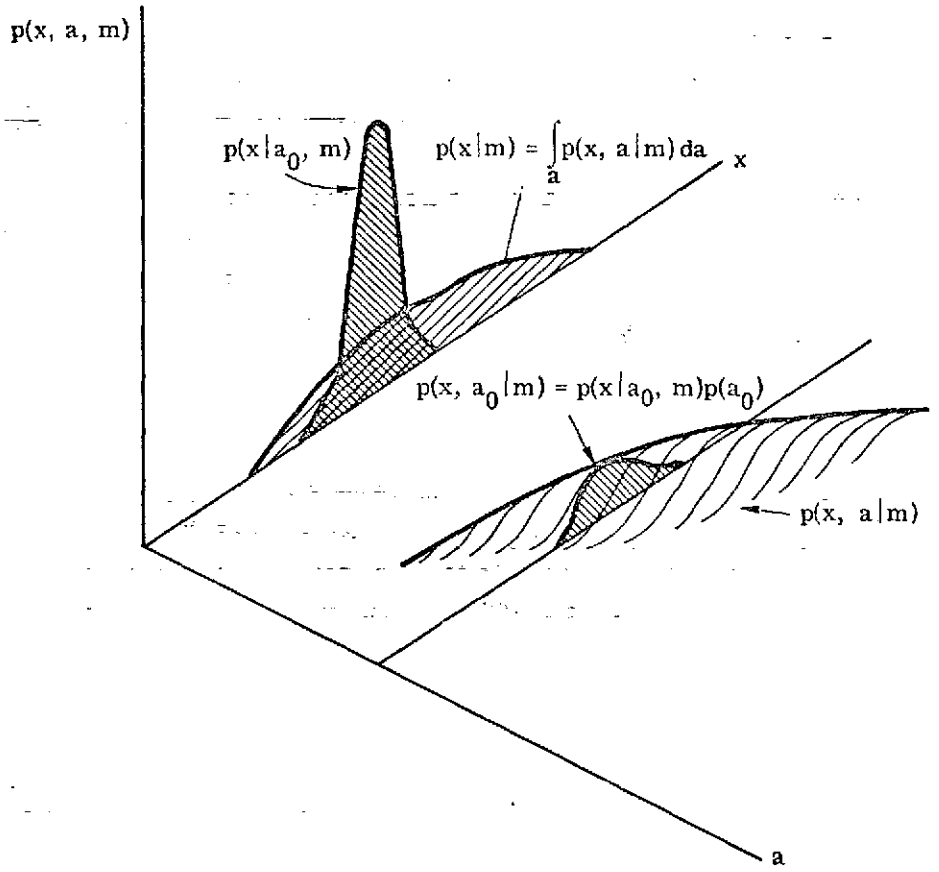

FIGURE 1. ILLUSTRATION OF THE USEFULNESS OF AUXILIARY INFORMATION, a_0, IN DELIMITING THE SIGNAL SPACE OCCUPIED BY SIGNALS, x, FROM MATERIAL CLASS, m

spite of these advantages, the multivariate normal approximation is merely an assumption, the validity of which is subject to test. The average probability of misclassification is a convenient criterion for deciding whether to use the multivariate normal approximation, some higher-order approximation, or, possibly, some simpler form.

Systematic trends in multispectral data result in large variances and covariances for various classes of materials. In addition, they can cause the multivariate density functions to depart from a normal form. We can remove the effects of systematic trends in the data by changing the parameters of the likelihood function according to changes in auxiliary information signals and/or measurement parameters. Alternatively, the average effect of the systematic trends on the means of signals can be removed by preprocessing the data, again as a function of the auxiliary signals and/or measurement parameters of the prime signal channels.

1.1.3. PREPROCESSING TRANSFORMATIONS

Preprocessing has several advantages, even though it is not the most accurate method of accounting for systematic variations in signals. First, preprocessing is efficient because only one set of corrections is applied to the data. Second, preprocessing separates the correction process from the decision process. Finally, preprocessing is a proven technique; its usefulness has been demonstrated for several applications in feasibility studies carried out at The University of Michigan.

There are several reasons for implementing preprocessing transformations. These include: (1) decreasing the time of digital recognition computations and/or reducing the complexity of analog computing hardware by reducing the number of information channels used in decision calculations; (2) removing systematic variations from the data and thereby improving recognition; and (3) producing variables that are more directly interpretable in terms of the physical processes being observed. In pattern-recognition literature, feature extraction is frequently used to describe some of these functions.

1.1.4. SYSTEM MODELING

Although the procedures described above might be approached from a purely empirical basis, we believe that a balanced program of empirical and theoretical studies provides the most reasonable approach to defining future remote sensing systems because the two types complement each other and permit more efficient and effective use of developmental resources. Such a program would use a model for simulating the entire system from the generation of radiation signals through recognition processing. The accuracy required of the model can vary, depending on the type of system being studied and other factors.

An overall system model serves several functions. It provides a mechanism for gaining a greater understanding of the physical nature of the problem being studied. For example, it

permits one to perform studies to determine the sensitivity of received signals or recognition performance to changes in the conditions or parameters of measurement. This type of information can be useful in the design of sensors and processors, and in the evaluation of operational system concepts. Finally, the system model can be used for testing and evaluating empirical techniques by simulating scanner signals and suggesting modifications of these techniques.

1.2. SUMMARY OF WORK PERFORMED DURING THE YEAR

During the past year of the contract period, progress has been made toward understanding and solving the problems of improving multispectral recognition performance and extending the applicability of recognition procedures beyond areas used to program (i.e., to set the decision rule parameters of) the recognition computers.

Work in four areas is reported herein: (1) simulation of the physical processes that produce the radiance signals sensed by a multispectral scanner and examination of the systematic variations in these signals; (2) investigation of techniques for overcoming the effects of these systematic variations during recognition processing operations, including a generalized development and application of a generalized preprocessing transformation; (3) completion of an investigation (begun last year) of the suitability of the multivariate normal likelihood function for recognition decision rules; and (4) collection of multispectral data for future analysis and testing of processing techniques in an operational area-survey context.

1.2.1. SIMULATION AND EXAMINATION OF SYSTEMATIC VARIATIONS IN DATA

During the past year, we have improved and used a radiative transfer model which characterizes the spatial, spectral, and temporal distribution of electromagnetic radiation on Earth's atmosphere. (The initial development of the model is described in Ref. [1].) Since we are primarily concerned with radiation in the visible and near infrared portion of the electromagnetic spectrum, we have neglected absorption. For this model, the atmosphere is assumed to be plane-parallel, homogeneous, and bounded by a uniform, perfectly diffuse surface. Similar models of radiative transfer through planetary atmospheres have been devised by other authors but their models usually suffer from one or more of the following restrictions: (1) an atmospheric state that is highly idealized and not representative of realistic conditions; (2) a radiation field that is determined only at the extremities of an atmosphere; and (3) surface reflectance conditions that are not realistic.

Our model has removed the first restriction by taking into consideration quantitatively the haze content of the atmosphere. We can calculate the spectral transmittance, spectral irradiance, and spectral radiance in any hazy or clear atmosphere for which a relationship between optical depth and altitude for each wavelength can be specified. We have eliminated the second restriction by finding a simple solution of the radiative transfer equation for radiance within

the atmosphere. Thus, our model can be used to calculate irradiance and radiance at any altitude in the atmosphere.

In calculations of the radiometric quantities, irradiance, sky radiance, and path radiance, one usually assumes a surface albedo independent of wavelength. In our model we consider a spectrally dependent surface albedo. Although at the present time, we do not include bidirectional reflectance in the model, such an effect will be included later.

One of our major innovations this year has been the inclusion of time as an independent parameter. We can now simulate actual flight conditions, taking into consideration the change in the solar zenith angle and the position of the sensor over the surface. By analyzing computer-generated graphs of radiance and irradiance, we can optimize flight conditions for the least amount of atmospheric variability, thereby reducing the burden on the processing system. Varieties of graphs have been produced and are presented in Section 2.

The graphs were selected to demonstrate the systematic variations present in scanner data and to illustrate the dependence of radiation quantities, such as transmittance, irradiance, total radiance, path radiance, and sky radiance, on a variety of parameters and conditions of measurement. The ultimate goal is to help develop processing techniques that are insensitive to systematic variations. The measurement parameters considered include wavelength, scan angle, azimuth angle relative to the sun, altitude, time of day, time of year, latitude, and longitude. Measurement conditions were varied primarily by changing the haze content and distribution in the atmosphere; various standardized atmospheres, labeled according to their horizontal visual range at ground level, were used for most of the calculations. Time was also varied to simulate the changes in date that result when data are collected over a period of time, as in an area-survey operation.

A question which has not been answered satisfactorily in remote sensing problems is the degree to which one surface element affects a neighboring element. In a haze, there is considerable scattering of radiation, and analysis of experimental data does seem to show an influence of one element on another. A partial solution to this rather difficult mathematical problem has been given in Section 2.3.3, in which single scattering in a haze is considered. An empirical method of data correction is described in Section 3.1.4.

The verification of the radiative transfer model depends, of course, on how well it agrees with experimental data. Well defined experiments with simple, geometrical and physical conditions, for which this model is applicable, are not always available, and therefore only partial verification of the model is possible. Nevertheless, as the computer-generated plots in this report show, the agreement between the model and exact calculations and experimental sky-radiance data under clear conditions is very good. Any deviation between model calculations and experimental data can be attributed to: (1) approximations used in the development of the

model: (2) inability to specify accurately the parameters used in the model; or (3) idealized surface conditions.

A simple radiative transfer model which includes multiple scattering in a hazy atmosphere has been developed and tested with a limited amount of actual experimental data. Furthermore, the model has been used to simulate flight conditions and to study preprocessing transformations. For the most comprehensive model, one should include discrete clouds, absorption, and a non-Lambertian surface.

1.2.2. INVESTIGATION OF TECHNIQUES FOR OVERCOMING SYSTEMATIC VARIATIONS

Simulation of the type described in the preceding section and examination of real scanner data have both shown that there are systematic variations in data that degrade recognition performance. We have studied methods for overcoming these variations in recognition processing.

Major emphasis during the year was on generalization of some of the preprocessing transformations that had been developed and tested earlier. A generalized transformation, called the U-V transformation, was developed; it applies both additive and multiplicative corrections to scanner data. Section 3.1 describes the transformation and Section 4 presents results of its application to real and simulated scanner data. The transformation was applied to a data set collected under very hazy conditions, first to correct for scan angle effects and then to extend decision-rule parameters for data collected from a 1000-ft altitude to data collected from 5000 ft. The scan angle correction is continuous, whereas the altitude correction is discrete or discontinuous. Both can be classed as one-dimensional corrections. Two-dimensional corrections are discussed in Section 3.1.3.

Another type of preprocessing, discussed in Section 3.1.4, is a method for removing the effects on the radiance signals of differences between the reflectances of the observed surface elements and those adjoining it through coupling by the atmosphere. The method can be related to the modeling effort mentioned in the previous section.

In Section 3.2, we consider, as an alternative to preprocessing, the adjustment of decision-rule parameters rather than the transformation of input data. The alternative approach has several potential advantages which are discussed.

The final presentation in Section 3 is of supporting analysis of interdependencies of radiation quantities related to sensor outputs. In other words, Section 3.3 presents results of radiative transfer-model calculations in ways that make clear interdependenceis such as: (1) total downward irradiance at any altitude versus that at the surface; and (2) the path radiance as a function of time of day versus the corresponding total received radiance.

1.2.3. INVESTIGATION INTO THE SUITABILITY OF THE NORMAL LIKELIHOOD FUNCTION FOR DECISION RULES

Likelihood functions are used in classification decision (i.e., recognition) processes on multispectral scanner data. These functions are usually represented by a multivariate normal (Gaussian) density function, the statistical parameters of which are determined for the various decision classes from subsets of the data. Last year, tests were made of the normality of subsets of data corresponding to single fields, and all were found to be non-normal. This year, the question of how much might be gained by use of a processing rule that does not assume multivariate normality was investigated. A comparison of two maximum likelihood decision rules was made on the basis of paired receiver operating characteristic curves, one curve for a decision rule based on a multivariate normal density function and the other for an empirical histogram density function. An operating characteristic curve is a plot of Type I versus Type II errors (probability of miss versus false alarm). We conclude that, for the cases considered, the improvement in performance resulting from using the histogram likelihood function is not sufficient to warrant the added complexity in processing and the development work necessary to implement it.

1.2.4. DATA-COLLECTION MISSIONS PERFORMED

One primary and two secondary data-collection missions were flown during the summer of 1971 to obtain multispectral scanner data for future use in the testing and continued development of processing techniques to overcome the systematic trends introduced into scanner data by the atmosphere, sun position, and scan geometry during area survey operations. The test site is located in Ingham County, Michigan.

2
EXAMINATION OF SYSTEMATIC VARIATIONS IN MULTISPECTRAL SCANNER RADIATION SIGNALS BY SIMULATION

As seen on a global scale, a number of factors can affect the radiation from a given field point that is incident upon an airborne or spacecraft remote sensing device. These factors are as follows for reflected radiation (~0.3-3.0 μm):

(1) Astronomical Factors

- (a) The solar emission spectrum in a given wavelength interval
- (b) Variable sun-earth distance (time of year)
- (c) Variation in solar declination angle (time of year)
- (d) Variation of hour angle of sun (time of day)

(2) Geographical Factors

- (a) Latitude of field point
- (b) Longitude of field point
- (c) Elevation (above sea level) of field point

(3) Geometrical Factors

- (a) Solar zenith angle
- (b) Solar azimuth angle
- (c) Zenith angle of surface normal
- (d) Azimuth of surface normal relative to solar azimuth
- (e) Altitude of sensor
- (f) View angles of sensor to surface element

(4) Physical Factors

- (a) Attenuation and scattering by atmospheric gases
  - (1) Temperature versus altitude
  - (2) Pressure versus altitude
  - (3) Relative humidity versus altitude
  - (4) Ozone density versus altitude
- (b) Attenuation and scattering by atmospheric aerosol particles
  - (1) Aerosol particle density versus altitude
  - (2) Aerosol particle size distribution
  - (3) Relative humidity versus altitude

(c) Cloudiness of sky

(d) Surface reflectance

Some of the factors can significantly affect the radiance, whereas other factors have only a small influence on the radiance received by a sensor. The overall effect on remote sensing is that Earth's atmosphere can seriously and systematically alter the intrinsic and observed radiation of surface objects. Hence, we need to gain an understanding of these phenomena and to develop methods to correct the received radiance for the systematic variations caused by the atmosphere or account for these variations in recognition processing. A radiative transfer model of the atmosphere is an important tool in the process of developing this understanding. It can be used to simulate mean radiance signals for multispectral scanners and to study parametrically the dependence of radiation quantities on the parameters and conditions of measurement.

2.1. THE RADIATIVE TRANSFER MODEL

A radiative transfer model has been developed for remote sensing studies. A detailed description of it is presented in a technical report produced last year under this contract [1] and in The University of Michigan Engineering Summer Conference Notes [2]. In this section, the key aspects of the model are noted, the improvements made in the model during the past year discussed, and a verification of the model is made by comparison with experimental measurements.

2.1.1. ASPECTS OF THE MODEL

The important aspects of a radiative transfer model, briefly summarized in this section, are reviewed in more detail in Appendix I. The reader also may wish to refer to Appendix IV.

In radiative transfer theory, the most fundamental radiometric quantity is the spectral radiance for a particular state of polarization. In a vacuum, spectral radiance is invariant with changes in distance. However, when traversing a medium, radiation is attenuated as a result of its electromagnetic interactions with the particles that compose the medium. In the visible and near-infrared regions of the electromagnetic spectrum, only (elastic) Rayleigh scattering by atoms and molecules and (inelastic) Mie scattering by aerosol particles are important as far as remote sensing applications are concerned.

The scattering by aerosol particles is highly anisotropic and accounts for most of the scattering occurring in hazy atmospheres. The calculation of radiative transfer through an anisotropic medium is a difficult problem because one must use or approximate the highly anisotropic scattering phase function that describes the way that radiation is distributed following a single scattering.

One quantity of great importance in estimating the scattering or absorbing properties of a medium and in interpreting the results of calculations is the optical depth, τ, defined as:

$$\tau = \int_h^\infty \kappa(z)\,dz \tag{1}$$

where h is some base altitude above sea level, and κ is the extinction coefficient for the particular polydispersion of aerosol particles.

Another important parameter, visibility or visual range, is frequently used to describe the atmospheric state. Following the convention of Koschmieder [3], the visual range, V is defined as that horizontal range at which the visual contrast between a black object and the sky horizon reaches 2%. In our model calculations, V designates particular atmosphere profiles that have been identified by Elterman [4]. A theoretical, hazeless atmosphere has a visual range of 336 km. Elterman identifies an atmosphere with V = 23 km as a typical clear atmosphere bordering on one with a light haze. The transition between a dense haze and a fog is usually taken to be V = 1.2 km.

The spectral* radiance, $L(\tau, \mu, \phi)$, received by a sensor in an aircraft or spacecraft which is viewing Earth's surface is given by the following very simple formula:

$$L(\tau, \mu, \phi) = L_I(\mu, \phi)T(\tau, \mu) + L_p(\tau, \mu, \phi) \tag{2}$$

where τ = the optical depth
μ = the cosine of the view angle
ϕ = the azimuthal angle

$L_I(\mu, \phi)$ is the intrinsic spectral radiance at Earth's surface and is given by:

$$L_I(\mu, \phi) = \int_0^{2\pi}\int_0^1 \mu'\rho'(\mu, \phi, -\mu', \phi')L(\tau_0, -\mu', \phi')\,d\mu'\,d\phi' \tag{3}$$

where $\rho'(\mu, \phi, -\mu', \phi')$ is the bidirectional spectral reflectance function of the surface, and

*All physical quantities described in this section are spectral in nature, but, for simplicity, the notation does not show this dependence explicitly.

$L(\tau_0, -\mu', \phi')$ is the total (diffuse plus solar) spectral radiance at the surface. For the special case of a perfectly diffuse (Lambertian) surface, $\rho'(\mu, \phi, -\mu', \phi')$ is independent of direction, and we have

$$L_I(\mu, \phi) = \frac{\rho}{\pi} \tilde{E}_-(\tau_0) = L_I \tag{4}$$

where ρ is the hemispherical spectral reflectance or albedo, and $\tilde{E}_-(\tau_0)$ is the total downward spectral irradiance on the surface. Hence, in this particular case, the intrinsic radiance is independent of direction.

The quantity $T(\tau, \mu)$ is called the spectral transmittance and is given by

$$T(\tau, \mu) = e^{-(\tau_0 - \tau)/\mu} \tag{5}$$

$L_p(\tau, \mu, \phi)$, the last quantity in Eq.(2), is the spectral path radiance, i.e., that radiance which results from the multiple scattering of nontarget radiation into the sensor's field of view.

To help understand variations in radiance caused by the atmosphere, we use the radiative transfer model to calculate transmittance, irradiance, and total path radiances as functions of the parameters on which they depend.

2.1.2. MODEL IMPROVEMENTS DURING THE PAST YEAR

Several significant improvements have been made in the radiative transfer model during the past year. The following changes result in increased reliability and accuracy of our model:

(1) We have included time as an independent parameter in our analysis so that we can now calculate spectral irradiance, spectral path radiance, spectral sky radiance, and total spectral radiance in terms of local standard time and location on Earth's surface.

(2) Instead of using approximations to the single-scattering phase functions, we now use the exact phase functions, as calculated according to Mie scattering theory, and realistic particle size distribution functions, as determined by Deirmendjian [5]. Using these general polydisperse phase functions in Eqs.(72) and (73) in Appendix I, we have calculated path and sky radiances and compared the results with other computational techniques and with experimental data. As we have already seen, the general agreement is quite good.

(3) A correction term, which accounts for a more realistic boundary condition for a diffuse (Lambertian) surface, was included in the formulas for irradiance and radiance.

(4) Some work has been done on a large scale plotting program. One of the advantages of this program, aside from its utility in the production of useful plots, is that we can now interpolate in altitude, wavelength, and visual range. Hence, we are no longer restricted to discrete data points.

(5) In order to examine the effect which one surface element has on a neighboring element, we have had to consider the two-dimensional radiative transfer problem. The complete problem of multiple scattering in the two-dimensional situation is quite complicated mathematically, but it can be simplified somewhat by consideration of single scattering only. In Section 2.3.3, we present the analysis for solving this simplified problem.

2.1.3. VERIFICATION OF THE MODEL

The ultimate validity of any model of the physical world lies in its agreement with experimental data. Unfortunately, there are very few experimental determinations of irradiances and path and sky radiances for which a specification of all the boundary conditions is given. However, there are some comparisons that we can make.

Making use of Mie scattering theory and a knowledge of particle size distributions for typical aerosols, Deirmendjian [5] has calculated scattering phase functions for several wavelengths and aerosol types. These theoretically exact phase functions were used in the radiative transfer equations (Eqs. (60) and (61) of Appendix I) to calculate the path and sky radiances for atmospheric conditions under which Ivanov [6] measured sky radiances for six wavelengths from 0.40 μm to 0.70 μm at every 15^{o}, in planes coincident with, and at angles of 45^{o} and 90^{o} to, the solar plane. The atmosphere was free of clouds and the optical depth of the atmosphere also was measured at each wavelength. The surface of Earth was said to be composed of herbage; however, our calculations were made for several different values of the surface albedo. Figures 2 through 6 illustrate how well our model calculations agree with the experimental data. In all cases, the shapes of the theoretical curves agree quite well with those of the experimental data. The reflectance (albedo) necessary to cause each pair of curves to match at a zenith angle of 0^{o} (arbitrarily selected) was determined. Using these values, we drew a derived spectral reflectance curve for this particular surface for comparison with reflectance curves for standard surfaces. Figure 7 shows two reflectance curves, one derived in the manner just described and the other representing the mean of the reflectance curves for green vegetation that are present in ERSIS, the Earth Resources Spectral Information System that has been developed for NASA under this contract [7]. Except for one wavelength, the shapes of the curves are similar. The differences in magnitude might be caused by any one of several reasons: (1) some atmospheric absorption has taken place and absorption is not included in the model; (2) the actual surface is not well described by the mean curve for vegetation; or (3) we arbitrarily chose a scan angle of zero degrees for a matching point, and another choice

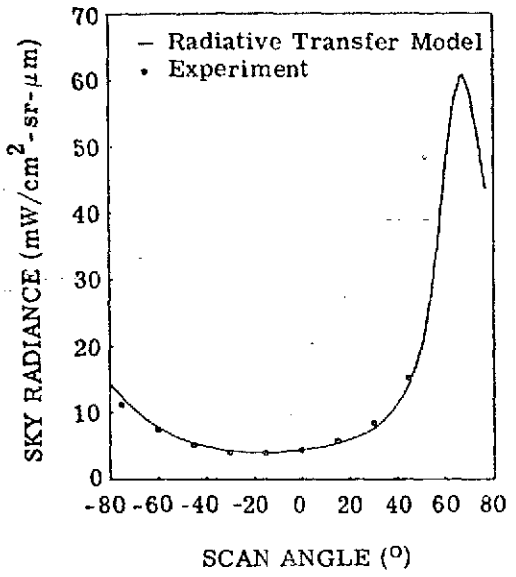

FIGURE 2. DEPENDENCE OF SKY RADIANCE ON SCAN ANGLE (IN THE SOLAR PLANE); SOLAR ZENITH ANGLE = 65.8°. Visual range = 269 km; wavelength = 0.404 μm; surface albedo = 45%

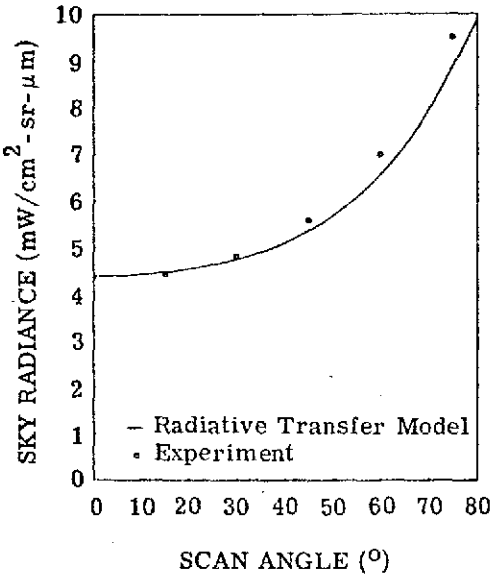

FIGURE 3. DEPENDENCE OF SKY RADIANCE ON SCAN ANGLE (PERPENDICULAR TO THE SOLAR PLANE); SOLAR ZENITH ANGLE = 65.8°. Visual range = 269 km; wavelength = 0.404 μm; surface albedo = 45%

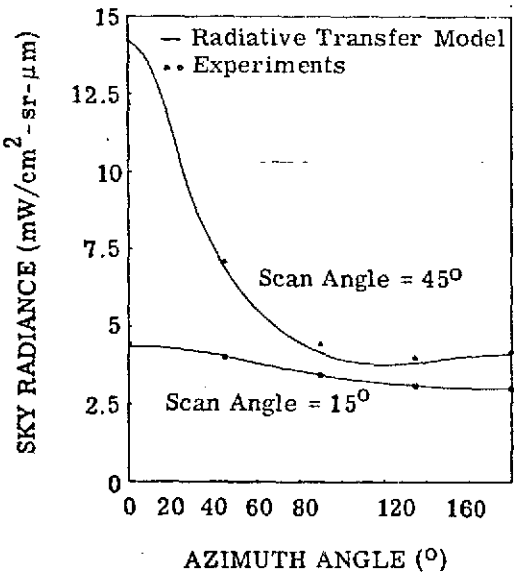

FIGURE 4. DEPENDENCE OF SKY RADIANCE ON AZIMUTH ANGLE. Visual range = 261 km; wavelength = 0.447 μm; surface albedo = 16%; solar zenith angle = 65.7°.

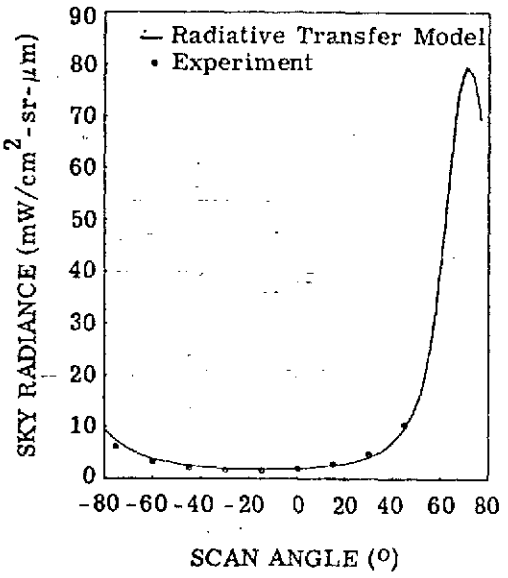

FIGURE 5. DEPENDENCE OF SKY RADIANCE ON SCAN ANGLE (IN THE SOLAR PLANE); SOLAR ZENITH ANGLE = 68.6°. Visual range = 205 km; wavelength = 0.553 μm; surface albedo = 46%.

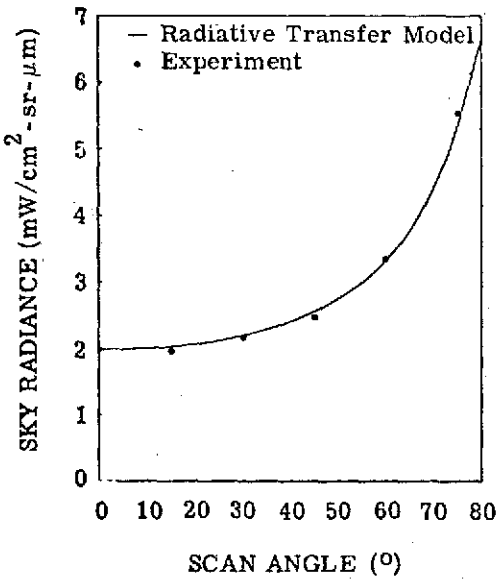

FIGURE 6. DEPENDENCE OF SKY RADIANCE ON SCAN ANGLE (PERPENDICULAR TO THE SOLAR PLANE); SOLAR ZENITH ANGLE = 68.6°. Visual range = 205 km; wavelength = 0.553 μm; surface albedo = 46%.

would bring the reflectance curves into closer agreement. On the whole, however, our model does show very good agreement with the limited amount of data available, at least as far as the angular dependence of sky radiance is concerned. We find good agreement for atmospheres with low haze content; additional confirmation is still needed for atmospheres with high haze content. Comparisons with multispectral scanner radiance data have been less successful to date because the model does not include bidirectional reflectance effects.

As an additional illustration of the general validity of our atmospheric radiation model, we can compare our sky radiances with those computed by Coulson et al. [8] using the results of Chandrasekhar's theory [9]. This comparison is shown in Figs. 8 through 12 (for a Rayleigh atmosphere). Figures 8 and 9 illustrate the sky radiance in and perpendicular to the solar plane, respectively, for a solar zenith angle of ~37° and Fig. 10 shows the sky radiance for a solar zenith angle of 0°. In all cases, the agreement is excellent although there is some deviation in the case of an extremely large solar zenith angle of ~84°.

2.2. RESULTS OF CALCULATIONS

In our radiative transfer model, the transmittance, irradiance, and radiance have the following functional dependences:

$$T = T(h, \theta, \lambda, V) \tag{6}$$

$$E = E(h, \theta_0, \lambda, V, \rho) \tag{7}$$

$$L = L(h, \theta_0, \lambda, V, \rho, \theta, \phi) \tag{8}$$

where h is the altitude in km, θ is the nadir or zenith scan angle, ϕ is the azimuthal angle between the scan plane and the solar plane, λ is the wavelength of the radiation, V is the visual range in km, θ_0 is the solar zenith angle, and ρ is the hemispherical reflectance or albedo. Implicitly, irradiance and radiance also depend on time of day and year and on location over the Earth's surface, i.e.,

$$\theta_0 = \theta_0(t, d, \text{latitude, longitude}) \tag{9}$$

where t is the local solar time (hours) and d is the day of the year.

Overcoming the variation of sensor radiation signals with respect to all the parameters listed above constitutes the main problem in extending recognition performance. Perhaps the greatest variations are the results of changes in scan angle, visual range, and time of day.

The remainder of this section presents results of calculations made for a variety of values for each parameter listed. Additional results are presented in the reprint that is included as Appendix IV. For example, the reprint contains both a discussion of contrast transmittance and a number of graphs that illustrate its dependence on a variety of parameters. Methods for overcoming systematic variations during recognition processing are discussed in Section 3.

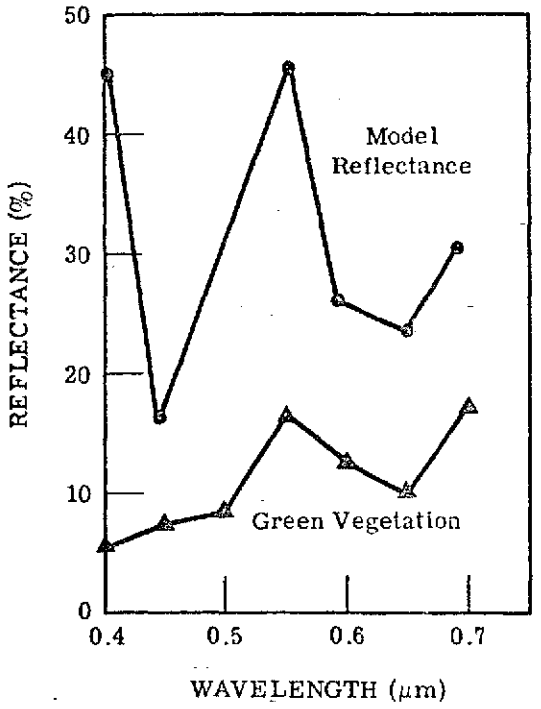

FIGURE 7. COMPARISON OF REFLECTANCE CURVES — FROM MODEL CALCULATIONS AND ERSIS DATA

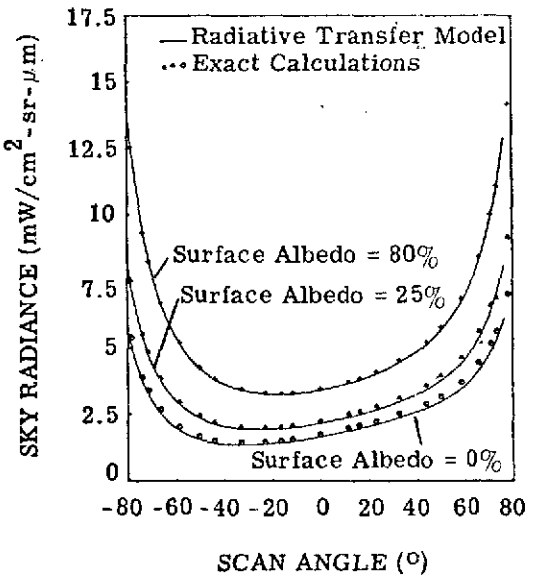

FIGURE 8. DEPENDENCE OF SKY RADIANCE ON SCAN ANGLE (IN THE SOLAR PLANE); SOLAR ZENITH ANGLE = 36.9°. Visual range = 336 km; wavelength = 0.546 μm.

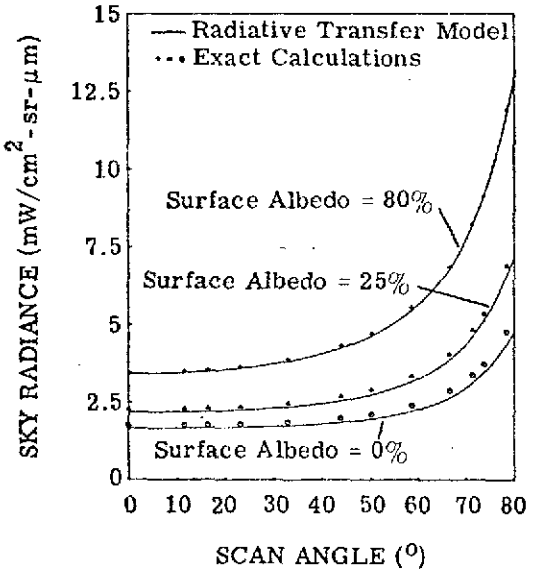

FIGURE 9. DEPENDENCE OF SKY RADIANCE ON SCAN ANGLE (PERPENDICULAR TO THE SOLAR PLANE); SOLAR ZENITH ANGLE = 36.9°. Visual range = 336 km; wavelength = 0.546 μm.

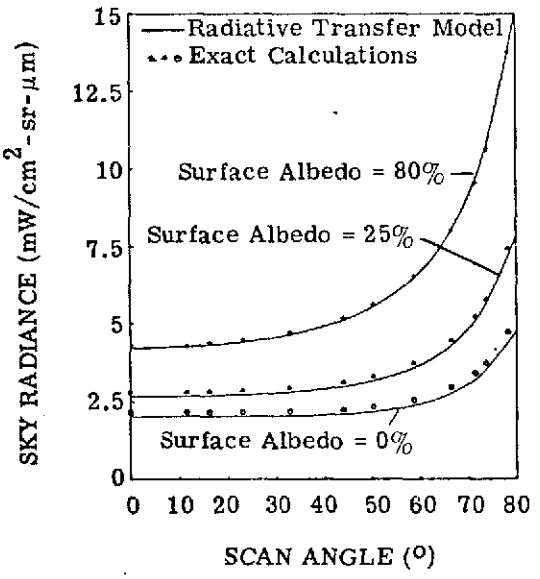

FIGURE 10. DEPENDENCE OF SKY RADIANCE ON SCAN ANGLE (IN THE SOLAR PLANE); SOLAR ZENITH ANGLE = 0°. Visual range = 336 km; wavelength = 0.546 μm.

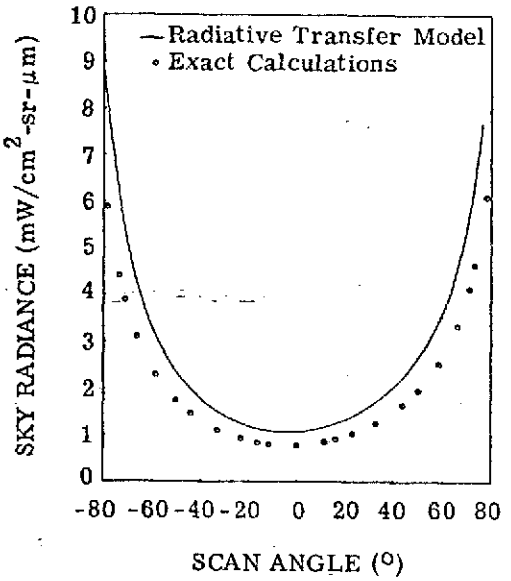

FIGURE 11. DEPENDENCE OF SKY RADIANCE ON SCAN ANGLE (IN THE SOLAR PLANE); SOLAR ZENITH ANGLE = 84.3°. Surface albedo = 25%; visual range = 336 km; wavelength = 0.546 μm.

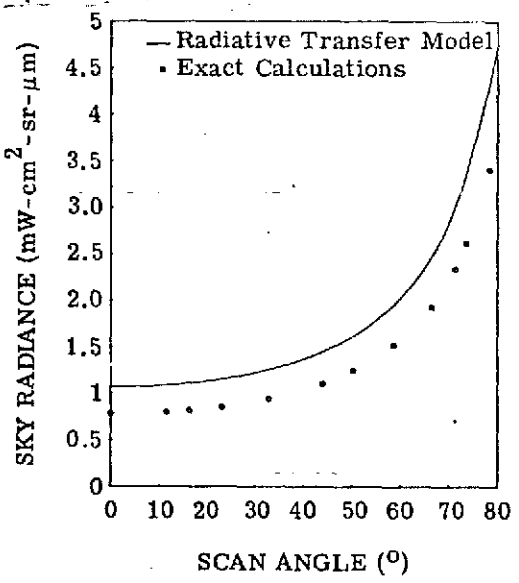

FIGURE 12. DEPENDENCE OF SKY RADIANCE ON SCAN ANGLE (PERPENDICULAR TO THE SOLAR PLANE); SOLAR ZENITH ANGLE = 84.3°. Visual range = 336 km; wavelength = 0.546 μm; surface albedo = 25%.

2.2.1. VARIATION OF SENSOR SIGNALS WITH SCAN ANGLE

During data collection, scan angle is the most rapidly changing measurement parameter. Substantial variations associated with scan angle are observed frequently in scanner signals. The two principal sources of these variations are the atmosphere and the bidirectional reflectance characteristics of the surface materials. In this section, we present graphs that illustrate the extent of scan angle variations associated with the presence of the atmosphere as calculated with the radiative transfer model. As seen in Eq. (2), the transmittance and path radiance are the two atmospheric parameters of prime interest.

Figures 13 and 14 illustrate the dependence of transmittance on scan angle and wavelength and on scan angle and visual range, respectively. The transmittance decreases as the scan angle increases, and the changes are greatest for low visual ranges.

The variation of path radiance with scan angle and visual range is illustrated in Fig. 15. Increasing values for large scan angles and low visual ranges are evident, as is a peak corresponding to the antisolar angle, which occurs because the scan is in the plane of the sun. This asymmetry can complicate the compensation for systematic variations. If the flight path is toward or away from the sun, however, the antisolar peak is not observed and the path radiance is a symmetric function of scan angle.

Figure 16 shows the variation of total radiance with scan angle and visual range. It is the total radiance that is measured by the scanner. Here, the variation for radiance from a diffuse surface observed from 1 km is not as great as it was in the case of path radiance, since the transmittance changes tend to oppose those in the path radiance. Nevertheless, a distinct antisolar peak still occurs because the scan is in the plane of the sun for this illustration.

By definition, there can be no dependence of irradiance on scan angle. However, dependence of sky radiance on scan angle and visual range is shown in Fig. 17. Note the high peak near the solar zenith angle, particularly in the case of very hazy conditions. The sun sensor at the top of The University of Michigan's aircraft responds to the weighted integral of sky radiance in the hemisphere above the aircraft in addition to the direct solar signal.

2.2.2. VARIATION OF SENSOR SIGNALS WITH VISUAL RANGE

Earth's atmosphere has varying degrees of haziness, depending on the density distribution of aerosol particles. In our model, the degree of haziness is characterized by the horizontal visual range at sea level. During a long data-collection flight, slow changes can occur in haze content and, from day to day, there are usually discrete changes in haze content. The effects of such changes must be overcome in processing for large area surveys.

Figure 18 shows the dependence of spectral transmittance on visual range and wavelength for a nadir scan angle of zero degrees. The greatest change occurs when the atmosphere is

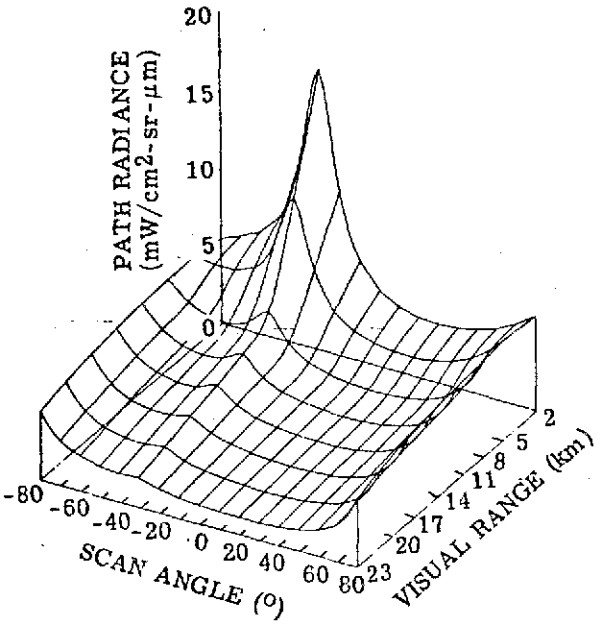

FIGURE 15. DEPENDENCE OF PATH RADIANCE ON VISUAL RANGE AND SCAN ANGLE. Solar zenith angle = 30°; wavelength = 0.55 μm; altitude = 1 km; azimuthal angle = 0° (in the plane of the sun); surface albedo for green vegetation.

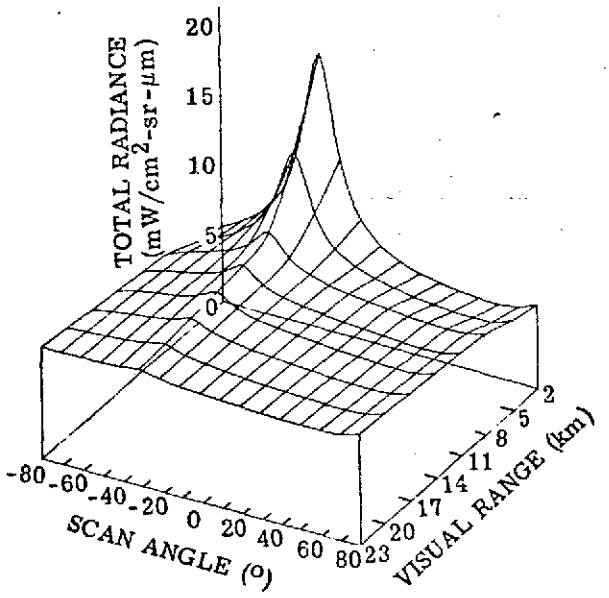

FIGURE 16. DEPENDENCE OF TOTAL RADIANCE FROM DIFFUSE SURFACE ON VISUAL RANGE AND SCAN ANGLE. Wavelength = 0.55 μm; solar zenith angle = 30°; azimuthal angle = 0° (in the plane of the sun); altitude = 1 km; surface albedo for green vegetation.

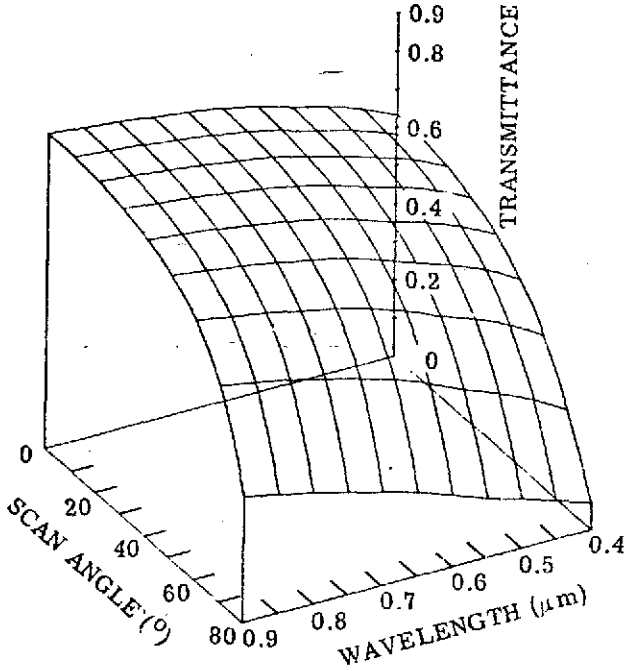

FIGURE 13. DEPENDENCE OF TRANSMITTANCE ON WAVELENGTH AND SCAN ANGLE. Visual range = 8 km; altitude = 1 km.

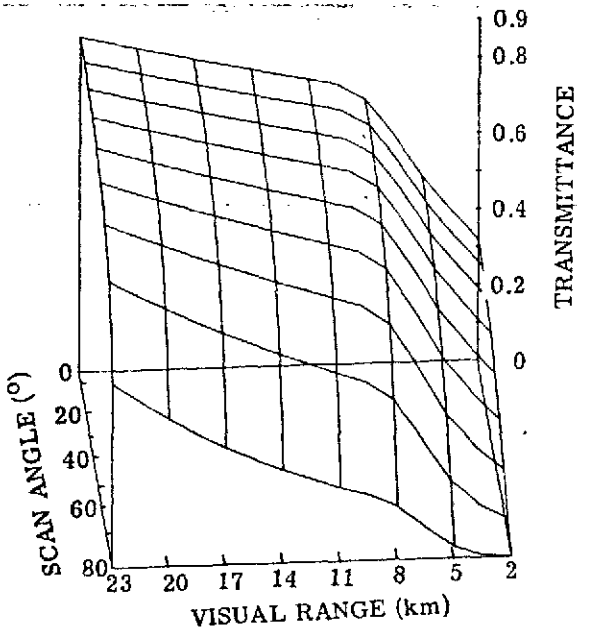

FIGURE 14. DEPENDENCE OF TRANSMITTANCE ON VISUAL RANGE AND SCAN ANGLE. Wavelength = 0.55 μm; altitude = 1 km.

Page intentionally left blank

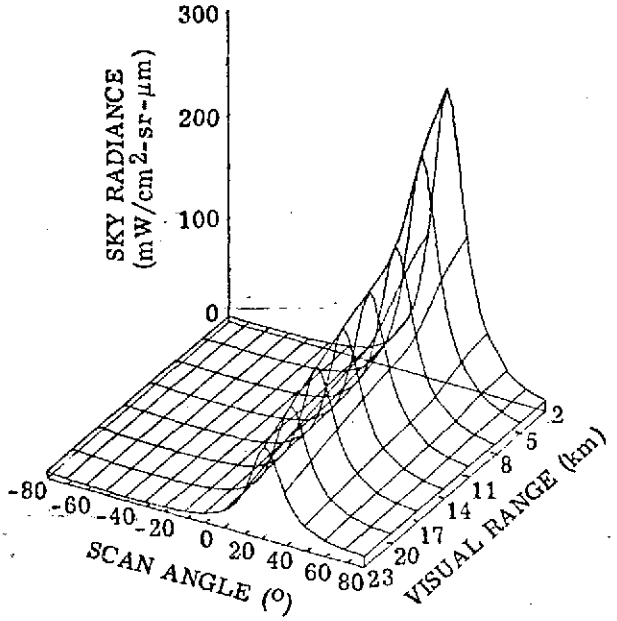

FIGURE 17. DEPENDENCE OF SKY RADIANCE ON VISUAL RANGE AND SCAN ANGLE. Solar zenith angle = 30°; wavelength = 0.55 μm; altitude = 0.1 km; azimuthal angle = 0° (in the plane of the sun); surface albedo for green vegetation.

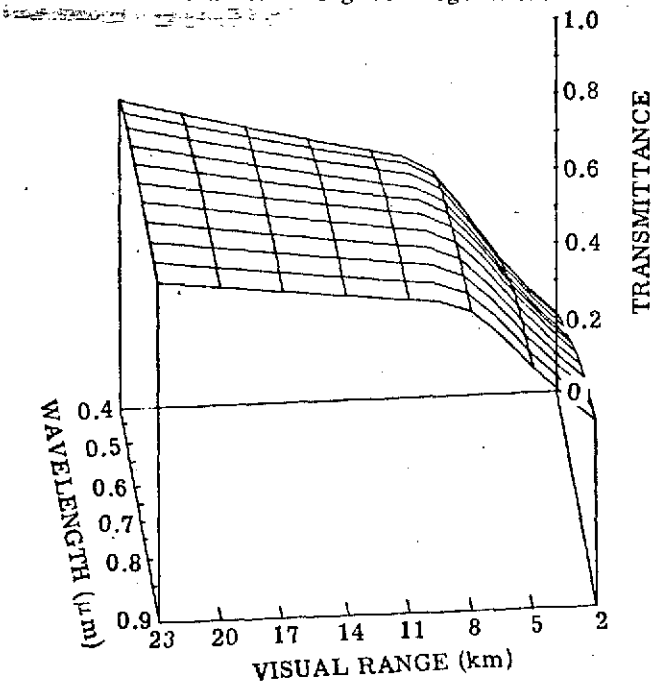

FIGURE 18. DEPENDENCE OF TRANSMITTANCE ON VISUAL RANGE AND WAVELENGTH. Scan angle = 0°; altitude = 1 km.

quite hazy, i.e. for visual ranges from 2 to 8 km. Transmittance does of course change rapidly with altitude, especially for very hazy conditions. This effect is illustrated in Fig. 19 for a wavelength of 0.55 μm.

The irradiance also depends on visual range. The dependence of the diffuse upward irradiance on visual range and altitude is shown in Fig. 20 for a wavelength of 0.55 μm. As in the case of transmittance, the diffuse upward irradiance varies most rapidly for low altitudes and small visual ranges. The change in the diffuse downward irradiance with visual range and altitude is even greater, as can be seen in Fig. 21. The spectral shape of the diffuse downward irradiance is almost independent of visual range (Fig. 22), but the magnitude roughly doubles as the visual range is reduced from 23 to 2 km.

At a wavelength of 0.55 μm, the overwhelming amount of irradiance results from directly attenuated solar radiation and, therefore, a plot of total irradiance (direct solar plus diffuse) should show little change with altitude and visual range. This is true, as is shown in Fig. 23, although one does see that the irradiance at the surface is lower than that above it, and that after 3 to 4 km, the irradiance is essentially constant.

Radiance also changes with visual range. The sky radiance at the Earth's surface can change rapidly with visual range and wavelength, as indicated in Fig. 24. The wavelength dependence is modified by the spectral albedo of the surface which, in this case, is green vegetation. Table 1 shows the average reflectance for green vegetation for several wavelengths. Path radiance is affected in approximately the same way by the surface albedo as shown in Fig. 25. Its variation with altitude and visual range is illustrated in Fig. 26 in which case there is little change with altitude above 4 km.

The wavelength/visual-range dependence of the total radiance from a vegetation surface is illustrated in Fig. 27 for an altitude of 1 km. For a large visual range, the path radiance is small and the total radiance is dominated by the intrinsic radiance from the surface as modified by atmospheric attenuation. Thus, we expect and see a spectral dependence similar to that for green vegetation at a visual range of 23 km. The spectral dependence is quite different for a visual range of 2 km, in which case the path radiance is a major contributor to the total radiance at the short wavelengths. The negative correlation between path radiance and transmittance again can be seen by comparing Figs. 25 and 27; in particular, the 0.9 μm total radiance decreases with visual range, whereas the path radiance increases.

2.2.3. VARIATION OF SENSOR SIGNALS WITH TIME OF DAY

Irradiance and radiance depend on the sun's position which, in turn, depends on the date and time of observation and the latitude and longitude. The passage of time is important in area survey operations. For simulating signals from an airborne scanner system and sun sensor, it is also necessary to specify the flight direction, the altitude, and some estimate of the amount of haze present. A typical flight configuration is depicted in Fig. 28.

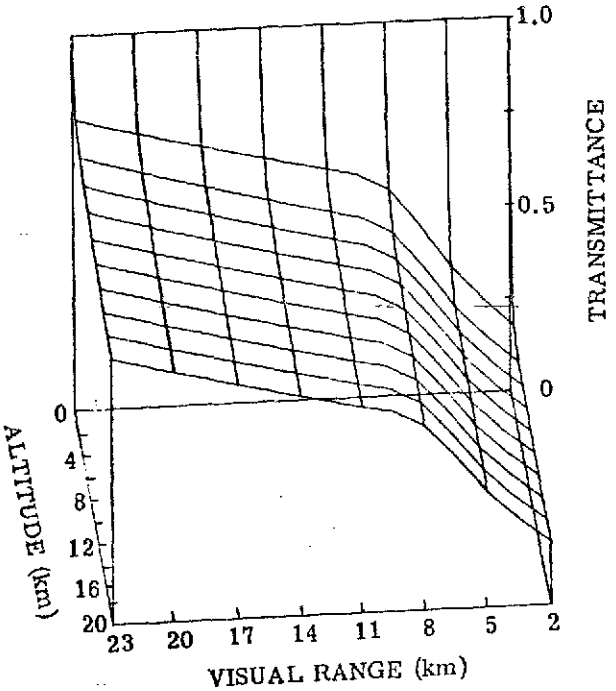

FIGURE 19. DEPENDENCE OF TRANSMITTANCE ON VISUAL RANGE AND ALTITUDE. Scan angle = 0°; wavelength = 0.55 μm.

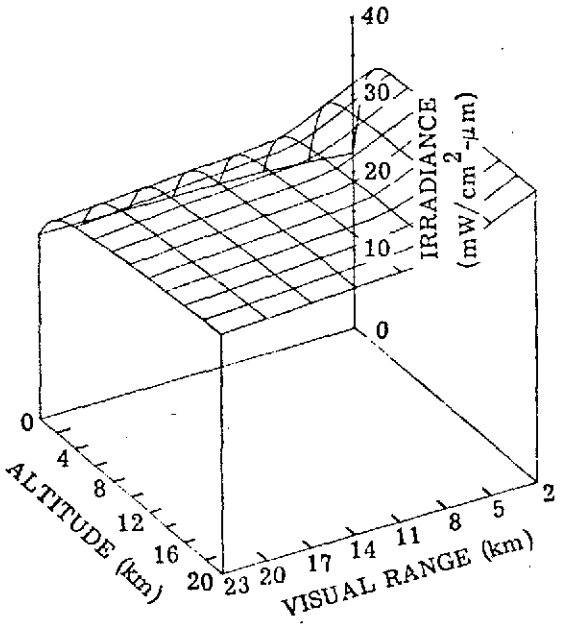

FIGURE 20. DEPENDENCE OF DIFFUSE UPWARD IRRADIANCE ON VISUAL RANGE AND ALTITUDE. Solar zenith angle = 30°; wavelength = 0.55 μm; surface albedo for green vegetation.

TABLE 1. AVERAGE REFLECTANCE FOR GREEN VEGETATION COMPILED FROM REAL DATA FOR SEVERAL WAVELENGTHS

Wavelength (μm)	Reflectance (%)
0.40	0.054
0.45	0.074
0.50	0.09
0.55	0.167
0.60	0.127
0.65	0.101
0.70	0.185
0.80	0.483
0.90	0.523
1.06	0.518

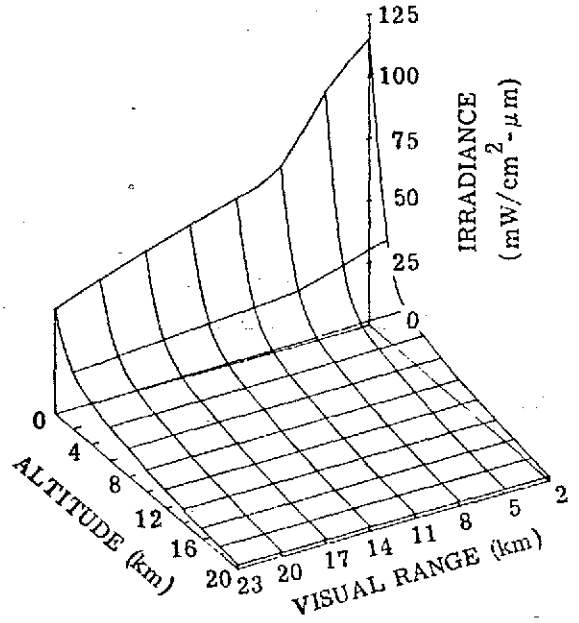

FIGURE 21. DEPENDENCE OF DIFFUSE DOWNWARD IRRADIANCE ON VISUAL RANGE AND ALTITUDE. Solar zenith angle = 30°; wavelength = 0.55 μm; surface albedo for green vegetation.

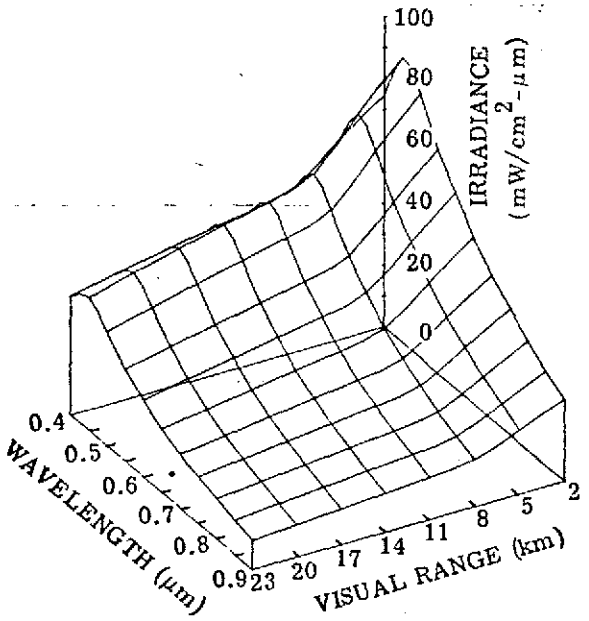

FIGURE 22. DEPENDENCE OF DIFFUSE DOWNWARD IRRADIANCE ON VISUAL RANGE AND WAVELENGTH. Solar zenith angle = 30°; altitude = 1 km; surface albedo for green vegetation.

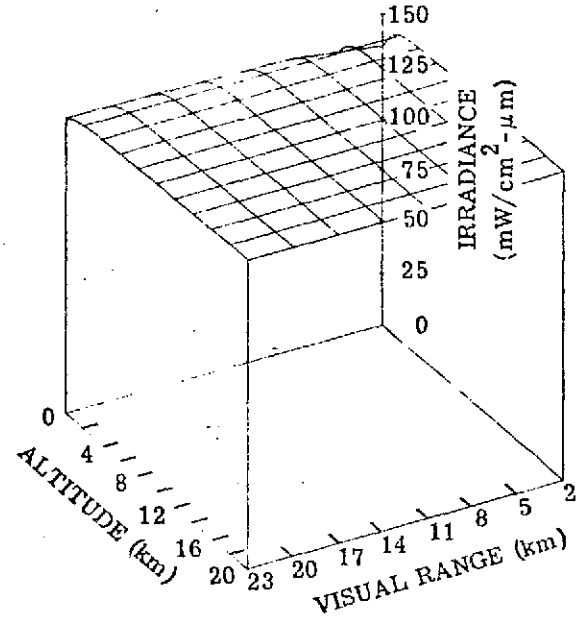

FIGURE 23. DEPENDENCE OF TOTAL DOWNWARD IRRADIANCE ON VISUAL RANGE AND ALTITUDE. Solar zenith angle = 30°; wavelength = 0.55 μm; surface albedo for green vegetation.

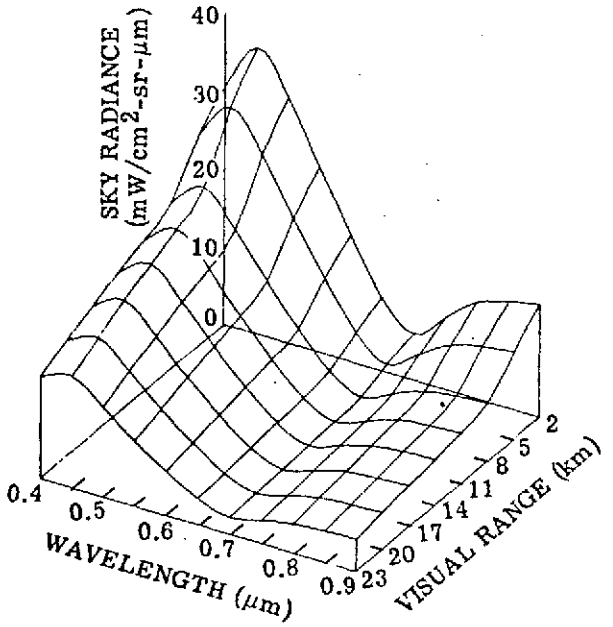

FIGURE 24. DEPENDENCE OF SKY RADIANCE ON VISUAL RANGE AND WAVELENGTH. Solar zenith angle = 30°; scan angle = 0°; altitude = 0 km; azimuthal angle = 0° (in the plane of the sun); surface albedo for green vegetation.

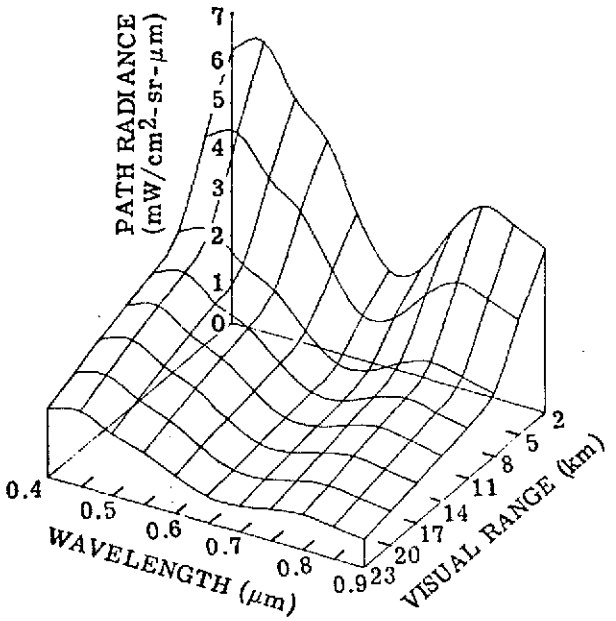

FIGURE 25. DEPENDENCE OF PATH RADIANCE ON VISUAL RANGE AND WAVELENGTH. Solar zenith angle = 30°; scan angle = 0°; azimuthal angle = 0° (in the plane of the sun); altitude = 1 km; surface albedo for green vegetation.

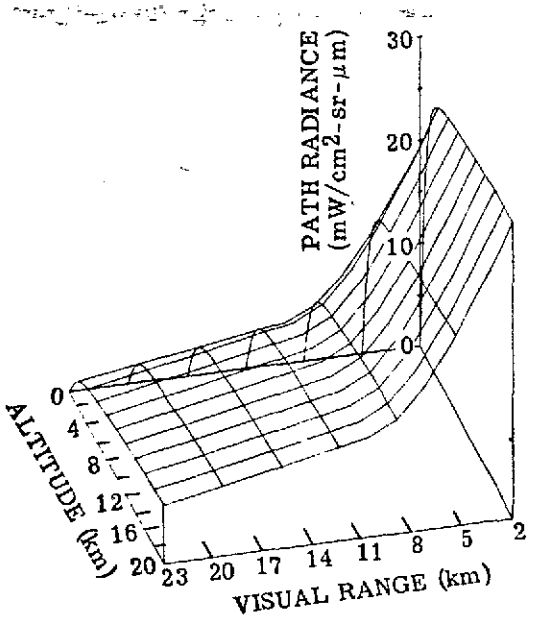

FIGURE 26. DEPENDENCE OF PATH RADIANCE ON VISUAL RANGE AND ALTITUDE. Wavelength = 0.55 μm; solar zenith angle = 0°; scan angle = 0°; azimuthal angle = 0° (in the plane of the sun); surface albedo for green vegetation.

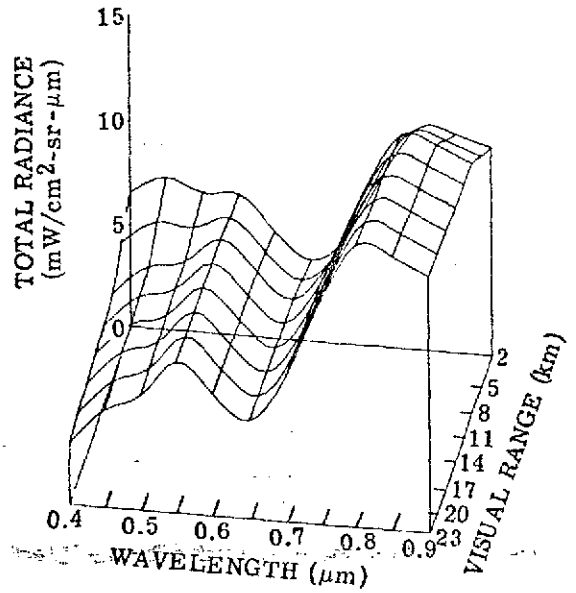

FIGURE 27. DEPENDENCE OF TOTAL RADIANCE ON VISUAL RANGE AND WAVELENGTH. Solar zenith angle = 30°; azimuthal angle = 0° (in the plane of the sun); altitude = 1 km; scan angle = 0°; surface albedo for green vegetation.

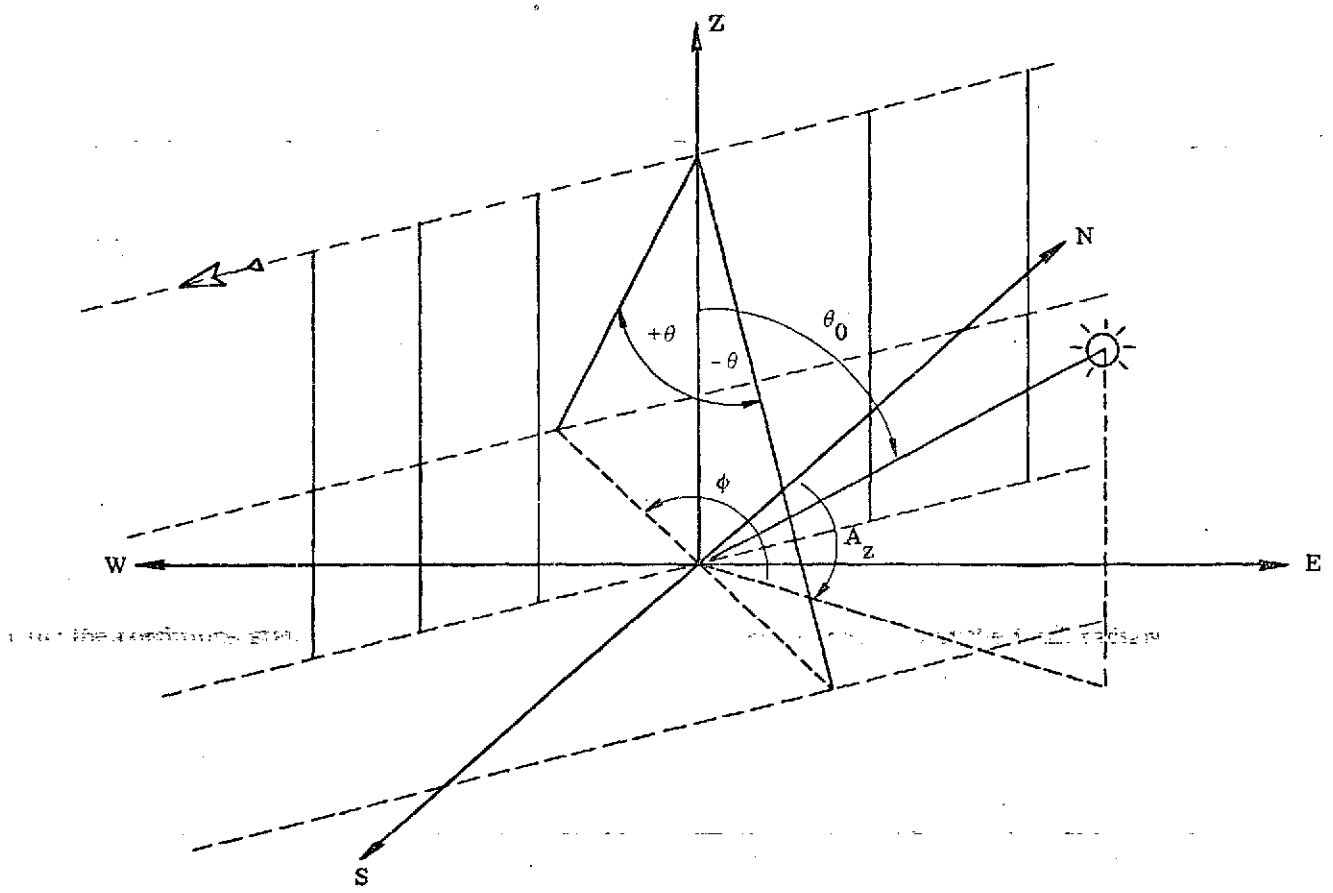

FIGURE 28. TYPICAL FLIGHT CONFIGURATION FOR AIRBORNE SCANNER SYSTEM

θ_0 = Solar Zenith Angle
A_z = Solar Azimuthal Angle
$+\theta$ = Right Scan Angle
$-\theta$ = Left Scan Angle
ϕ = Relative Azimuthal Angle Between Scan Plane and Solar Plane

We can consider a definite place on Earth's surface, Southeastern Michigan, on a specific date, September 1, 1971 and study the variation of irradiance and radiance as a function of time of day. Figure 29 shows the diffuse downward irradiance for the conditions stated above. The greatest changes occur early in the morning and late in the afternoon, when the visual range is small. Figure 30 illustrates the variation of the total downward irradiance. Here, there is very little dependence on visual range because: (1) most of the effect is the result of direct solar irradiance, which is still the major contributor of total downward irradiance, even at an altitude of 1 km; and (2) there is the negative correlation between path radiance and transmittance.

If one scans the local North-South meridian continuously, the sun will cross that meridian near local noon. Such an effect is clearly seen in the sky radiance plot (Fig. 31) for a moderately hazy day.

Now consider a flight due west on a hazy day, at an altitude of 1 km, over a green field in Southeastern Michigan, on September 1, 1971. The path radiance is shown in Fig. 32 in terms of scan angle and eastern standard time. Path radiance increases rapidly near the horizon, especially when the sun is high in the sky. Also, the antisolar peak is clearly noticeable near noon.

Finally, we can look at the total radiance received by a scanner for the conditions stated above. In Fig. 33, we see that this radiance has a less rapid change as a function of scan angle than does path radiance, although a distinct antisolar peak is still visible. The slower variation in this case is the result of the compensating effect of transmittance, i.e. transmittance causes the directly attenuated radiance from the surface to decrease with increasing scan angle, whereas path radiance increases with scan angle. Significantly, in Fig. 33, the dominant changes of signal are associated with time and the position of the sun.

2.2.4. VARIATION OF SENSOR SIGNALS WITH SEASON

The amount of solar radiation reaching a point on the Earth's surface at any time depends on the time of year as well as on the time of day. Figure 34 illustrates the variation of the diffuse upward irradiance with local solar time in Southeastern Michigan for the winter solstice (December 21), the vernal equinox (March 21), and the summer solstice (June 21).

Atmospheric scattering decreases the intensity of the direct solar radiation, forming diffuse downward radiation as a result. This diffuse downward irradiance is shown in Fig. 35 as a function of the local solar time for the four seasons.

The total (solar plus diffuse) irradiance as a function of local solar time is illustrated in Fig. 36 for the same dates as in the previous cases.

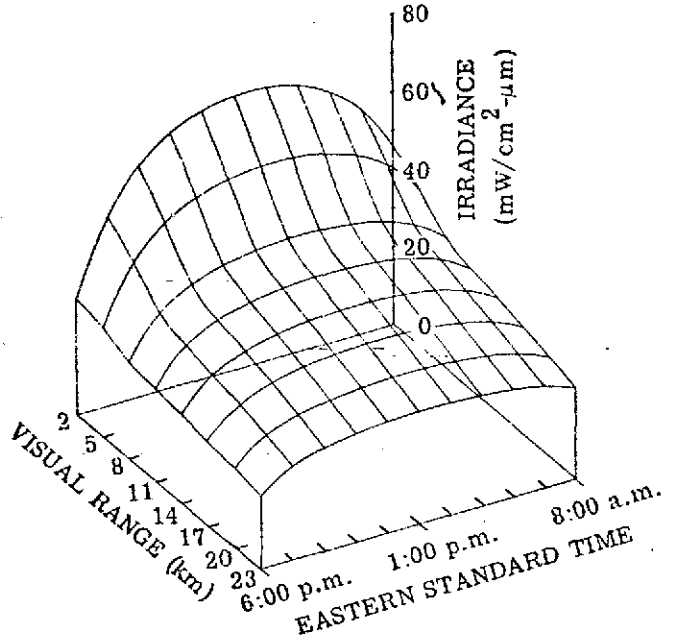

FIGURE 29. DEPENDENCE OF DIFFUSE DOWNWARD IRRADIANCE ON TIME AND VISUAL RANGE. Southeastern Michigan, 1 September 1971. Wavelength = 0.55 μm; altitude = 1 km; surface albedo for green vegetation.

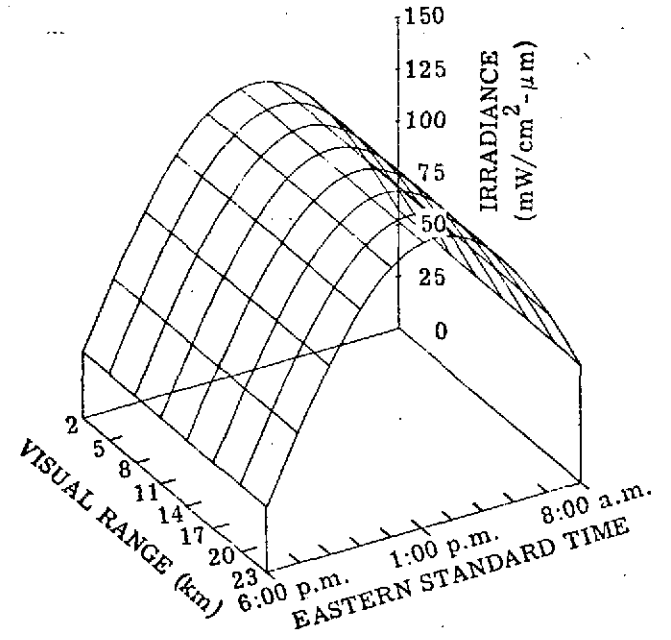

FIGURE 30. DEPENDENCE OF TOTAL DOWNWARD IRRADIANCE ON TIME AND VISUAL RANGE. Southeastern Michigan, 1 September 1971. Wavelength = 0.55 μm; altitude = 1 km; surface albedo for green vegetation.

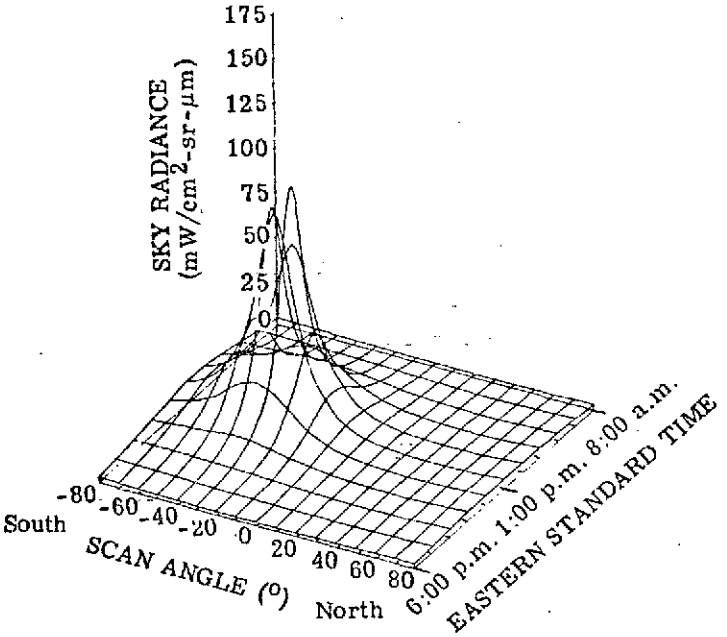

FIGURE 31. DEPENDENCE OF SKY RADIANCE ON TIME AND SCAN ANGLE. Southeastern Michigan, 1 September 1971. Altitude = 0 km; wavelength = 0.55 μm; visual range = 8 km; surface albedo for green vegetation.

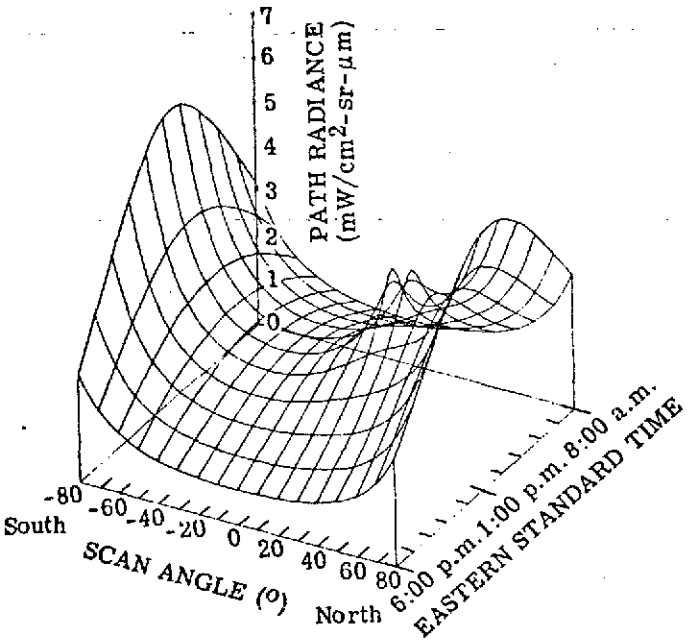

FIGURE 32. DEPENDENCE OF PATH RADIANCE ON TIME AND SCAN ANGLE. Southeastern Michigan, 1 September 1971. Wavelength = 0.55 μm; altitude = 1 km; visual range = 8 km; surface albedo for green vegetation.

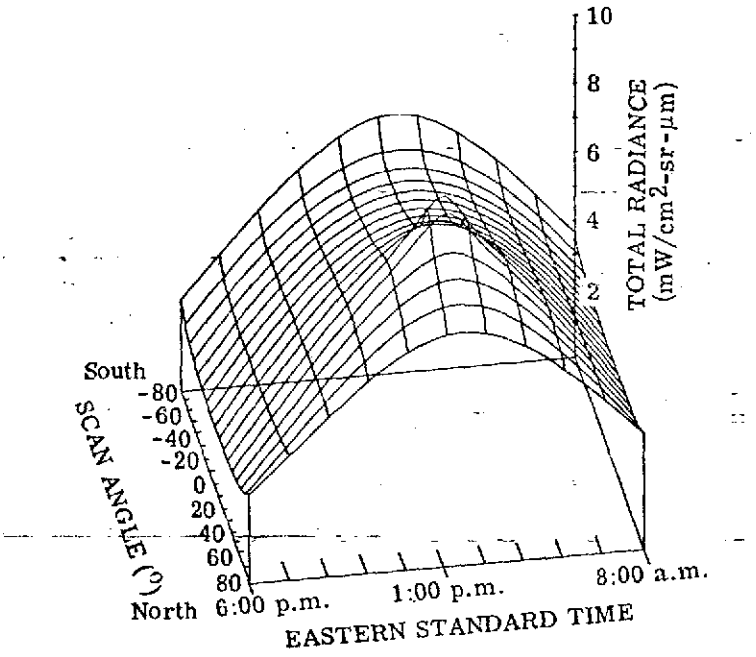

FIGURE 33. DEPENDENCE OF TOTAL RADIANCE ON TIME AND SCAN ANGLE. Southeastern Michigan, 1 September 1971. Wavelength = 0.55 μm; altitude = 1 km; visual range = 8 km; surface albedo for green vegetation.

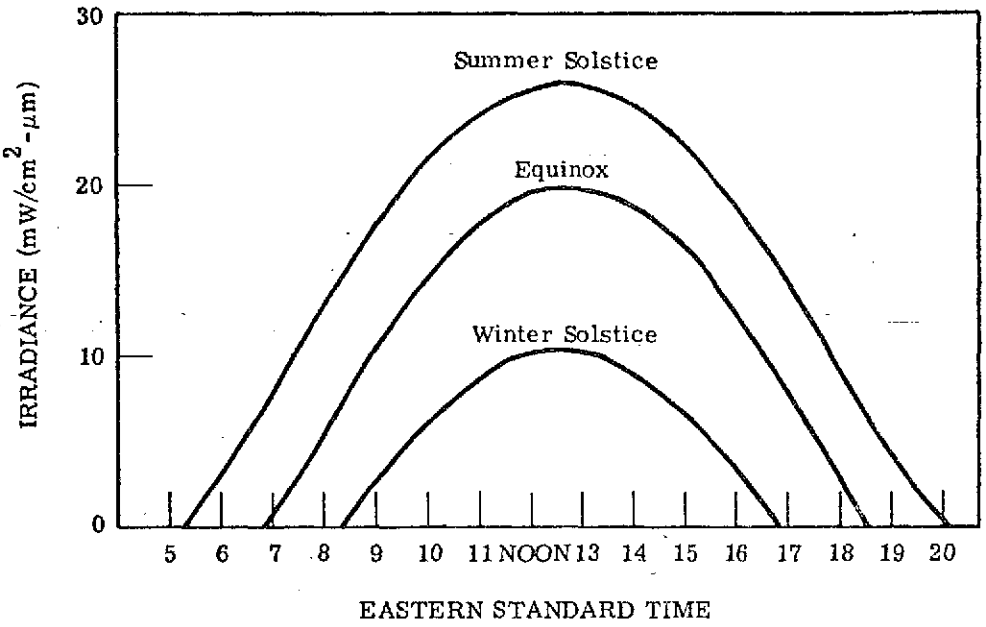

FIGURE 34. VARIATION OF DIFFUSE UPWARD IRRADIANCE WITH TIME AT AN ALTITUDE OF 0 km OVER A SURFACE OF GREEN VEGETATION. Southeastern Michigan; visual range = 8 km; wavelength = 0.55 μm.

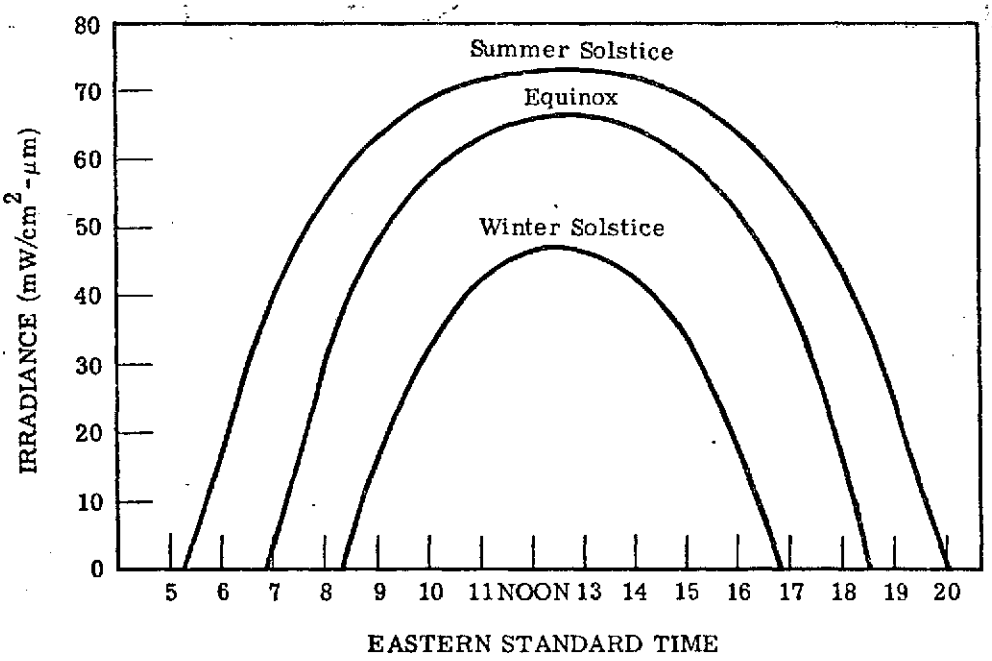

FIGURE 35. VARIATION OF DIFFUSE DOWNWARD IRRADIANCE WITH TIME AT AN ALTITUDE OF 0 kin OVER A SURFACE OF GREEN VEGETATION. Southeastern Michigan; visual range = 8 km; wavelength = 0.55 μm.

We can now consider the relative magnitude of direct solar irradiance, downward diffuse irradiance, and total downward irradiance as a function of time of day and time of year. These effects are illustrated in Figs. 37 and 38. In June, the sun is higher in the sky and all irradiances will be greater than those in December. On June 21, from sunrise to 8:30 a.m. and from 5:00 p.m. to sunset, most of the solar energy goes into scattered radiation (diffuse component), whereas on December 21 most of the irradiance is diffuse from sunrise to sunset because the sun is always low in the sky. For longer wavelengths or greater visual ranges, the direct solar irradiance is larger.

2.3. OTHER SOURCES OF VARIATION

The preceding section presents calculations that demonstrate the systematic variations introduced in multispectral scanner signals by changes in the sun's position, in the viewing geometry, and in the condition of the atmosphere. In the real world, one would also expect both random variations in the characteristics of the atmosphere and the presence of clouds to introduce less predictable changes in scanner signals.

Three other sources of variation have not been discussed yet. These are: (1) the sensor itself; (2) the reflectance properties of the surface being viewed; and (3) the reflectance properties of the surface elements adjacent to the element being viewed.

2.3.1. SENSOR CHARACTERISTICS

No measurement device is noise-free, and the multispectral scanner can introduce random and, perhaps, systematic variations into the signals. It is impossible to distinguish between random sensor noise and random variations in the radiation signals. However, potentially, instability and drift in electrical circuits can produce serious problems for area-survey operations.

2.3.2. REFLECTANCE CHARACTERISTICS OF ELEMENT BEING VIEWED

The radiative transfer model discussed above incorporates a simple model for the reflectance properties of the Earth's surface; it assumes a diffuse (Lambertian) reflector. There is evidence in reflectance measurement and modeling efforts that many materials have bidirectional reflectance characteristics which must be taken into account [10]. In other words, the amount of radiation reflected depends on both the direction of the illumination and the direction of observation.

In order to see how a bidirectional reflectance property might come about for an agricultural field, for example, one can argue heuristically that a sensor looking straight down sees a maximum amount of soil and a minimum amount of vegetation. At some angle off the nadir, there might be no soil visible and hence a different reflectance spectrum. Therefore,

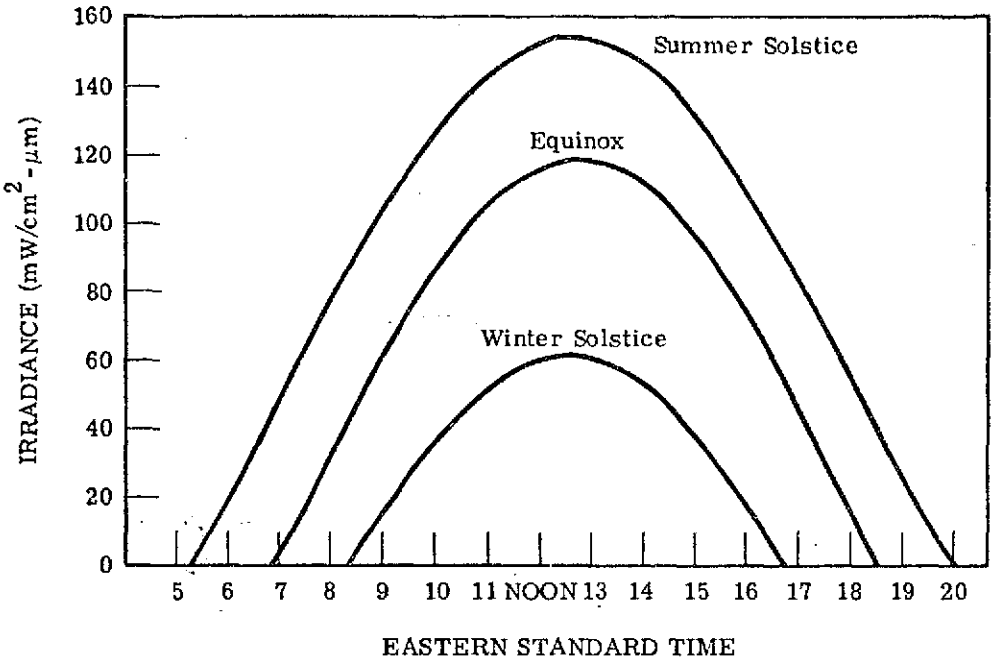

FIGURE 36. VARIATION OF TOTAL DOWNWARD IRRADIANCE WITH TIME AT AN ALTITUDE OF 0 km OVER A SURFACE OF GREEN VEGETATION. Southeastern Michigan; visual range = 8 km; wavelength = 0.55 μm.

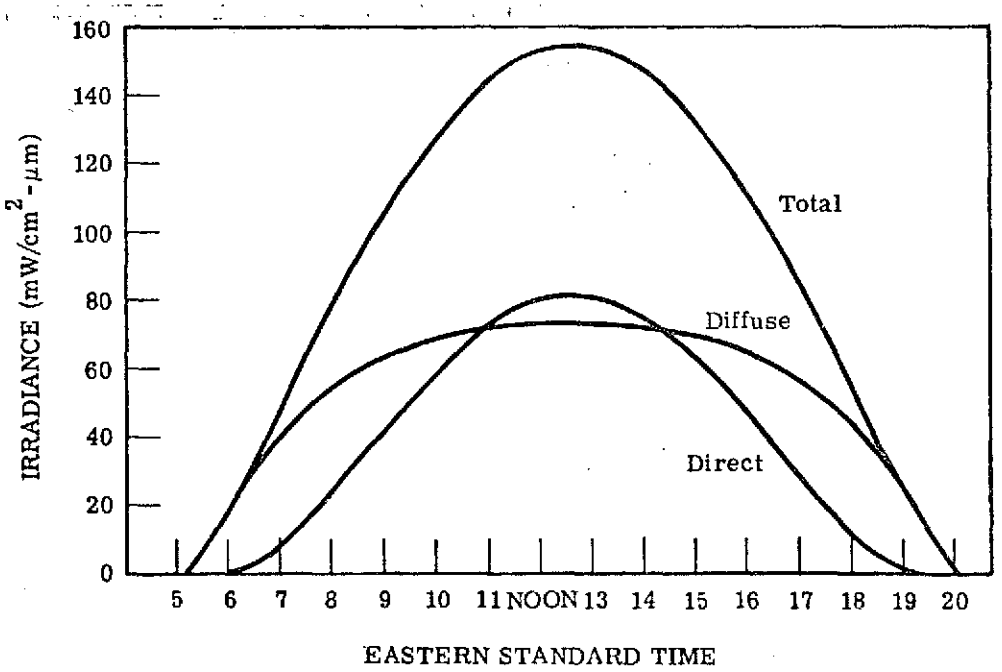

FIGURE 37. VARIATION OF DIRECT SOLAR, DIFFUSE DOWNWARD, AND TOTAL IRRADIANCES WITH TIME AT AN ALTITUDE OF 0 km OVER A SURFACE OF GREEN VEGETATION. Southeastern Michigan; June 21; visual range = 8 km; wavelength = 0.55 μm.

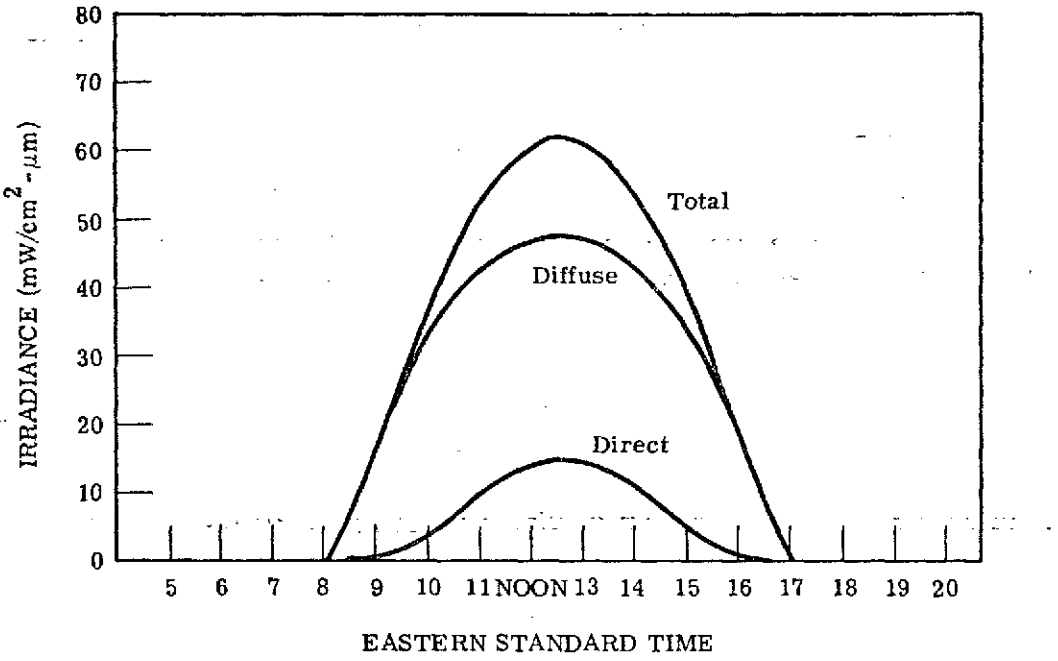

FIGURE 38. VARIATION OF DIRECT SOLAR, DIFFUSE DOWNWARD, AND TOTAL IRRADIANCES WITH TIME AT AN ALTITUDE OF 0 km OVER A SURFACE OF GREEN VEGETATION (DECEMBER 21). Southeastern Michigan; visual range = 8 km; wavelength = 0.55 μm.

the action of scanning a uniform surface, even in the absence of an atmosphere, can produce systematic signal variations if the reflector is nondiffuse.

A method for incorporating a nondiffuse surface reflectance characteristic into the radiative transfer model has been identified and should be implemented. While not exact, the approximation should allow more realistic simulations of scanner signals.

Random variations of two types are introduced by the surface materials being viewed. For agricultural problems, we can label these within-field variations and within-class, or field-to-field, variations. Frequently, these two types of random variations are confused with each other and with systematic variations.

Within a single field, there are random variations in the reflectance characteristics of a crop in addition to systematic trends associated with measurement parameters, such as scan angle. The statistical decision rules are designed to accommodate this type of random variation. Within-class variations, on the other hand, are not as well understood and are more difficult to predict and account for in recognition processing.

2.3.3. REFLECTANCE CHARACTERISTICS OF ELEMENTS ADJOINING THE ELEMENT BEING VIEWED

In last year's report [1], it was shown that both the irradiance on an element and the path radiance received when the element is observed depend on the reflectances of the elements that surround that element. Consequently, the received signal depends in part on the surrounding elements. This year, a formulation has been made of a method for analytical evaluation of the magnitude of this effect.

To understand how the radiation field (path radiance) varies in a medium above a surface on which the surface albedo changes spatially, it is necessary to consider the mathematically complex problem of radiative transfer in a two- or three-dimensional model. The complete problem with multiple scattering and an arbitrary single-scattering phase function has not been solved, but one can solve the problem if only one scattering is assumed. We can make the following simplifying assumptions for a two-dimensional radiative transfer model:

a. a perfectly diffuse (Lambertian) surface
b. a monotonically decreasing phase function
c. homogeneous atmosphere
d. only single scattering
e. surface composed of two half spaces, each having a different albedo

The basic geometry for radiation being emitted from the surface is illustrated in Fig. 39. We shall assume the simple case in which the observer is at point P, receiving radiation which

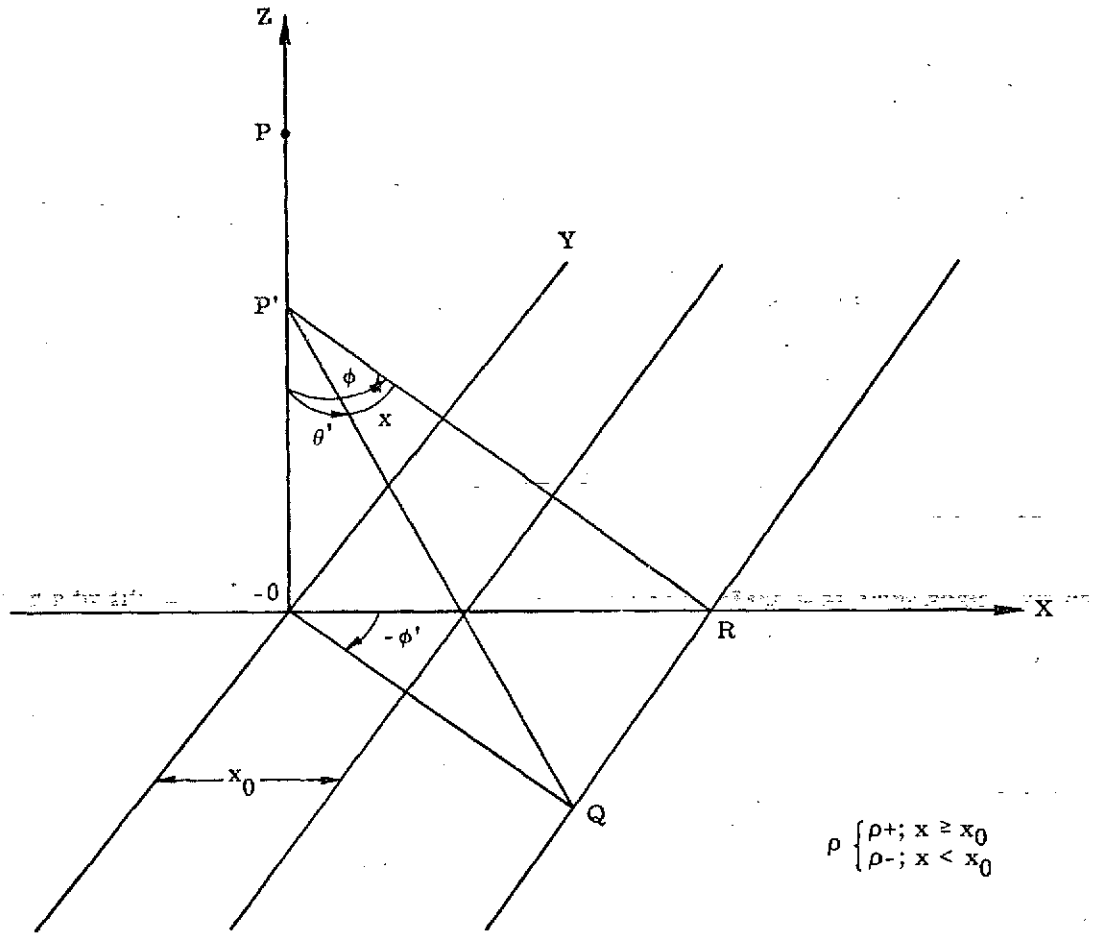

FIGURE 39. GEOMETRY FOR TWO-DIMENSIONAL ATMOSPHERIC MODEL

originates at Q and is scattered once at P'. Also, assume that the irradiance on the surface is known and is independent of a spatial change in albedo and that the radiance from the atmospheric scattering can easily be calculated. Hence, the once-scattered spectral radiance from the right half space is given by:

$$L(\tau, \mu, \phi) = \int_{\tau_0}^{\tau} \int_{0}^{\pi/2} \int_{0}^{1} L(\tau_0)\, e^{-(\tau_0 - \tau')/\mu'} p(\mu, \phi, \mu', \phi') e^{-(\tau' - \tau)/\mu}\, d\mu'\, d\phi'\, d\tau' \tag{10}$$

where, for our particular geometry $\mu = 1$, i.e., $\theta = 0^{\circ}$ and $L(\tau_0)$ is the intrinsic radiance from the surface.

We will consider the atmosphere to be composed of a light haze which scatters the radiation in a highly anisotropic manner. A mathematically convenient phase function approximating the actual phase function is given by:

$$p(\nu) = \begin{cases} Ae^{-a/\nu} & ; 0 \le \nu \le 1 \\ 0 & ; -1 \le \nu \le 0 \end{cases} \tag{11}$$

where ν is the cosine of the scattering angle. We can determine the constants A and a by fitting this function to a realistic phase function at $\nu = 1$ and by normalization, i.e.:

$$p(1) = Ae^{-a} = p_0 \tag{12}$$

and

$$1/2 \int_{-1}^{1} p(\nu)\, d\nu = 1 = \frac{A}{2} \int_{0}^{1} e^{-a/\nu}\, d\nu = \frac{A}{2} \int_{1}^{\infty} \frac{e^{-ax}}{x^2}\, dx = \frac{A}{2} E_2(a) \tag{13}$$

where $E_2(a)$ is an exponential integral. Thus, from Eqs. (12) and (13), and the recursion formula for exponential integrals, we have:

$$p_0[1 - aE_1(a)] = 2 \tag{14}$$

can be solved for the constant a.

Equation (10) now becomes:

$$L(\tau, 1, \phi) = \int_{\tau_0}^{\tau} \int_{0}^{\pi/2} \int_{0}^{1} L(\tau_0) e^{-(\tau_0 - \tau')/\mu'} A e^{-a/\mu'} e^{-(\tau' - \tau)} d\mu' d\phi' d\tau' \tag{15}$$

Hence, the inner integrals (I) have the form:

$$I = \int_{0}^{\pi/2} \int_{0}^{1} e^{-\alpha/\mu'} e^{-\beta/\mu'} d\mu' d\phi' \tag{16}$$

where

$$\alpha = \tau_0 - \tau'$$

$$\beta = a$$

From Fig. 39, we see that $\mu' = \cos \chi \cos \psi$, and

$$d\mu' d\phi' = J \, d\chi \, d\psi \tag{17}$$

The Jacobian of this coordinate transformation is $-\cos \chi$. Thus,

$$I = -2 \int_{0}^{\pi/2} \int_{0}^{\pi/2} e^{-k \sec \chi \sec \psi} \cos \chi \, d\chi \, d\psi \tag{18}$$

where $k = \alpha + \beta$. Making the transformation $x = \sec \chi$, transforms the integral into:

$$I = -2 \int_{1}^{\infty} \int_{0}^{\pi/2} \frac{e^{-kx \sec \psi}}{x^2 \sqrt{x^2 - 1}} dx \, d\psi \tag{19}$$

but, $\bar{S}(kx) = \int_{0}^{\pi/2} e^{-kx \sec \psi} \, d\psi$ is Sievert's integral

Tables exist of $\bar{S}(kx)$ versus kx and therefore the complete integral I can be integrated numerically. Thus,

$$I = -2\int_1^\infty \frac{\bar{S}(kx)}{x^2\sqrt{x^2 - 1}}\,dx \tag{20}$$

Carrying out this integration will allow one to see how rapidly the radiance decreases with distance from the edge of the surface.

3
TECHNIQUES FOR OVERCOMING SYSTEMATIC VARIATIONS IN SCANNER DATA

Several kinds of systematic variations in multispectral scanner data have been discussed, and the nature and extent of these variations have been illustrated. There are also random variations in the data which have led to the use of statistical decision rules in recognition processing. In this section, we examine possible methods for overcoming systematic variations before or during recognition processing and consider the consequences of these methods on one's ability to handle the random variations. The succeeding sections present results of studies carried out to test some of these ideas.

The decision rules that we consider in this section are those which assume that the signals have multivariate normal distributions and use the likelihood function in the decision process. This is, by far, the most common approach taken toward the recognition processing of multispectral scanner signals. All one needs for evaluating the likelihood functions are the mean vector and covariance matrix for each recognition class considered.

We have already seen that the received radiance signal consists of two parts, a desired part that originates at the ground surface and an extraneous part that is a result of the atmosphere's presence between the surface and the sensor. There is a third part that must be considered for any practical use of the detected radiation signal. It is the additive noise-equivalent radiance that represents noise added by the detector and subsequent electronics and storage media. That is:

$$L(\theta, i, j) = \rho'_{ij} E_j(\theta) T_j(\theta) + L_{pj}(\theta) + L_{nj} \qquad (21)$$

where: L = the radiance signal,

i = the class of ground cover being scanned

j = the spectral channel

$*\theta$ = a vector that describes the parameters and conditions of the measurement

ρ'_{ij} = the bidirectional reflectance of the surface (for a diffuse surface, $\rho'_{ij} = \rho_{ij}/\pi$, where ρ_{ij} is the diffuse or directional reflectance)

E_j = the irradiance in channel j

T_j = the corresponding atmospheric transmittance

L_{pj} = the path radiance in channel j

L_{nj} = the noise-equivalent radiance in channel j

*Note that the definition of θ has been generalized in this section to include all parameters and conditions of measurement.

Equation (21) has exact physical meaning only when the reflectance of the surface is diffuse and, consequently, has no angular dependence. In Section 3.1, we discuss a generalization in which angular dependence is allowed.

We shall assume for simplicity that any systematic variations in the data depend on θ, and that there are only two independent sources of randomness in the data, ρ'_{ij} and L_{nj}. The mean vector and the elements of the covariance matrix needed for the likelihood calculations are respectively:

$$<L(\theta, i, j)> = <\rho'_{ij}> E_j(\theta)T_j(\theta) + L_{pj}(\theta) + <L_{nj}> \tag{22}$$

and

$$<[L(\theta, i, j) - <L(\theta, i, j)>] [L(\theta, i, k) - <L(\theta, i, k)>] > =$$
$$E_j(\theta)T_j(\theta)E_k(\theta)T_k(\theta)<[\rho'_{ij} - <\rho'_{ij}>] [\rho'_{ik} - <\rho'_{ik}>]> +$$
$$<(L_{nj} - <L_{nj}>)(L_{nk} - <L_{nk}>)> \tag{23}$$

where <> denotes an ensemble average. If we assume that the mean system noise and therefore also the mean noise-equivalent radiance is zero, we have for the mean:

$$<L(\theta, i, j)> = <\rho'_{ij}> E_j(\theta)T_j(\theta) + L_{pj}(\theta) \tag{24}$$

and for the spectral covariance matrix element:

$$Cov_{jk}\ L(\theta, i) = E_j(\theta)T_j(\theta)E_k(\theta)T_k(\theta)<[\rho'_{ij'} - <\rho'_{ij}>][\rho'_{ik} - <\rho'_{ik}>]> + <L_{nj}L_{nk}> \tag{25}$$

In the next two subsections, we first explore the implications of preprocessing the data to remove systematic effects from each channel and then consider the advantages of alternatively changing the decision rule parameters, i.e., the mean and, if necessary, the covariance matrix. Both empirical methods and a method based on the radiative transfer model are considered. The final subsection examines the interdependencies of the various radiation quantities to gain insight for the other analyses.

In Section 4, we describe the use of the $U(\theta, j)$ and $V(\theta, j)$ method when applied to scan angle correction and extension of recognition from one altitude to another. We are faced with the question of how to evaluate the performance improvement. Since the desire is to improve recognition performance, the probability of misclassification seems obvious. In fact, we show that, for the data set that was tested, an improvement in performance was easily noticeable. There are, however, other ways to visualize and evaluate the improvement. For the scan angle effect, the use of an incorrect mean vector in recognition processing can easily be seen to cause degraded performance. Thus, a measurement of the dependence of the data mean on scan angle both before and after preprocessing, is an easily measureable criterion for data corresponding

to one type of ground cover. While any one field might exhibit some residual variations with scan angle, the same variations should not occur in the majority of fields.

3.1. PREPROCESSING

Equations 24 and 25 show that the mean vector and covariance matrix of signals received from a given ground cover depend on the vector, θ, which describes the measurement parameters and measurement conditions. However, if the material reflectance functions are independent of θ (e.g., are diffuse or Lambertian reflectors), appropriate preprocessing of the data will remove the θ effects from the signal means. When this is done, however, the covariance matrix of the transformed data in general will not be independent of θ.

As discussed in Appendix V, appropriate preprocessing includes both an additive and a multiplicative correction function. Our generalized preprocessing transformation, called the U-V transformation, meets this requirement.

The operating principle of the U-V transformation is one of adjusting a signal, $L(\theta, i, j)$, (measured under any arbitrary set of measurement parameters and conditions that are represented by θ) to $L(\theta_0, i, j)$, the value it would have had, had it been measured under a reference set of conditions and measurement parameters represented by θ_0. Mathematically:

$$L(\theta_0, i, j) = U(\theta, j)L(\theta, i, j) + V(\theta, j) \tag{26}$$

where $U(\theta, j)$ and $V(\theta, j)$ are functions that can be determined empirically from a data set or calculated with a radiative transfer model and auxiliary measurements and information. Once transformed, we process the data, using a fixed, maximum likelihood decision rule.

The U-V transformation can be applied to more than just diffuse reflectors. For example, if ρ'_{ij} is not independent of θ for all materials, but has a systematic variation that is well approximated by

$$\rho'_{ij}(\theta) = \rho^*_{ij}K_{1j}(\theta) + K_{2j}(\theta) \tag{27}$$

where ρ^*_{ij} depends only on the material, and $K_{1j}(\theta)$ and $K_{2j}(\theta)$ depend only on θ, the U-V transformation will remove the θ dependence from the signal means. Equation (21) now takes the form:

$$L(\theta, i, j) = \rho^*_{ij}K_{3j}(\theta) + K_{4j}(\theta) \tag{28}$$

where $K_{3j}(\theta)$ and $K_{4j}(\theta)$ are functions that can be thought of as being apparent, rather than measurable, (irradiance × transmittance) and path radiance, respectively. This form also handles a simple dependence of the actual path radiance on the surface reflectance. To the extent that the actual surface reflectance properties depart from the above approximations, the transformation applies an average correction factor which minimizes the errors remaining after correction.

We now consider the nature of the U and V correction functions for the simple diffuse model of the radiance signal (Eq. 21). The functions take the forms:

$$U(\theta, j) = \frac{E_j(\theta_0)T_j(\theta_0)}{E_j(\theta)T_j(\theta)} \tag{29}$$

$$V(\theta, j) = L_{pj}(\theta_0) - U(\theta, j)L_{pj}(\theta) \tag{30}$$

When we combine Equations (21), (26), (29), and (30), we have

$$L(\theta_0, i, j) = \rho'_{ij}(\theta)E_j(\theta_0)T_j(\theta_0) + L_{pj}(\theta_0) + \frac{E_j(\theta_0)T_j(\theta_0)}{E_j(\theta)T_j(\theta)} L_{n_j} \tag{31}$$

We now need to consider the likelihood function for the set of transformed signals $L(\theta_0, i, j)$. For the mean, we have

$$\langle L(\theta_0, i, j)\rangle = \langle\rho'_{ij}(\theta)\rangle E_j(\theta_0)T_j(\theta_0) + L_{pj}(\theta_0) \tag{32}$$

when we make the usual assumption that $\langle L_{nj}\rangle = 0$. For the elements of the covariance matrix

$$\langle[L(\theta_0, i, j) - \langle L(\theta, i, j)\rangle][L(\theta_0, i, k) - \langle L(\theta_0, i, k)\rangle]\rangle$$

$$= E_j(\theta_0)T_j(\theta_0)E_k(\theta_0)T_k(\theta_0)\langle(\rho'_{ij} - \langle\rho'_{ij}\rangle)(\rho'_{ik} - \langle\rho'_{ik}\rangle)\rangle + \left[\frac{E_j(\theta_0)T_j(\theta_0)}{E_j(\theta)T_j(\theta)}\right]\left[\frac{E_k(\theta_0)T_k(\theta_0)}{E_k(\theta)T_k(\theta)}\right]\langle L_{nj}L_{nk}\rangle \tag{33}$$

Examination of Eqs. (32) and (33) reveals that, for a Lambertian reflector with $\rho'_{ij}(\theta) = \langle\rho'_{ij}(\theta)\rangle$, the mean vector is independent of θ, but the covariance matrix is θ-independent as noted earlier.

3.1.1. POTENTIAL USES AND LIMITATIONS OF PREPROCESSING TRANSFORMATION

Thus far we have described θ as a measurement parameter or condition of measurement. Let us now examine θ in more detail, by considering specific identities for θ and corresponding potential uses of preprocessing transformations. We can consider two classes of uses for preprocessing, depending on whether we consider θ to be continuous or discontinuous. An example of a continuous function is when θ is the scan angle. The received radiance is scan angle dependent because the amount of atmosphere between the ground cover and the multispectral scanner depends upon the scan angle. Another example is when θ represents the along-track direction

(and time). The received radiance can change gradually because of gradual atmospheric changes or sun-position movement. Preprocessing can be used to adjust for such changes.

If we consider θ to be discontinuous, we again have many potential applications for preprocessing. We might let $L(\theta_0)$ represent signals from sunlit portions of the ground and $L(\theta)$ represent cloud-shadowed portions. We would then have a simple processing (or preprocessing) scheme to extend signatures obtained from sunlit areas to the shadowed areas. We could let $L(\theta_0)$ and $L(\theta)$ represent data taken at two different times at either the same or different altitudes. Again we would be extending recognition capability without using separate training areas. With this particular extension, we would be capable of making area surveys in which one set of training data, in principle, would be used for the entire survey. Another possibility is to let θ represent an idealized measurement condition, such as a laboratory condition for reflectance measurements; then a transformation could be made to convert the measured radiance values into reflectance values.

The potential uses of this $L(\theta)$ and $L(\theta_0)$ preprocessing concept are numerous. But, before we become too enthusiastic, let us examine some of the limitations. An obvious limitation is the assumption that the ground acts as a Lambertian reflector or that all materials have the same bidirectional characteristic. Although this limitation is frequently quoted, there are few reliable measurements with which to evaluate the bidirectional reflectance of the various ground covers. Another limitation is that the reflectance of a given type of ground cover is not always invariant. For example, the reflectance of a corn field can vary from field to field and even within any one field, and these variations can affect recognition processing results. An effect of field-to-field variations is that the training area may not adequately represent the identification class. An effect of within-field variations becomes apparent when we look at the derivation of the functions $U(\theta, j)$ and $V(\theta, j)$. These functions must be derived either directly from the data or, when the radiative transfer model is used, from measurements of the condition of the atmosphere and the geometry of the data collection. When the functions are derived from the data, intrafield variations can affect the accuracies of measurement and correction. The actual method for deriving $U(\theta, j)$ and $V(\theta, j)$ from the data will be discussed presently.

Another limitation is the dependence of radiance upon the albedo (average diffuse reflectance) of the ground at and around the point being measured. Measurements made near boundaries of fields indicate that the reflectance of one field can influence the measurements of the adjacent fields through atmospheric effects (see Section 2.3.3). This is a measurable effect near the boundaries, but it becomes negligible at some distance away from the boundary. In Section 3.1.4, and Appendix II, we present a model and a suggested algorithm for removal of this effect.

The noise in the data provides another limitation. There is always inaccuracy present in measurements of the mean vector and covariance matrix for each training set. If we are

developing $U(\theta, j)$ and $V(\theta, j)$ from the data, measurement errors will introduce additional inaccuracy. In addition, the noise statistics may vary under different conditions of θ.

3.1.2. PREPROCESSING TECHNIQUES FOR ONE-DIMENSIONAL CORRECTION

In order to use the preprocessing algorithm in which $U(\theta, j)$ and $V(\theta, j)$ are used, it is necessary to find these functions. One method is to consider Eq. (26) to be a function of $U(\theta, j)$. If we have measurements of two materials under conditions θ and θ_0, we will have two simultaneous linear equations in two unknowns. If we label the two materials $i = 1, 2$, we can find the data:

$$U(\theta, j) = \frac{L(\theta_0, 1, j) - L(\theta_0, 2, j)}{L(\theta, 1, j) - L(\theta, 2, j)} \tag{34}$$

Similarly, for the function $V(\theta, j)$

$$V(\theta, j) = \frac{L(\theta, 1, j)L(\theta_0, 2, j) - L(\theta, 2, j)L(\theta_0, 1, j)}{L(\theta, 1, j) - L(\theta, 2, j)} \tag{35}$$

Because $U(\theta, j)$ and $V(\theta, j)$ are independent of the material i, these correction functions can be used for all data. Obviously, the reflectances of materials 1 and 2 must be different if one is to obtain good estimates of U and V.

A redundant method of calculating $U(\theta, j)$ and $V(\theta, j)$ is better suited to our purpose, since our measurements are noisy and the materials chosen to be $i = 1, 2$ may actually have variations for different values of θ. By averaging, we obtain a more representative value for each of the correction functions. If we adapt a linear regression method of averaging, we have:

$$U(\theta, j) = \frac{\sum_{i=1}^{n}\left[L(\theta_0, i, j) - \frac{1}{n}\sum_{k=1}^{n} L(\theta_0, k, j)\right]\left[L(\theta, i, j) - \frac{1}{n}\sum_{k=1}^{n} L(\theta, k, j)\right]}{\sum_{i=1}^{n}\left[L(\theta, i, j) - \frac{1}{n}\sum_{k=1}^{n} L(\theta, k, j)\right]^2} \tag{36}$$

$$V(\theta, j) = \frac{1}{n}\sum_{i=1} L(\theta_0, i, j) - U(\theta, j)\frac{1}{n}\sum_{i=1}^{n} L(\theta, i, j) \tag{37}$$

For two fields ($n = 2$), Eqs. (36) and (37) reduce to Eqs. (34) and (35), as expected. Therefore, we will only be considering Eqs. (36) and (37). In the above derivation, there was no assumption that the two correction functions were continuous functions of θ. Thus, they apply even when θ is discontinuous. In fact, the principle application of these formulas is for discontinuous θ. Even when θ is continuous, the calculated functions can vary considerably for small changes of θ

because of measurement noise. Therefore, it may be necessary to combine Eqs. (36) and (37) with a smoothing procedure to obtain usable correction functions.

One method of deriving smoothed functions, $U(\theta, j)$ and $V(\theta, j)$, from the data is to assume that they are of known form but depend upon unknown parameters. For example, we can assume that the correction functions are polynomial functions of θ, and estimate the coefficients. We used this method and second-order polynomials where

$$U(\theta, j) = 1 + u_{1j}(\theta - \theta_0) + u_{2j}(\theta - \theta_0)^2 \tag{38}$$

$$V(\theta, j) = v_{1j}(\theta - \theta_0) + v_{2j}(\theta - \theta_0)^2 \tag{39}$$

We found the maximum likelihood estimator for the unknown coefficients, which is equivalent to minimizing S(j), where:

$$S(j) = \sum_{i=1}^{n}\sum_{k=1}^{k_i}[L(\theta_0, i, j) - U(\theta_k, j)L(\theta_k, i, j) - V(\theta_k, j)]^2 \tag{40}$$

where θ_k is the k-th sample point of θ.

An alternative method of applying parameter estimation is to derive the form of the correction functions from the radiative transfer model. This method has not been used yet, but is discussed in Section 3.1.4.

3.1.3. EXTENSION OF TECHNIQUES TO TWO DIMENSIONS

The uses of the preprocessing method that were mentioned in the last section can be considered one-dimensional corrections. We discussed letting θ represent either scan angle or along-track measurement conditions. If we were to consider both effects at the same time, we could first make a scan angle correction, followed by an along-track correction. Another method is to find a pair of correction functions dependent upon the two conditions in such a way that it is not possible to correct for first one, and then the other, condition. Such a scheme is a generalization of the one-dimensional approach. Intuitively, such a scheme makes sense, since one would expect the scan angle correction functions to change as the along-track measurement conditions change.

3.1.4. TECHNIQUES FOR REMOVING SYSTEMATIC VARIATIONS IN SCANNER DATA WITH THE USE OF THE RADIATIVE TRANSFER MODEL

The radiative transfer model, with a diffuse surface, has been used to investigate systematic variations in scanner data caused by atmosphere. For the calculation of total radiance, however, it is necessary to include bidirectional reflectance functions for the surface elements in

view. Assuming that these have been included, we can develop the formalism to be used in removing systematic variations caused by atmospheric effects and bidirectional reflectance.

Let us consider the total spectral radiance, given by:

$$L(\xi) = L_0(\xi)T(\xi) + L_p(\xi) \tag{41}$$

where $L_0(\xi)$ is the intrinsic radiance at the surface, $T(\xi)$ is the transmittance from the surface to the scanner, and $L_p(\xi)$ is the path radiance. The independent parameter ξ is used to represent a typical independent variable. Inverting Eq. (41) allows us to solve for the intrinsic radiance, i.e.,

$$L_0(\xi) = F(\xi)L(\xi) + G(\xi) \tag{42}$$

where one can easily see that the F and G functions are given by:

$$F(\xi) = [T(\xi)]^{-1} \tag{43}$$

$$G(\xi) = -L_p(\xi)/T(\xi) \tag{44}$$

which are directly calculable from the model. Thus, by performing the (F, G) transformation on real scanner data, $L(\xi)$, we could use the radiative transfer model to correct for atmospheric effects. According to the model, however, we can also write the intrinsic radiance as

$$L_0(\xi) = R(\xi)L_c(\xi) \tag{45}$$

where $R(\xi)$ is a known function which depends on the bidirectional reflectance properties of the surface element being viewed, and $L_c(\xi)$ is the final corrected radiance. One should note that $L_c(\xi)$ depends on the magnitude of the surface reflectance but not on its bidirectional reflectance properties. Hence, one can write the corrected radiance as:

$$L_c(\xi) = [R(\xi)]^{-1}L_0(\xi) = S(\xi)L_0(\xi) \tag{46}$$

or, combining Eqs. (46) and (42), we get

$$L_c(\xi) = P(\xi)L(\xi) + Q(\xi) \tag{47}$$

where

$$P(\xi) = F(\xi)S(\xi) \tag{48}$$

$$Q(\xi) = G(\xi)S(\xi) \tag{49}$$

The lack of a reliable model for bidirectional reflectances of natural surfaces has contributed to our previous omission of bidirectional surface effects. Recently, however, such a model has been developed [11] and we can now use it to determine the P and Q transformation functions. Therefore, by using the atmospheric correction functions (F and G), followed by the bidirectional correction function, S, one can remove all of the known systematic variations in real

scanner data. One also can use functional forms based on these correction functions in empirical techniques like those discussed in Section 3.1.2.

3.1.5 REMOVING THE EFFECTS OF NEIGHBORING MATERIALS FROM RADIANCE SIGNALS NEAR BOUNDARIES

Earlier sections (e.g., Section 2.3.3) have shown that the reflectances of adjoining surface elements can affect the received radiance in two ways: (1) they govern the amount of path radiance to an extent; and (2) they affect the magnitude of irradiance on the surface and, therefore, the amount of radiance received directly from the element. Insofar as the reflectances of the adjoining elements are different from those of the observed element, we have developed a method for removing the effect of the differences in a preprocessing operation. The result of applying the preprocessing transformation would be to make each point appear as it would have had it been surrounded by material of its own reflectance; the transformation would not remove the effect of the atmosphere entirely.

Appendix II presents a derivation of the correction formula. A block diagram that illustrates its application is presented here in Fig. 40. The function, $K(\omega)$, depends on a function, $h(x, y)$, which is measured from the data and describes the spatial spreading effect that the atmospheric haze has on the radiation. When it is completed, the modeling effort described in Section 2.3.3 should provide a functional form for $h(x, y)$.

3.2. ADJUSTMENT OF DECISION-RULE PARAMETERS

The preceding section discusses methods for preprocessing data to remove systematic variations prior to recognition processing. There are several reasons why it might be preferable to change the decision rule parameters instead (i.e., to change the mean vector and, perhaps, the covariance matrix of each class of material):

(1) If the covariance matrix is independent of the controlling measurement parameter, θ, changes in the mean vector do not change the variances as they do in preprocessing.

(2) The correction functions can be different for each material rather than being fitted to a few (or averaged over all) materials.

(3) Corrections can be made at relatively slow rates corresponding to the scan rate of the scanner or slower rather than at the video rate (i.e., the rate at which resolution elements are scanned).

In computing the likelihood for an individual data point, the stored mean value for the class of interest is subtracted from the input data point and the difference is used in the computation. Since the operation of changing the mean value is a linear one, it has no effect on the variance of the signal.

In a case analogous to preprocessing, the mean value in channel j for a given material class, i, can be written in a new form:

$$<L(\theta, i, j)> = A(\theta, j)<L(\theta_0, i, j)> + B(\theta, j) \quad (50)$$

where $A(\theta, j)$ and $B(\theta, j)$ are correction functions independent of material class, and where $L(\theta_0, i, j)$ represents the radiance under a standard or arbitrarily chosen reference condition of measurement, θ_0. In general, however, the correction functions A and B could depend on the material class as well as on the channel. The use of a correction function of the form of Eq. (50) would permit a different pair of correction functions for each class of material.

Data rates and bandwidth requirements are important aspects in the design of processing systems. The bandwidth is particularly important for analog processing systems. Slow rates of change of decision-rule parameters are ideally suited for implementation in hybrid (digital/analog) processors.

Just as discussed earlier for the correction functions U and V, the functions A and B might be determined empirically from the data, might depend on auxiliary inputs and theoretical relationships, or might combine the two methods. We also can introduce a method which can be used to improve either of the others; it is the concept of feedback or adaptive processing. With this concept, each time a datum point is classified, that point is included in the training set for the particular decision outcome and will slightly alter the likelihood function for subsequent decisions. For example, if we let θ represent the along-track direction of data collection, the mean vector and covariance matrix associated with each decision outcome would gradually change as the illumination conditions and atmosphere changed.

3.3. SUPPORTING ANALYSIS OF INTERDEPENDENCIES OF RADIATION QUANTITIES

Both the preprocessing techniques (Section 3.1) and the decision-rule-adjustment techniques (Section 3.2) depend on theinterrelationships between the various physical radiation quantities and their relationships with primary and auxiliary sensor signals. The radiative transfer model provides a mechanism for simulating the radiation quantities and analyzing these interdependencies.

In Fig. 41, we consider the ratio of the total downward irradiance at an altitude of 5 km to the total downward irradiance at the surface versus wavelength for three visual ranges. As expected, there is a greater change for the V = 23-km case than for the V = 2-km case because, in the former, we approach pure Rayleigh scattering which has a λ^{-4} wavelength dependence. In a dense haze, the wavelength dependence is much weaker.

Figure 42 illustrates the variation of the ratio of diffuse downward irradiance to total downward irradiance with respect to visual range for three altitudes. The haze present at low altitudes scatters much of the direct solar radiance and, hence, a large amount of solar

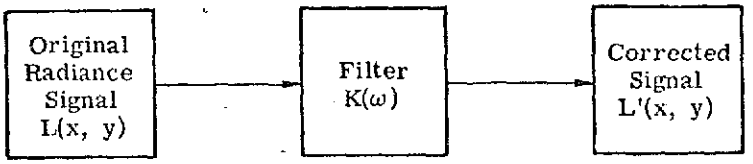

FIGURE 40. BLOCK DIAGRAM OF CORRECTION TO REMOVE THE EFFECT OF NEIGHBORING MATERIALS FROM RADIANCE SIGNALS NEAR BOUNDARIES

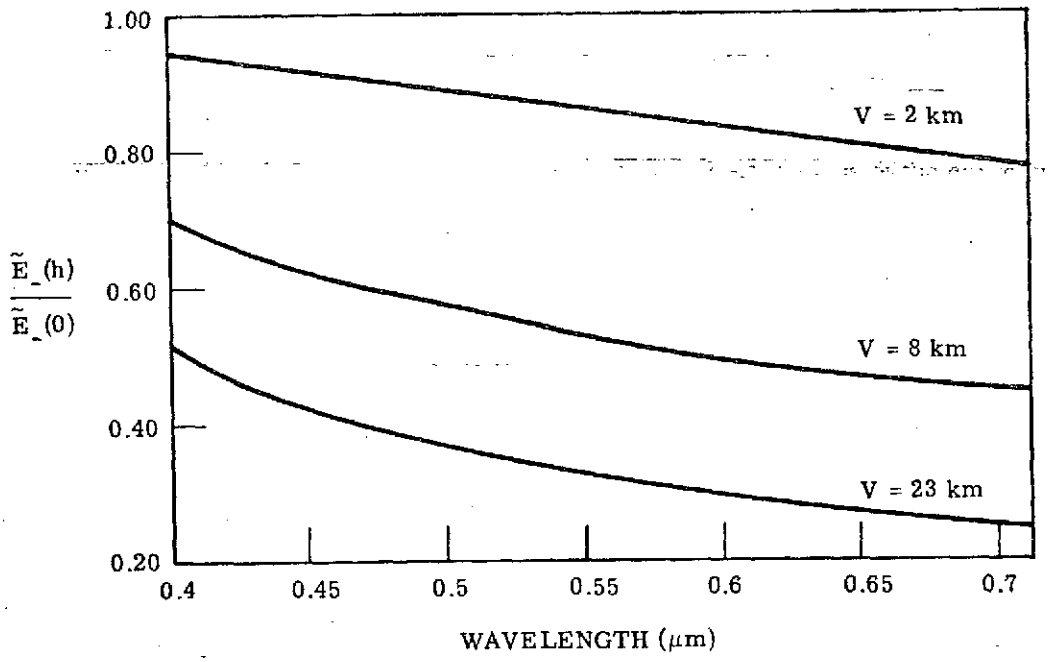

FIGURE 41. RATIO OF TOTAL DOWNWARD IRRADIANCE AT AN ALTITUDE OF 5 km TO TOTAL DOWNWARD IRRADIANCE AT EARTH'S SURFACE AS A FUNCTION OF WAVELENGTH. Solar zenith angle = 30°; surface albedo = 0.5.

energy is redistributed in the form of downward diffuse radiation. For higher altitudes, above the majority of the haze, only a relatively small amount of radiation exists in the diffuse state and therefore the ratio is independent of visual range.

We can now simulate the response of a sensor which is measuring the total downward irradiance at some altitude as a function of the time of day. Such an effect is clearly seen in Fig. 43 for three visual ranges. For large solar zenith angles there is considerable attenuation in the direct solar radiation, and since the attenuation is less at higher altitudes, the ratio of total radiance at some altitude to its value at the surface is always greater than unity. From Eq. (70) one can see that this ratio is given by:

$$\frac{\tilde{E}_{-}(\tau)}{\tilde{E}_{-}(\tau_0)} \sim \frac{\tau_0 - \tau}{\mu_0} \tag{51}$$

for large solar zenith angles, θ_0.

If a sensor mounted on top of an aircraft were responsive only to diffuse sky radiation, we could compare the irradiance at some altitude to its value at the surface. This comparison is shown in Fig. 44. At the Earth's surface, the two irradiances are of course equal and we then get a 45° line. At the top of the atmosphere, by definition, there is no downward diffuse component. For intermediate altitudes, the slope of the curve simply reflects the attenuated solar spectrum.

Now consider the variation of spectral radiance. The equation for total radiance is:

$$L_t = L_0 T + L_p = L_b + L_p \tag{52}$$

where L_0 is the intrinsic radiance from a surface, T is the transmittance, L_p is the path radiance, and $L_b = L_0 T$ is called the bare radiance. Also, transmittance and path radiance are negatively correlated in relation to the scan angle. Figure 45 illustrates the ratio of path radiance to total radiance, plotted as a function of time of day. As the solar zenith angle increases, the intrinsic radiance decreases and, therefore, the ratio of L_p to L_t increases. For very hazy conditions, the path radiance increases and the transmittance decreases, thereby increasing the ratio. The slight maximum near noon is the result of strong backscattering of radiation by the haze layer. The important point of Fig. 45 is that the ratio of path radiance to total radiance is essentially constant during a major part of the day for the downlooking case illustrated there.

There exist simplified experimental methods for determining the total transmittance of Earth's atmosphere from the ground. Therefore, it is interesting to compare the path radiance and transmittance in terms of visual range and wavelength. This dependence is shown in Fig. 46, in which we see that a relatively small change in transmittance (~10%) corresponds to a large change (~100%) in path radiance, at least for the spectral region 0.50 μm-0.70μm. Path radiance is a monotonically decreasing function of transmittance for a constant wavelength.

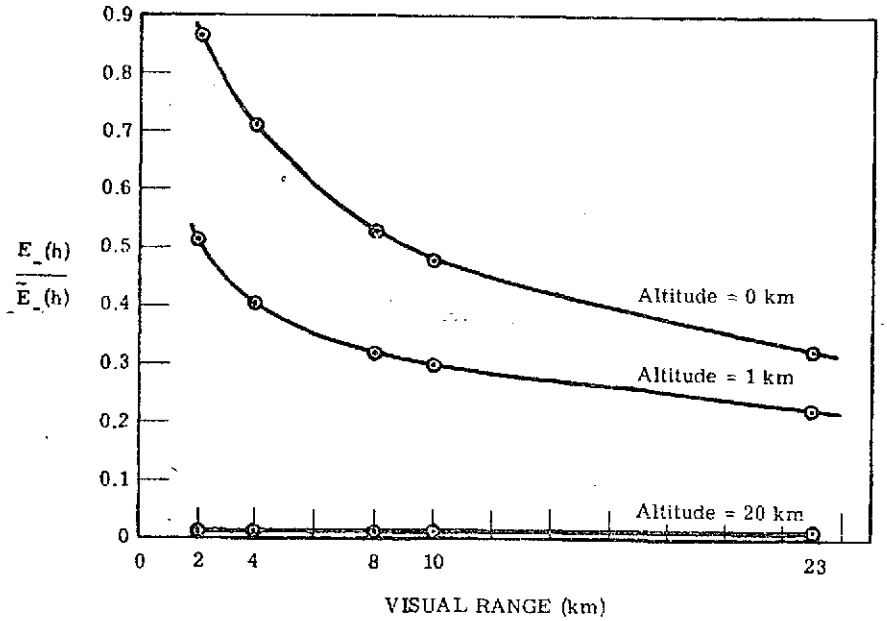

FIGURE 42. RATIO OF DIFFUSE DOWNWARD IRRADIANCE TO THE TOTAL DOWNWARD IRRADIANCE AS A FUNCTION OF VISUAL RANGE. Southeastern Michigan; solar zenith angle = 30°; wavelength = 0.55 μm; surface albedo = 0.5.

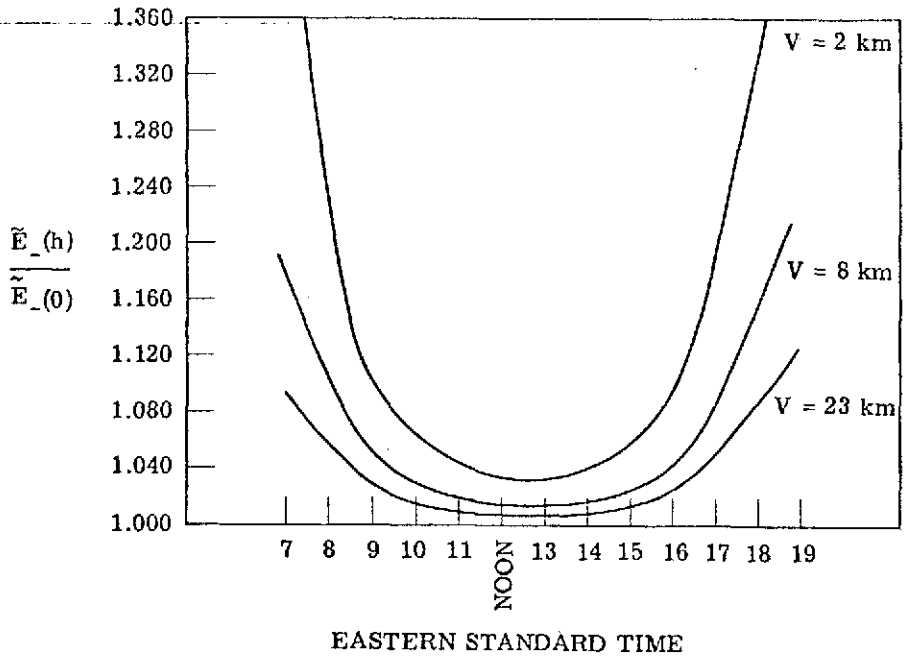

FIGURE 43. RATIO OF TOTAL DOWNWARD IRRADIANCE AT AN ALTITUDE OF 5 km TO TOTAL DOWNWARD IRRADIANCE AT EARTH'S SURFACE AS A FUNCTION OF TIME. Southeastern Michigan; wavelength = 0.55 μm; surface albedo = 0.5.

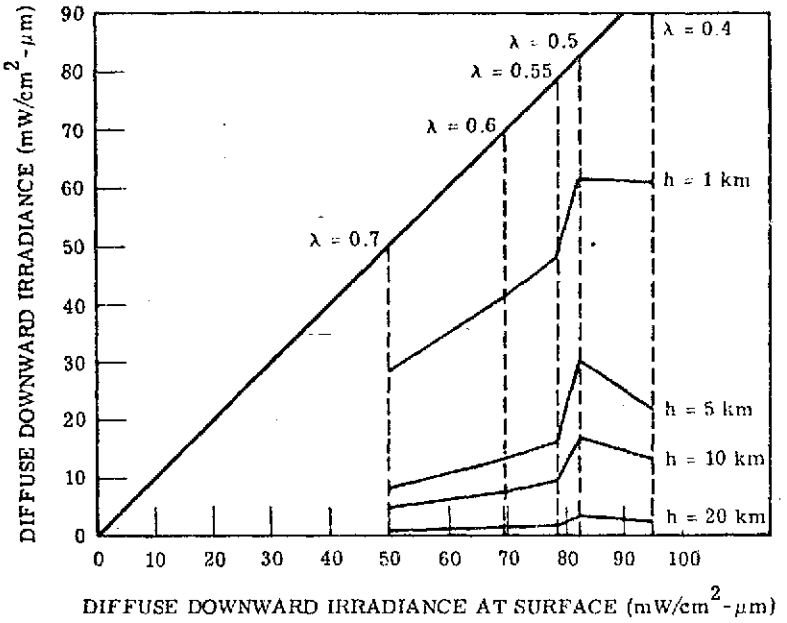

FIGURE 44. DEPENDENCE OF DIFFUSE DOWNWARD IRRADIANCE AT ALTITUDE h ON DIFFUSE DOWNWARD IRRADIANCE AT EARTH'S SURFACE. Solar zenith angle = 30°; visual range = 8 km; surface albedo = 0.5.

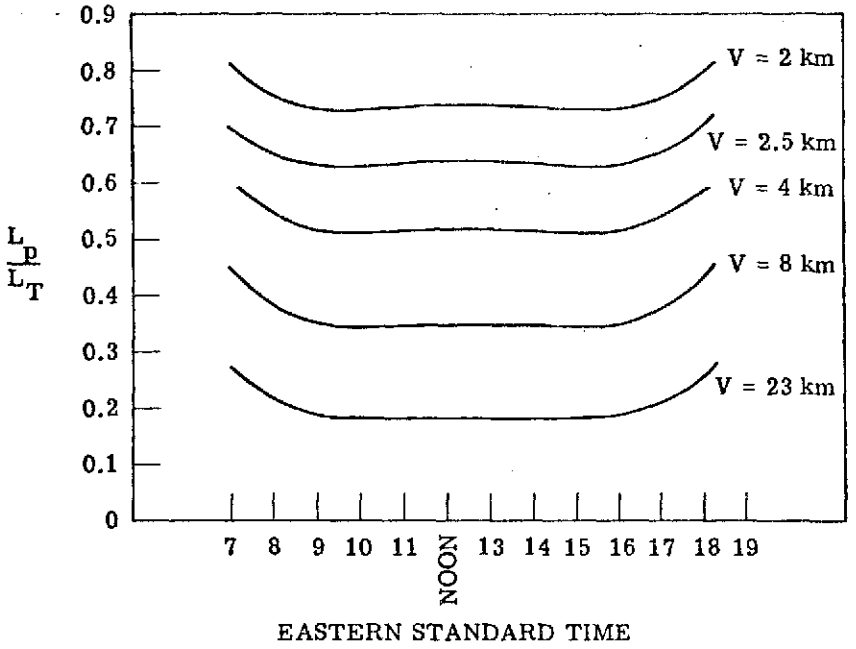

FIGURE 45. RATIO OF PATH RADIANCE TO TOTAL RADIANCE AT AN ALTITUDE OF 5 km AS A FUNCTION OF TIME. Wavelength = 0.55 μm; nadir scan angle = 0°; surface albedo = 0.5.

Finally, we can compare (Fig. 47) the path radiance to the attenuated intrinsic radiance (bare radiance) for various wavelengths and visual ranges. From 0.40 μm to 0.50 μm, a relatively large change occurs in bare radiance as a result of the increase of the solar irradiance with increasing wavelength and because transmittance increases with wavelength. Beyond 0.50 μm, the solar spectrum decreases and transmittance increases, leading to an almost constant value for bare radiance, whereas path radiance decreases rapidly with increasing wavelength. As in Fig. 46, the path radiance in Fig. 47 decreases monotonically with bare radiance for a given wavelength.

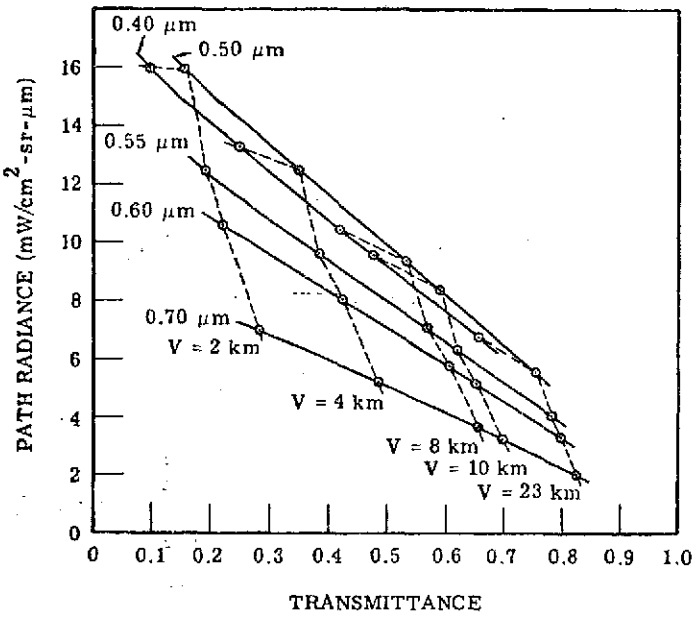

FIGURE 46. DEPENDENCE OF PATH RADIANCE AT AN ALTITUDE OF 5 km ON TOTAL ATMOSPHERIC TRANSMITTANCE. Solar zenith angle = 30°; nadir scan angle = 0°; surface albedo = 0.5.

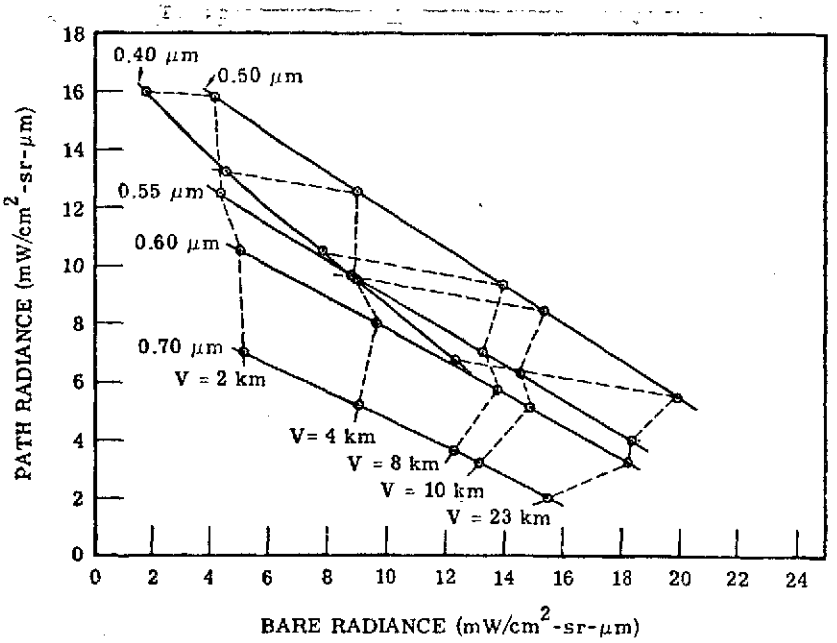

FIGURE 47. DEPENDENCE OF PATH RADIANCE ON BARE RADIANCE AT AN ALTITUDE OF 5 km. Solar zenith angle = 30°; nadir scan angle = 0°; surface albedo = 0.5.

4
APPLICATION OF PREPROCESSING TECHNIQUES

A description of preprocessing techniques is presented in Section 3. In this section, we apply the U-V transformation to both simulated and real scanner data. For purposes of these tests, the parameter vector, θ, is used to represent the sensor scan angle in most instances, and altitude in one instance.

4.1. RESULTS OF USING THE U-V TRANSFORMATION ON SIMULATED DATA

The radiative transfer model was used to generate simulated data to make an initial test on the U-V correction procedure. Simulated data can be made noiseless, so only a small amount of data need be analyzed in order to obtain a qualitative performance evaluation.

Data were generated for the following conditions:

Visual Range (V):	2, 8, 23 km
Surface Reflectance (ρ):	0.1, 0.2, 0.3, 0.4
Wavelength (λ):	0.8, 0.6, 0.4 μm
Altitude (h):	500, 1000, 5000 ft
Scan Angle:	-40^{o} to 40^{o}, every 10^{o}
Sun Position (^{o}):	30^{o} from overhead, in plane of scan

Figure 48 shows the calculated radiance values for V = 2 km, λ = 0.4 μm, altitude = 1000 ft, and reflectance values of 0.1, 0.2, 0.3 and 0.4. The solid curves represent the radiance values before U-V correction. A considerable amount of scan angle effect can be seen in these curves. For example, the radiance received at a scan angle of -30^{o} (the antisolar angle) from a 0.1 reflector exceeds the radiance from a 0.3 reflector at $+30^{o}$.

The dashed curves show the U-V corrected radiance curves as a function of scan angle. The U and V correction functions (Eqs. 34 and 35) were derived with the data for $\rho \approx 0.1$ and 0.4 for each angle and were then applied to all the data. Within the accuracy of the calculations, the corrected radiance values are independent of scan angle, as expected, because the present radiative transfer model does not include bidirectional reflectance effects. Figures 49 and 50 show the U and V curves, respectively, for the three different visual ranges. Figure 49 shows very little multiplicative correction used on the data, the maximum being less than 1.04. Almost all of the correction comes from the additive correction shown in Fig. 50. In Section 4.2, we will find that more multiplicative correction is used when measured, rather than computed, data are used.

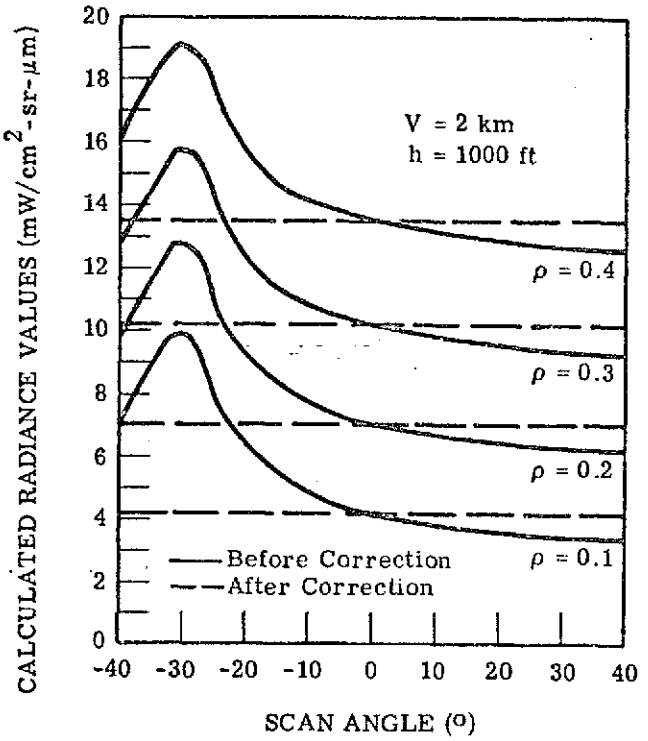

FIGURE 48. CALCULATED 0.4-μm RADIANCE VALUES AS A FUNCTION OF SCAN ANGLE

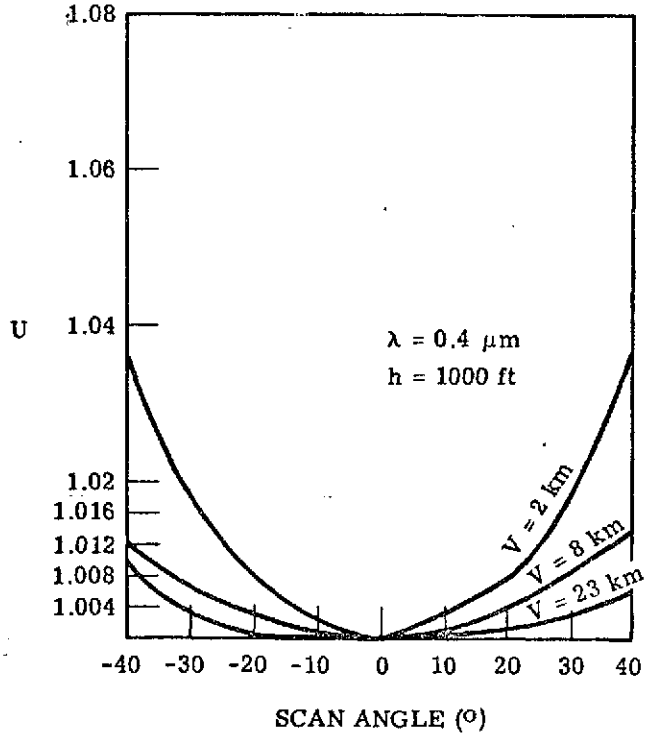

FIGURE 49. U FOR CALCULATED RADIANCE VALUES

We used a quadratic U-V correction (using equations derived from Eq. 40) to reduce the scan angle effect in Fig. 48. The results are shown in Fig. 51 in which a residual scan angle effect is seen. The correction was designed to have the corrected radiance, for any reflectivity, be that measured at a scan angle of 0°. The deviation of the curves from straight lines is relatively large, which is predictable since, in looking at Fig. 48, one would not expect quadratic additive and multiplicative corrections to be effective.

In Fig. 52, we show data corresponding to the parameters used for Fig. 48, except that the wavelength is 0.8 μm rather than 0.4 μm. At this wavelength, very little scan angle effect is present.

As one might expect, the scan angle effect became more noticeable with decreasing wavelength and visibility and increasing altitude. More explicitly, the following chart lists those parameter combinations that showed radiance values at one scan angle and one reflectance to be greater than values computed at a different scan angle for a lower value of reflectance:

λ (μm)	Visibility (km)	Altitude (ft)
0.4	2	1000
0.4	2	5000
0.6	2	5000
0.4	8	5000
0.4	23	5000

Note that the first parameter combination corresponds to Fig. 48.

It is premature to use the above list to define conditions under which the scan angle effect is severe. For instance, the radiation transfer model does not include bidirectional reflectance, but rather assumes Lambertian reflectance. One could expect that atmospheric phenomena alone might cause a severe scan angle problem for those parameter combinations in the table and that other combinations of parameters might be added when the model is expanded to include bidirectional reflectance.

4.2. RESULTS OF THE USE OF THE U-V TRANSFORMATION ON REAL SCANNER DATA

Our choice of multispectral scanner data to test the U-V concept was based on several considerations. First, we wanted more than one data set gathered over the same ground area to enable us to try signature extension from one set of data to another. Thus, we could compute the mean and covariance signatures for training areas in one data set, and then find a U-V transformation which can convert the signatures so they can be used for processing a second data set. One of the data sets should be collected from a fairly low altitude (where fields are large in angular subtense) in order to use Eqs. (36) and (37). To use these equations for scan angle

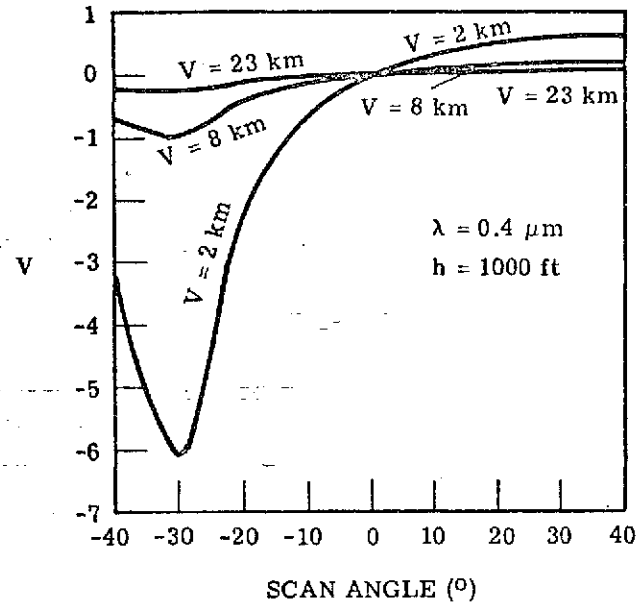

FIGURE 50. V FOR CALCULATED RADIANCE VALUES

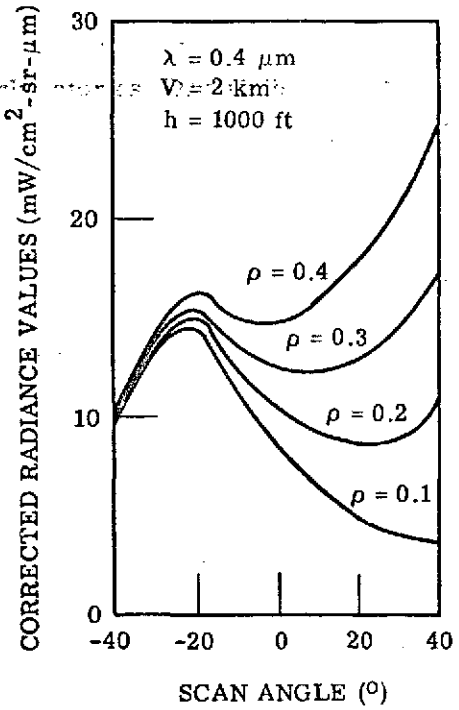

FIGURE 51. CALCULATED RADIANCE VALUES AFTER APPLICATION OF QUADRATIC CORRECTION

correction, measurements on the same ground covers at both scan angles θ and θ_0 were necessary. Data taken on a relatively hazy day were desired so that a measurable scan angle effect would be present that could be at least partially caused by the atmosphere. We also wanted data for which ground truth was available, to test not only the ability to remove the scan angle effect but also the change in ensuing recognition performance. There is not a direct relationship between the presence of the scan angle effect and the ability to recognize correctly, because recognition is limited by other factors, e.g., interfield and intrafield reflectance variations.

Another consideration in the choice of data was that the data correspond to an agricultural area in which the fields were easily delineated and each field was homogeneous (more or less). Recent data were desired because continuing improvements in our data collection equipment make the more recent data more representative of the present-day state of the art. To be confident of the datas' quality we wanted data collected close in time to one of the periodic calibrations. We wanted the day of the flight to be cloudfree, or almost so, since we were not immediately concerned with the problem of recognizing both shadowed and sunlit ground covers in the same data set. Finally, to reduce time and expense, we wanted data already digitized, if possible.

The data set that was chosen seems to have fulfilled our requirements. The data were collected on 3 September 1969, over a rural area near the Willow Run Laboratories. The visibility was estimated to have been 4 miles, and the flight log noted that heavy haze was present. A few small clouds were present at high altitude. From the photographs, the ground cover we studied appears to be free of cloud shadows, although it is possible that shadows might explain some of the intrafield variations that were noticed. Two data sets had already been digitized, taken at 1000 and 5000 ft, respectively. Data from 2000 and 10,000 ft also are available, but not digitized.

A total of 29 fields were chosen for study. From these fields, 7 were chosen for U-V calculations and 14 for training for recognition. The 29 fields chosen had recognizable boundaries and represented multiple types of ground cover. Each of the 7 fields used for the U-V determinations encompassed at least half of the total angular coverage. The area overflown was divided in approximately the middle of the scan by Willow Road, so three fields on one side of the road could be used to find the U-V correction; the other four on the other side could also be used, with Eqs. (36) and (37).

The 29 fields along with the ground truth are listed in Table 2. A map of the fields appears in Fig. 12 in [11].

The 1000-ft data were processed to compute the U-V functions. Filtering of data reduced the number of scan angles and scan lines, each by a factor of four. Figures 53 and 54 show the computed U and V functions, respectively, for channel 1 (0.40-0.44 μm). There is considerable

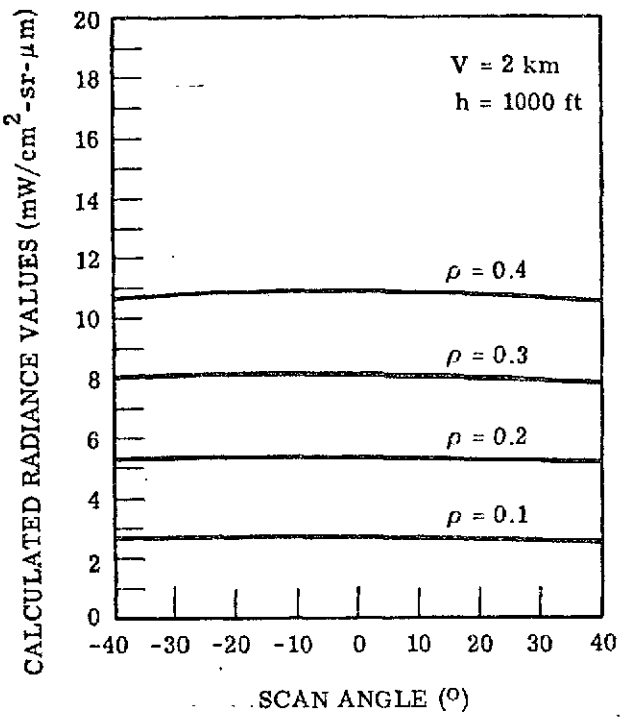

FIGURE 52. CALCULATED 0.8-μm RADIANCE VALUES AS A FUNCTION OF SCAN ANGLE

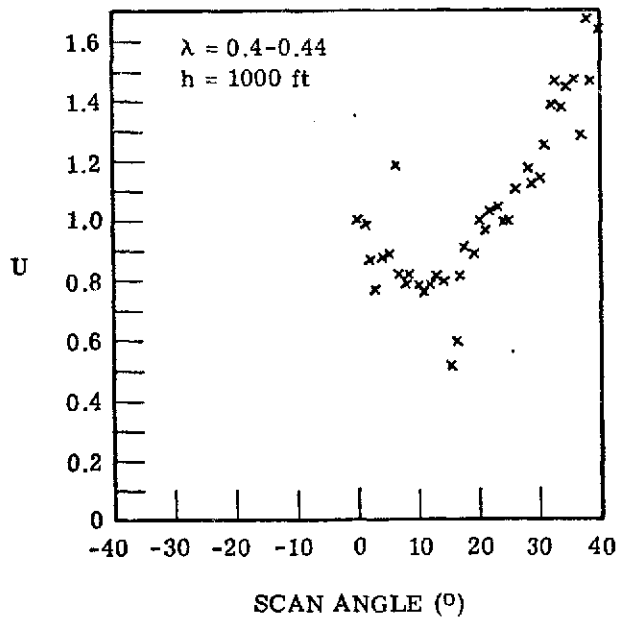

FIGURE 53. U CALCULATED FROM MEASURED RADIANCE

TABLE 2. FIELDS SELECTED FOR TESTING U-V TRANSFORMATION

Field Type	Number	Fields Used for Determining U and V Functions	Fields Used for Recognition Training
Corn	4	X	X
	10		
	17-18		
	40	X	X
	52		X
	66		
Soybean	67		X
	3		X
	15		X
	20-21		X
	39		
	49		
Grain Stubble	55		
	9	X	
	23	X	X
	25		X
	42		
	53		
Idle	56		
	5		
	44		X
	54	X	X
	11		
Bare Soil	24	X	X
	38		
	57		
Alfalfa	16		X
Alfalfa Mix	26	X	X
	27		

variation in the two figures, caused at least partially by the noise in the data and by rapid local changes in reflectance of the fields. Some of the changes are caused by the scanning, since the instantaneous field of view of the scanner is small enough to produce aliasing at 1000 ft. Therefore, we used Eqs. (38) and (39) (the quadratic formulation) to compute the U-V corrections.

In Fig. 55, we have a plot of the scan angle effect as seen in the means of six soybean fields for scanner channel 1 (0.40-0.44 μm). In each field, the along-track averages of the data for the 10 channels was computed, and these averages were plotted as a function of scan angle. It appears that there is a general trend followed by all of the fields, as well as some field variations. In fact, the variation over any one field with scan angle exceeds the field-to-field variation at constant scan-angle.

In Fig. 56, the same fields are shown after the U-V corrections were applied. The isolated points are believed to be caused by noise bursts in the data introduced during the A-D process. The fields are shown to exhibit much less scan angle effect than before correction. In these data, the field-to-field variations are larger than the scan angle effect observed in any one field, which is just the opposite of the effect observed in the uncorrected data. Generally, a desirable goal for scan angle correction would be to make the scan angle effect somewhat less than the field-to-field variations. Usually, refinements in the correction beyond this criterion will not be reflected in the recognition results.

In Figs. 57 and 58, we see for six corn fields the same kind of plots as Figs. 55 and 56. The trends observed in the soybean fields are clearly repeated. Our plots show the scan angle effect directly, so it is evident that the U-V correction does reduce this effect. A much less sensitive method of testing for the removal of the effect is to use recognition results. The intrafield and interfield variations tend to obscure the improvement gained by the scan angle correction. The U-V correction would not remove all of the limitations to perfect recognition. Still, it is desirable to see the effects of the U-V correction on recognition, not as a measure of U-V effectiveness, but rather as an indication of how well data can be recognized before and after corrections. This knowledge would be useful in deciding whether correction should be applied and in predicting the resultant improvement in recognition capability.

Recognition results were obtained for both the 1000-ft data and the 5000-ft data for the 29 fields. For the 1000-ft data, an area located near the center of the scan was selected to derive the likelihood functions used in the maximum likelihood decision rule, in each of the 14 training fields. Recognition processing was performed; no decision was made for any point for which the maximum likelihood did not exceed a level calculated to reject one point in 10^3 (assuming normal data).

This recognition procedure was repeated for the 1000-ft data set in three conditions: 1) as collected; 2) after filtering; and 3) after both filtering and U-V corrections were applied.

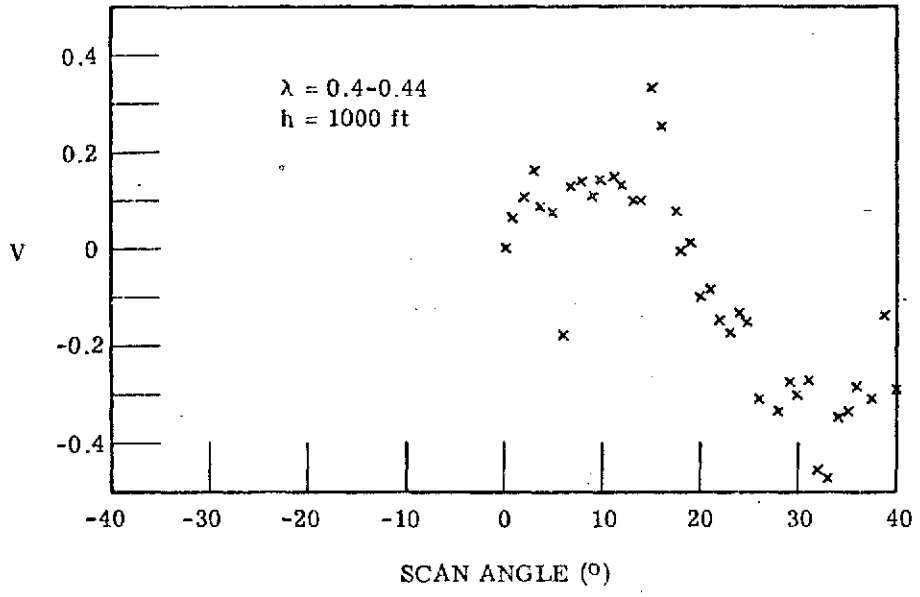

FIGURE 54. V CALCULATED FROM MEASURED RADIANCE

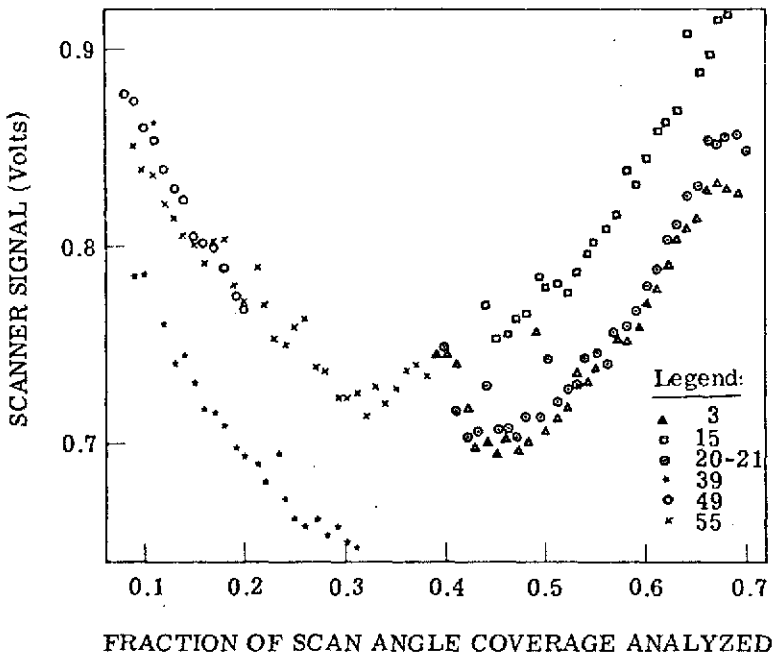

FIGURE 55. SCAN ANGLE EFFECT IN SIX SOYBEAN FIELDS (UNCORRECTED)

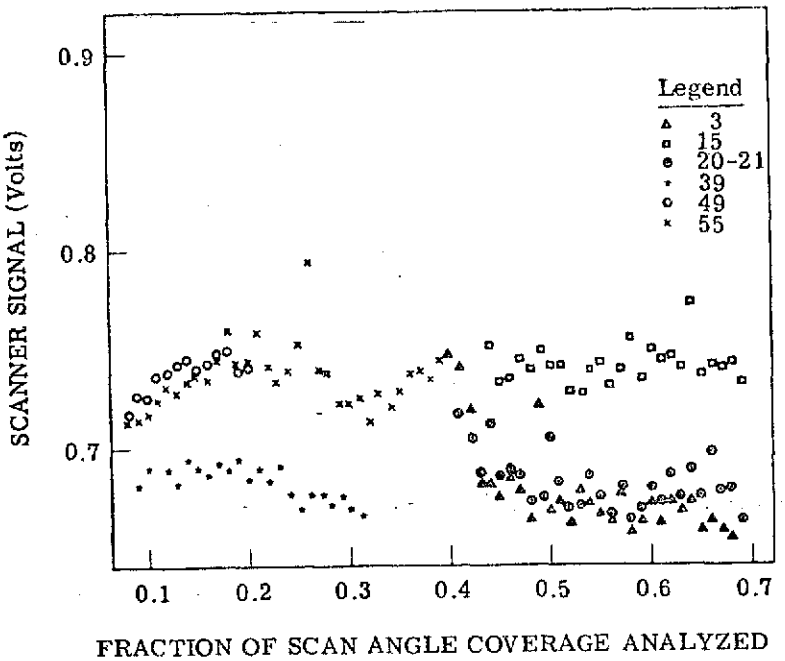

FIGURE 56. SCAN ANGLE EFFECT IN SIX SOYBEAN FIELDS AFTER QUADRATIC U-V CORRECTION

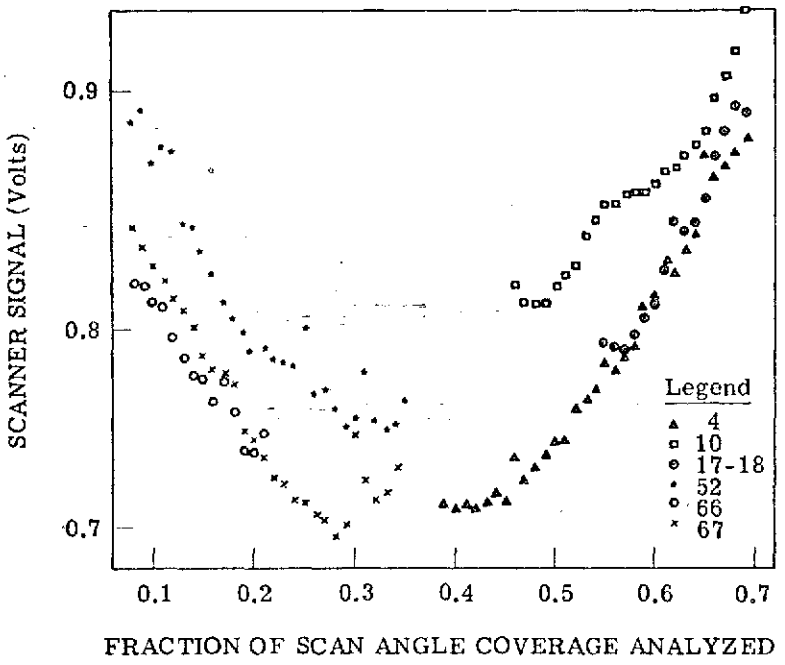

FIGURE 57. SCAN ANGLE EFFECT IN SIX CORN FIELDS (UNCORRECTED)

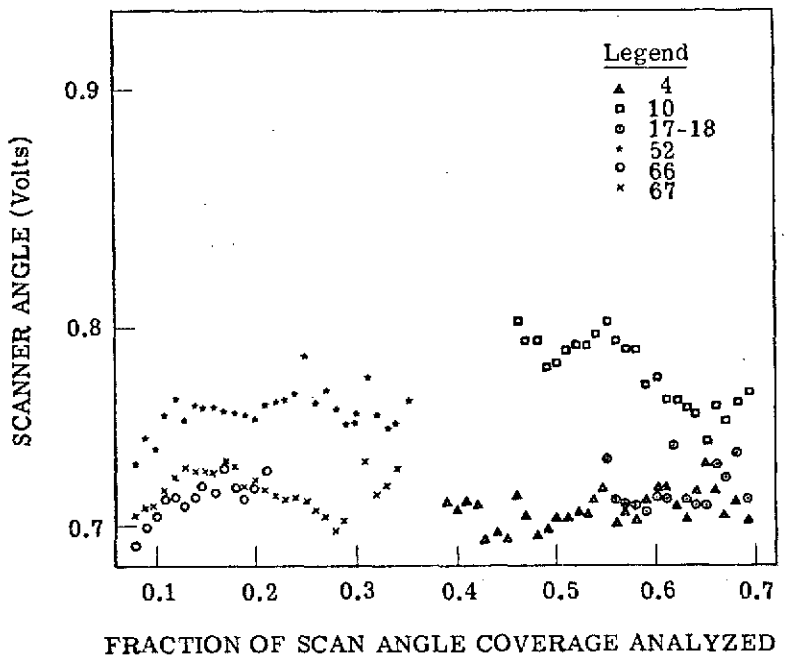

FIGURE 58. SCAN ANGLE EFFECT IN SIX CORN FIELDS AFTER QUADRATIC U-V CORRECTION

Different decision-rule parameters were used for each of the data conditions, each derived from the data set for which the rules would be applied. In addition, the 5000-ft data were processed as collected and after U-V corrections were applied. For the second condition, the likelihood decision-rule parameters were obtained from the 1000-ft data, after it had been corrected (condition 3). The 7 fields that were used for deriving the scan angle correction were used to correct the 1000-ft rules for use on the 5000-ft data. The procedure was to use Eqs. (36) and (37) on the mean vectors of the likelihood rules, with θ_0 and θ denoting the 5000-ft and 1000-ft data, respectively. In this manner, we are directly testing the U-V concept for signature extension between data sets. The covariance matrices in the likelihood functions were used without change. Probably a preferable method would be to change the matrices in accordance with the gain changes in the scanner amplifiers. Another alternative would be to use measured variances in the channels at a constant scan angle.

A summary of the recognition results is shown in Table 3. The first three columns are for the 1000-ft data and the last two for the 5000-ft data. The first three columns correspond to data that are: 1) uncorrected; 2) filtered; and 3) filtered and U-V corrected, respectively. The final two columns are for 5000-ft data that have been either: 1) scan angle corrected and recognized with the use of the 1000-ft likelihood decision functions with corrected mean vectors; or 2) noncorrected and recognized with training sets from 5000-ft data. To obtain the first row, we simply counted recognitions in each field. For the second row, a field was assumed to be composed of the material with the largest number of recognitions. The third row is the average probabilities of no-decisions in the 29 fields, caused by the maximum likelihood function being less than the critical value. These numbers reflect the variance changes caused by filtering and the variation of the data with scan angle; they also reflect data from material types not represented in the training sets. Also, the training areas were all taken near the center of the scan. The fifth row is similar to the first, except that only the decisions were used, so that all of the no-decision points were ignored. The last row is similar to the first, although only the 14 training fields were examined. Thus, this row excludes the interfield variations which are confusion factors as far as U-V scan angle corrections are concerned.

As we mentioned earlier, several phenomena in addition to the scan angle effect cause differences in the table. However, it can be seen that the U-V scan angle correction does indeed improve recognition capability over the unfiltered condition. We can also see that, to a limited extent, signature extension between data sets at two different altitudes has been accomplished. This is best seen by comparison of the last two columns of Table 3.

In order to obtain the results indicated, the fields identified as grain stubble, idle, and bare soil were grouped together, as were alfalfa and alfalfa mix. This was done because the recognition showed that there was a considerable amount of confusion within the two groups, possibly caused by the inaccuracy or incompleteness in the ground information.

We also used the mean value of the data from one field to represent that field, and performed a recognition using the likelihood decision rules developed from the 14 fields. This method incorrectly replaces intrafield variations with interfield variations in deriving the decision rule. When the tests were run, it was found that a large number of fields were not recognized, in the uncorrected data, especially. The experiment was repeated, with a decision made by a criterion that would reject five points in 10^{20} if the likelihood functions accurately described the interfield distributions. The results are shown in Table 4. The columns are the same as were used in Table 3. The rows represent correct, incorrect, and no decisions, respectively. One might expect the second row to be the same as the second row of Table 3 (majority rule), but it is not. The difference is caused by the nonlinear scan angle function and by the fact that the recognition process is nonlinear.

4.3. COMPARISON BETWEEN SIMULATED AND REAL DATA

We can now compare calculations with actual flight data. Model calculations were made for a sun position, an atmospheric state, and scanner geometry that matched the flight conditions as closely as possible. Figure 59 shows the calibrated spectral radiance as measured by the scanner over five soybean fields on 4 September 1969, for an aircraft flying due west at an altitude of 1000 ft. The solid line is the result of our calculations for a wavelength of 0.56 μm normalized arbitrarily at a nadir scan angle of zero degrees. The fact that the actual data points do not approximate the almost linear condition represented by the model indicates that the assumptions used in the model do not completely represent real conditions. One could vary the state of the atmosphere, and a variation in the density profile would cause a greater change in radiance with scan angle, but it seems more likely that the omission of bidirectional reflectance in the model accounts for the difference in shape between the calculated and measured data.

Figure 60 seems to indicate a more systematic, uniform variation in measured radiance data than that for the data in Fig. 59. This occurs at a shorter wavelength (0.42 μm) where more scattering takes place and hence we can expect the atmospheric effects to be more important, that is, the scattering tends to mask the intrinsic variations caused by surface reflectances.

Nonstandard atmospheric states can be taken into account by changing the vertical density profile of the aerosol distribution and various angular functions can be used to simulate bidirectional reflectance. Therefore, by making minor changes in the mathematical formulation of the model, to accommodate bidirectional reflectances, one should be able to remove all the known systematic variations in real scanner data.

TABLE 3. COMPARISON OF RECOGNITION RESULTS

	DATA				
	1K	1KF	1KUV	5K-5K	5K-1K
Number of fields with probability of correct recognition less than 0.5 (out of a total of 29)	14	13	7	14	13
Number of fields with wrong recognition using majority rule (out of a total of 29)	4	4	1	7	5
Average probability of no decision	0.12	0.32	0.21	0.01	0.02
Average ratio of the probability of an incorrect decision to the probability of any decision	0.35	0.20	0.18	0.45	0.50
Number of fields with more incorrect recognitions than correct decisions (out of a total of 29)	12	4	4	15	13
Number of training fields with the probability of a correct recognition less than 50% (out of a total of 14)	6	4	0	5	8

TABLE 4. RESULTS OF THE USE OF FIELD MEAN FOR RECOGNITION WITH AN INTRAFIELD LIKELIHOOD DECISION RULE

	DATA				
	1K	1KF	1KUV	5K-5K	5K-1K
Number of correct decisions*	19	21	25	10	17
Number of incorrect decisions	10	7	3	19	12
Number of data points not recognized	0	1	1	0	0

*Out of 29

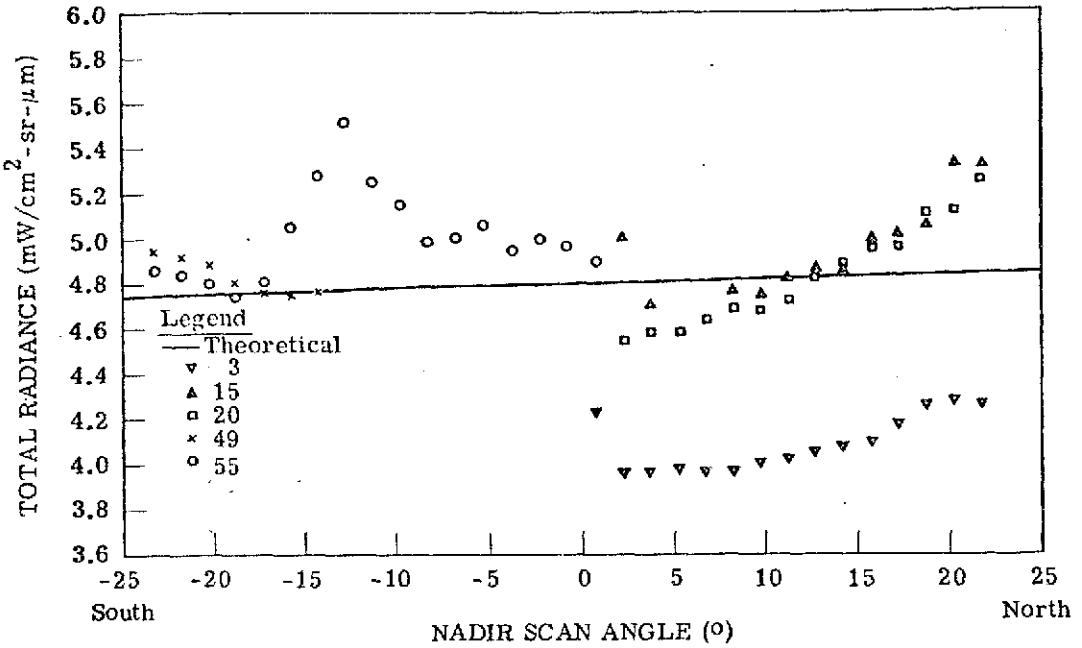

FIGURE 59. COMPARISON BETWEEN CALCULATED AND MEASURED RADIANCE DATA FOR SOYBEAN FIELDS (WAVELENGTH = 0.56 μm). Altitude = 1000 ft; visual range = ~6 km.

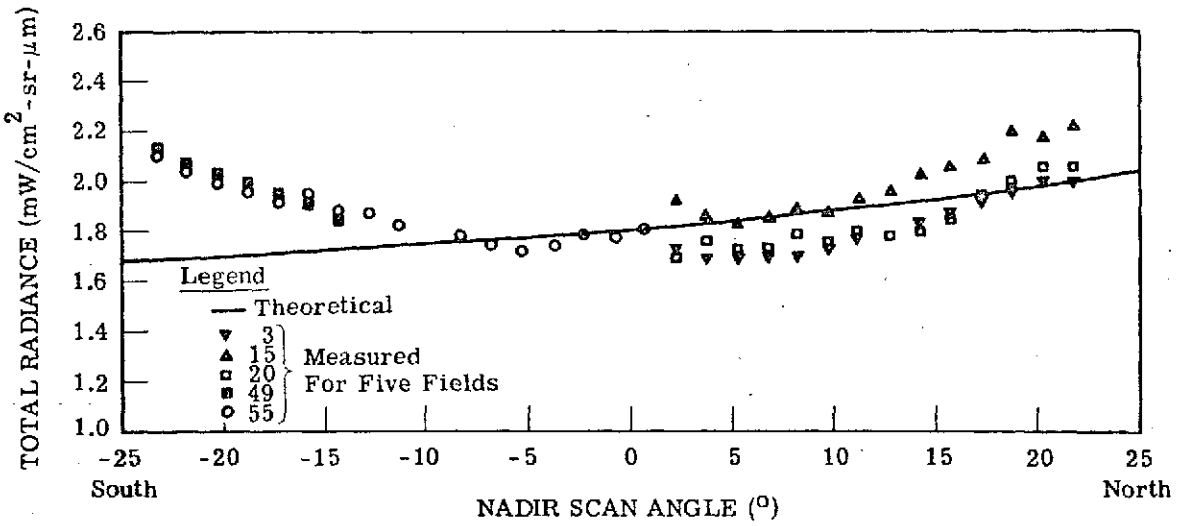

FIGURE 60. COMPARISON BETWEEN CALCULATED AND MEASURED RADIANCE DATA FOR SOYBEAN FIELDS (WAVELENGTH = 0.42 μm). Altitude = 1000 ft; visual range = ~6 km.

5
INVESTIGATION INTO THE SUITABILITY OF THE NORMAL LIKELIHOOD FUNCTION FOR RECOGNITION DECISION RULES

Likelihood functions are used in classification decision (i.e., recognition) processes on multispectral scanner data. These functions are usually represented by a multivariate normal (Gaussian) density function, statistical parameters of which are determined for the various decision classes from subsets of the data. Last year, tests were made of the normality of individual subsets of data corresponding to single fields, and all were found to be non-normal at the 1% level of significance when a standard χ^2 goodness of fit test was used [12]. A review of that work, as well as a more detailed discussion which is summarized in the remainder of this section, is presented in Appendix III. A comparison of two maximum likelihood decision rules was made on the basis of paired receiver operating-characteristic (ROC) curves, one member of each pair representing a multivariate normal decision rule and the other a rule based on an empirical density function. For each data set, an alternative hypothesis was assumed, and the Type I versus Type II errors (probability of miss versus false alarm) were plotted for different decision levels for each decision rule; see Fig. 61 for a typical pair of ROC curves. From such curves, a direct comparison can be made between the two likelihood function decision rules.

The choice of an alternative hypothesis is an important consideration. If we consider the data to be points in a hyperspace of which each coordinate corresponds to a transformed spectral channel, then the question becomes one of where the alternative hypothesis will be located in the hyperspace. The location and shape of the alternative distribution can be expected to affect the decision errors. A distribution was chosen that was uniformly located in the hyperspace. The use of this distribution corresponds to the use of many different separate distributions located uniformly in the hyperspace. Thus, the results correspond to an average of the performance that we would obtain using a large number of separate distributions. This choice of an alternative distribution has the additional advantage of making it possible to test each data set individually.

Using first one decision rule, then the other, we found the Type I errors by selecting a decision level and counting of the percentage of points that were rejected. The Type II errors were found by direct calculation. Data points for the alternative were assumed to be located uniformly throughout a hyper-rectangular parallelepiped, the dimensions of which were set so that 0.9995 of the volume of the Gaussian distributions would be included.

As a result of our tests, we have decided that the use of the normal likelihood function for individual fields is justified for recognition processing of multispectral scanner data. This

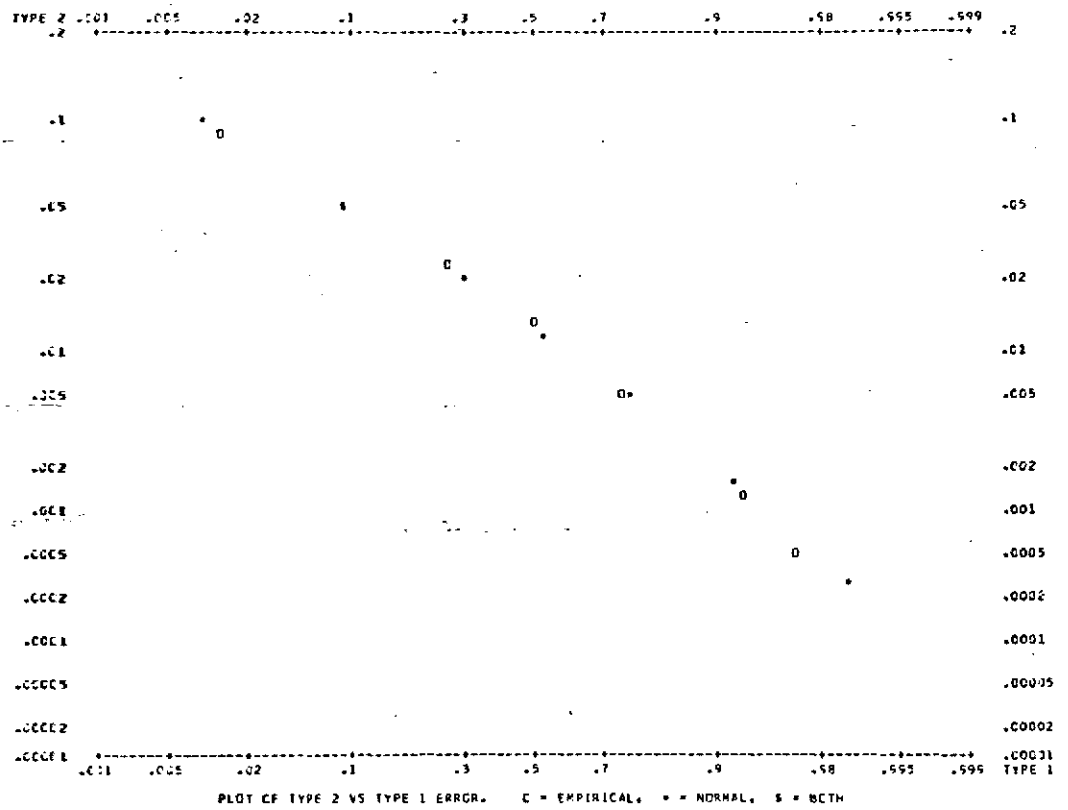

FIGURE 61. EFFECT OF LIKELIHOOD FUNCTION ON OPERATING CHARACTERISTICS (TYPICAL FOR THE FIRST THREE VARIABLES)

function is much quicker to generate and use than the histogram function. Also, the improvement in performance resulting from use of a histogram likelihood function and all of the channels is not believed to be significant. More promising approaches are: (1) preprocessing of the data to compensate for scan angle and similar systematic effects; and/or (2) compensation by changing the decision rule parameters. By using the first approach, we would expect the transformed data to have distributions that would be more nearly normal and, at the same time, have reduced-variances.

6
DATA-COLLECTION MISSIONS

One primary and two secondary data-collection missions were flown during the summer of 1971 to obtain multispectral scanner data for future use in the testing and continued development of processing techniques to overcome the systematic trends introduced into scanner data by the atmosphere, sun position, and scan geometry during area survey operations.

The primary flight was made between two missions flown for the 1971 Corn Blight Watch, and the secondary missions were carried out enroute from corn blight missions. Ground instrumentation and reference reflectance panels were deployed during the primary mission.

The chosen test site is located in Ingham County, Michigan, partly on and partly south of the Michigan State University Agricultural Farm. These areas were chosen because: (1) information on the types of crops present was to be available from other sources; (2) they were conveniently located for coverage enroute to or from the Corn Blight flight line in Indiana; and (3) space was available for laying out the reflectance panels and setting up ground instrumentation.

The basic cycle of coverage included one pass at 5000 ft altitude over a 1 mile x 8 mile area south of Michigan State University (MSU), two adjacent passes over the MSU Agricultural Farm and campus, and three short passes,each at 1000 ft over areas of special interest. This cycle was flown on the secondary missions on 17 August and 21 September 1971, but was modified somewhat for the primary mission. Three additional passes were made on the primary mission over the instrumented test site at altitudes of 1000, 2000, and 5000 ft. This expanded cycle was repeated three times, roughly at 9 a.m., 10:30 a.m., and 12 p.m. on 6 August 1971. Between these groups of passes, six consecutive passes were made over the 1 mile x 8 mile test area. These passes will provide data with which to evaluate the time-dependent changes occurring in the scanner signals and to campare these changes with model calculations.

An additional set of passes was made along flight lines that are perpendicular to the 1 mile x 8 mile strip and extended over it. Each pass was displaced by one mile from the previous one, so that an area coverage was obtained in which each pass contains a portion of the area for which ground information is available.

The ground instrumentation was used to measure spectral irradiance at the surface of the ground (0.4-1.3 μm), spectral radiance from the reflectance panels, sky radiance at three wavelengths, incoming global radiation over the 0.4-to 3-μm wavelength interval, both outgoing short wavelength radiation and net radiation over bare soil and vegetation stands, surface radiometric temperatures, and meteorological parameters.

7
CONCLUSIONS AND RECOMMENDATIONS

7.1. SIMULATION AND MODELING OF SCANNER SIGNALS

7.1.1. CONCLUSIONS

The principal conclusions regarding the application of the radiative transfer model are:

(1) A model has been developed which accounts for the transfer of radiation through Earth's atmosphere and the model has been partially verified by comparison of calculations based on the model to experimental sky radiance data.

(2) The present model is versatile enough to simulate a large number of conditions. Many of these conditions, which correspond to realistic flights, have been simulated and are discussed in this report.

(3) The mathematical formalism has also been developed to enable us to correct the actual scanner data for atmospheric effects and surface bidirectional reflectance effects.

(4) A potential advantage of the radiative transfer model as opposed to an empirical technique lies in the saving of processing time.

Therefore, we conclude that by using the radiative transfer model one can gain greater insight into the geometric and physical aspects of the radiometric quantities involved in the analysis of scanner data.

7.1.2. RECOMMENDATIONS

The radiative transfer model developed during the past two years can be applied to the simulation of sensor response under realistic flight conditions. One can expect some discrepancies, (as seen in Figs. 59 and 60) to arise as a result of the inherent limitations of the model. To remove these limitations and therefore bring the model into closer agreement with actual conditions, one should consider several improvements in the extension of our model.

We have compared radiances calculated from the radiative transfer model for different stratospheric aerosol densities; however, the change in radiance, irradiance, and transmittance caused by a large variation in the tropospheric vertical density profile has not been explored. The particle size distribution and the aerosol density profile should be varied for investigation of the corresponding variation in transmittance, irradiance, and radiance, to simulate unusual weather conditions.

A surface which is perfectly diffuse (Lambertian) in reflectance properties has been assumed for almost all work done in radiative transfer through planetary atmospheres. The results of some theoretical and experimental studies on the reflectance properties of natural surface conditions indicate, however, that the Lambertian assumption is not always valid. Many deviations between mathematical models and actual data could, in fact, be attributed to failure to consider bidirectional reflectance in the expanded radiative transfer models.

The question of how much one surface element affects the radiance from a contiguous surface element has not been answered satisfactorily, primarily because of the mathematical complexities in the modeling efforts. Nevertheless, a simplified two-dimensional analysis of this problem has been carried out as described in this report. So far we have only considered single scattering in the two-dimensional analysis but it might be necessary also to investigate multiple scattering.

The effect of discrete cloud formations has not been studied in a mathematical model of radiative transfer through Earth's atmosphere. Previously, detailed studies of the transmittance and reflectance properties of clouds have been done at Willow Run Laboratories [13] and the results of this work should be included in an advanced radiative transfer model.

For this report, we have investigated the interdependencies of irradiance, transmittance, radiance, and various combinations of these on the parameters, visual range, wavelength, scan angle, time, and surface albedo. We have seen how the various quantities are correlated for a particular atmospheric state. By varying the atmospheric condition, we should be able to discern the most important features to be used in a comprehensive, unified radiative transfer model.

Finally, for normal or standard hazy atmospheres predominantly composed of water, there is little absorption in the visual region of the spectrum. However, in certain industrial areas, a considerable amount of absorption by aerosol particles can take place. Therefore, we must investigate the overall effects of absorption on the transmittance, irradiance, and radiance in both the visible and near infrared spectral regions.

7.2. TECHNIQUES FOR REMOVING SYSTEMATIC EFFECTS

7.2.1. CONCLUSIONS

A straightforward method of scan angle correction and signature extension has been developed and tests have been conducted. The correction scheme should practically eliminate most systematic data variations caused by the presence of the atmosphere. The limitations seem to be noise present in the data and interfield reflectance variations. Theoretically, the

c.2

bidirectional reflectance patterns of the ground covers should also be a limitation if their angular properties strongly depend on material type; in the tests conducted to date, this effect was not noticeable. In deriving the correction functions for scan angle correction, we selected areas of assumed constant ground cover to derive the correction function. For data set-to-data set signature extension, the corrections are derived by location of at least two pairs of areas for which one member of each pair is in each data set, the reflectances of each pair can be assumed to be identical, but the reflectances of the pairs are quite different. Once the areas are located, the scan angle correction and signature extension are straightforward calculations.

An initial test was made to determine whether we could recognize fields by using the average measured radiance for each field. This method shows promise for large area-survey applications, although more experience is needed for an evaluation.

7.2.2. RECOMMENDATIONS

The studies performed have led to the following recommendations.

(1) To account for systematic variations in scanner data, the technique of varying the parameters of the likelihood functions in the recognition process in correspondence with the data measurement parameters and conditions should be investigated. Preprocessing was used in the reported tests of scan angle correction and it is an efficient method when all materials exhibit the same angular effects. This other method provides theoretical advantages, when scan angle effects depend on material. It also provides greater versatility and, thus, the potential for more sophisticated processing. For example, various forms of adaptive processing can be used to aid in recognition of intrafield variations, bidirectional reflectance differences between ground cover types, and slowly changing interfield variations. Perhaps, combinations of the two methods will prove useful.

(2) The correction methods should be tested on other data, a logical choice being data collected over a larger area. With this choice, the one-pass multispectral scanner operation could be extended to an area survey operation. For a large area, the correction also would have to handle gradual changes in the data not connected with scan angle; i.e., changes dependent on time and distance.

(3) Interfield variations and methods for handling them should be studied with a larger data set than the one used for this study. After scan angle corrections, the recognition capability available at present appears to be limited by such variations.

(4) The length of time required for recognition processing should be decreased. Using presently available digital methods, the time required for the recognition operation substantially limits the amount of data that can be processed in technique-development

and feasibility studies. Undersampling, filtering, and channel selection are now commonly used; additional methods are still needed.

(5) There is a need to study data sets and model calculations specifically to determine whether radiance measured from the edges of fields differs sufficiently from that in central positions to warrant the immediate development of our proposed correction method for minimizing this effect of the atmosphere.

(6) A model should be developed that would explain the sources of the terms in the covariance matrix in order to increase understanding of the physical basis of the variations in the data, as well as to better match the likelihood functions to the data.

7.3. INVESTIGATION OF DECISION-RULE LIKELIHOOD FUNCTIONS

The use of the multivariate normal likelihood function for individual fields in recognition processing is justified because: (1) it is much quicker to generate and use than are histogram likelihood functions; and (2) the improvement that would result from the use of histogram functions instead is insignificant. More promising approaches are preprocessing of the data to remove systematic effects and/or change of decision rule parameters.

Appendix I
THE RADIATIVE TRANSFER MODEL

This appendix contains a description of the most important aspects of a radiative transfer model for use in correction of remote sensing scanner data for hazy atmospheric conditions.

I.1. ELECTROMAGNETIC INTERACTIONS

In radiative transfer theory, the most fundamental radiometric quantity is the spectral radiance for a particular state of polarization. In a vacuum, spectral radiance is an invariant, i.e., it does not depend on distance. In traversing a medium, however, radiation is attenuated as a result of its interaction with the particles composing the medium. Some of the most common electromagnetic interactions are the following:

(1) Elastic scattering
   a. Rayleigh scattering by atoms and molecules
   b. Thomson scattering by free electrons
   c. resonance scattering

(2) Inelastic scattering
   a. ordinary Compton scattering (energy loss)
   b. inverse Compton scattering (energy gain)
   c. Raman scattering by atoms and molecules
   d. Mie scattering by aerosol particles
   e. fluorescence

(3) Capture
   a. line absorption
   b. photo-ionization
   c. inverse Bremsstrahlung
   d. photodissociation of molecules
   e. pair production
   f. photonuclear reactions

In the visible and near infrared regions of the electromagnetic spectrum, only Rayleigh scattering by atoms and molecules and Mie scattering by aerosol particles are important for remote sensing applications. Any aerosol absorption which takes place in this spectral region will vary slowly with wavelength as opposed to the rapid change in absorption properties in the case of gaseous absorption.

I. 2. THE ATMOSPHERE

Earth's atmosphere consists primarily of gas molecules such as O_2, N_2, H_2O, CO_2, and O_3 as well as aerosol particles, i.e., much larger groupings of molecules having a definite shape. Typical aerosol particles would be water droplets, dust, smoke particles, or any other semi-permanent suspension in the atmosphere.

For visible and near infrared radiation, the density fluctuations in the atmosphere act as scattering centers, and since the wavelength of the radiation is much greater than the size of a scattering center, an oscillating electric dipole radiation is created. This is called Rayleigh scattering. The dependence of the intensity of the scattered radiation on wavelength and scattering angle is as follows:

$$\text{Intensity} \propto \lambda^{-4}(1 + \cos^2 \theta) \qquad (53)$$

where λ is the wavelength of the radiation and θ is the angle between the direction of the scattered and incident radiation. It is this strong dependence on wavelength which led Lord Rayleigh to conclude that the scattering of sunlight by scattering centers in the atmosphere accounts for the blue color of the sky. Although this type of scattering does account for the general blueness of the sky, certain serious discrepancies occur when one attempts to use Eq. (1) to describe the sky radiation in detail. In general, the spectral and angular dependence of the sky radiation is not given by Eq. (1) and the polarization points in the sky do not correspond exactly with those as determined from Rayleigh's analysis. Two explanations can usually be given for these discrepancies: (1) Rayleigh's theory considered only single scattering, but multiple scattering can be important, especially in the visible spectral region; and (2) scattering by larger particles (aerosols) was neglected.

During the past 25 years, much work has been done to remove the discrepancy caused by consideration of single scattering only. In particular, the efforts of Chandrasekhar [9] and Mullikin [14] have resulted in the climatic achievement of providing an exact formulation for the radiation field in a homogeneous*, plane-parallel atmosphere with multiple scattering according to Rayleigh's scattering law. Although the mathematical formalism is rather involved, Coulson et al. [8] performed a computer analysis of the equations and determined the radiation field emerging from the top and bottom of a plane-parallel, homogeneous, Rayleigh-type atmosphere. Additional work by Bellman and Kalaba [15] and Grant and Hunt [16] have yeilded results which give the radiation field in an inhomogeneous atmosphere with Rayleigh scattering.

* Homogeneous means that the scattering properties of the atmosphere do not depend on altitude.

Unfortunately, the atmosphere is never free of particulate matter, and there is evidence that the aerosol component is increasing with time [17, 18]. Thus, computations based on a Rayleigh-type atmosphere cannot accurately represent the real Earth's atmosphere. In fact, in the case of hazy atmospheres, most of the scattering is caused by aerosol particles. The theoretical analysis of nonRayleigh-type atmospheres has not met with the same degree of success as for Rayleigh-type atmospheres, primarily because of the nature of scattering by aerosols. Instead of following the angular dependence of dipole scattering as in the Rayleigh case, the angular dependence of radiation scattered by particles the sizes of which are comparable to the wavelength of the incident radiation, is a more rapidly changing function of the scattering angle. This strong dependence on angle is illustrated in Fig. 62. The high degree of anisotropy characteristic of aerosol scattering is very difficult to deal with mathematically and certain approximations are needed to solve the problem of radiative transfer in a plane-parallel, homogeneous aerosol atmosphere.

Assuming that aerosol particles are basically spherical in shape, their scattering, absorption, and total cross sections and the angular scattering properties (scattering phase function) can be calculated according to classical electrodynamics. This is called Mie scattering, the mathematical development of which is given by Stratton [19], van de Hulst [20], and Kerker [21]. If one knows the particle size distribution, then one can easily determine the scattering, absorption, and extinction coefficients as well as the complete scattering phase function for the polydispersion of spherical aerosol particles. We shall designate the absorption, scattering, and extinction coefficients by $\alpha(z)$, $\beta(z)$, and $\kappa(z)$ respectively, where z is the altitude above sea level.

One quantity of great importance in estimating the scattering or absorbing properties of a medium is the optical depth, τ. It is defined as

$$\tau = \int_{h}^{\infty} \kappa(z)\,dz \tag{54}$$

where h is some base altitude above sea level. The total optical depth of an atmosphere is given by

$$\tau_0 = \int_{0}^{\infty} \kappa(z)\,dz \tag{55}$$

Thus, τ is a variable optical depth, varying from zero at the top of an atmosphere to its total value, τ_0, at the bottom of an atmosphere. For Rayleigh atmospheres, τ_0 lies between 0.1 and

1.0 in the visible and near infrared spectral regions, whereas for aerosol atmospheres τ_0 can be considerably greater than 1.0. The physical significance of optical depth is that it is a measure of the number of interaction lengths or mean free paths of a photon of a certain energy. Therefore, a large optical depth, which occurs at short wavelengths, implies an optically thick medium and hence a large number of scatterings. A small optical depth, such as 0.1, which usually occurs at long wavelengths, indicates that few scatterings take place. An example of the relationship between optical depth and altitude for a standard atmosphere is shown in Fig 63, and is shown with the percent deviation in Fig. 64. Further details on the physical of Earth's atmosphere can be found in Bullrich [22], Fleagle and Businger [23], Junge [24], and Robinson [25].

I.3. VISIBILITY

To remove the effects of the atmosphere on the radiation received by an airborne detector, we need to define the state of the atmosphere. One measure of the atmospheric state is the visibility or visual range.

If a black object is moved away from an observer in a horizontal plane, the contrast between that object and the sky horizon background gradually diminishes until a limit is reached beyond which the object will no longer be distinguishable. The apparent brightness of the black object at a horizontal distance, x, from an observer is

$$B_0 = B_b(1 - e^{-\kappa x}) \tag{56}$$

where B_b is the brightness of the horizon and κ is the extinction coefficient. The contrast (C) is defined as

$$C = \frac{B_b - B_0}{B_b} = e^{-\kappa x} \tag{57}$$

The convention followed for the limiting contrast is that given by Koschmieder [4] as 2%, i.e., C = 0.02. Thus, the range corresponding to this contrast is

$$x_0 = V = \frac{\ell n\, 50}{\kappa} \tag{58}$$

or

$$V = \frac{3.912}{\kappa} \tag{59}$$

Equation (59) is then a simple formula relating horizontal visual range (km) to the atmospheric extinction coefficient. The clearest day possible would be one in which there were no

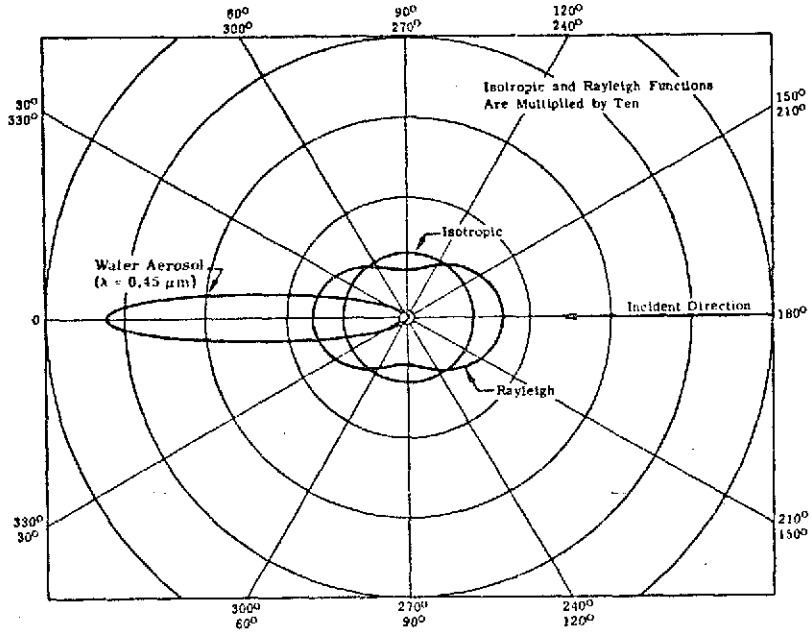

FIGURE 62. ANGULAR DEPENDENCE OF SINGLE-SCATTERING PHASE FUNCTIONS IN ANY AZIMUTHAL PLANE

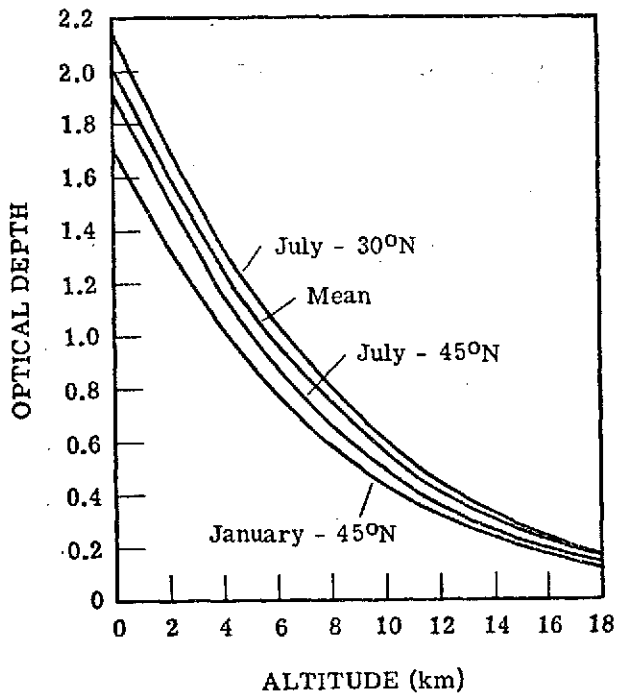

FIGURE 63. RELATIONSHIP BETWEEN OPTICAL DEPTH AND ALTITUDE FOR A CLEAR, U. S , STANDARD ATMOSPHERE (WAVELENGTH = 0.27 μm)

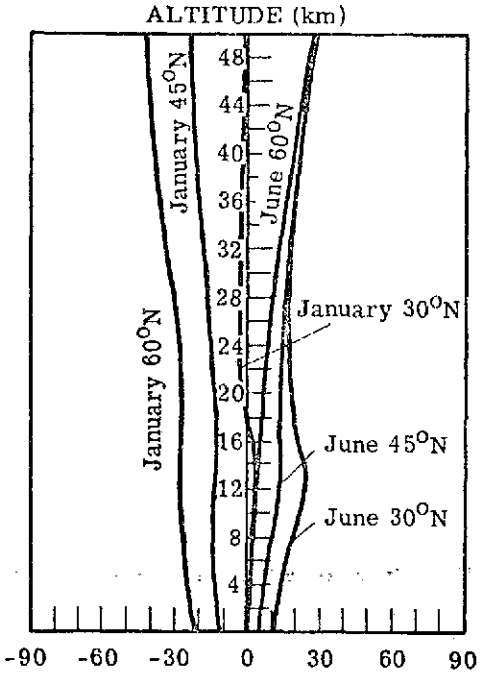

FIGURE 64. RELATIONSHIP BETWEEN OPTICAL DEPTH AND ALTITUDE FOR A CLEAR, U. S., STANDARD ATMOSPHERE WITH PERCENT DEVIATION

particulates. At a wavelength of 0.55 μm, the corresponding Rayleigh extinction coefficient is 1.162×10^{-2} km^{-1} and hence the visual range is 336 km. Actually, however, some haze is always present and 23-km visual range is taken by Elterman [5] to represent the line between a clear and a hazy atmosphere. Excellent pictures of the effect of haze on seeing ability from an aircraft are given by Larmore and Hall [26] for a variety of conditions. The line of demarcation between a haze and a fog is usually taken to be 1.2-km visual range. A more complete treatment of visibility is given by Middleton [27], and Johnson [28].

I.4. THE RADIATIVE TRANSFER EQUATION

In this section, we shall discuss briefly the radiative transfer equation which is used to determine the radiation field within a plane-parallel, homogeneous atmosphere with aerosol scattering. A more complete discussion and derivation of the equation is given by Turner [2] and Malila et al. [1].

The basic integro-differential equation of radiative transfer for a plane-parallel, homogeneous atmosphere illuminated by solar radiation is given by

$$\mu\frac{dL}{d\tau} = L(\tau, \mu, \phi) - \frac{\omega_0}{4\pi}\int_0^{2\pi}\int_{-1}^{1} p(\mu, \phi, \mu', \phi')L(\tau, \mu', \phi')d\mu'd\phi' - \frac{\omega_0}{4\pi}E_s(\tau)p(\mu, \phi, -\mu_0, \phi_0)$$

$$- (1 - \omega_0)B(\tau) \tag{60}$$

where

$$E_s(\tau) = E_0 e^{-\tau/\mu_0} \tag{61}$$

$L(\tau, \mu, \phi)$ is the spectral radiance at optical depth τ, zenith angle θ (of which the cosine is μ), and azimuthal angle ϕ. $E_s(\tau)$ is the solar irradiance at optical depth τ and $p(\mu, \phi, \mu', \phi')$ is the single-scattering phase function which describes the function of energy scattered from the direction μ', ϕ' into the direction μ, ϕ. $B(\tau)$ is the Planck radiation function and ω_0 is called the single scattering albedo defined as

$$\omega_0 = \frac{\beta}{\kappa} \tag{62}$$

The direct solar radiation enters Earth's atmosphere with a zenith angle the cosine of which is μ_0 and azimuthal angle ϕ_0.

For the visible spectral region, $B(\tau)$ is usually negligible and $\omega_0 \approx 1$ since there is very little absorption by either gases or particulate matter. Nevertheless, Eq. (60) is quite difficult

to solve exactly and has been done only for isotropic and Rayleigh-type scattering. For realistic atmospheres with an aerosol component, the phase function is highly anisotropic and approximations must be made to solve the transfer equation. One approximation to simplify Eq. (60) is the following:

$$p(\mu, \phi, \mu', \phi') = F\,\delta(\mu - \mu')\delta(\phi - \phi') + B\delta(\mu + \mu')\delta(\pi + \phi - \phi') \tag{63}$$

where F is the fraction of energy scattered into the forward direction and B is the fraction scattered into the backward direction. Since scattering by aerosols is strongly peaked in the forward direction, this approximation seems to be a reasonable one. Use of Eq. (63) in Eq. (60) permits a solution in terms of arbitrary constants which are determined from boundary conditions. The general boundary conditions are,

$$L(0, -\mu, \phi) = 0 \tag{64}$$

$$L(\tau_0, \mu, \phi) = \int_0^{2\pi}\int_0^1 \mu'\rho'(\mu, \phi, -\mu', \phi')[\,L(\tau_0, -\mu', \phi') + L_s(\tau_0, -\mu', \phi')]\,d\mu'\,d\phi' \tag{65}$$

where Eq. (64) simply states that there is no diffuse radiation entering the top of Earth's atmosphere and Eq. (65) indicates that we must integrate the diffuse and solar radiance with the bidirectional reflectance over the hemisphere of incoming radiation. If we deal with a Lambertian (perfectly diffuse) surface, the boundary conditions reduce to

$$E_-(0) = 0 \tag{66}$$

$$E_+(\tau_0) = \rho\left[E_-(\tau_0) + \mu_0 E_0\, e^{-\tau_0/\mu_0}\right] \tag{67}$$

where $E_-(0)$ is the downward diffuse irradiance at the top of the atmosphere, $E_-(\tau_0)$ is the downward diffuse irradiance at the bottom of the atmosphere, $E_+(\tau_0)$ is the upward diffuse irradiance at the bottom of the atmosphere, E_0 is the direct solar irradiance at the top of the atmosphere, and ρ is the hemispherical reflectance of the surface.

Breaking the radiation fields up into two components, an anisotropic one for $\rho = 0$, and an isotropic one for $\rho \neq 0$, we can solve for the irradiances at any point within the atmosphere, i.e.,

$$E_+(\tau) = \frac{\mu_0 E_0}{\mu_0 + (1 - \eta)\tau_0}\left[(1 - \eta)(\tau_0 - \tau) + \rho\mu_0 \frac{1 + 2(1 - \eta)\tau}{1 + 2(1 - \eta)(1 - \rho)\tau_0}\right] \tag{68}$$

$$E_-(\tau) = \frac{\mu_0 E_0}{\mu_0 + (1 - \eta)\tau_0}\left[\mu_0 + (1 - \eta)(\tau_0 - \tau) - [\,\mu_0 + (1 - \eta)\tau_0]e^{-\tau/\mu_0} + \frac{2\rho\mu_0(1 - \eta)\tau}{1 + 2(1 - \eta)(1 - \rho)\tau_0}\right] \tag{69}$$

$$\tilde{E}_{-}(\tau) = \frac{\mu_0 E_0}{\mu_0 + (1 - \eta)\tau_0}\left[\mu_0 + (1 - \eta)(\tau_0 - \tau) + \frac{2\mu_0\rho(1 - \eta)\tau}{1 + 2(1 - \eta)(1 - \rho)\tau_0}\right] \tag{70}$$

where η is $F/4\pi$ and $\tilde{E}_{-}(\tau)$ is the total downward irradiance.

Having determined the irradiances, we can now find the radiances by using the approximation

$$L(\tau, \mu, \phi) = \frac{1}{\mu_0}\left[E'_{+}(\tau)\delta(\mu - \mu_0)\delta(\pi + \phi_0 - \phi) + E'_{-}(\tau)\delta(\mu + \mu_0)\delta(\phi - \phi_0)\right] + \frac{E''_{+}(\tau) + E''_{-}(\tau)}{2\pi} \tag{71}$$

where the primed irradiances represent the radiation field with $\rho = 0$ and the double primed irradiances represent the radiation field with $\rho \neq 0$. The complete spectral path radiance in the upward and downward hemispheres are then, respectively

$$L_p(\tau, \mu, \phi) = \frac{E_0}{4\pi[\mu_0 + (1 - \eta)\tau_0]}$$

$$\left(\left\{(1 - \eta)\tau_0[p(\mu, \phi, \mu_0, \pi + \phi_0) + p(\mu, \phi, -\mu_0, \phi_0)] + \mu_0 p(\mu, \phi, -\mu_0, \phi_0)\right.\right.$$

$$\left. + \frac{2\mu_0^2\rho}{1 + 2(1 - \eta)(1 - \rho)\tau_0}\right\}\left[1 - e^{-(\tau_0 - \tau)/\mu}\right] + \left\{(1 - \eta)[p(\mu, \phi, \mu_0, \pi + \phi_0)\right.$$

$$\left.\left. + p(\mu, \phi, -\mu_0, \phi_0)] - \frac{8(1 - \eta)\mu_0^2\rho}{1 + 2(1 - \eta)(1 - \rho)\tau_0}\right\}\left[(\tau_0 + \mu)e^{-(\tau_0 - \tau)/\mu} - (\tau + \mu)\right]\right) \tag{72}$$

$$L_p(\tau, -\mu, \phi) = \frac{E_0}{4\pi[\mu_0 + (1 - \eta)\tau_0]}$$

$$\left(\left\{(1 - \eta)\tau_0[p(-\mu, \phi, \mu_0, \pi + \phi_0) + p(-\mu, \phi, -\mu_0, \phi_0)] + \mu_0 p(-\mu, \phi, -\mu_0, \phi_0)\right.\right.$$

(equation continued)

$$+\frac{2\mu_0^2\rho}{1+2(1-\eta)(1-\rho)\tau_0}\Bigg\}(1-e^{-\tau/\mu})-\Bigg\{(1-\eta)[p(-\mu,\phi,\mu_0,\pi+\phi_0)$$

$$+p(-\mu,\phi,-\mu_0,\phi_0)]-\frac{8(1-\eta)\mu_0^2\rho}{1+2(1-\eta)(1-\rho)\tau_0}\Bigg\}(\mu e^{-\tau/\mu}+\tau-\mu)\Bigg) \tag{73}$$

where the single-scattering phase functions are given by

$$p(\mu,\phi,\mu_0,\pi+\phi_0)=p\left[\mu\mu_0-\sqrt{(1-\mu^2)\left(1-\mu_0^2\right)}\cos(\phi-\phi_0)\right] \tag{74}$$

$$p(\mu,\phi,-\mu_0,\phi_0)=p\left[-\mu\mu_0+\sqrt{(1-\mu^2)\left(1-\mu_0^2\right)}\cos(\phi-\phi_0)\right] \tag{75}$$

$$p(-\mu,\phi,\mu_0,\pi+\phi_0)=p\left[-\mu\mu_0-\sqrt{(1-\mu^2)\left(1-\mu_0^2\right)}\cos(\phi-\phi_0)\right] \tag{76}$$

$$p(-\mu,\phi,-\mu_0,\phi_0)=p\left[\mu\mu_0+\sqrt{(1-\mu^2)\left(1-\mu_0^2\right)}\cos(\phi-\phi_0)\right] \tag{77}$$

Appendix II
DERIVATION OF AN EMPIRICAL TECHNIQUE FOR CORRECTING HAZE EFFECTS NEAR BOUNDARIES

Analyses of scanner data and radiative transfer model calculations have shown that the material surrounding the material being observed contributes to the received spectral radiance. [2]. It is because of the atmosphere that some of the radiation reflected from the surrounding materials is scattered directly into the scanner's field of view and some irradiates the element being viewed and is reflected to the scanner. Both components are detected as part of the target's radiance and are indistinguishable from it. If a white or grey panel is surrounded by green vegetation, the spectral content of the path radiance resembles that of a green material and, therefore, the effect has been called green haze.

This appendix describes a mathematical technique which can be implemented empirically to remove the contribution of the surrounding materials to the observed radiance when they differ from the material being observed. The first step is to find a boundary between two different fields. If we choose x, y coordinates so that the boundary is on the y axis, a plot of the measured radiance across the boundary might be that shown in Fig. 65. Here a and b are the measured asymptotic values of radiance. We then proceed as follows:

(1) Form f(x), where:

$$f(x) = \frac{d}{dx} \cdot \frac{1}{b - a} [L_0(x, y) - a] \tag{78}$$

(2) Find $F(\omega)$, the Fourier transform of f(x).

$$F(\omega) = \int e^{-j\omega x} f(x)\, dx \tag{79}$$

(3) Form

$$K(\omega) = \frac{1}{F(\omega)} G(\omega) \tag{80}$$

where $G(\omega)$ is a low pass filter corresponding to the desired system bandpass.

(4) Find the inverse transform of $K(\omega)$.

$$k(x) = \frac{1}{2\pi} \int_{-\infty}^{\infty} e^{j\omega x} K(\omega)\, d\omega \tag{81}$$

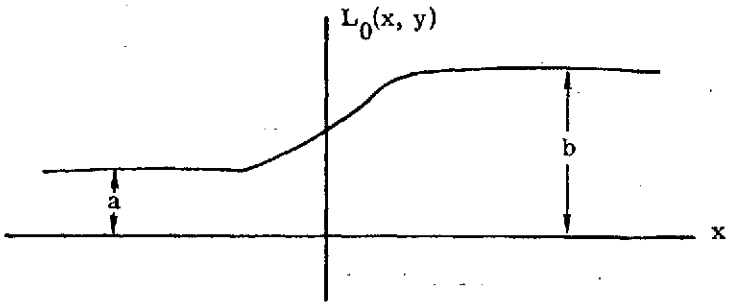

FIGURE 65. PLOT OF THE MEASURED RADIANCE ACROSS FIELD BOUNDARY

(5) Transform the data by the equation

$$L'(x, y) = \iint L(x - u, y - v)k(\sqrt{u^2 + v^2})\,du\,dv \tag{82}$$

The above algorithm has the property that (1) if the radiance can be written as:

$$L(x, y) = ET\rho(x, y) \pm L_p + \iint ET\rho(x', y')h(x - x', y - y')\,dx'\,dy' \tag{83}$$

where h(x, y) is function that represents the spatial spreading effect of the atmospheric haze, and (2) if the measurements shown in Fig. 63 were of a surface with reflectance

$$\rho_0(x, y) = \rho_a, \quad x < 0$$

$$= \rho_b, \quad x \geq 0 \tag{84}$$

then

$$L'(x, y) = [1 + H(0, 0)]ET\rho(x, y) + L_p \tag{85}$$

where $H(\omega_x, \omega_y)$ is the Fourier transform of h(x, y).

$$H(0, 0) = \iint h(x, y)\,dx\,dy, \quad \text{a constant.} \tag{86}$$

and h(x, y) is assumed to have radial symmetry, i.e.,

$$h(x, y) = H(\sqrt{x^2 + y^2}) \tag{87}$$

We can demonstrate the property mentioned above by assuming Eqs. (83) and (84). We first write $\rho_0(x, y)$ in a one-dimensional form:

$$\rho_0(x, y) = (\rho_b - \rho_a)U(x) + \rho_a \tag{88}$$

where U(x) is the unit step function. From Eq. (83) we have, for the two steady state values of $L_0(x, y)$:

$$a = ET\rho_a + L_0 + ET\rho_a H(0, 0)$$

$$= ET\rho_a[1 + H(0, 0)] + L_p \tag{89}$$

$$b = ET\rho_b[1 + H(0, 0)] + L_p \tag{90}$$

Combining Eqs. (89) and (90)

$$b - a = ET(\rho_b - \rho_a)[1 + H(0, 0)] \tag{91}$$

From Eqs. (83), (88), and (89) we derive:

$$L_0(x, y) - a = ET\rho_0 + L_p + ET\rho_0 * h(x, y) - ET\rho_a[1 + H(0, 0)] - L_p$$

$$= ET(\rho_b - \rho_a)[U(x) + U * h_1(x)] \tag{92}$$

Now from Eqs. (78), (91), and (92):

$$f(x) = \frac{\delta(x) + h_1(x)}{1 + H_1(0)} \tag{93}$$

Thus, from Eqs. (79) and (80) we find:

$$K(\omega) = \frac{1 + H_1(0)}{1 + H_1(\omega)} G(\omega) \tag{94}$$

Let us now consider the use of $K(\omega)$. From Eq. (82) we see that:

$$L'^t = L^t K(\omega) \tag{95}$$

where L^t denotes the Fourier transform of L. From Eq. (83):

$$L^t = ET\rho^t + L_p\delta(\omega) + ET\rho^t H_1$$

$$= ET\rho^t(1 + H) + L_p\delta(\omega) \tag{96}$$

After applying $K(\omega)$, we have

$$L'^t = \left[ET\rho^t[1 + H_1(0)] + L_p\delta(\omega)\right]G(\omega) \tag{97}$$

which has the inverse transform of Eq. (85) for $G(\omega) = 1$. This completes the development.

One additional point should be mentioned. The data are unchanged in the middle of large fields, since the green haze effect is a local phenomenon.

Appendix III
AN EMPIRICAL INVESTIGATION INTO THE SUITABILITY OF THE NORMAL LIKELIHOOD FUNCTION FOR PROCESSING MULTISPECTRAL SCANNER DATA

by

R. B. Crane
W. A. Malila
W. Richardson

Abstract

Likelihood functions are usually used in classification decision (i.e., recognition) processes on multispectral scanner data. These functions can be represented by a multivariate normal (Gaussian) density function, the statistical parameters of which are determined for the various decision classes from subsets of the data. A comparison was made to determine whether or not improved classification results could be obtained by use of a different form to represent the likelihood functions, namely, an empirical, multivariate probability, density histogram of decorrelated variables. First, tests were made of the normality of the individual subsets of data, and all were found to be non-normal at the 1% level of significance when a standard chi-square goodness-of-fit test is used. Operating characteristic curves then were generated to represent decisions made with each form between each given class and a uniformly distributed alternative class; a uniform distribution was chosen because the results are then least dependent on the choice of the alternative data set. It was found that the probabilities of misclassification with the two forms were approximately identical for almost every data set, even though a large number of individual data points were classified differently. It was concluded that the conventional assumption of a multivariate normal distribution of multispectral scanner signals from individual fields is sufficiently accurate to warrant its use in recognition processing rather than a more complicated empirical distribution function.

III.1. INTRODUCTION

A multispectral scanner is a mapping instrument that collects and stores infrared, visible, and ultraviolet images in electrical form on magnetic tape. The scanning itself is similar to that employed by an infrared scanner, whereby the circular scan of the collecting optics and the forward motion of the scanner provide the two-dimensional scanning pattern. The images collected by the optics are then separated into wavelength bands by a prism, grating, or

interference filters before detection and storage for subsequent recognition processing. Either before or after storage, the signals can be digitized by an appropriate sampling procedure, if digital processing is to be used.

The likelihood function plays an important role in the processing of multispectral scanner data. It is used in the Bayesian decision rule, as well as more classical rules such as the Neyman-Pearson, minimax, and maximum likelihood. The likelihood of an observed set of values is the joint density function for continuous data or the joint probability function for discrete data. In this appendix, we restrict our attention to discrete data. For the data that are considered, the likelihood functions are not known, but must be estimated from the data set itself. Subsets of the data are chosen from which various likelihood functions are derived, each function corresponding to a separate decision outcome. Such subsets are often known by additional information to represent materials to be recognized and are therefore called training sets. These tests will not include the possibility of interfield variations which cause differences between the statistics of the training sets and those of other fields of the same class. A convenient approximate method of calculating the likelihood function from the data subsets is made possible by the assumption that the data are generated by a Gaussian or normal process. The normal likelihood function is completely determined by first- and second-order moments of the data subsets. Although the normality assumption can sometimes be justified by an application of the central limit theorem, that argument cannot be justified here.

The alternative to the normal assumption that we will consider is that of constructing, from histograms, an empirical likelihood function for each subset of data. Each data point of a subset of data, consisting of the values from the spectral channels for each particular sample, is linearly transformed into a new set of values. The transformation is chosen so that the values in any pair of channels are uncorrelated. Histograms are then formed for each of the new channels, and these histograms, properly normalized, become the new approximation to the likelihood function.

Practical considerations led to the use of this particular method of deriving a likelihood function. The likelihood function should represent the data that are to be analyzed; hence, it is derived from the same data. The subset has a finite number of members, as would any subset used for multispectral analysis; thus, one would not expect exact agreement between data and the underlying likelihood function. Finally, the histogram method can be justified if two assumptions concerning the data are made: 1) the channels are independent when they are uncorrelated; and 2) each histogram accurately describes the marginal distribution. Because data from several sources are to be analyzed, the effect of the first assumption, at least for many of the data sets, can be expected to be small when compared to the effects of using the Gaussian assumption. In fact, the first assumption would be true if the data were distributed normally. The

second assumption is justified by the limited data analyzed. Since there is going to be an uncertainty in the estimation of each marginal distribution, that uncertainty is reflected in the number of intervals of the histograms. The histogram describes the distribution function as accurately as the measurements permit.

III.2. DESCRIPTION OF TEST PROCEDURES

The multispectral scanner data analyzed were obtained from agricultural fields overflown in two different years, at different locations. The set of 1966 data was collected over one growing season in Indiana, on and near the Purdue University Agricultural farm. The 1969 data set was selected from one run over the Imperial Valley in California. Each set of data corresponds to one field, with one agricultural crop. Care was taken to collect data from the interior of the fields, and not to include any boundary samples. Since the present method of processing multispectral scanner data assumes that the data are from a normal process, the marginal distribution of amplitudes of the original data sets were tested for non-normality. In addition, similar tests were made of the data after transformation by a normalized eigenvector basis.

The non-normality test is based on histograms of the amplitudes in each channel or in each transformed variable. By choosing the intervals for the histogram (frequency distribution) so that each interval is equally likely to be populated by a normal distribution, one can readily see any significant departures from a normal population. To quantify the non-normality of the distributions, a χ^2 test is applied to each histogram.

The χ^2 test for non-normality (goodness of fit) is one of several that could be applied. It was selected because it is convenient to apply, has a well defined, asymptotic distribution, and provides a quantitative criterion for rejecting the normal hypothesis. The usual χ^2 statistic (called X^2) was calculated, and its significance (i.e., the probability of an X^2 this large or larger arising from a normal distribution) was determined from the χ^2 distribution, with the appropriate number of degrees of freedom. The lower this probability, the less likely there is a normal distribution; we have used a value of 0.01 as a decision threshold for rejection.

A linear transformation of the signals does not affect the normality of their joint-probability distribution, but it can produce a new basis of uncorrelated variables (vectors) for describing the distribution. There is more than one transformation that will produce uncorrelated variables. One, a Cholesky decomposition into triangular matrices, is used in our recognition-processing algorithms. Another, the eigenvector transformation, rotates the coordinates and aligns them with the major axes of the signal distribution in N-space for Gaussian data. We decided to apply the eigenvector transformation to the data to remove any interchannel correlation, in order to perform a scaling for producing unit variances and to test the marginal distributions of the transformed variables for univariate non-normality using the χ^2 test. The

χ^2 test does provide us with quantitative estimates for deciding when the transformed variables are not normally distributed, but normality of the marginal distributions is not theoretically sufficient to prove that the overall distribution is multivariate normal, even when the variables are uncorrelated; they must be shown to be independent as well.

After the data sets were tested for normality and histogram likelihood function derived, a comparison was made between the use of normal and histogram likelihood functions in a decision process. The comparison was made on the basis of receiver operating characteristic (ROC) curves. For each data set, an alternative hypothesis was assumed, and the Type I versus Type II errors were plotted for different decision levels. The Type I and Type II errors are the errors made when the hypothesis and alternative hypothesis, respectively, are present. From these curves a direct comparison could be made between the two likelihood function decision rules.

The choice of an alternative hypothesis is an important consideration. If we consider the data to be points in a hyperspace, of which each coordinate corresponds to a spectral channel, then the question becomes one of where the alternative hypothesis will be located in the hyperspace. The location and shape of the alternative distribution can be expected to affect the decision errors. A distribution was chosen that was uniformly located throughout the hyperspace. Use of this distribution corresponds to the use of many different separate distributions located uniformly in the hyperspace. Thus, the results correspond to an average of the performance that we would obtain using a large number of separate distributions. This choice of an alternative distribution has the additional advantage of making it possible to test each data set individually.

III.3. SUMMARY OF EXPERIMENTAL RESULTS: NON-NORMALITY TESTS

An examination was made of each channel of the data subsets recorded throughout the summer of 1966 from 38 fields, under a variety of conditions. It was found that 310 of the 456 channels, or 68%, were non-normal according to our χ^2 test at the 1% significance level. The results of these tests and the conditions of measurement are summarized in Table 5. All of the channels tested normal for only one field, and that one had two transformed margins that tested non-normal. None of the fields tested was multivariate normal, as measured at the 1% level of significance.

In a similar manner, we examined data recorded in 1969 from 16 fields in the Imperial Valley. We found 88 out of 160 channels, or 56%, were non-normal. None of the fields had all channels normal. Table 6 shows the number of non-normal channels in each field.

In carrying out the tests, we were careful to account for the discreteness of the data. Because the data values were in the form of 9-bit integers, the histogram intervals were chosen

TABLE 5. SUMMARY OF 1966 DATA USED IN EMPIRICAL DISTRIBUTION STUDY

Crop	Tape	File	Date	Altitude (ft)	Approximate Angle Between Scan Line and Sun's Direction	Eigenvalues λ_1	Eigenvalues λ_2	Eigenvalues λ_1/λ_2	Number of Negative Components in Principal Eigenvector	Number of Non-Normal Margins x	Number of Non-Normal Margins y
Corn	1	16	7/29	700	5°	0.297	0.0206	14.42	0	12	2
Soy	1	19	7/29	700	85°	0.792	0.0363	21.82	0	12	2
Corn	1	20	7/29	700	85°	0.126	0.0220	5.73	0	3	1
Wheat	2	16	6/30	700	5°	0.487	0.0106	49.94	0	12	2
Wheat	2	18	6/30	700	85°	0.0542	0.0104	5.21	0	8	1
Wheat	3	15	6/30	2000	5°	0.186	0.0939	1.98	0	12	5
Corn	3	16	9/15	700	10°	0.191	0.0315	6.06	0	5	2
Soy	3	18	9/15	2000	10°	0.161	0.0362	4.45	0	9	1
Corn	3	19	9/15	2000	10°	0.0403	0.0186	2.17	0	0	2
Soy	3	20	9/15	4000	10°	0.0964	0.0401	2.40	0	1	2
Corn	3	21	9/15	4000	10°	0.198	0.0373	5.31	6	5	2
Soy	3	22	9/15	6000	10°	0.115	0.0479	2.40	5	1	2
Corn	3	23	9/15	6000	10°	0.148	0.0381	3.88	5	1	2
Corn	3	25	9/15	8000	10°	0.0993	0.0282	3.52	5	1	1
Soy	4	5	6/29	700	0°	0.0898	0.0255	3.52	0	12	6
Corn	4	6	6/29	700	0°	0.0175	0.0107	1.63	0	8	3
Corn	4	7	6/29	700	45°	0.0235	0.0088	2.67	5	9	6
Corn	4	16	6/30	700	0°	0.0370	0.0073	5.07	1	12	2
Corn	4	20	6/30	700	90°	0.0108	0.0028	3.86	0	2	0
Soy	4	21	6/30	700	90°	0.0599	0.0189	3.17	0	12	3
Corn	4	22	6/30	700	45°	0.0302	0.0058	5.21	0	11	2
Wheat	4	25	6/30	700	0°	0.339	0.0026	130.4	0	12	4
Wheat	5	4	6/30	700	45°	0.124	0.0033	37.6	0	12	5
Corn	5	9	7/27	700	85°	0.0433	0.0119	3.64	0	8	1
Soy	5	8	7/27	700	85°	0.303	0.0432	7.01	0	11	6
Corn	5	12	7/28	700	90°	0.0884	0.0073	12.1	0	6	3
Soy	5	15	7/28	700	90°	0.0537	0.0087	6.17	0	3	2
Corn	5	16	7/28	700	5°	0.394	0.0110	35.8	0	11	6
Corn	5	18	7/28	700	40°	0.0031	0.0016	1.93	0	5	0
Corn	5	25	9/15	700	85°	0.151	0.0180	8.39	0	11	5
Corn	6	2	9/15	700	15°	0.145	0.0355	4.08	0	12	3
Corn	6	7	6/30	700	50°	0.0545	0.0256	2.13	0	12	2
Corn	6	11	6/30	700	40°	0.0221	0.0079	2.80	2	8	2
Corn	6	13	6/30	700	5°	0.0447	0.0085	5.26	2	11	2
Wheat	6	16	6/30	700	50°	0.0227	0.0018	12.6	0	11	2
Wheat	6	17	6/30	700	40°	0.0905	0.0068	13.3	0	12	2
Wheat	6	20	6/30	700	5°	0.336	0.0066	50.9	0	12	3
Wheat	6	21	6/30	2000	50°	0.0209	0.0019	11.0	0	7	2

TABLE 6. SUMMARY OF 1969 DATA USED IN EMPIRICAL DISTRIBUTION STUDY. (Imperial Valley, California; 3/12/69; 1025 hours PDT; altitude = 5000 ft; east-west flightline.)

Crop	Field Number	Principal Eigenvalues λ_1	λ_2	Number of Non-Normal Margins x	y
Rye	21	0.0342	0.0193	10	5
Alfalfa	29	0.0289	0.0103	8	3
Sugar	39	0.0139	0.0073	2	2
Soil	45	0.0235	0.0110	6	1
Soil	76	0.0498	0.0102	10	3
Soil	77	0.0135	0.0053	2	0
Barley	75	0.0254	0.0077	2	2
Rye	91	0.0312	0.0055	4	2
Lettuce	155	0.0179	0.0102	3	0
Soil	156	0.0631	0.0076	6	4
Alfalfa	180	0.0503	0.0161	9	3
Sugar	179	0.0111	0.0087	2	2
Sugar	190	0.0088	0.0059	1	2
Lettuce	191	0.0461	0.0120	6	3
Alfalfa	205	0.0417	0.0112	10	3
Barley	202	0.0125	0.0113	7	2

to correspond to an integral multiple of possible data values. The hypothesized normal distribution in each channel was determined by the mean and variance of the sample, but extreme points introduced during digitization were excluded. In the case of the 1969 data, the dynamic range of the digitized values was small enough that quantization noise can significantly affect the non-normality tests.

There is no typical pattern of distribution found among the non-normal channels. Figure 66 shows one of the normal distributions; the extremes of the distribution have been compressed because of the method of presentation in intervals of equal probability. Figure 67 shows the distribution of a margin of the data which has a pronounced scan angle effect. The shape can be explained, at least in part, by the change of mean signal with scan angle. Figures 68 and 69 are examples of unsymmetrical and bimodal distributions, respectively.

The analysis of the transformed data yielded some interesting results. The transformation was an eigenvector transformation, with the vectors ordered according to decreasing eigenvalue and weighted so that the transformed variables had unit variance. Thus, the first transformed variable corresponds to variation in the direction of maximum uncertainty in the untransformed hyperspace.

Figure 70 is a representative sample of the results of the analysis. It contains the analysis of the first two transformed variables for one of the fields of corn. Let us consider the analysis of the first variable, y(1). The bar chart on the left shows the number of data points that had amplitudes within each of twenty ranges. These ranges were chosen so that if y(1) were normally distributed, as the number of sample points was increased, the percentage of points in each range would approach 5%. Therefore, the bars would have equal lengths. The first and last ranges were subdivided into two intervals each, so that any extremely unlikely points could be shown separately and excluded from the χ^2 test. Thus, the first two lines form the first equally likely interval, and the last two lines form the twentieth. The intervals that were used are shown to the left of the bars in terms of standard deviations from the mean.

In this example, because it is quite apparent that the bars are not of equal length, we might say that the distribution is non-normal. As noted on the figure, this data set has a large number of sample points (4077), a X^2 value of 245.06, and a significance level of 0 (to 8 places). Since the significance level is below 0.01, we say that y(1) is non-normal.

The second bar chart for y(1) portrays the form of the probability-density function. Because intervals of equal probability are used rather than intervals of equal amplitude (deviation from the mean), the top and bottom of the curve have been compressed relative to the middle portion. Yet, the skewness of the distribution is quite apparent in this chart, where it might have been overlooked in the left-hand chart.

CHANNEL 6 Crn, A62-64, 7/29/66, 0802, T1, R05, 700 Ft, 90 Deg, File 20, TP 01, 05 Jun 67

Interval		Frequency	%	Normal	No.	Normal
*	.54		.00	.00	1	.1
.54	.75	***	.01	.01	34	27.8
.75	.79	***	.01	.01	37	34.1
.79	.83	*****	.02	.02	61	64.9
.83	.87	**********	.03	.03	115	112.8
.87	.91	**************	.05	.05	172	178.9
.91	.95	********************	.06	.07	244	258.9
.95	.99	******************************	.09	.09	344	341.9
.99	1.03	**********************************	.10	.11	390	412.1
1.03	1.06	**	.12	.12	463	453.3
1.06	1.10	**	.13	.12	479	455.0
1.10	1.14	************************************	.11	.11	419	416.8
1.14	1.18	**********************************	.10	.09	368	348.5
1.18	1.22	**********************	.07	.07	248	265.9
1.22	1.26	*****************	.05	.05	191	185.2
1.26	1.30	*********	.03	.03	104	117.7
1.30	1.34	******	.02	.02	77	68.2
1.34	1.38	***	.01	.01	32	36.1
1.38	1.59	**	.01	.01	29	29.8
1.59	*		0	.00	0	.1

3808 Points, χ^2 = 11.39, Significance Level = .72419039, 15 Degrees of Freedom

FIGURE 66. EXAMPLE OF A GAUSSIAN SIGNAL DISTRIBUTION

CHANNEL 5 Wht, C32-3A, 6/30/67, 0830, T1, R04, 700 Ft, 180 Deg, File 16, TP 02, 07 Jun 67

Interval		Frequency	%	Normal	No.	Normal
*	.31		0	.00	0	15.5
.31	.37		0	.00	0	12.7
.37	.43		0	.01	0	21.0
.43	.49		0	.01	0	33.3
.49	.54		0	.01	0	50.6
.54	.60		0	.02	0	73.4
.60	.66	*	.00	.03	12	102.1
.66	.72	******	.02	.04	86	135.7
.72	.78	**********	.08	.05	293	172.7
.78	.84	**	.16	.06	570	210.3
.84	.90	**	.16	.07	572	245.0
.90	.95	*****************************	.11	.08	393	273.1
.95	1.01	******************	.07	.08	246	291.3
1.01	1.07	**********	.04	.08	144	297.4
1.07	1.13	********	.03	.08	121	290.4
1.13	1.19	*********	.03	.08	122	271.4
1.19	1.25	******	.03	.07	92	242.7
1.25	1.31	*******	.03	.06	101	207.7
1.31	1.36	********	.03	.05	120	170.1
1.36	1.42	********	.03	.04	115	133.2
1.42	1.48	*********	.04	.03	134	99.9
1.48	1.54	*********	.03	.02	122	71.7
1.54	1.60	*******	.03	.01	94	49.2
1.60	1.66	*******	.03	.01	95	32.3
1.66	1.72	*****	.02	.01	65	20.3
1.72	1.85	****	.01	.01	53	26.9
1.85	*		0	.00	0	.1

3550 Points, χ^2 = 2243.13, Significance Level = 0, 22 Degrees of Freedom

FIGURE 67. EXAMPLE OF A SIGNAL DISTRIBUTION FROM DATA WHICH HAS A LARGE SCAN-ANGLE EFFECT

CHANNEL 4 Wht, C32-3, 6/30/66, 1400, T1, R08, 2000 Ft, 360 Deg, File 15, TP 03, 15 Jun 67

Interval		Frequency	%	Normal	No.	Normal
*	.42		0	.00	0	.1
.42	.65		0	.01	0	21.5
.65	.69		.00	.01	3	20.4
.69	.73	*	.00	.01	6	35.2
.73	.77	****	.01	.02	37	57.3
.77	.81	*******	.02	.03	70	87.7
.81	.85	**************	.04	.04	129	126.5
.85	.89	*********************	.06	.05	201	171.5
.89	.93	**********************************	.09	.07	300	218.9
.93	.97	**	.11	.08	355	262.9
.97	1.01	**	.12	.09	373	297.1
1.01	1.04	**	.12	.10	376	316.0
1.04	1.08	************************	.07	.10	225	316.3
1.08	1.12	*********************	.06	.09	203	298.0
1.12	1.16	**********************	.06	.08	191	264.1
1.16	1.20	******************	.05	.07	166	220.3
1.20	1.24	**************	.04	.05	141	172.9
1.24	1.28	**********	.04	.04	117	127.8
1.28	1.32	**********	.03	.03	93	88.8
1.32	1.36	******	.02	.02	58	58.1
1.36	1.40	******	.02	.01	53	35.8
1.40	1.44	***	.01	.01	29	20.7
1.44	1.68	******	.02	.01	54	22.0
1.68	*	******	.02	.0	60	.1

3240 Points, χ^2 = 325.02, Significance Level = 0, 19 Degrees of Freedom

FIGURE 68. EXAMPLE OF A SKEWED SIGNAL DISTRIBUTION

CHANNEL 5 Soy, A32-5, 6/29/66, 1308, T1, R02, 7000 Ft, 90 Deg, TP 04, File 6 05 Dec 67

Interval		Frequency	%	Normal	No.	Normal
*	.22		0	.00	0	.0
.22	.36		0	.01	9	8.7
.36	.38		0	.01	0	7.8
.38	.40	**	.01	.01	10	13.3
.40	.42	***	.01	.02	14	21.3
.42	.44	**********	.04	.03	46	32.3
.44	.46	********************	.06	.04	81	46.2
.46	.48	**************************	.08	.05	102	62.4
.48	.50	******************************	.09	.06	115	79.8
.50	.52	********************	.07	.08	85	96.4
.52	.54	**************	.04	.09	57	110.0
.54	.56	*************	.04	.09	53	118.6
.56	.58	******************	.06	.09	72	120.9
.58	.60	**********************	.08	.09	101	116.4
.60	.62	*****************************	.09	.08	114	106.0
.62	.63	**	.13	.07	164	91.1
.63	.65	*************************	.08	.06	97	74.1
.65	.67	*******************	.06	.04	72	56.9
.67	.69	**********	.03	.03	40	41.3
.69	.71	*****	.02	.02	20	28.3
.71	.73	***	.01	.01	14	18.3
.73	.75	*	.00	.01	5	11.2
.75	.77	*	.00	.01	3	6.5
.77	.91	*	.00	.01	5	7.0
.91	*	*	.00	.00	5	.0

1275 Points, χ^2 = 257.01, Significance Level = 0, 20 Degrees of Freedom

FIGURE 69. EXAMPLE OF A BIMODAL DISTRIBUTION

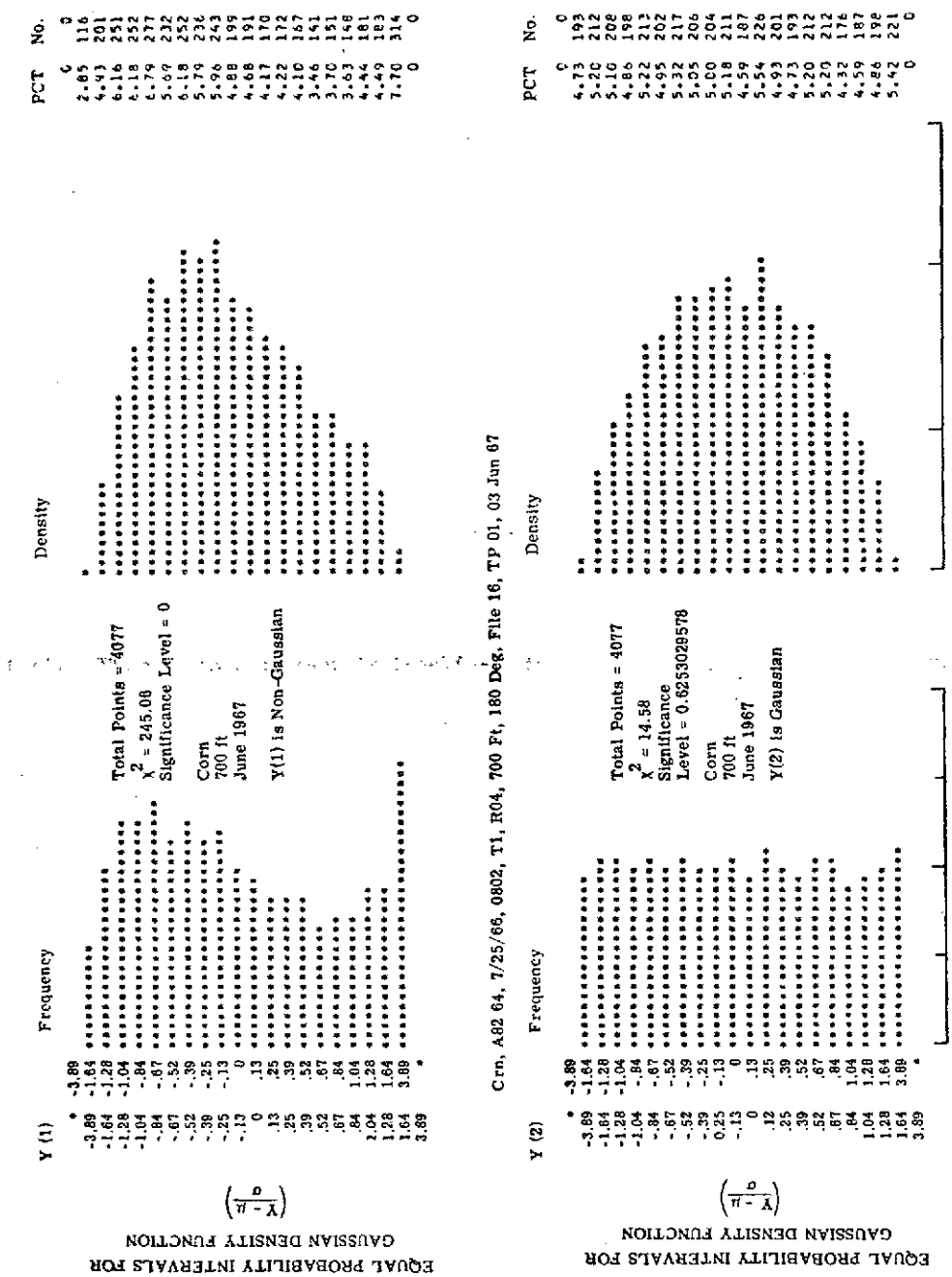

FIGURE 70. EMPIRICAL DISTRIBUTIONS OF DECORRELATED MULTICHANNEL SCANNER DATA

The final two columns of figures shows the percentage and the number of points in each range. The expected percentages, assuming normality for the first and last intervals, is 0.005%, meaning that 20,000 points would be needed before one value in each of these intervals would be expected. The percentages for the remaining intervals should be close to 5% if y(1) are normally distributed.

The two bottom bar charts in Fig. 70 are for y(2) of the same data set. Since the significant level is greater than 0.01, we say that y(2) is normal. The bars on the left-hand chart have very nearly the same length. The right-hand chart shows the previously mentioned compression of the normal curve.

A total of 54 sets of data were analyzed. From the 1969 data, we selected 38 fields (each with 10 channels of data), and from the 1966 data we selected 16 (each with 12 channels); a total of 616 variables were tested with results as tabulated in Tables 5 and 6. Of these 616, 136, or 22% were non-normal, with y(1) and y(2) (the variables associated with the two largest eigenvalues) accounting for 71 or 52% of the total. The variation of the data in the direction of maximum eigenvalue tends to be the most non-normal.

Since the total number of transformed variables that were classified as nonGaussian is 136, the average per data set is 2.5. Only four sets were found that had all channels normal, while three had the maximum number found, six. Thus, it appears that the transformation we chose did tend to isolate the non-normal variations into a small number of variables.

The results of our χ^2 tests for non-normality of the signature distributions are summarized in Table 7. The 1% criterion used for the tests of the normal hypothesis is quite conservative. Also, the χ^2 tests is not as powerful as more complicated tests would be. Consequently, we must conclude that a processor designed under the assumption that we have data with normal statistics is not optimum for data like those studies here, although we have not yet discussed the extent to which this nonoptimality affects recognition performance.

Previous examination of the 700-ft data (Fig. 67) has shown that it has a regular or systematic variation [29]. As seen by the sensor, at this altitude, the fields subtend a large angle. Thus, there is a scan angle effect present which causes the data to have a mean value that is angle dependent.

For the low-altitude data we tested, it is appropriate to use a filtering or preprocessing scheme to eliminate the scan angle effect. This approach, however, would not completely eliminate the problem of non-normality. One reason is that the scan-angle effects, in general would be reduced but could not be eliminated because of the noise in the data. In addition, we have evidence that the resulting preprocessed data would not necessarily be multivariate normal. For example, none of the high-altitude data we tested fully satisfied the simple hypothesis tests for normality we used, and these data subtended angles much smaller than the low-altitude data did.

TABLE 7. SUMMARY OF NON-NORMALITY TESTS ON SIGNATURES

	Untransformed (%)	Transformed (%)
% Non-Normal Margins*	65	22
% Non-Normal Margins Found in First Two Variables	17	52
% Non-Normal Margins from 700-ft-Altitude Data	78	24
% Non-Normal Margins from Higher Altitude Data	47	20

* Failed χ^2 test at 1% level of significance.

III. 4. SUMMARY OF EXPERIMENT RESULTS: CLASSIFICATION TESTS

The final step in the testing procedure was to compare the ability of the two (normal and histogram) likelihood functions to classify correctly. We found the Type I errors by selecting a decision level and counting the percentage of points that were rejected using first one, then the other, decision rule. The Type II errors were found by direct calculation. Data points for the alternative were assumed to be located uniformly throughout a hyperrectangular parallelepiped, the dimensions of which were set so that 0.9995 of the volume of the Gaussian distributions would be included.

All of the comparisons were made with only three channels of data (after application of the eigenvalue transformation). The first three channels, corresponding to the largest eigenvalues were used for some of the comparisons; in other comparisons, the last three channels were used. When the last three channels were used, there was no noticeable difference between the results using the two decision rules. This was true for all of the data sets.

When the first three channels were used, there was a difference in the performance of the two decision rules for a small fraction of the data sets. The Type II errors were compared for Type I errors of 0.1 to 0.3. Only three data sets were found where there was a noticeable improvement in performance when the histogram likelihood functions were used. One set produced twice the Type II error rate for the same Type I probability, while the other two had one and one-half times the error rate. These ratios could be expected to be reduced if all of the channels were used. Figure 71 shows the distribution of the first transformed variable for each of the three data sets. Note the obvious departure from normality. The importance of the two-to-one ratio of errors depends upon the actual separation between alternative hypotheses in the decision process. For two hypotheses with close separation between mean values, this decrease in performance when the Gaussian rule is used could be significant.

Figure 72 shows the plot of Type I versus Type II errors for the data set with the largest difference in performance. The top curve shows the performance when we use Gaussian likelihood function in the decision rule while the bottom corresponds to the histogram rule. A Gaussian scale was used in preparing the graphs. If the data were normal, the normal decision rule would be approximately a straight line, with only minor deviations because a finite number (3550) of data points were used to find the Type I errors.

Figure 73 shows the results of the use of the last three channels for the same data set as was used for Fig. 67. The two curves overlap. The curves in this figure are typical of all of the curves for which the last three channels of the data were used. The curves were also found to be typical of the large majority of results from the first three channels. Figure 61 shows one such graph. The two curves tend to overlap, especially for probabilities of Type I errors in the range of 0.1 to 0.3. Various decision levels were assumed for computation of the points on the

WHT, C32-3, 6/30/66, SEC.11,R04, 700 FT,180 DEG,TP 05,FILE 25 11 DEC 67 — WHT,4,25

VC 11		O/O	NO.
*	-3.85	0	0
-3.85	-1.64	0	0
-1.64	-1.28	0	0
-1.28	-1.04	.54	14
-1.04	-.84	13.63	355
-.84	-.67	24.04	626
-.67	-.52	11.79	307
-.52	-.39	4.45	113
-.39	-.25	2.57	67
-.25	-.13	2.65	69
-.13	0	2.57	67
0	.13	3.15	82
.13	.25	3.15	82
.25	.39	2.34	61
.39	.52	2.30	60
.52	.67	2.65	69
.67	.84	2.34	61
.84	1.04	2.19	57
1.04	1.28	3.46	90
1.28	1.64	4.38	114
1.64	3.85	11.52	300
3.85	*	.23	6

TOTAL POINTS = 2604, CHI SQUARE = 3424.67, SIGNIFICANCE LEVEL =

CRN,462 24, 5/15/66,1745,12,R 5, 4000 FT,360 DEC,FILE 21,TP 03,15 JUN 67 — CRN,3,21

VC 11		O/O	NO.
*	-3.85	0	0
-3.85	-1.64	12.82	75
-1.64	-1.28	.34	2
-1.28	-1.04	0	0
-1.04	-.84	0	0
-.84	-.67	1.20	7
-.67	-.52	.85	5
-.52	-.39	1.37	8
-.39	-.25	2.39	14
-.25	-.13	2.39	14
-.13	0	2.91	17
0	.13	3.76	22
.13	.25	9.43	55
.25	.39	13.33	78
.39	.52	17.61	103
.52	.67	16.24	95
.67	.84	8.89	52
.84	1.04	3.76	22
1.04	1.28	.51	3
1.28	1.64	0	0
1.64	3.85	0	0
3.85	*	2.22	13

TOTAL POINTS = 585, CHI SQUARE = 769.56, SIGNIFICANCE LEVEL = 0

WHT,C32-24, 6/30/67,0830,11,R 4, 700 FT,180 DEG,FILE 16,TP 02,07 JUN 67 — WHT,2,16

VC 11		O/O	NO.
*	-3.85	0	0
-3.85	-1.64	0	0
-1.64	-1.28	0	0
-1.28	-1.04	1.52	54
-1.04	-.84	13.75	488
-.84	-.67	19.49	692
-.67	-.52	11.38	404
-.52	-.39	8.00	284
-.39	-.25	4.28	152
-.25	-.13	2.65	94
-.13	0	3.01	107
0	.13	2.87	102
.13	.25	1.66	59
.25	.39	1.61	57
.39	.52	1.94	69
.52	.67	1.97	70
.67	.84	2.06	73
.84	1.04	2.37	84
1.04	1.28	3.80	135
1.28	1.64	6.08	216
1.64	3.85	11.55	410
3.85	*	0	0

TOTAL POINTS = 3550, CHI SQUARE = 3657.58, SIGNIFICANCE LEVEL = 0

FIGURE 71. DISTRIBUTION OF FIRST TRANSFORMED VARIABLE FOR THE THREE DATA SETS SHOWING LARGEST DIFFERENCES IN OPERATING-CHARACTERISTIC CURVES

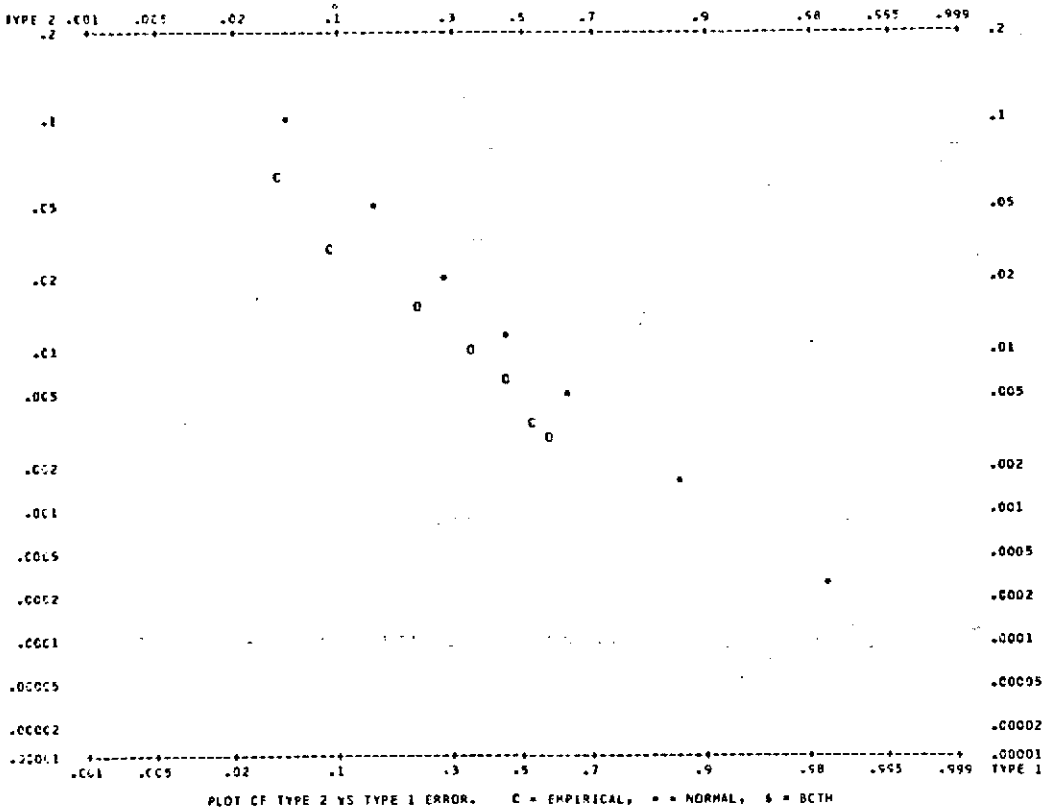

FIGURE 72. EFFECT OF LIKELIHOOD FUNCTION ON OPERATING CHARACTERISTICS—WORST CASE WHEN FIRST THREE VARIABLES ARE USED

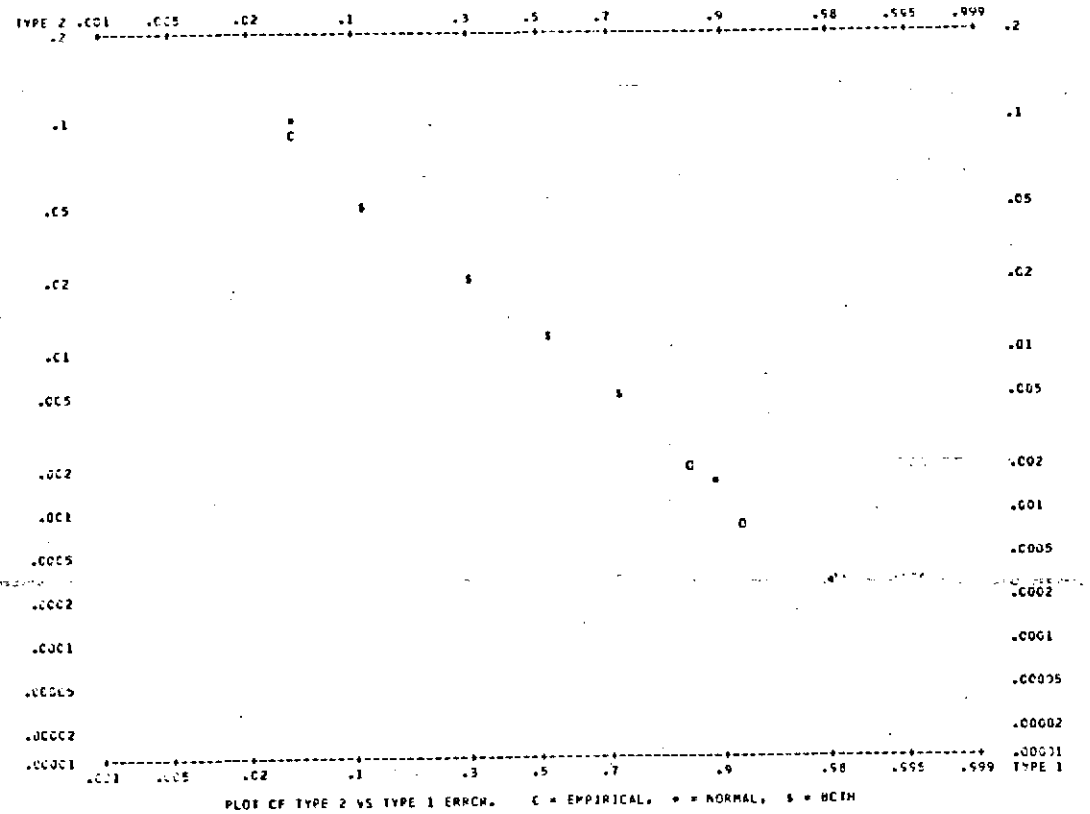

FIGURE 73. EFFECT OF LIKELIHOOD FUNCTION ON OPERATING CHARACTERISTICS— WORST CASE WHEN LAST THREE VARIABLES ARE USED

graph. The same decision level, when used with the two decision rules, produces different Type I and II errors. This can be seen by the location of the plotted points for the Type I error probability of approximately 0.3. For this example, at the same decision level, 8.17% of the points were classified differently by the two rules, although the two curves appear to overlap. Figure 74 a, b, c shows the complete set of operating characteristic curves for the 54 data sets when the 3 largest eigenvalue channels were used.

For all of the curves, the Type II errors are correct within a multiplying factor. Remember that the uniform distribution was used to generate the Type II errors. Thus, the extent of values of the distribution is arbitrary, the choice having been made as a compromise between accuracy and computation time. The accuracy is limited by the number of data points available for our curves, rather than by the extent of the uniform distributions.

III.5. CONCLUSIONS

As a result of our tests, we have decided that the use of the normal likelihood function is justified for recognition processing of multispectral scanner data. This function is much quicker to generate and use than the histogram function. Also, the improvement in performance that would result from the use of a histogram likelihood function and all of the channels, rather than only three channels, is not believed to be significant. If one were to include the effects of interfield variations, even smaller differences probably would result. More promising approaches are: (1) to preprocess the data to compensate for scan angle and similar systematic effects (Refs. 2, 3, and 4, Appendix V) and then use the normal assumption in the decision rule; or (2) to compensate by changing the decision rule parameters. By using the first approach, we would expect transformed data which had distributions that are more nearly normal and, at the same time, which had reduced variances.

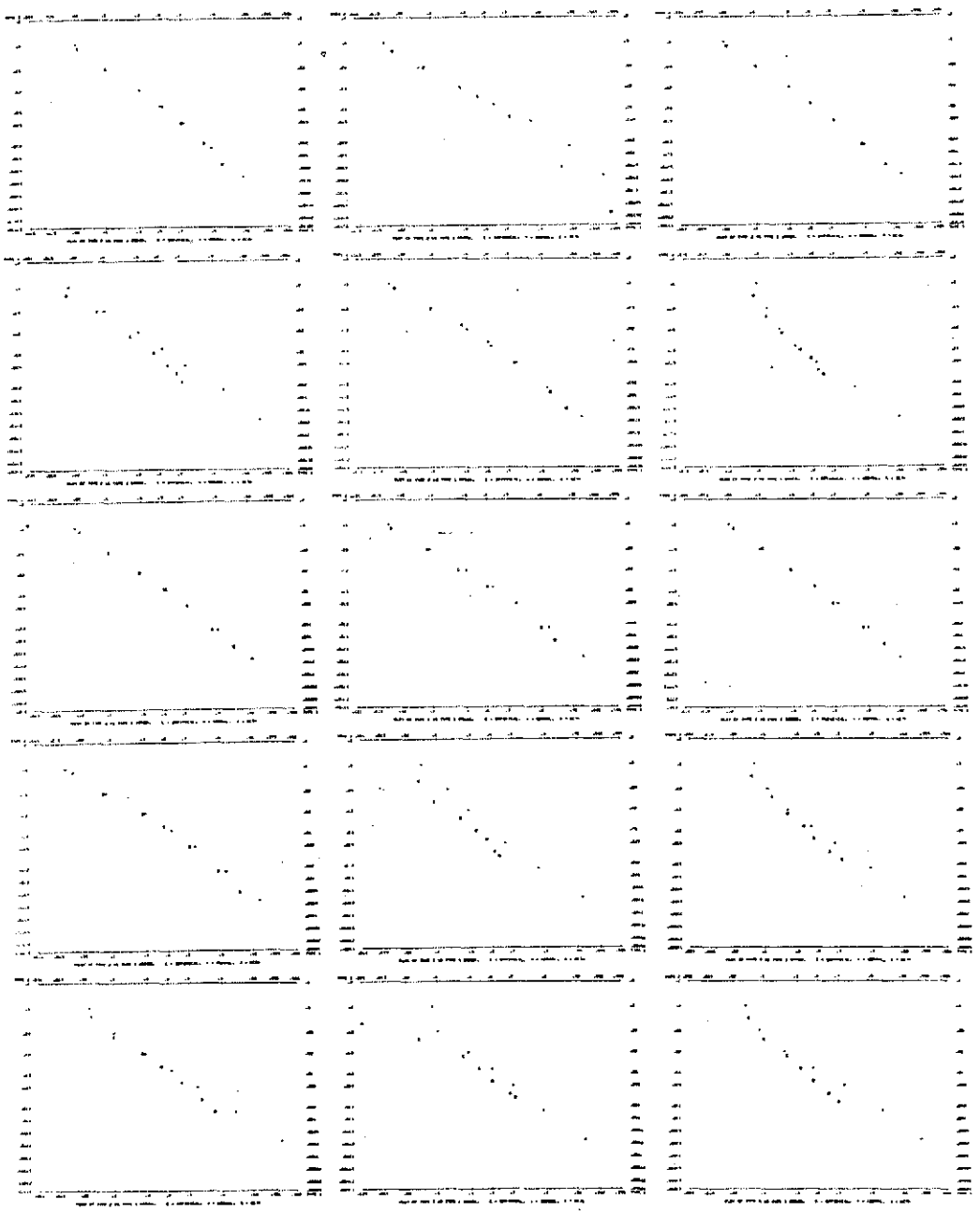

(a)

FIGURE 74. EXAMPLES OF OPERATING CHARACTERISTIC CURVES WHEN FIRST THREE VARIABLES ARE USED

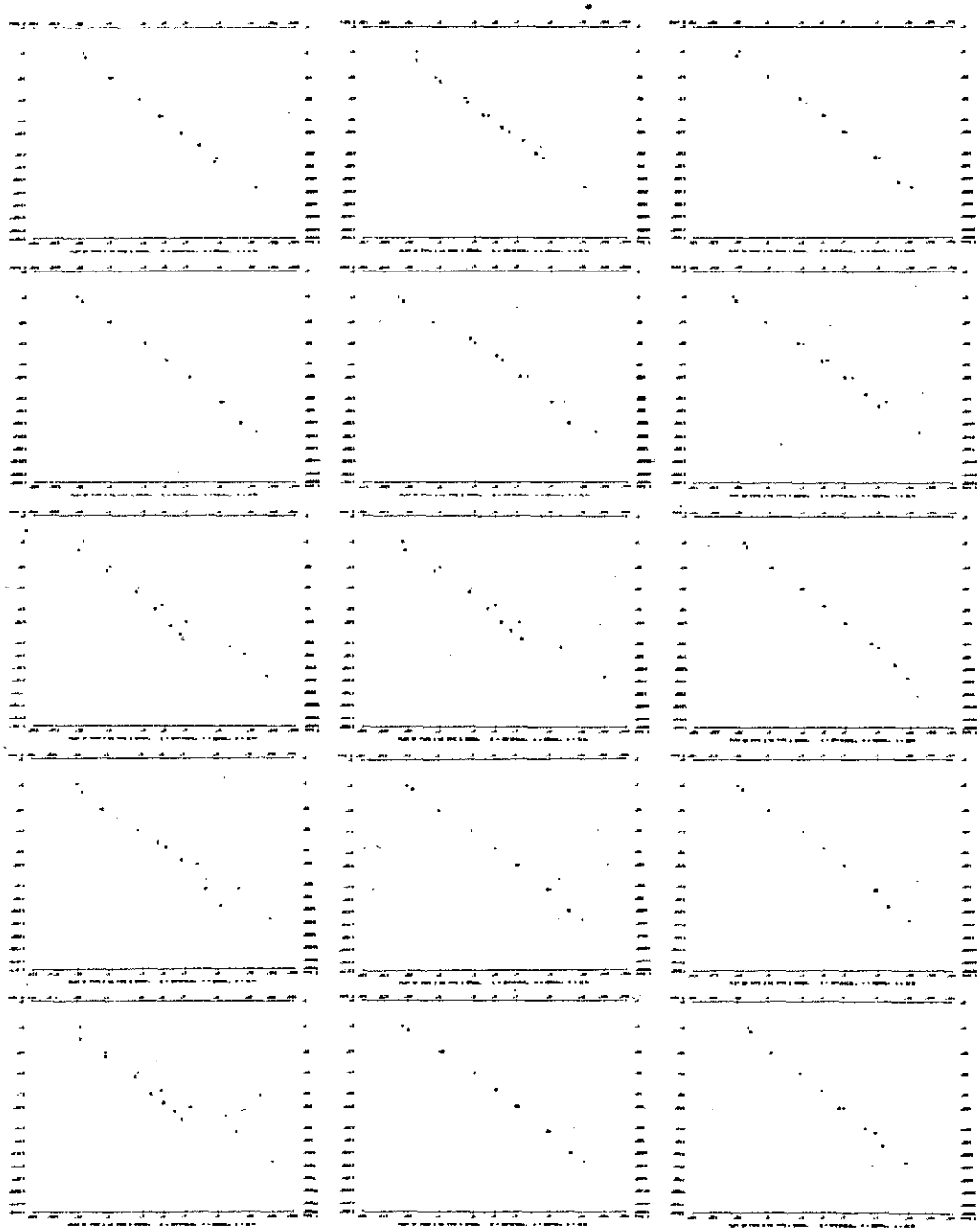

(b)

FIGURE 74. EXAMPLES OF OPERATING CHARACTERISTIC CURVES WHEN FIRST THREE VARIABLES ARE USED (Continued)

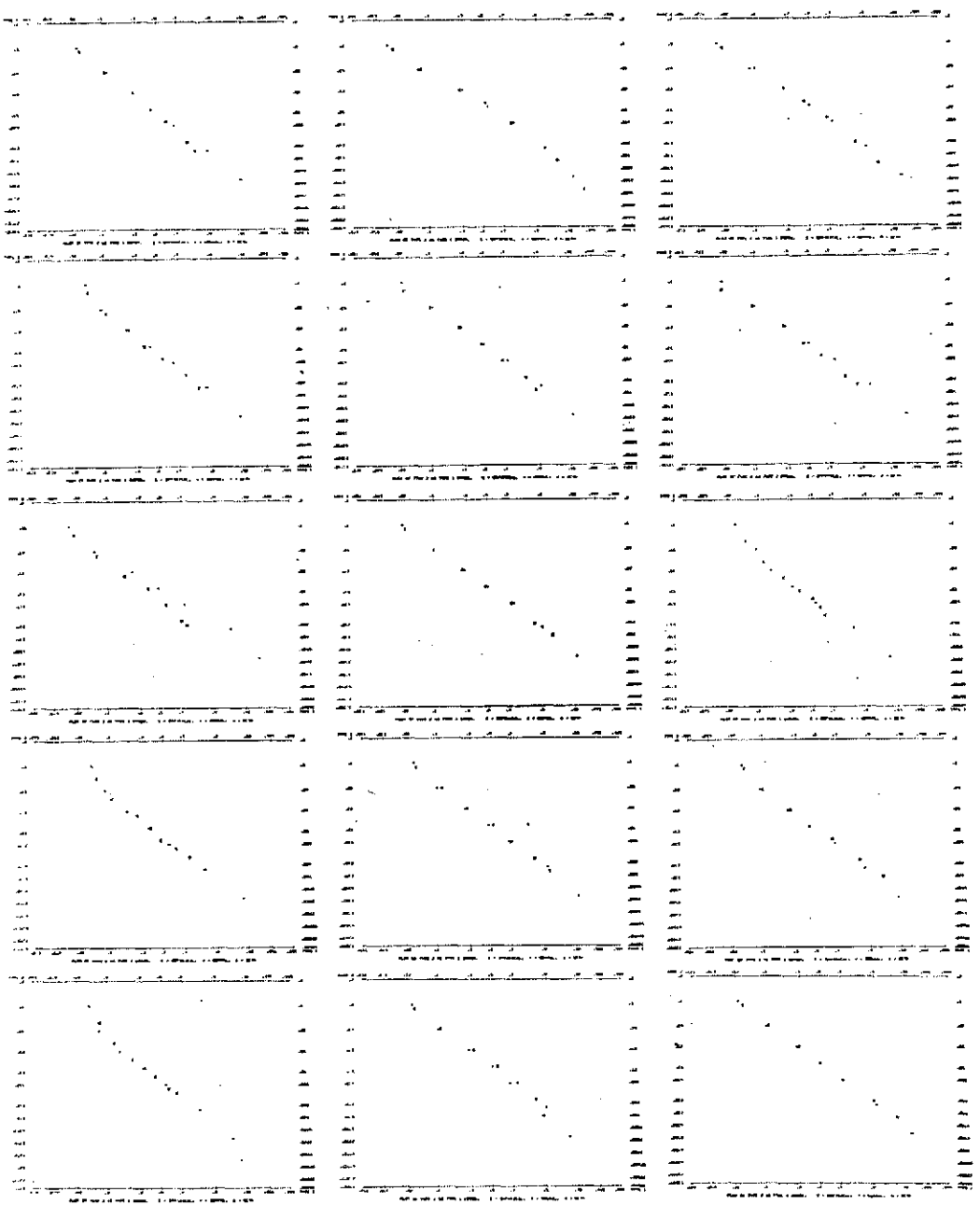

(c)

FIGURE 74. EXAMPLES OF OPERATING CHARACTERISTIC CURVES WHEN FIRST THREE VARIABLES ARE USED (Concluded)

Appendix IV

IMPORTANCE OF ATMOSPHERIC SCATTERING IN REMOTE SENSING*

R. E. Turner
W. A. Malila
R. F. Nalepka

* Reprinted from Proceedings of the Seventh International Symposium on Remote Sensing of Environment, Willow Run Laboratories of the Institute of Science and Technology, The University of Michigan, Ann Arbor, 1971, pp. 1651-1697.

IMPORTANCE OF ATMOSPHERIC SCATTERING IN REMOTE SENSING, OR EVERYTHING YOU'VE ALWAYS WANTED TO KNOW ABOUT ATMOSPHERIC SCATTERING BUT WERE AFRAID TO ASK*

R.E. Turner
W.A. Malila
R.F. Nalepka**

Willow Run Laboratories
Institute of Science and Technology
The University of Michigan
Ann Arbor, Michigan

ABSTRACT

One's ability in remote sensing to discriminate between target and background materials on Earth's surface is diminished by the presence of atmospheric haze which scatters and/or absorbs parts of the radiation. The extent to which the atmosphere affects the process of discrimination depends on the specific condition of the atmosphere existing at the time of observation as well as on the discrimination technique employed. Remote sensing operations in environmental and natural science applications would benefit from a better and more quantitative understanding of the effects of the atmosphere on discrimination.

This paper asks and answers questions that are of interest to users of remote sensor data and presents calculations designed to improve one's understanding of radiation transfer in Earth's atmosphere. The spectral region considered lies between 0.4 and 3 μm. A recently developed radiative transfer model was used in computing irradiance, path radiance, sky radiance, transmittance, and contrast transmittance in a cloudless atmosphere for a variety of sun angles, viewing (nadir) angles, altitudes, surface reflectances, and atmospheric haze conditions. The results are presented parametrically. One interesting result is the effect which neighboring materials have on the spectral character of a target as a result of aerosol scattering by the haze.

The model described was developed using radiative transfer theory as applied to a plane-parallel, homogeneous, aerosol-filled atmosphere with a surface, the reflectance of which is assumed to be perfectly diffuse. The haze content of the atmosphere is designated by the horizontal visual range at sea level.

1. WHY SHOULD A USER OF REMOTE SENSOR DATA BE CONCERNED ABOUT ATMOSPHERIC SCATTERING?

Many problems associated with target recognition and image interpretation in remote sensing are caused by the presence of Earth's atmosphere. One problem is clearly evident in photographs of the Earth's surface taken from orbiting spacecraft[1]. The general bluish tint in many of these photo-

* The work reported in this paper was supported by NASA under Contract NAS9-9784.

** The authors are employees of: Infrared and Optics Laboratory, Willow Run Laboratories, Institute of Science and Technology, University of Michigan.

graphs arises from radiation that has been scattered one or more times by the molecules and particulate material which compose the atmosphere. This scattered radiation adds spectral variations to the received signals which are not truly representative of surface features.

Since most remote sensing operations involve observation paths within or through Earth's atmosphere, each investigator must consider the effects of the atmosphere on the radiation signals produced by the sensors and on his use and interpretation of the data. If the atmospheric effects on the signals are serious enough, he should then consider ways and means of reducing or overcoming these effects.

There are several deleterious effects of atmospheric haze on remote sensor data, whether in the form of imagery or of electrical signals processed on computers. First, haze reduces the contrast between adjacent surface features on imagery and makes the interpretation of that imagery more difficult. Figure 1 illustrates the way that contrasts are reduced on images obtained in two spectral bands at 5000-ft. altitude from those at 1000-ft. altitude.

Second, as a result of scattering in the atmosphere, the spectral distribution of radiation received by a detector is different from that which originates at the ground surface, i.e., the atmospheric effects are more pronounced at some wavelengths than at others. For example, in Figure 1, the effect of the haze is much greater for the wavelength band, 0.55 μm to 0.58 μm, than for the band at longer wavelengths, 0.80 μm to 1.0 μm. It is this spectral dependence of scattering which accounts for the blueness in color photography and color composite imagery taken from high-altitude aircraft and spacecraft.

Finally, atmospheric effects can reduce the amount and quality of information that can be extracted from the data by computer processing. That is, the first two effects discussed with regard to imagery and its interpretation also are important in the recognition processing of multispectral remote sensor data. The effects of atmospheric haze can reduce the recognition computer's ability to discriminate between surface materials that resemble each other, and can limit the extent of the area over which satisfactory recognition results can be obtained easily.

2. HOW DOES THE ATMOSPHERE AFFECT REMOTE SENSOR SIGNALS?

The atmosphere affects visible and near-infrared remote sensor signals in three ways. First, it modifies the spectral and spatial distributions of the radiation incident on the surfaces being observed. Second, it attenuates the radiation that passes through it to the sensor after being reflected by the surface. Third, it adds an extraneous component of scattered radiation, called path radiance, to the transmitted component. (See Figure 2).

The total radiance received by a sensor at altitude, h, with nadir view angle, θ, and azimuthal angle, ϕ, can be expressed as:

$$L(h,\theta,\phi) = L_T(h,\theta,\phi) + L_p(h,\theta,\phi) \qquad (1)$$

where: $L_T(h,\theta,\phi)$ is the transmitted radiance and $L_p(h,\theta,\phi)$ is the path radiance. Although not noted explicitly, these radiances also depend on wavelength, solar zenith and azimuthal angles, the amount and distribution of haze particles and molecules in the atmosphere, and the surface reflectance.

The transmitted radiance is the product of the radiance emanating from the surface, here called the intrinsic radiance, and the transmittance of the atmosphere, $T(h,\theta)$. That is:

$$L_T(h,\theta,\phi) = L_I(\theta,\phi)T(h,\theta) \qquad (2)$$

Here, $L_I(\theta,\phi)$, the intrinsic radiance of the surface, is given by:

$$L_I(\theta,\phi) = \int_0^{2\pi} \int_0^1 \mu' \rho'(\mu,\phi,-\mu',\phi') L(0,-\mu',\phi') d\mu' d\phi' \qquad (3)$$

where: $L(0,-\mu',\phi')$ is the radiance incident on the surface, $\rho'(\mu,\phi,-\mu',\phi')$ is the bidirectional reflectance of the surface, and $\mu = \cos\theta$. The primed variables indicate a downward direction, and the unprimed quantities indicate an upward direction.

The quantity $T(h,\theta)$ is the transmittance and is given by:

$$T(h,\theta) = e^{-(\tau_o - \tau)/\mu} \qquad (4)$$

where τ and τ_o are the optical depth at altitude h and the total optical depth, respectively, for the atmosphere, and can be determined for any wavelength and atmospheric condition.

3. WHY IS A DETAILED RADIATIVE TRANSFER MODEL IMPORTANT FOR REMOTE SENSING APPLICATIONS?

One can learn about atmospheric effects from either experimental measurements or theoretical calculations with a radiative transfer model, or both. A large number of variables must be considered, and an extensive measurement or calculation program would be required to get a full understanding of the severity of the effects under a wide variety of conditions.

The use of radiative transfer model calculations has several advantages over the use of experiments: lower cost, more flexibility, better control, and a freedom to study effects parametrically. To keep from drawing erroneous or misleading conclusions from the calculations, however, the model must be a detailed and accurate one and must be verified by comparison with experimental data.

A knowledge of atmospheric effects is useful in all phases of remote sensing operations. In the data collection phase, it can be useful in the specification and design of sensors and in mission planning. In the recognition processing phase, it can be used to remove signal variations introduced by the atmosphere thereby making large-area surveys more feasible. That is, this knowledge may be used directly to specify parameters of preprocessing transformations or may be used in their development through the simulation of sensor data exhibiting various atmospheric effects. Finally, in the interpretation phase, it can help the investigator better understand features in imagery and recognition maps and extract quantitative estimates of surface radiation characteristics.

4. HAVEN'T SCATTERING PHENOMENA IN EARTH'S ATMOSPHERE BEEN UNDERSTOOD FOR A LONG TIME?

We are all aware of many beautiful phenomena which occur in the sky from time to time, such as the red and orange sunsets, the green flash, the aurora borealis, and rainbows, but by far the most obvious phenomenon we notice is the blue sky. Why is the sky blue? Lord Rayleigh[2] found that the blue color of the sky could be explained by considering the single scattering of light by scattering centers in the atmosphere. The scattering centers, usually assumed to be molecules, are actually molecular density fluctuations, the sizes of which are much smaller than the wavelength of the radiation. If incident radiation is scattered once by an inhomogeneity, then, for Rayleigh scattering, the intensity of the scattered radiation varies as:

$$I(\text{Rayleigh}) \propto \lambda^{-4}(1 + \cos^2\theta) \qquad (5)$$

where λ is the wavelength of light and θ is the scattering angle. Thus, we see from (5) that short wavelength radiation is scattered much more than long wavelength radiation.

Actual measurements of the sky radiation reveal, however, large deviations from Rayleigh's theory. The spectral character can differ strongly from the inverse fourth power relationship given by (5), and the degree of polarization is also different from that predicted by the theory.

The discrepancies between theory and experiment can be explained by the following: (1) Rayleigh considered only single scattering whereas multiple scattering is also important, and (2) the real atmosphere contains particulate matter which can scatter radiation in a manner quite different from that given by (5).

Significant advances were made in radiative transfer theory by Schuster in 1906 and by Schwarzschild[3] in 1914 but the exact solution of the multiple scattering problem in plane-parallel, homogeneous, conservative atmospheres which have a Rayleigh scattering law was found by Chandrasekhar.[4] Using Chandrasekhar's theory, Coulson et al.,[5] computed the sky radiation for a Rayleigh-type atmosphere with multiple scattering and polarization. The optical thickness considered, however, was small and only recently[6] have similar calculations been performed for atmospheres of large optical thicknesses.

In recent years, the theory of radiative transfer has been extended to include absorption,[7] inhomogeneities,[8] and internal field calculations.[9] In all these investigations, only Rayleigh-type scattering or scattering according to a slightly anisotropic distribution was used, but, even with these developments, theory and experiment did not agree, especially for hazy atmospheres in which scattering by particulate material is predominant.

Thus, we can say that scattering phenomena are now understood for Rayleigh-type atmospheres under special conditions. However, for a realistic atmosphere, characteristic of Earth's atmosphere, the particulate component, typical of haze, must be taken into account.

5. WHY IS THE RADIATIVE TRANSFER PROBLEM FOR HAZY ATMOSPHERES SO DIFFICULT TO SOLVE?

As we have just noted, Rayleigh scattering refers to the scattering of electromagnetic radiation by objects much smaller than the wavelength of the incident radiation. In the case of Earth's atmosphere, the scattering centers are regions where the molecular density fluctuates and, hence, Rayleigh scattering is also referred to as molecular scattering. For the theoretical case of a pure Rayleigh-type atmosphere, the visibility is very great, about 300 kilometers or more. The actual atmosphere, however, consists of a turbulent mixture of gases and particulate matter, a combination which is called an aerosol. Typical aerosol particles have radii in the range 10^{-1} μm to 10^{0} μm but can vary from 10^{-4} μm to 10^{2} μm. For radiation in the visible region of the spectrum, it is a particle in the range 10^{-1} μm to 10^{0} μm (haze particle) which scatters radiation most strongly.

If a simple shape, e.g., a sphere, and an index of refraction are assumed for a haze particle, then classical electromagnetic theory can be applied to determine the cross-section and scattering properties of the particle. For the special case of a homogeneous sphere irradiated by a plane electromagnetic wave in one direction, standard electromagnetic scattering theory (Mie scattering) is applicable. The results of calculations show that the cross section for a particle of radius r is strongly dependent upon the dimensionless ratio $2\pi r/\lambda$, where λ is the wavelength of the radiation. An actual aerosol distribution is, however, a polydispersion, i.e., a collection of particles of varying sizes and therefore an effective cross section must be found for the distribution.

Although we need the scattering, absorption, and total cross sections of the polydispersion, it is also necessary that we have knowledge of the angular distribution of the radiation scattered by a particle in order to solve the transfer equation. The quantity which describes the angular variation is called the single-scattering phase function, a dimensionless function which represents the fraction of the radiation scattered through the angle θ. Examples of these functions in terms of wavelength are shown in Figure 3 for a typical haze condition.[10] The most striking characteristic associated with aerosol particles is the very high degree of anisotropy in the scattered radiation field. Typically, the amount of radiation scattered into the forward hemisphere is $\sim$ 95% with most of that being within the first four degrees.

The use of such anisotropic functions in radiative transfer problems usually involves extensive analysis and computation. To illustrate, consider the expansion of the phase function in spherical harmonics, i.e.,

$$p(\mu) = \sum_{\ell=0}^{N} (2\ell + 1)\, A_\ell\, P_\ell(\mu) \qquad (6)$$

where $p(\mu)$ is the actual polydisperse phase function, μ is the cosine of the scattering angle θ, $P_\ell(\mu)$ is a Legendre polynomial, and A_ℓ are constants given by:

$$A_\ell = 1/2 \int_{-1}^{1} p(\mu)\, P_\ell(\mu) d\mu \qquad (7)$$

Using values of the actual phase function $p(\mu)$ from Deirmendjian[10] we calculated the coefficients A_ℓ numerically and inserted them into Equation 6. The results are shown in Figure 4 where only the backward hemisphere is depicted since there is almost perfect agreement for the forward hemisphere. One must use some 36 or 38 terms to approximate the actual phase function, while only two terms are needed to represent the simple Rayleigh function.

Thus, there are two factors which serve to complicate the problem of radiative transfer in hazy atmospheres; (1) the uncertainty in the specification of the parameters needed to define an atmospheric condition, and (2) the mathematical complexities involved in solving the transfer equation which has a highly anisotropic phase function.

6. WHICH PARAMETERS ARE USEFUL FOR DESCRIBING THE STATE OF THE ATMOSPHERE?

Earth's atmosphere consists of semi-permanent gases such as nitrogen, oxygen, and argon and highly variable components such as ozone, water vapor, and aerosols. The latter take on many forms; water droplets, smoke particles, dust, fumes, etc.. For the purposes of remote sensing in the ultraviolet or infrared spectral regions, we need information on the atmospheric content of gases such as water vapor, carbon dioxide, and ozone, since these gases absorb significant amounts of radiation. Radiosonde data can supply the pressure, temperature, density, and relative humidity data and independent measurements provide data on gaseous composition.

In the visible spectral region, very little absorption occurs by gases or aerosol particles so that the primary attenuating mechanism is scattering. Since the tropospheric aerosol is highly variable in nature, it is desirable to have some information concerning the amount of particulate material present at times of interest.

One useful parameter for the visible region is the sea level horizontal visual range, V. Assuming a 2% relative contrast between a black object and the sky background we have:

$$\frac{L_B - L}{L_B} = e^{-\kappa X} = 0.02 \tag{8}$$

where κ is the extinction coefficient (km^{-1}) and X is a standard distance. Defining the variable distance X to be equal to V for this particular relative contrast we have:

$$V = \frac{3.912}{\kappa} \tag{9}$$

a simple relation which enables us to define the extinction coefficient κ for a haze according to the easily measured parameter visual range (km).

Other parameters can of course be specified to define the state of the atmosphere more accurately, but from the practical point of view used in remote sensing applications, the horizontal visual range will usually suffice.

7. DOES A RADIATIVE TRANSFER MODEL EXIST FOR HAZY ATMOSPHERES?

The mathematical complexities in a radiative transfer model arises from attempts to solve the integro-differential equation of radiative transfer. The equation to be solved for the description of radiative transfer through a plane-parallel atmosphere is the following:

$$\mu \frac{dL}{d\tau} = L(\tau,\mu,\phi) - \frac{\omega_o}{4\pi} \int_0^{2\pi} \int_{-1}^{1} p(\tau,\mu,\phi,\mu',\phi') L(\tau,\mu',\phi') d\mu' d\phi' \tag{10}$$

$L(\tau,\mu,\phi)$ is the scalar spectral radiance at an optical depth, τ, where we define the dimensionless quantity τ to be:

$$\tau = \int_h^{\infty} \kappa(z) dz \tag{11}$$

$\kappa(z)$ being the extinction coefficient at altitude z, and h being the base altitude. The quantity ω_o is the single-scattering albedo, defined as the ratio of the scattering coefficient to the extinction coefficient and is usually very close to unity for the visible spectral region. The function $p(\tau,\mu,\phi,\mu',\phi')$ is the single-scattering phase function which describes the angular distribution of radiation scattered through the angle χ, where

$$\cos\chi = \mu\,\mu' + \sqrt{(1-\mu^2)(1-\mu'^2)}\,\cos(\phi-\phi') \tag{12}$$

There are three general methods used to determine the spectral radiance $L(\tau,\mu,\phi)$. These are: (1) the classical approach, in which the radiance function $L(\tau,\mu,\phi)$ and the phase function are treated as continuously varying functions of $\theta(=\cos^{-1}\mu)$ and ϕ; (2) discrete space theory, where the transfer equation is solved for the radiance at specific angles θ_i, ϕ_i; and (3) the statistical technique, i.e., one which makes use of sampling theory such as the Monte Carlo method. The decision as to which method should be used depends somewhat on the personal preferences of the investigator and also on the accuracy desired.

In the classical approach, one can expand the radiance functions $L(\tau,\mu,\theta)$ in spherical harmonics and, using the orthogonality properties, convert the transfer equation into an eigenvalue problem. Although the analytical formulation is complicated because of the large number of terms needed, this is one of the approaches we are now examining at The University of Michigan.

There are several other methods in the classical approach, one being the conversion of the transfer equation into an integral equation which can be reduced to a Neumann series. Each member of the series corresponds to a higher degree of scattering. The main reason why this method is not used often is that convergence of the series is very slow under certain conditions.

Discrete space theory is more readily adaptable to computer methods but is quite time consuming, especially when inhomogeneous atmospheres are considered. An example of this method is the invariant imbedding technique in which the linear equation 10 with a two-point boundary condition is replaced by a nonlinear equation with an initial condition. Various thin layers of an atmospheric medium are added successively until the total thickness is obtained. Thus, the internal field can be obtained for any atmospheric thickness, but so far the method has not been used with highly anisotropic phase functions that are characteristic of a hazy atmosphere. In this case too, an excessive amount of computer time is necessary in order to simulate real atmospheres with large optical depths.

The Monte Carlo technique has enjoyed great success in recent years and has as its most desirable feature, versatility. That is, one can simulate many unusual atmospheric and surface conditions easily and hence eliminate the enormous analytical complexities using the other methods. Unfortunately, much computer time is needed to achieve reasonable accuracy.

Therefore, we can say that, in spite of all the research over the past thirty years or so, no detailed, comprehensive radiative transfer model has been developed which can be applied directly to the problems in remote sensing. In order to rectify this situation, we have developed a simplified model at The University of Michigan and are presently extending the development to include a large variety of atmospheric and terrestrial conditions.

8. WHAT ARE THE CAPABILITIES OF THE RADIATIVE TRANSFER MODEL DEVELOPED AT THE UNIVERSITY OF MICHIGAN?

For immediate application to problems of discrimination in remote sensing, a user needs a simplified, workable model which can be applied to a wide range of atmospheric and surface conditions with a minimum of computational effort. Our model is especially equipped to deal with plane-parallel, homogeneous,* hazy atmospheres, under a variety of situations.

Realizing that aerosol scattering occurs predominantly in the forward direction, we can approximate the phase function by a sum of delta functions, i.e.,

$$p(\mu,\phi,\mu',\phi') = F\delta(\mu-\mu')\delta(\phi-\phi') + B\delta(\mu+\mu')\delta(\pi+\phi-\phi') \qquad (13)$$

where $F = 4\pi\eta$ and $B = 4\pi(1-\eta)$, η being the fraction of the radiation which is scattered into the forward hemisphere. Inserting Equation 13 into the following radiative transfer equation:

$$\mu \frac{dL}{d\tau} = L(\tau,\mu,\phi) - \frac{1}{4\pi}\int_0^{2\pi}\int_{-1}^{1} p(\mu,\phi,\mu',\phi')L(\tau,\mu',\phi')d\mu'd\phi' - \frac{E_s(\tau)}{4\pi} p(\mu,\phi,-\mu_o,\phi_o) \qquad (14)$$

allows us to separate the equation into two simple differential equations. $E_s(\tau)$ is the attenuated solar spectral irradiance, and $\mu_o(=\cos\theta_o)$, ϕ_o are the coordinates of the sun. Assuming a surface

* By homogeneous, we mean that the proportions of constituents are constant throughout all altitudes, even though the actual density varies drastically with altitude. We are presently modifying our model to include inhomogeneous atmospheres.

reflectance of zero, we solve the equations for the spectral irradiances in the upward and downward hemispheres at any optical depth τ. Then, assuming a perfectly diffuse surface reflectance, we find the radiation field resulting from surface reflection and combine these irradiances to determine a "source" radiance, i.e.,

$$L(\tau,\mu,\phi) = \frac{1}{\mu_o}\left[E_+'(\tau)\delta(\mu-\mu_o)\delta(\pi+\phi_o-\phi)+ E_-'(\tau)\delta(\mu+\mu_o)\delta(\phi-\phi_o)\right] + \frac{E_+''(\tau) + E_-''(\tau)}{2\pi} \qquad (15)$$

where here $L(\tau,\mu,\phi)$ represents the source radiance and is to be inserted into the integral of Equation 14. Equation 14 can then be solved to determine the spectral sky radiance and the spectral path radiance at any point in the atmosphere. The boundary conditions for the spectral radiance are:

$$L(0,-\mu,\phi) = 0 \qquad (16)$$

$$L(\tau_o,\mu,\phi) = \int_0^{2\pi}\int_0^1 \mu'\rho'(\mu,\phi,-\mu',\phi')\hat{L}(\tau_o,-\mu',\phi')d\mu'd\phi' \qquad (17)$$

where $\rho'(\mu,\phi,-\mu',\phi')$ is the bidirectional reflectance of the surface and $\hat{L}(\tau_o,-\mu',\phi')$ is the total (direct plus diffuse) spectral radiance at the surface. It should be noted that for the case of a perfectly diffuse (Lambertian) surface Equation 17 reduces to

$$L(\tau_o,\mu,\phi) = \frac{\rho}{\pi}\hat{E}_-(\tau_o) \qquad (18)$$

where ρ is the hemispherical reflectance, and $\hat{E}_-(\tau_o)$ is the total downward irradiance at the surface.

Finding the radiance in terms of optical depth τ instead of altitude h allows one to modify the state of the atmosphere without affecting the radiative transfer calculations. In the model currently being used at The University of Michigan, we utilize the optical depth-altitude-wavelength relationship as determined by Elterman[11] for visual ranges from 2km to 23km. The actual scattering phase functions for a haze, taken from Deirmendjian,[10] are then used in the solution of the radiative transfer equation. Assuming some surface reflectance, we can then determine the spectral radiances in the atmosphere for a variety of conditions. An outline of the general capabilities of our current radiative transfer program at The University of Michigan is illustrated in Figure 5.[12]

The ultimate test for the validity of any theoretical model lies in its agreement with experiment. In Figures 6 and 7, a comparison is made between calculations made with our model and experimental data obtained by Ivanov.[13] Although the surface conditions were not known exactly, it was known that the surface was one of vegetation and, therefore, had a reflectance of about 20%.

We are now continuing the development of our radiative transfer model to include a variation in atmospheric parameters. One long-term variation is illustrated in Figure 8 in which results of our model were presented for (1) data reported in 1964[14] but gathered prior to the Mt. Agung volcanic eruption in 1963 and (2) data gathered several years later (1968).[15] The volcanic eruption added considerable quantities of dust to the stratosphere and, hence, a reduction in irradiance occurred at the surface. Thus, there is a reduction in the upward scattered radiation and the path radiance is less.

9. HOW DOES THE TRANSMITTANCE DEPEND ON THE ATMOSPHERIC AND OBSERVATION CONDITIONS?

The transmittance function was described in Equation 4. It is a function of the various parameters that describe the path conditions as well as of wavelength. Figure 9 presents plots of spectral transmittance for several visual ranges. Note that transmittance is smallest for the shortest wavelengths. A more detailed presentation of the dependence of spectral transmittance on visual range is given in Figure 10 for a wavelength of 0.55 μm.

Both altitude and scan angle effect the length of the observation path and consequently affect the transmittance. Figure 11 illustrates the altitude dependence of spectral transmittance and Figure 12 illustrates its dependence on nadir scan angle for several visual ranges.

10. HOW DOES IRRADIANCE DEPEND ON THE ATMOSPHERIC AND OBSERVATION CONDITIONS?

There are two components of downward irradiance within Earth's atmosphere, the direct solar component and the diffuse downward component. As shown in Figure 13, the diffuse spectral irradiance component, $E_{\downarrow}(\tau)$, depends very strongly on the vertical distribution of haze particles and on the altitude of the observer. The total downward spectral irradiance, $E_{\downarrow}(\tau)$, however, exhibits a much smaller dependence on altitude.

As the visual range decreases, the diffuse component at any altitude increases as shown in Figure 14. The curves in this figure suggest that measurements of the diffuse irradiance at two or more low altitudes could be used to estimate the visual range or haze distribution in the atmosphere. Plans are being made to incorporate a diffuse irradiance sensor in the Michigan multispectral aircraft.

It is well known that scattering is more pronounced at shorter wavelengths than at longer ones. Figure 15 illustrates the spectral distribution of irradiance for two visual ranges at an altitude of 1 km.

Finally, Figure 16 presents ratios of irradiance at given altitudes to that at sea level for three visual ranges. This plot is of interest because an irradiance sensor aboard the multispectral aircraft is frequently used in extimating the irradiance at the ground surface. At an altitude of 3 km, there is a difference of about 4% under reasonable clear conditions (V=23 km), a 7% difference under moderate haze conditions (V=8 km), and a 14% difference under dense haze conditions (V=2 km).

11. HOW DOES PATH RADIANCE DEPEND ON THE ATMOSPHERIC AND OBSERVATION CONDITIONS?

The path radiance term is important because it is an additive term that tends to mask the transmitted scene radiances. As shown in Figure 17, path radiance is strongly dependent on the haze condition of the atmosphere and on the altitude of the observer.

In a scanning system, the observation path lengthens as the scan angle moves from the nadir. This increased path length results in substantial increases in path radiance as can be seen in Figure 18. For many situations, the path radiance can be an appreciable part of the received signal. The peak value seen on the V=2 km curve is at $\theta = 60°$, the antisolar angle. That is, the observer is looking directly away from the sun. Figure 19 illustrates the change in shape that occurs when other solar zenith angles are considered.

A fourth graph, Figure 20, clearly illustrates the interesting fact that the path radiance depends substantially on the albedo (diffuse reflectance) of the ground surface.

12. HOW CAN THE RADIATIVE TRANSFER MODEL HELP ONE UNDERSTAND THE EFFECTS OF THE ATMOSPHERE ON IMAGE CONTRASTS?

Investigators have often used a quantity called contrast transmittance to describe the manner in which the atmosphere reduces contrasts in imagery. The contrast between a target material and its background is usually defined to be:

$$C(h) = \frac{L_t(h) - L_b(h)}{L_b(h)}$$

where $L_t(h)$ is the target radiance at altitude h, and $L_b(h)$ is the corresponding background radiance. Recall that, from Equation 2, we have

$$L_b(h) = L_{I_b}(0)T(h) + L_p(h)$$

and

$$L_t(h) = L_{I_t}(0)T(h) + L_p(h).$$

Contrast transmittance is defined as the ratio of the contrast, C(h), at any altitude to that at sea level, C(0). Thus,

$$T_c(h) = \frac{C(h)}{C(0)} = \frac{L_{I_b}(0)T(h)}{L_{I_b}(0)T(h) + L_p(h)}$$

which reduces to:

$$T_c(h) = \frac{1}{1 + \frac{L_p(h)}{L_{I_b}(0)T(h)}}$$

where

$$L_{I_b}(0) = \frac{\rho_b}{\pi} \tilde{E}_{-}(0)$$

ρ_b = background albedo (diffuse reflectance) and $\tilde{E}_{-}$ = total downward irradiance. Note that T_c can be defined either spectrally or over a band of wavelengths, and also that it is independent of the target characteristics.

Calculations of contrast transmittance were made using quantities generated with our radiative transfer model for a variety of atmospheric and observation conditions. One normally sees plots of contrast transmittance versus altitude for various atmospheric conditions (visual ranges) as shown in Figure 21 for a wavelength of 0.55 μm. For a fixed altitude of 3 km, the spectral dependence of contrast transmittance in Figure 22 reveals the influence of the reflectance spectrum of the green vegetation background surface considered.

A useful presentation of contrast transmittance versus visual range is made in Figure 23 for several altitudes. Note there is little difference in contrast transmittance at a given altitude for visual ranges between 15 and 70 km; the dependence on visual range is greatest at short visual ranges.

Another interesting graph, Figure 24, shows the dependence of contrast transmittance on the solar zenith angle. There is a surprisingly strong dependence caused by the increase in path radiance that occurs as the solar zenith angle approaches 0° and the decrease in surface irradiance that occurs for low sun angles.

Up to this point, all contrast transmittance plots have been made for a green vegetation background. Figure 25, illustrates the dependence of contrast transmittance on the diffuse background reflectance (i.e., albedo). This type of plot can be misleading since T_c becomes zero for a background reflectance of zero while, on the other hand, C(0), the contrast being transmitted, becomes infinite according to its definition. This points out the fact that the investigator must consider both the inherent contrast in the scene and the contrast transmittance in his interpretation and analysis.

13. WHAT IS THE PRACTICAL UTILITY OF OUR RADIATIVE TRANSFER MODEL?

As mentioned earlier, a radiative transfer model which properly accounts for the characteristics of a real atmosphere will be an extremely useful tool for engineers and scientists involved in the many aspects of remote sensing, from system design to data analysis and interpretation.

A thorough understanding of the effects of the atmosphere on the radiation available for detection under the wide range of atmospheric conditions that may exist will permit the design of new and better remote sensing systems. For data being gathered with presently existing systems, such a model will provide a means for identifying and possibly reducing the deleterious effects of atmospheric scatter. Also, hypotheses which have been offered to explain effects noticed in the analysis of remotely sensed data can be verified or rejected. An example of the latter use of the radiative transfer model is described briefly in the next few paragraphs.

An interesting and perhaps significant effect was noticed while processing and analyzing a set of airborne multispectral data which was gathered under hazy atmospheric conditions*. It was

---

* A more detailed discussion than that given here can be found in [16].

determined that, under certain circumstances, the radiance spectrum being sensed from small objects at the receiver assumed the spectral characteristics of surrounding objects, that is, objects not in the receiver's instantaneous field of view (IFOV). The resulting signals therefore were not representative of the objects appearing within the IFOV. It is clear that this situation, whenever it might arise, would seriously reduce the accuracy of automatic recognition processing since the signature of each class of objects would vary depending on the background in which it was found.

As a part of the investigation, an attempt was made to extract a quantitative measure of the spectral path radiance existing at the time of data collection. This was accomplished by utilizing data gathered over a set of spectrally neutral (gray) reflectance panels which were placed in the scene. Having measured the reflectance of the panels in the laboratory and extracted the voltage generated when viewing them from the air, it was possible to construct a voltage-reflectance transfer curve in each of the airborne scanner spectral bands. An extrapolation of each of those curves was carried out and the voltage intercept corresponding to zero reflectance was determined. Those voltages were interpreted as resulting from viewing an object having zero reflectance. Therefore, the radiance associated with the zero reflectance voltage in each spectral band did not emanate from objects on the ground which were within the receiver IFOV.

Using sources of standard radiance in the scanner, it was possible to calibrate voltages in terms of radiance and to convert the zero reflectance voltages to path radiance values. The path radiance spectrum so computed is illustrated in Figure 26 where the vertical lines indicate the range of uncertainty due to scanner system noise. The shape of the distribution illustrated, which has a peak in the green portion and a maximum in the near-infrared portion of the spectrum was initially somewhat of a surprise. It was expected that the primary source of path radiance would result from the direct scattering of solar radiation into the receiver. However, if this were the case, the path radiance spectrum would have exhibited a maximum at considerably shorter wavelengths in the region where the solar spectrum peaks. This was certainly not true here and in fact the resulting path radiance spectrum looked suspiciously like a reflectance spectrum for green vegetation.

Since the reflectance panels were placed in a grassy area, several hypotheses which could explain the computed radiance spectrum were explored in detail. It was finally determined that a single hypothesis best explained the computed radiance spectrum; namely that radiation from nearby objects outside the receiver's IFOV (in this case grass) was being scattered into the receiver.

As a check on this hypothesis, our radiative transfer model was employed to calculate the expected path radiance spectrum under low visibility conditions when viewing a spectrally neutral object in a background of green vegetation. Although the atmospheric conditions existing during the time of data collection were rapidly varying and could not be accurately specified it was believed that the plausibility of the hypothesis could still be determined. The results of the model calculations are illustrated in Figure 27 for a 1-km altitude. Here again, the path radiance spectra exhibited local maxima at 0.55 and 0.80 μm thereby lending credence to the hypothesis.

An additional effect was noted during the analysis of the multispectral scanner data gathered on the same day. These data were gathered over an agricultural area at several flight altitudes to enable an empirical determination of the effect of flight altitude on the radiance spectra received when viewing objects of interest to the agricultural community. The mean radiance spectra received at flight altitudes of 1000 and 5000 feet for a field of bare soil and a field of soybeans are depicted in Figures 28 and 29. The interesting effect here is that while the entire 1000 ft. radiance spectrum for bare soil lies below the 5000 ft. spectrum this is not the case for the radiance spectra received when viewing the soybean field. For the soybean field, in the spectral bands centered at 0.71 and 0.80 μm, the spectral radiance received at 1000 ft. exceeds that received at 5000 ft.

Although the existence of such an effect was satisfactorily explained in a qualitative manner, the specific results could have been predicted through the use of the radiative transfer model. Figure 30 illustrates the spectral radiance computed using the radiative transfer model for viewing a small object having a reflectance of 8% surrounded by a background of green vegetation and an extended background of green vegetation. The results seen here are similar to those evident in Figures 28 and 29.

Hopefully, the examples illustrated above are sufficient to provide an indication of the practical utility of the radiative transfer model. The real advantage of such a model, however, is that it permits investigations of atmospheric effects not only for conditions that do exist during the collection of any particular data set but for conditions that, in the mind of the investigator, might exist at some future time. Because of this, individual parameters may be varied and the effect of their variation determined. From this information insight can be gained

into the results to be expected with present remote sensing systems and improved systems can be designed for the future.

In order to further illustrate the effects of certain parameters, we include in Figures 31 through 35 examples of results calculated of our radiative transfer model. These results demonstrate the variation of transmitted and apparent radiance with altitude, wavelength, and visual range for a variety of conditions.

14. WHAT ARE THE FUTURE DEVELOPMENTS OF THE RADIATIVE TRANSFER MODEL?

Having accounted for the main characteristics of radiative transfer in Earth's atmosphere, one should now take into consideration more subtle effects such as the following:

(1) Influence of background reflectance on target radiance as a result of atmospheric scattering.

(2) Absorption by aerosols and gases.

(3) Non-Lambertian surfaces.

(4) Inhomogeneous atmospheres.

(5) Cloud shadows and radiances of clouds.

(6) Unusual atmospheric conditions.

The influence of background reflectance on target radiance has been suspected for some time and this can seriously affect recognition processing of multispectral scanner data. Thus, a two-dimensional formulation of the radiative transfer problem is necessary to understand such phenomena.

Absorption by aerosols is usually negligible in the visible spectral region but can be of some importance in the near infrared. Ozone absorption is of some importance near 0.6 μm and the concentration varies significantly with altitude. Absorption by other gases is negligible in the visible region.

It is commonly assumed that most natural surfaces can be approximated by Lambertian surfaces, but there do exist cases in which this assumption breaks down. Thus, it is of some importance to be able to model surface features with a general bidirectional reflectance.

Inhomogeneous atmospheres can be modeled by assuming atmospheric layers. This should be done, especially for the inclusion of ozone absorption.

The presence of clouds can alter the radiance on a given target by either its own radiance contribution or by its shadowing effect. Thus, a two-or three-dimensional formulation of the radiative transfer problem is needed.

Finally, unusual atmospheric conditions can be studied by varying the aerosol density vertical profile. Thus, weather phenomena can be simulated under a wide range of conditions.

With these refinements included in an advanced model, there will result a considerable improvement in our ability to account for variations in scanner data which result from the scattering and absorption of radiation by Earth's atmosphere.

REFERENCES

1. Lowman, P.D. Jr., (1968) Space Panorama, WELTFLIGBILD, R.A. Muller, Fieldmeilen/Zurich, Switzerland.

2. Rayleigh, J.W.S., (1881), The Theory of Sound, Phil. Mag. 41 (1871) 274, 447; 47 (1899), 375.

3. Menzel, D.H. (1966) Selected Papers on the Transfer of Radiation, Dover Publications, Inc., New York, N.Y.

4. Chandrasekhar, S., (1960) Radiative Transfer, Dover Publications, Inc., New York, N.Y.

5. Coulson, K.L., Dave, I.V., and Sekera, Z., (1960) Tables Related to Radiation Emerging from a Planetary Atmosphere with Rayleigh Scattering, Univ. of California Press, Berkeley, California.

6. Sekera, Z., and Kahle, A.B., (1966), Scattering Function for Rayleigh Atmospheres of Arbitrary Thickness. The RAND Corporation, R-452-PR, Santa Monica, California.

7. Sweigart, A.B., (1970) Radiative Transfer in Atmospheres according to the Rayleigh Phase Function with Absorption, Ap. J. Suppl. 22, no. 182.

8. Pymat, A.A., and Abhyankar, F.D., (1969) Theory of Radiative Transfer in Inhomogeneous Atmospheres, I. Perturbation Method. Ap. J. 158, 315.

9. Mullikin, T.W., (1965) Multiple Scattering in Homogeneous Plane-Parallel Atmospheres, The RAND Corporation Memorandum RM-4846-PR.

10. Deirmendjian, D., (1969) Electromagnetic Scattering on Spherical Polydispersions, American Elsevier Publishing Co., Inc., New York, N.Y.

11. Elterman, L. (1970), Vertical-Attenuation Model with Eight Surface Meteorological Ranges 2 to 13 Kilometers, AFCRL-70-0200, Air Force Cambridge Research Laboratories, Bedford, Massachusetts.

12. Malila, W.A., Crane, R.B., Omarzu, C.A., and Turner, R.E., (1970) Studies of Spectral Discrimination, University of Michigan, Institute of Science and Technology, Willow Run Laboratories, WRL-31650-22-T.

13. Ivanov, A.I., (1970), Spectral Brightness of the Sky, Atmospheric Optics, N.B. Divari, editor, Consultants Bureau, New York, N.Y.

14. Elterman, L., (1964) Vertical Attenuation Model, 1964, in the Ultraviolet, Visible, and Infrared Regions for Altitudes to 50 km, AFCRL-64-740, Air Force Cambridge Research Laboratories, Bedford, Massachusetts.

15. Elterman, L., (1968), UV, Visible, and IR Attenuation for Altitudes to 50 km, AFCRL-68-0153, Air Force Cambridge Research Laboratories, Bedford, Massachusetts.

16. Nalepka, R.F., Horwitz, H.M., and Thomson, N.S., May 1971, Investigations of Multispectral Sensing of Crops, The University of Michigan, Institute of Science and Technology, Willow Run Laboratories, Report No. WRL-31650-30-T.

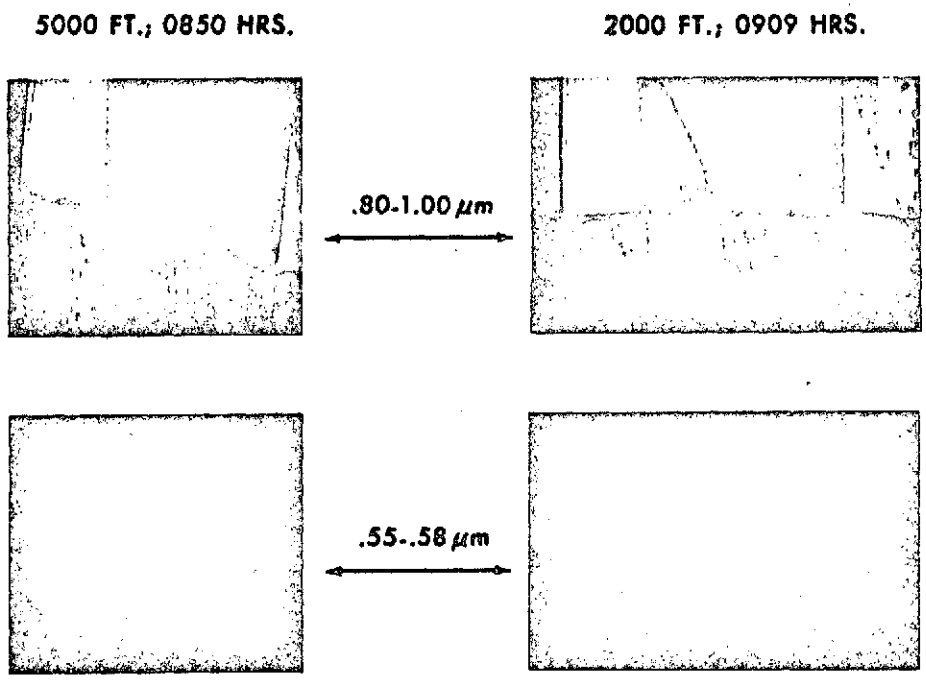

FIGURE 1. EFFECTS OF ATMOSPHERIC BACKSCATTER AS FUNCTIONS OF WAVELENGTH REGION AND ALTITUDE. Agricultural area near Ann Arbor, Michigan; 3 September 1969.

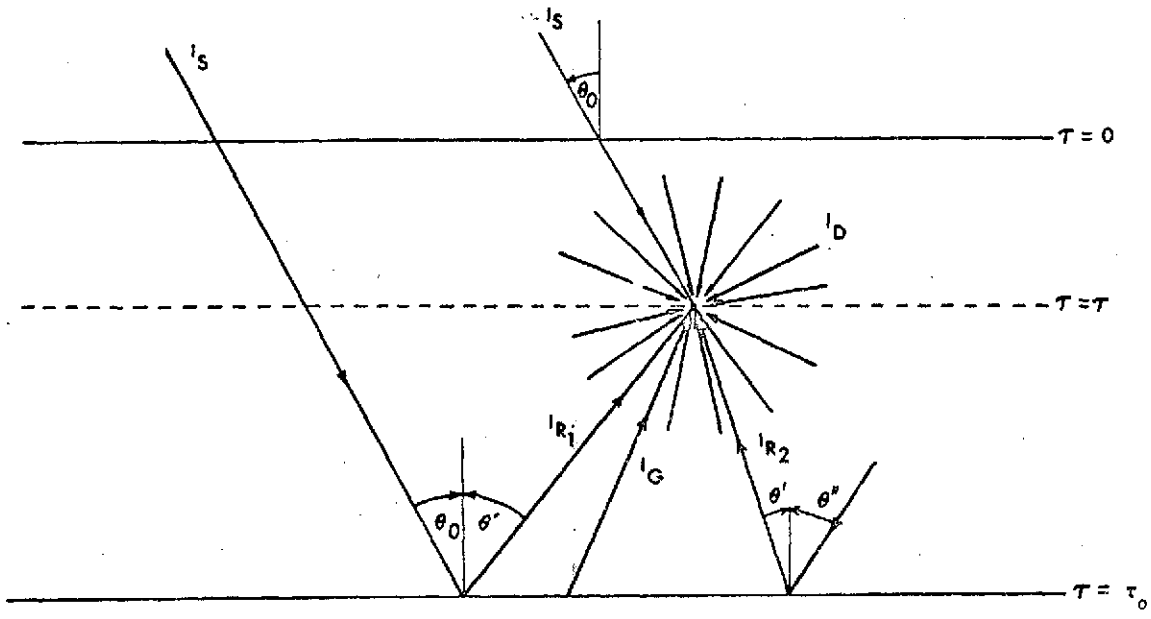

FIGURE 2. CONTRIBUTION TO RADIATION FIELD WITHIN EARTH'S ATMOSPHERE. I_S = Solar radiance; I_D = Diffuse radiance; I_{R_1} = Reflected radiance from sun; I_{R_2} = Reflected radiance from atmosphere; I_G = Ground radiance; θ_0 = Solar zenith angle.

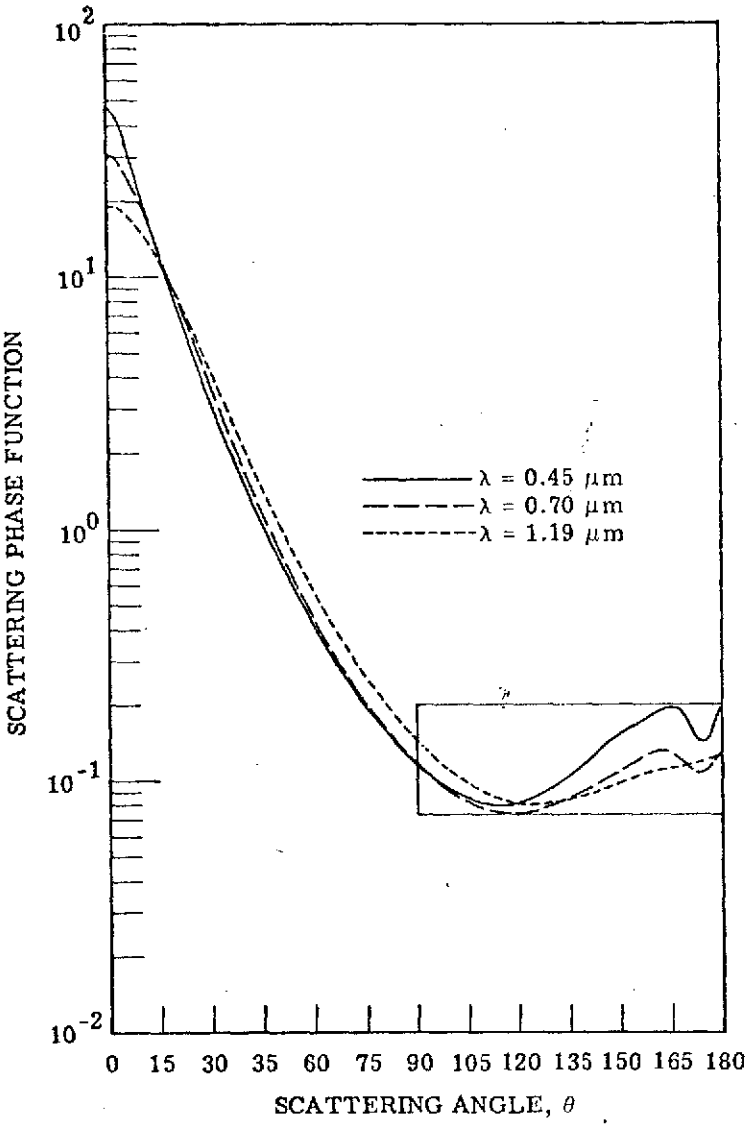

FIGURE 3. SINGLE SCATTERING PHASE FUNCTION FOR DEIRMENDJIAN'S CONTINENTAL TYPE AEROSOL

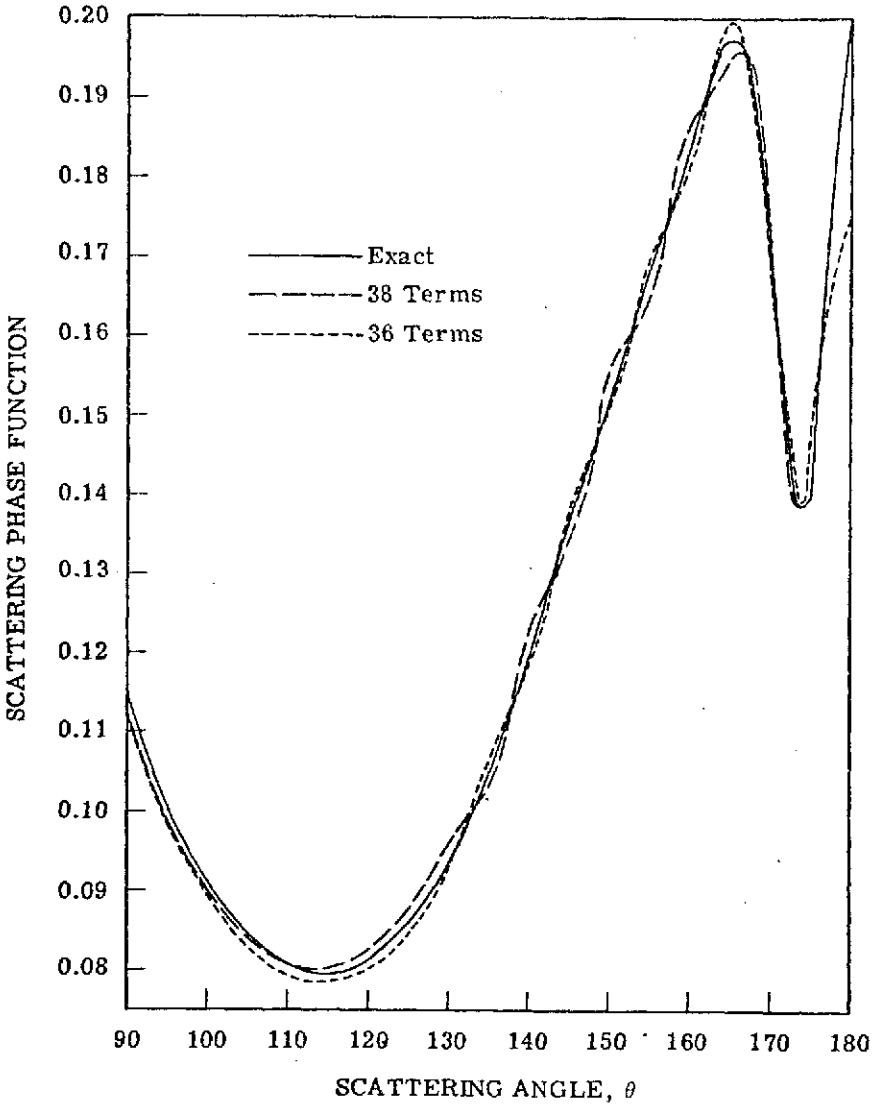

FIGURE 4. COMPARISON BETWEEN EXACT SINGLE SCATTERING PHASE FUNCTION AND APPROXIMATE LEGENDRE SERIES EXPANSION IN THE BACKWARD HEMISPHERE FOR DEIRMENDJIAN'S CONTINENTAL TYPE AEROSOL. $\lambda = 0.45\ \mu m$.

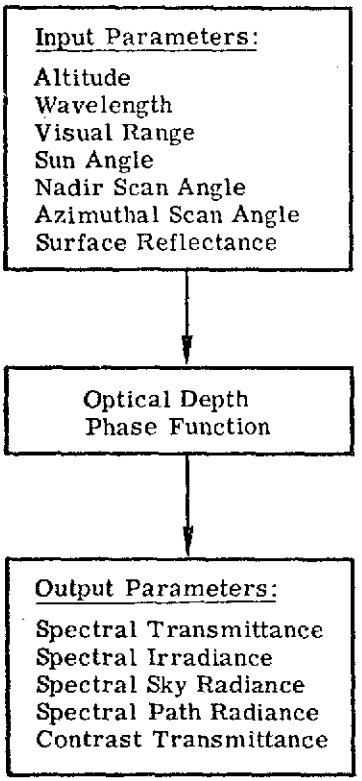

FIGURE 5. THE UNIVERSITY OF MICHIGAN, RADIATIVE TRANSFER MODEL FOR HAZY ATMOSPHERES

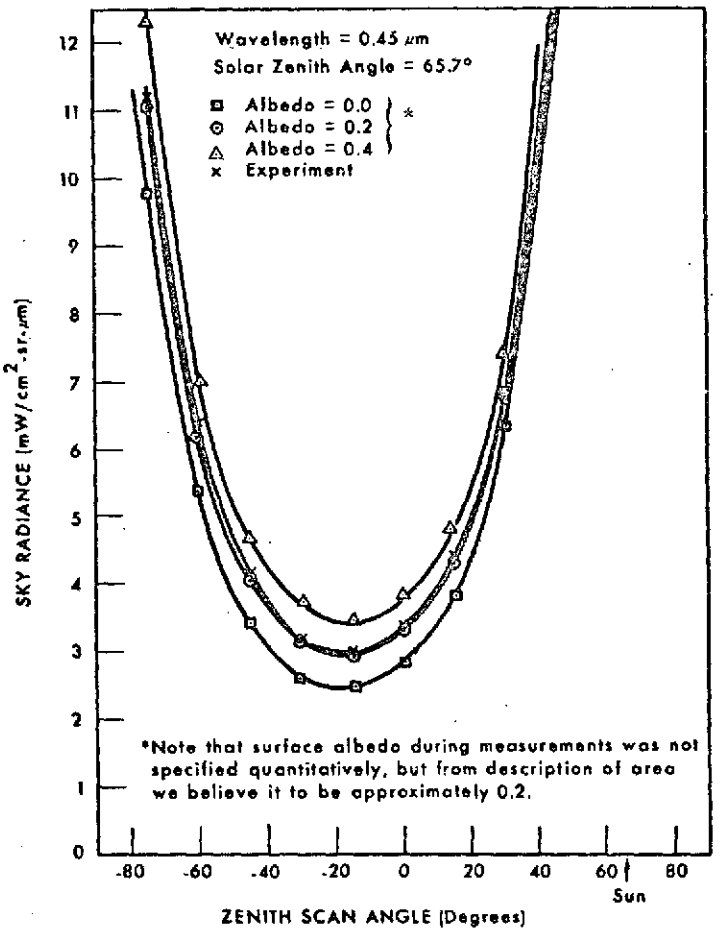

FIGURE 6. DEPENDENCE OF SKY RADIANCE ON ZENITH ANGLE IN SOLAR PLANE FOR CLEAR SKY CONDITIONS

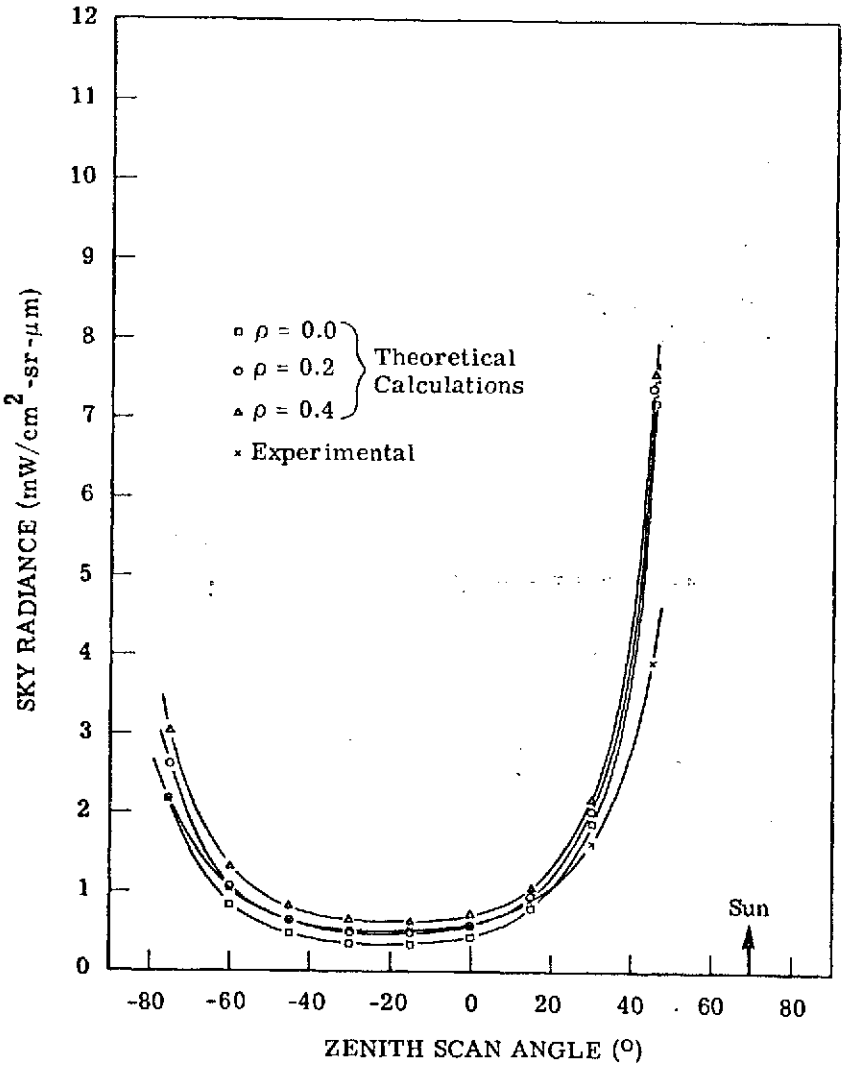

FIGURE 7. DEPENDENCE OF SKY RADIANCE ON ZENITH ANGLE IN SOLAR PLANE FOR CLEAR SKY CONDITIONS. Wavelength = 0.70 μm; solar zenith angle = 69.6°.

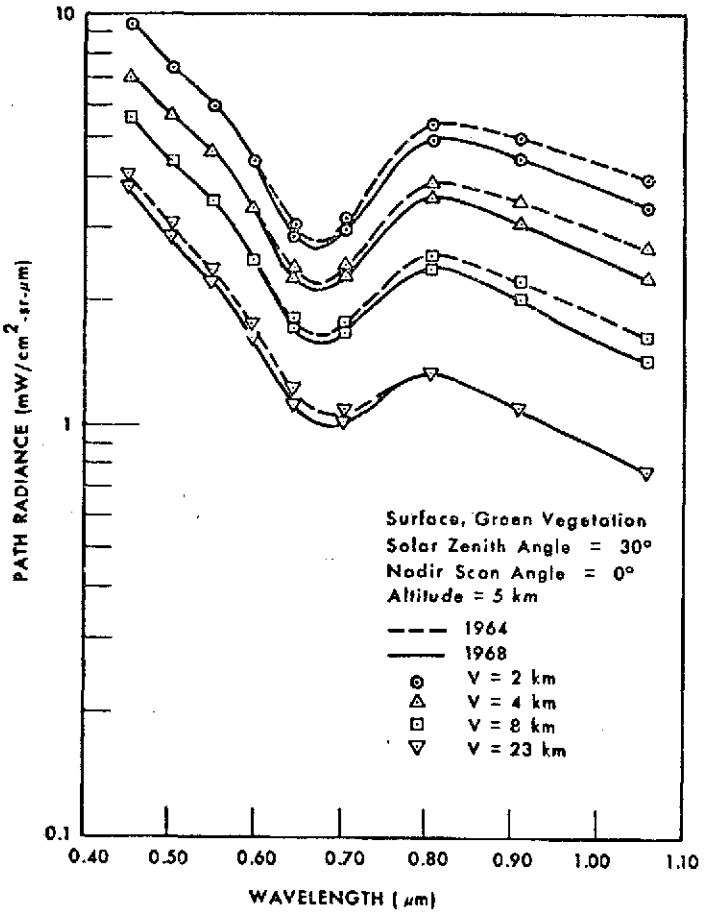

FIGURE 8. DEPENDENCE OF SPECTRAL PATH RADIANCE ON VISUAL RANGE FOR DIFFERENT STRATOSPHERIC AEROSOL DISTRIBUTIONS

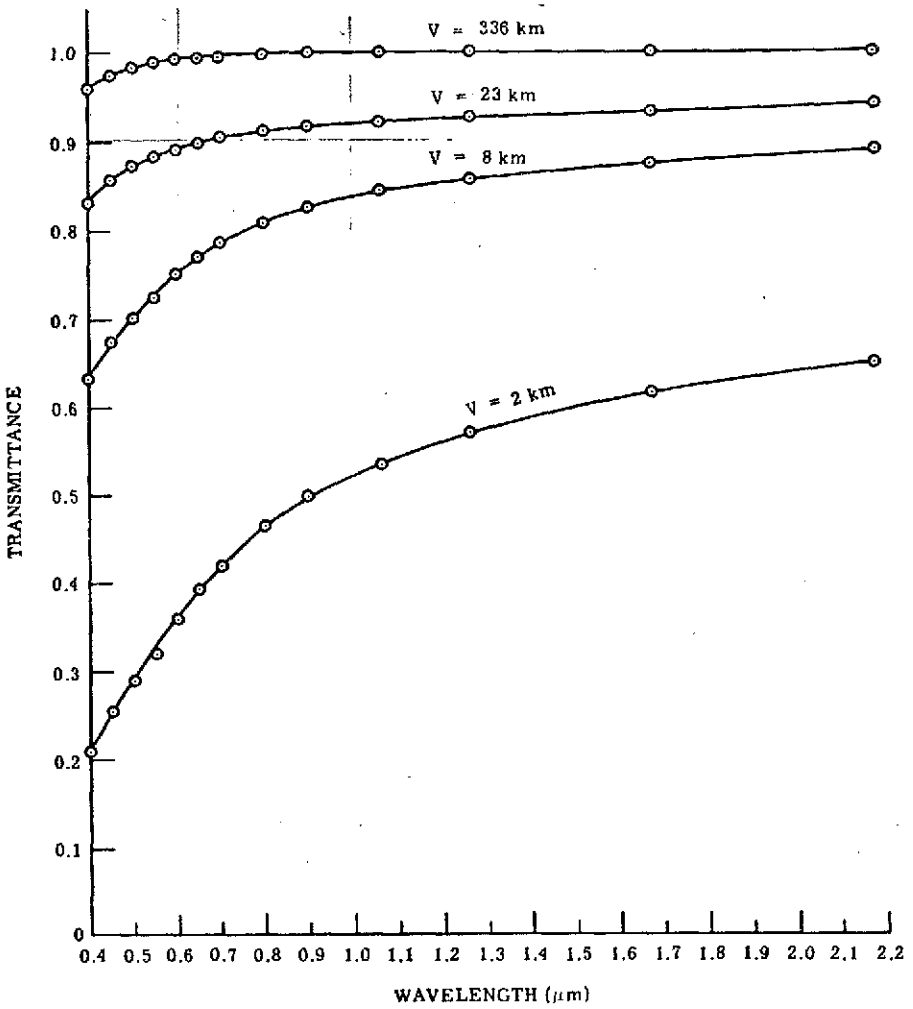

FIGURE 9. SPECTRAL DEPENDENCE OF ATMOSPHERIC TRANSMISSION FROM THE SURFACE TO AN ALTITUDE OF 1 km FOR A NADIR SCAN ANGLE OF 0°

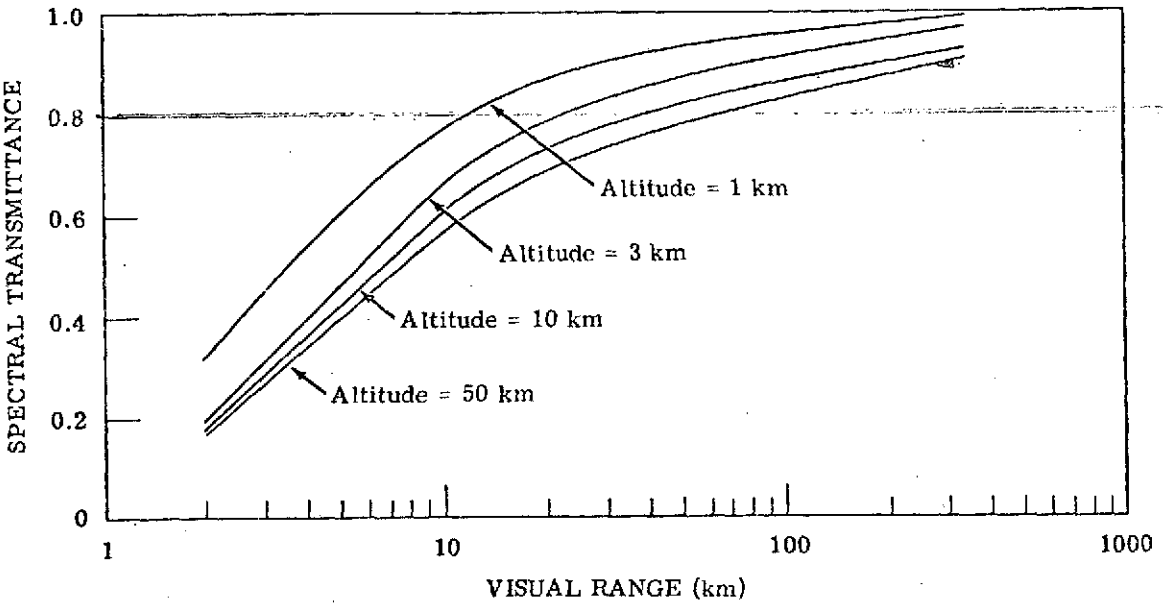

FIGURE 10. DEPENDENCE OF TRANSMITTANCE ON VISUAL RANGE FOR VARIOUS ALTITUDES. Wavelength = 0.55 μm; nadir scan angle = 0^{o}.

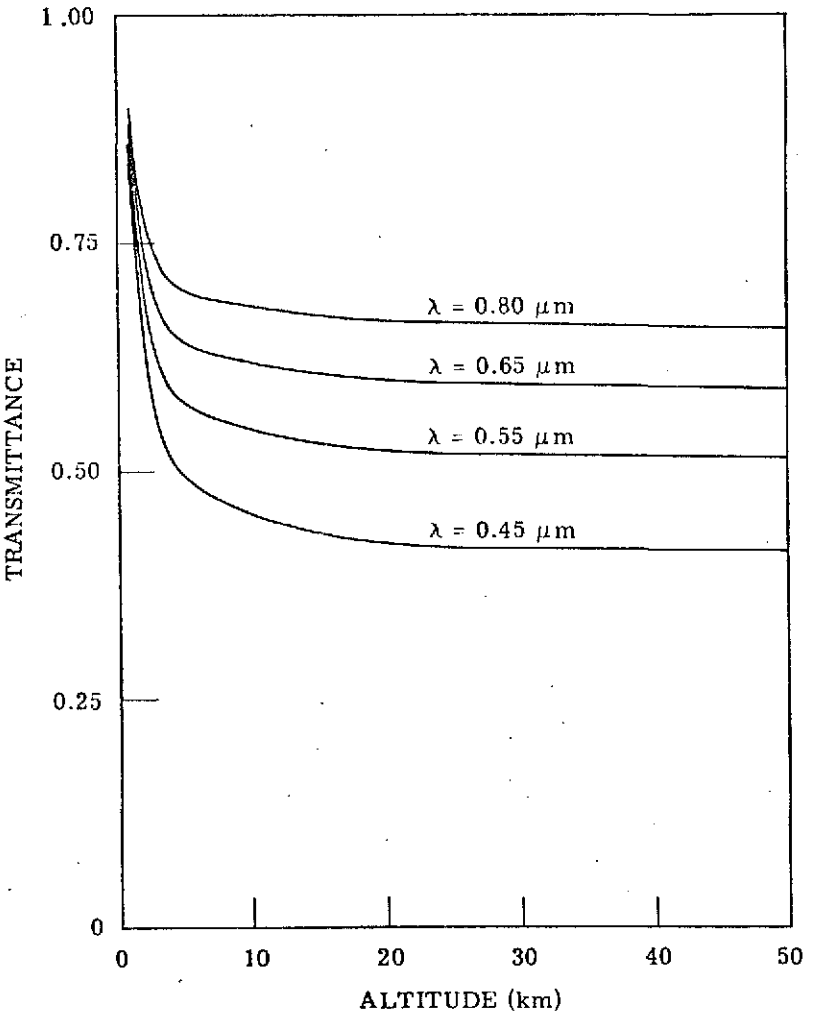

FIGURE 11. DEPENDENCE OF TRANSMITTANCE ON ALTITUDE FOR VARIOUS WAVELENGTHS. Visual range = 8 km; nadir scan angle = 0^{o}.

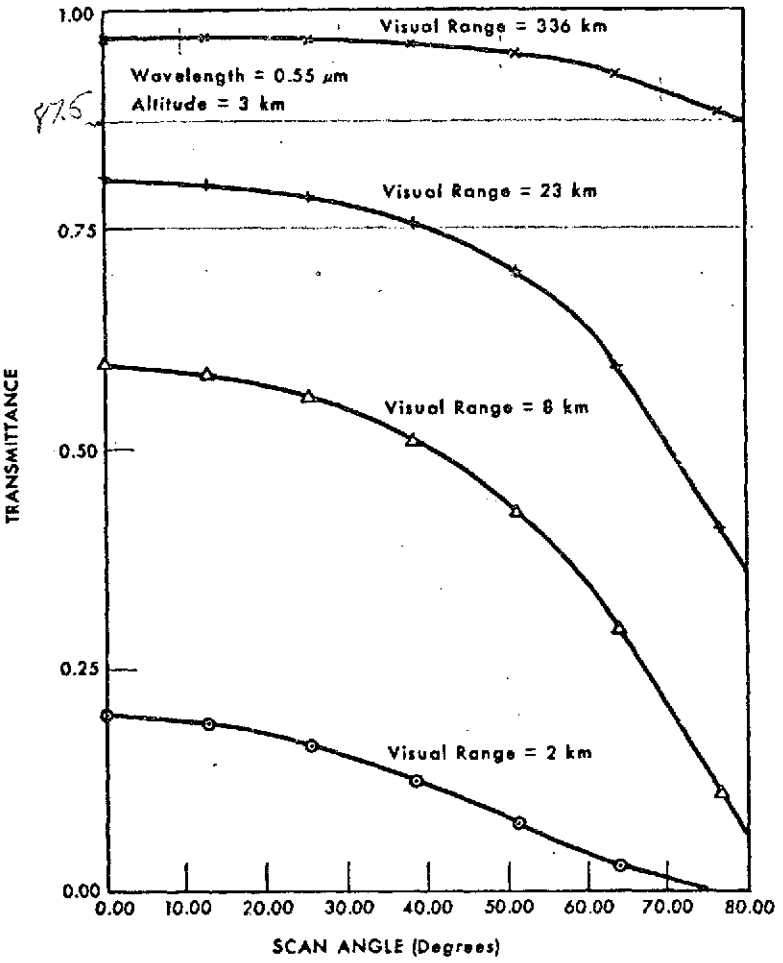

FIGURE 12. DEPENDENCE OF TRANSMITTANCE ON NADIR SCAN ANGLE FOR VARIOUS VISUAL RANGES

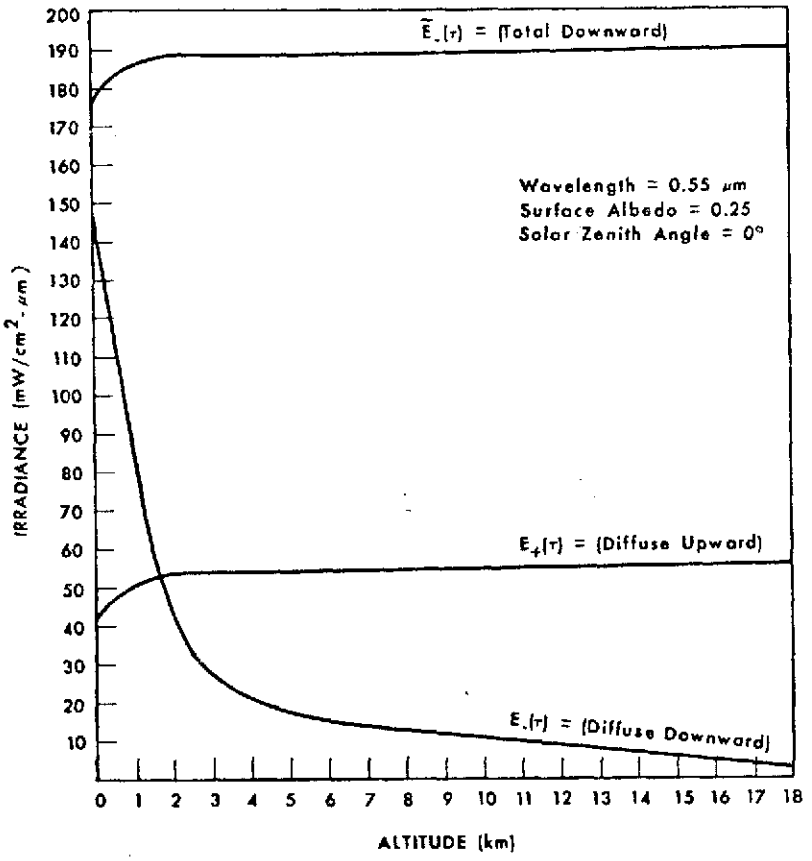

FIGURE 13. DEPENDENCE OF IRRADIANCE ON ALTITUDE — VISUAL RANGE = 2 km AND SURFACE ALBEDO = 0.25

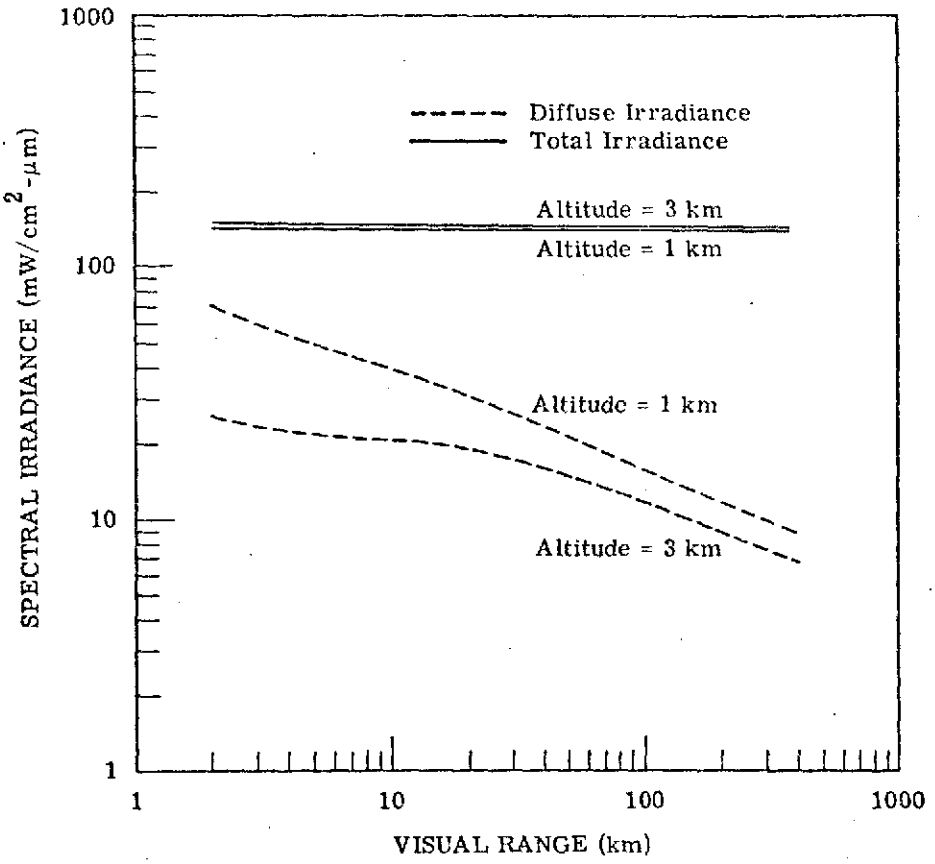

FIGURE 14. DEPENDENCE OF DIFFUSE AND TOTAL IRRADIANCE ON VISUAL RANGE FOR TWO ALTITUDES. Wavelength = 0.55 μm; green vegetation surface; solar zenith angle = 30°.

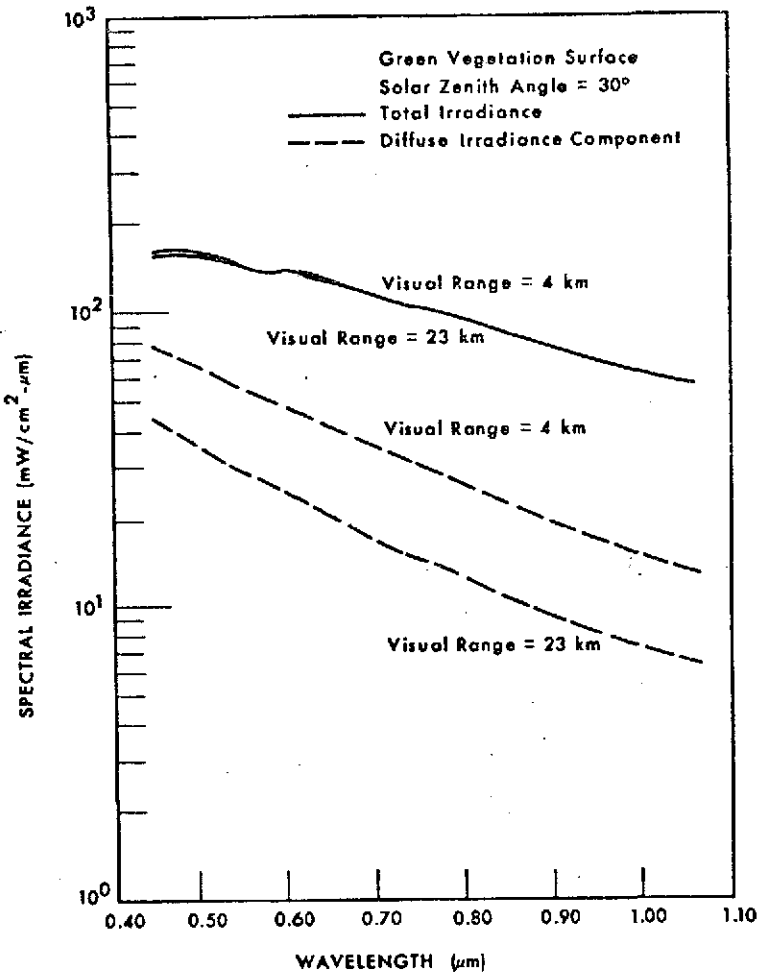

FIGURE 15. DIFFUSE AND TOTAL SPECTRAL IRRADIANCES FOR TWO VISUAL RANGES AT AN ALTITUDE OF 1 KM

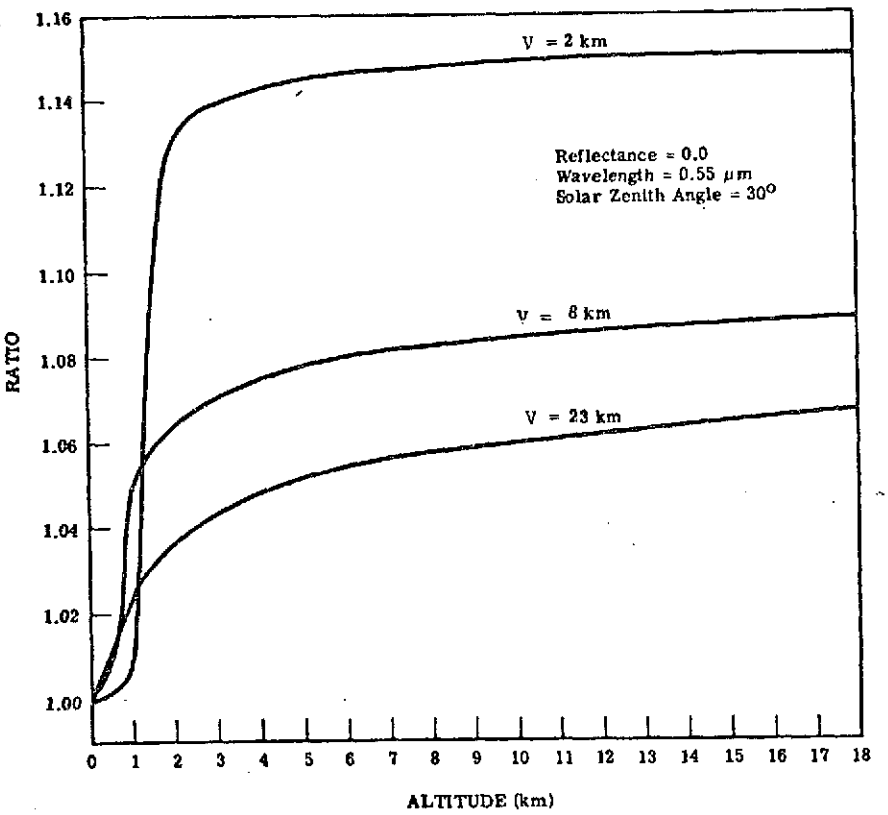

FIGURE 16. ALTITUDE DEPENDENCE OF RATIO OF THE TOTAL DOWNWARD IRRADIANCE AT ALTITUDE h TO THE TOTAL DOWNWARD IRRADIANCE AT THE SURFACE

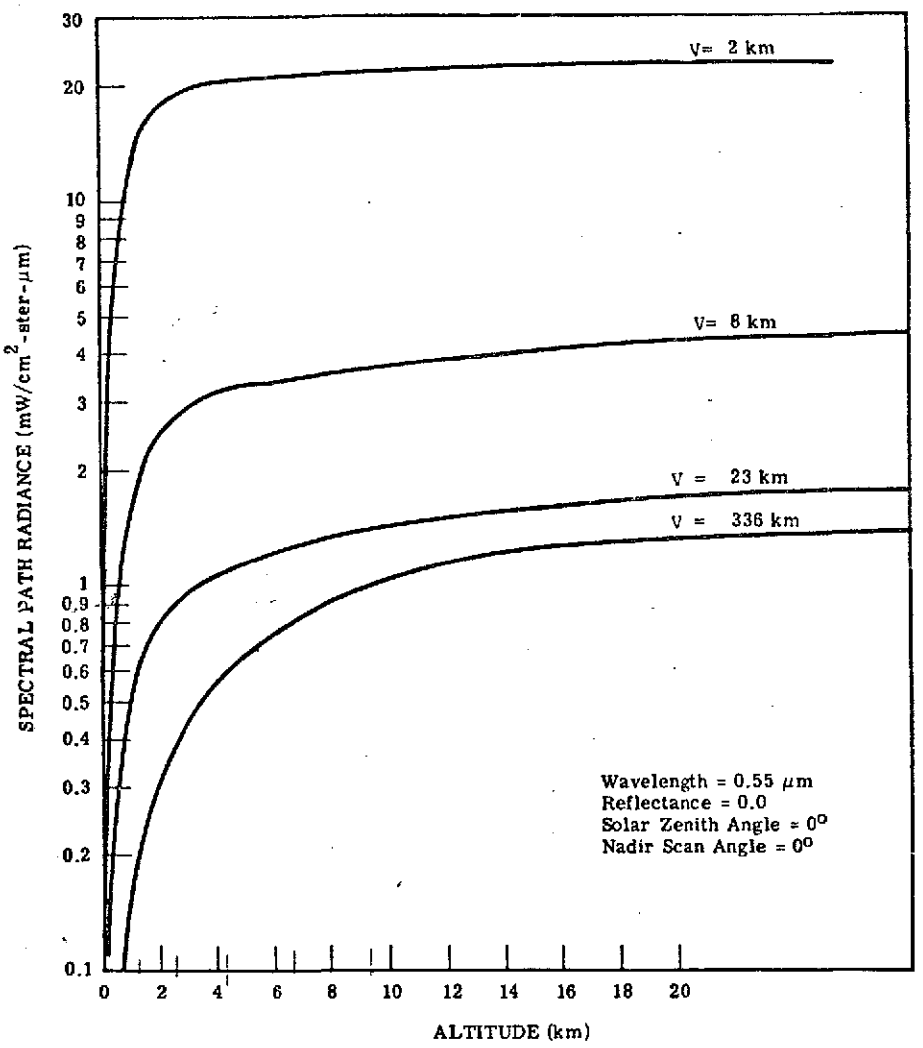

FIGURE 17. ALTITUDE DEPENDENCE OF PATH RADIANCE FOR A HOMOGENEOUS ATMOSPHERE

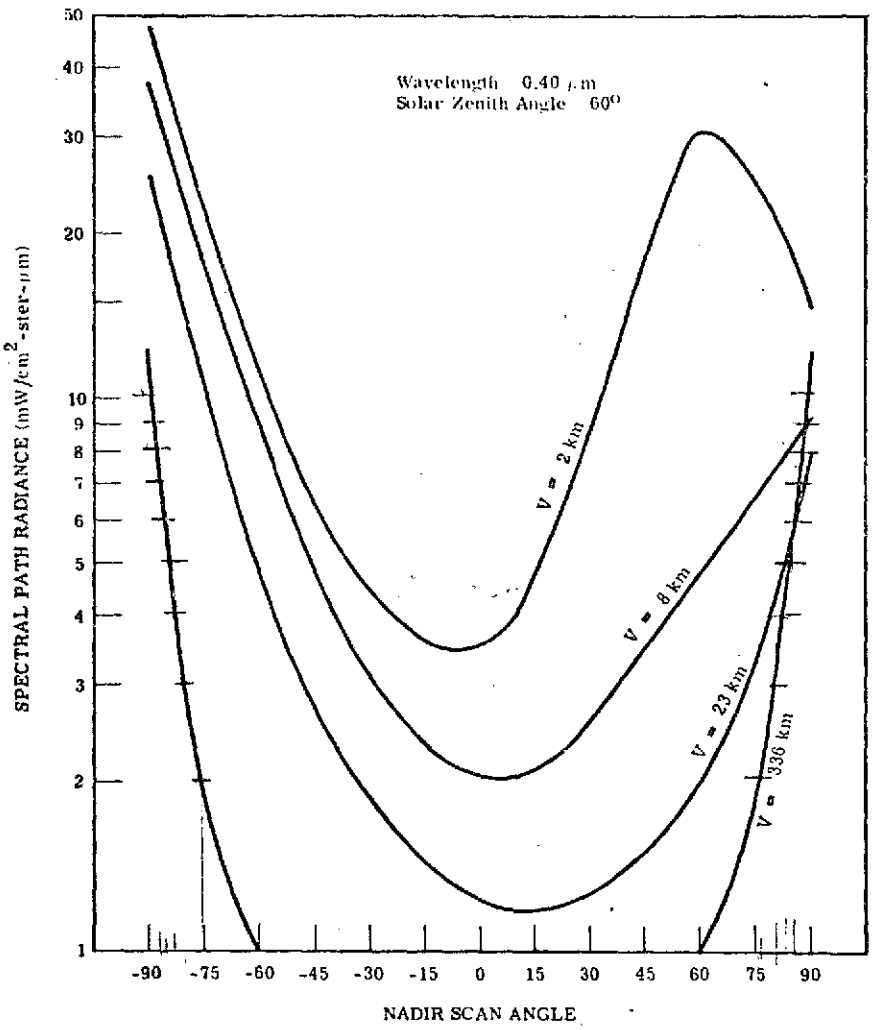

FIGURE 18. DEPENDENCE OF PATH RADIANCE ON NADIR SCAN ANGLE AT AN ALTITUDE OF 1 km FOR A HOMOGENEOUS ATMOSPHERE WITH A REFLECTANCE OF 0.0

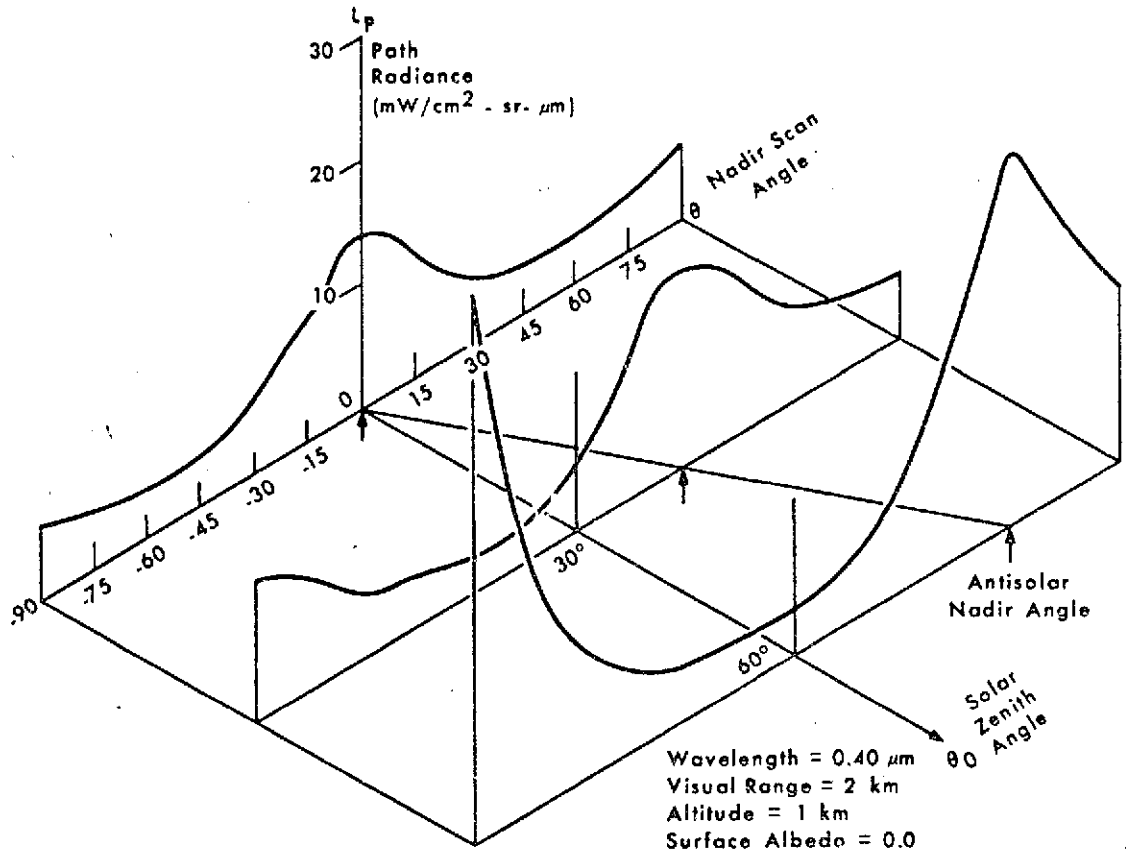

FIGURE 19. PATH RADIANCE VERSUS SCAN ANGLE AND SOLAR ZENITH ANGLE

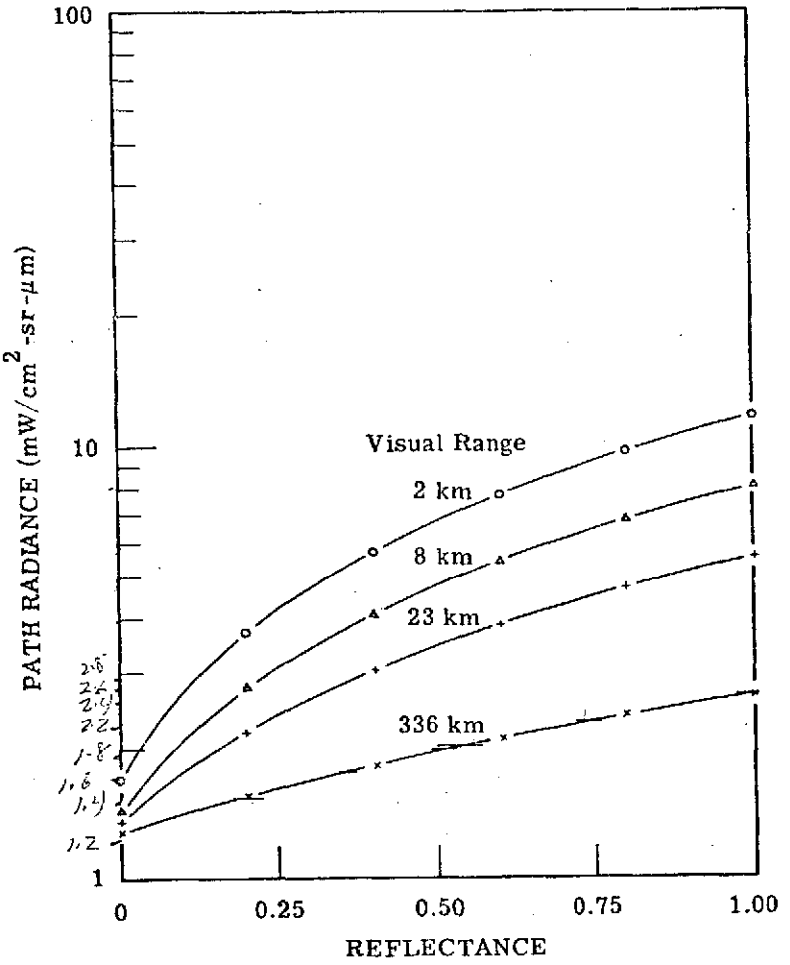

FIGURE 20. DEPENDENCE OF PATH RADIANCE ON DIFFUSE SURFACE REFLECTANCE (ALBEDO). Wavelength = 0.55 μm; solar zenith angle = 55°; nadir scan angle = 0°; altitude = 50 km.

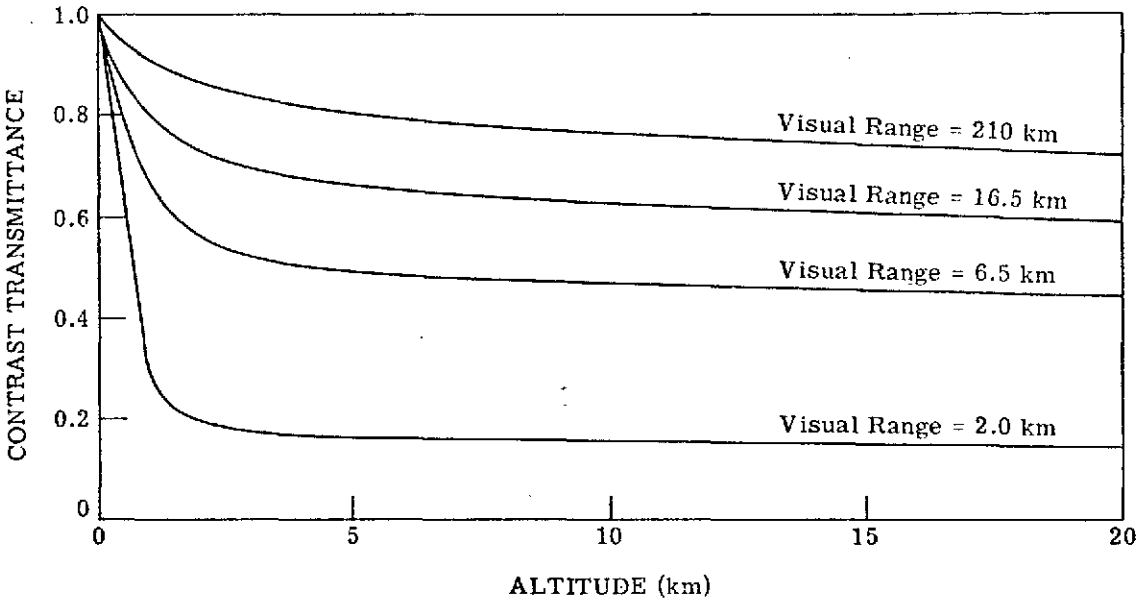

FIGURE 21. DEPENDENCE OF CONTRAST TRANSMITTANCE ON ALTITUDE FOR VARIOUS VISUAL RANGES. Wavelength= 0.55 μm; green vegetation surface; solar zenith angle = 30^{o}; nadir scan angle = 0^{o}; azimuthal angle = 0^{o}.

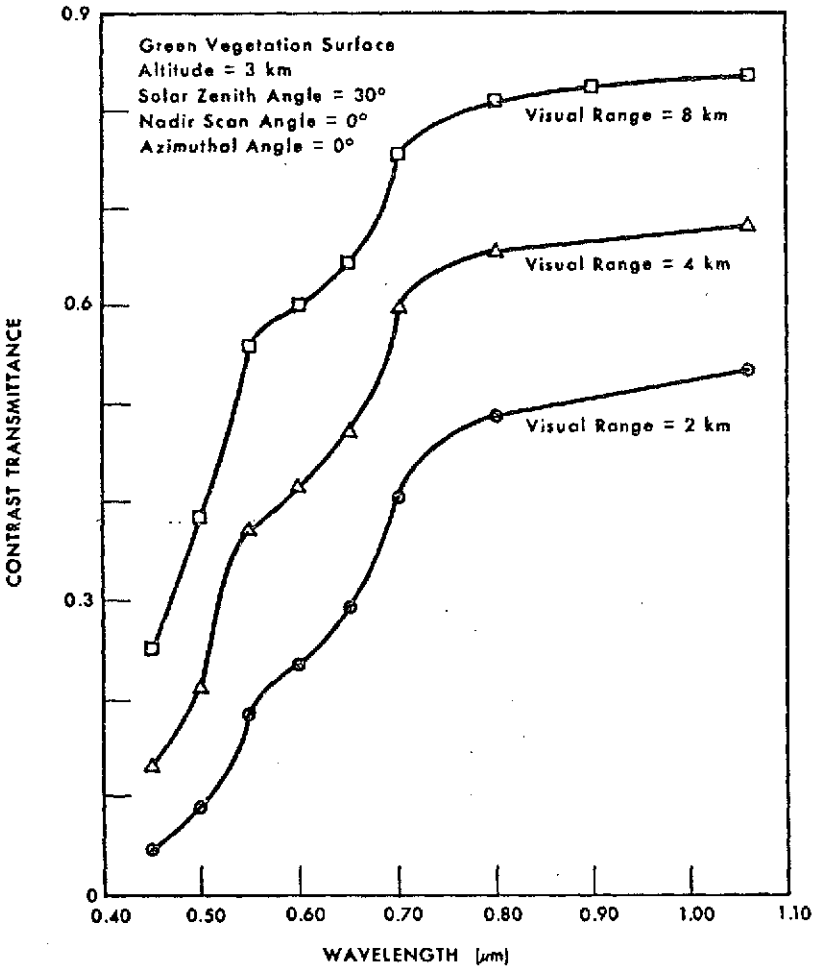

FIGURE 22. DEPENDENCE OF CONTRAST TRANSMITTANCE ON WAVELENGTH FOR VARIOUS VISUAL RANGES

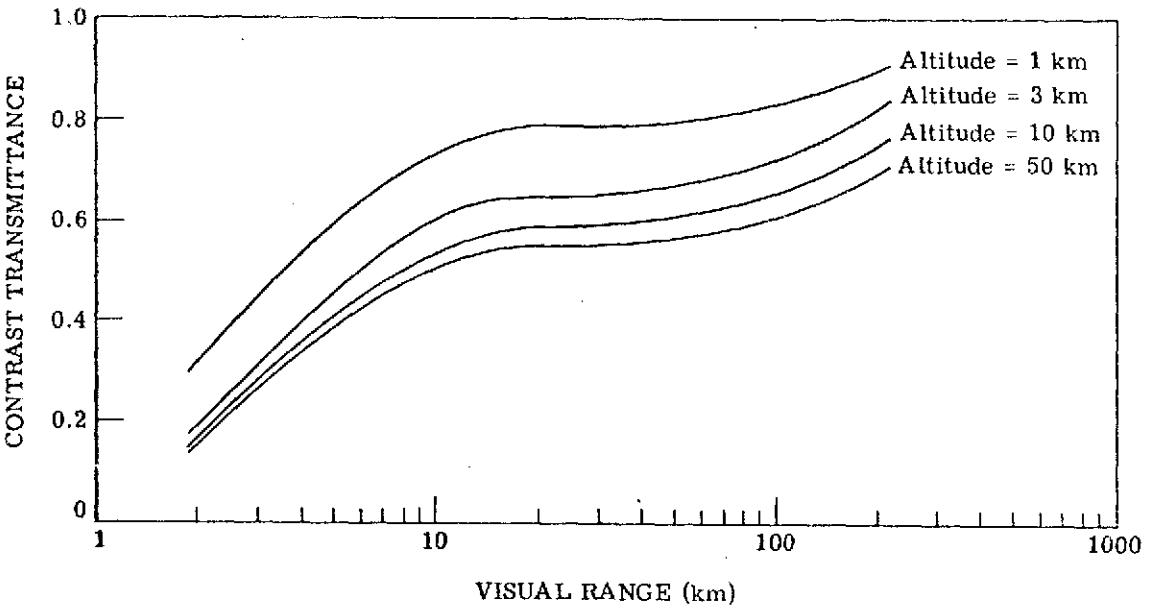

FIGURE 23. DEPENDENCE OF CONTRAST TRANSMITTANCE ON VISUAL RANGE FOR VARIOUS ALTITUDES. Wavelength = 0.55 μm; green vegetation surface; solar zenith angle = 30°; nadir scan angle = 0°; azimuth angle = 0°.

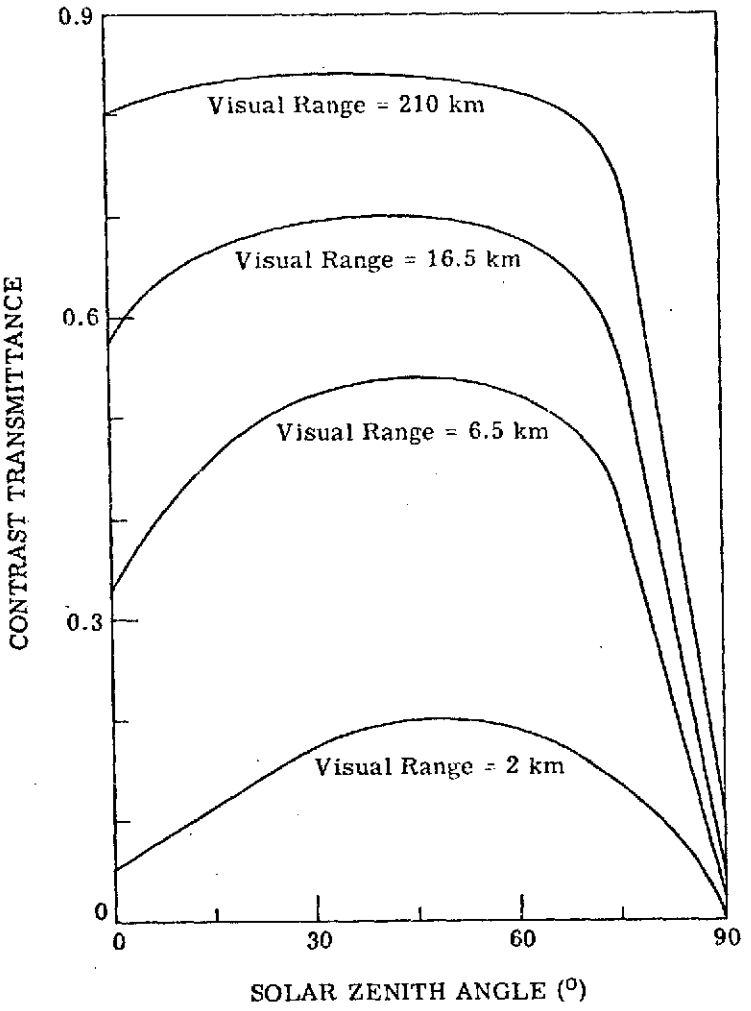

FIGURE 24. DEPENDENCE OF CONTRAST TRANSMITTANCE ON SOLAR ZENITH ANGLE FOR VARIOUS VISUAL RANGES. Wavelength = 0.55 μm; green vegetation surface; altitude = 3 km; nadir scan angle = 0^{o}; azimuthal angle = 0^{o}.

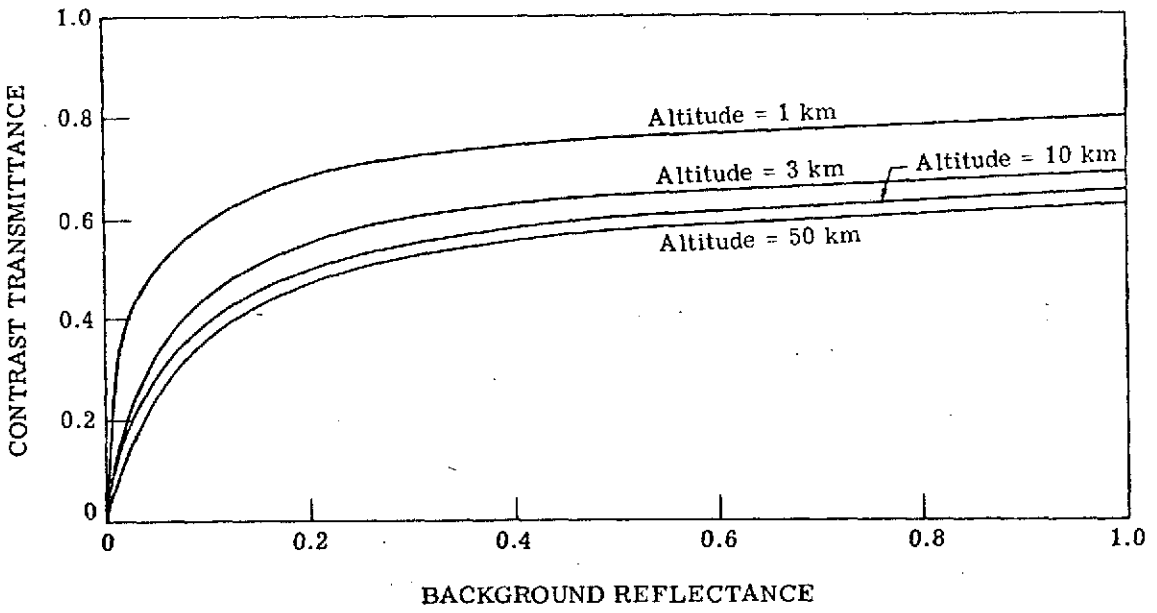

FIGURE 25. DEPENDENCE OF CONTRAST TRANSMITTANCE ON BACKGROUND REFLECTANCE FOR VARIOUS ALTITUDES. Wavelength = 0.55 μm; visual range = 6.5 km; solar zenith angle = 30^{o}; nadir scan angle = 0^{o}; azimuthal angle = 0^{o}.

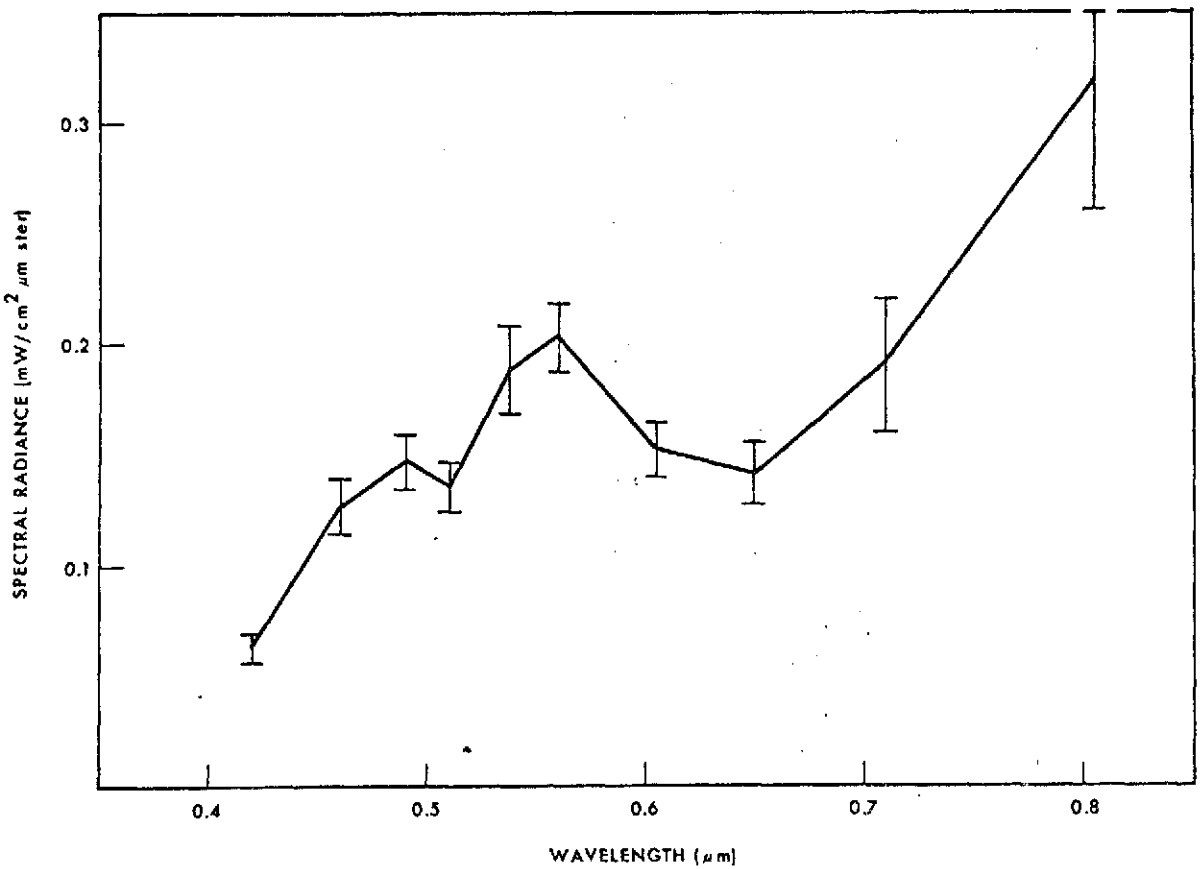

FIGURE 26. PATH RADIANCE SPECTRUM FOR 3 SEPTEMBER 1969, 500 FT. RAMP DATA

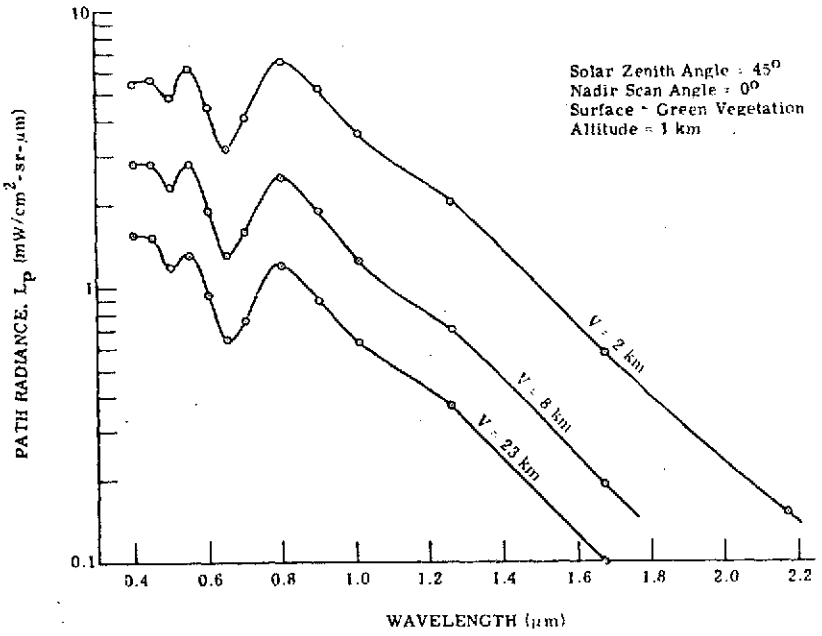

FIGURE 27. PATH RADIANCE (mW/cm^2-sr-μm) VERSUS WAVELENGTH AND VISUAL RANGE

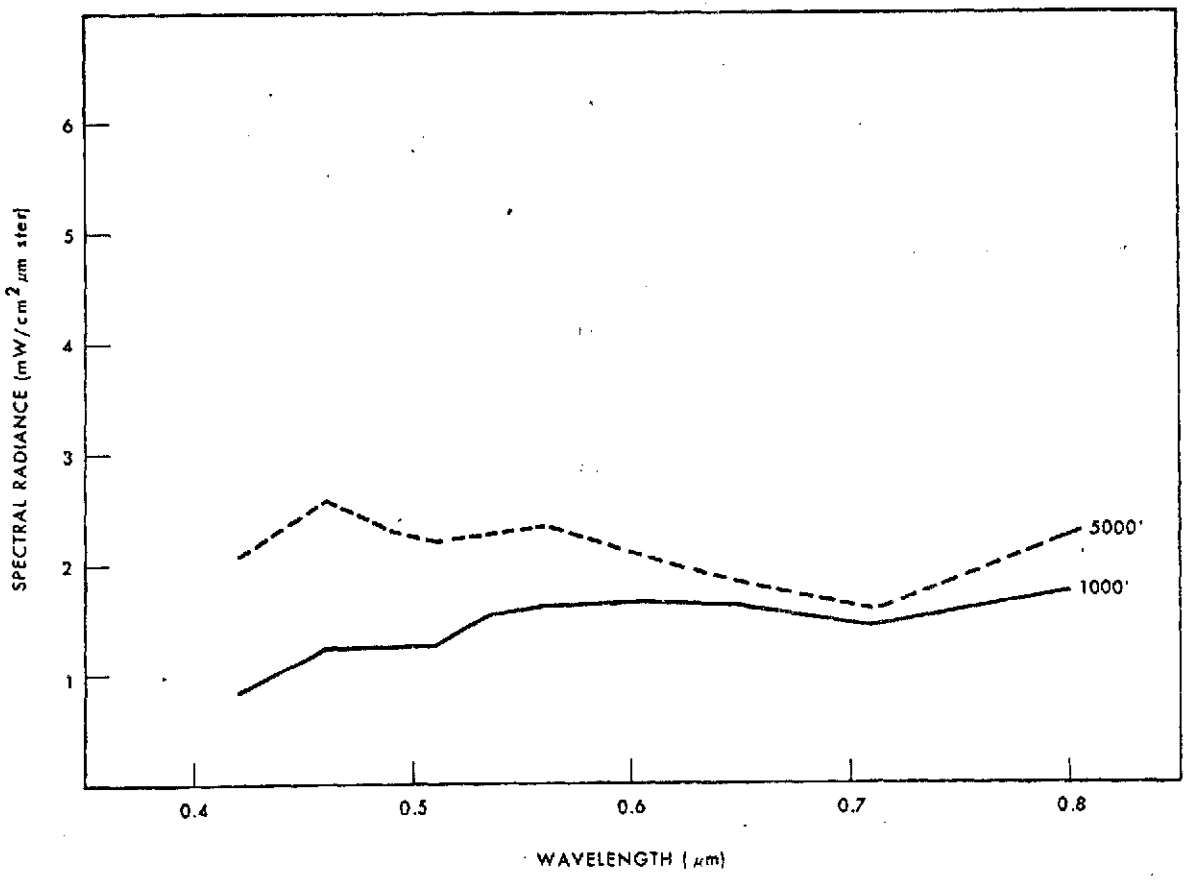

FIGURE 28. MEAN SPECTRAL RADIANCE FROM BARE SOIL FIELD AT 1000 AND 5000 FEET

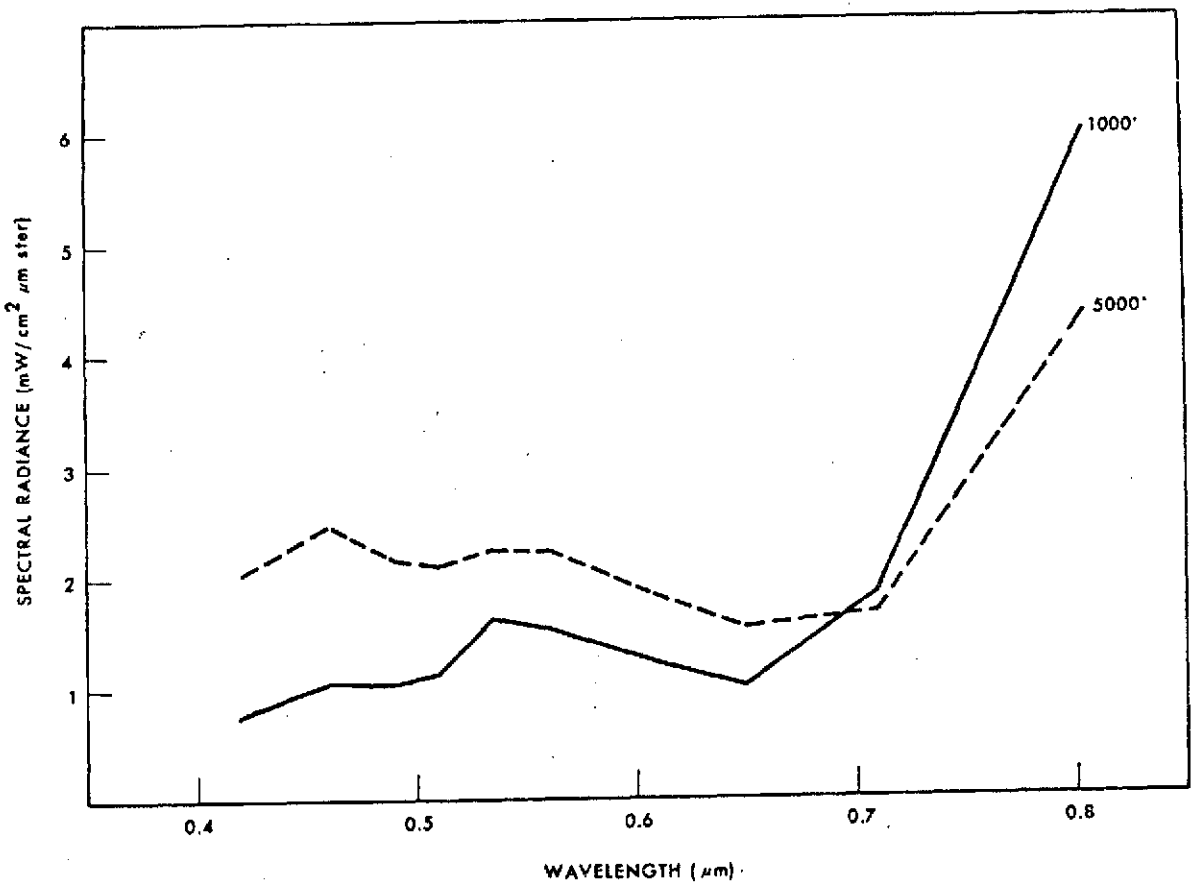

FIGURE 29. MEAN SPECTRAL RADIANCE FROM SOYBEAN FIELD AT 1000 AND 5000 FEET

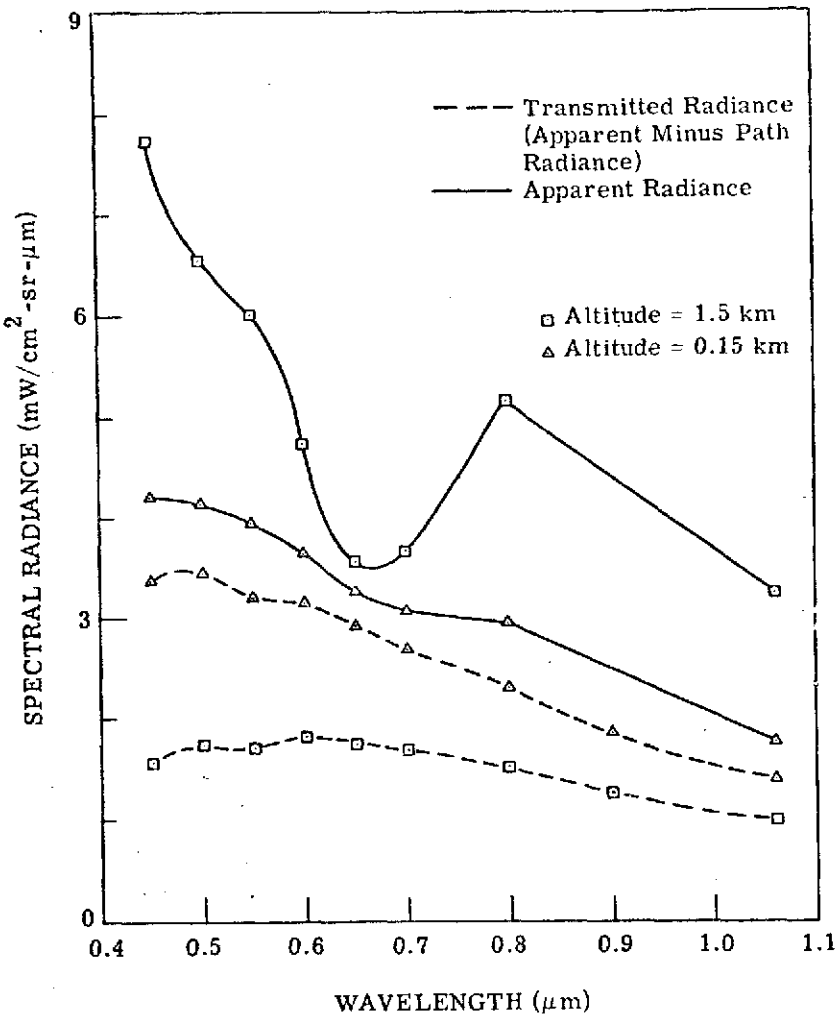

FIGURE 30. APPARENT AND TRANSMITTED TARGET SPECTRAL RADIANCES FOR TWO ALTITUDES. Visual range = 4 km; background surface, green vegetation; target surfaces, ρ = 0.08; solar zenith angle = 30°; nadir scan angle = 0°; azimuthal angle = 0°.

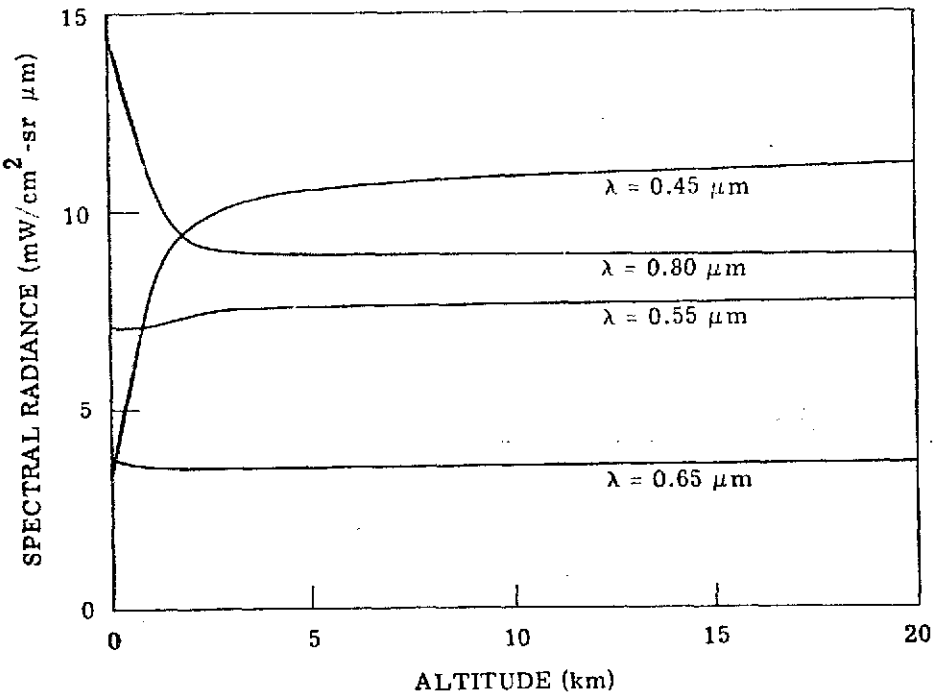

FIGURE 31. ALTITUDE DEPENDENCE OF SPECTRAL RADIANCE AT DETECTOR FROM GREEN VEGETATION BACKGROUND FOR SEVERAL WAVELENGTHS. Visual range = 2 km; solar zenith angle = 30°; nadir scan angle = 0°; azimuthal angle = 0°.

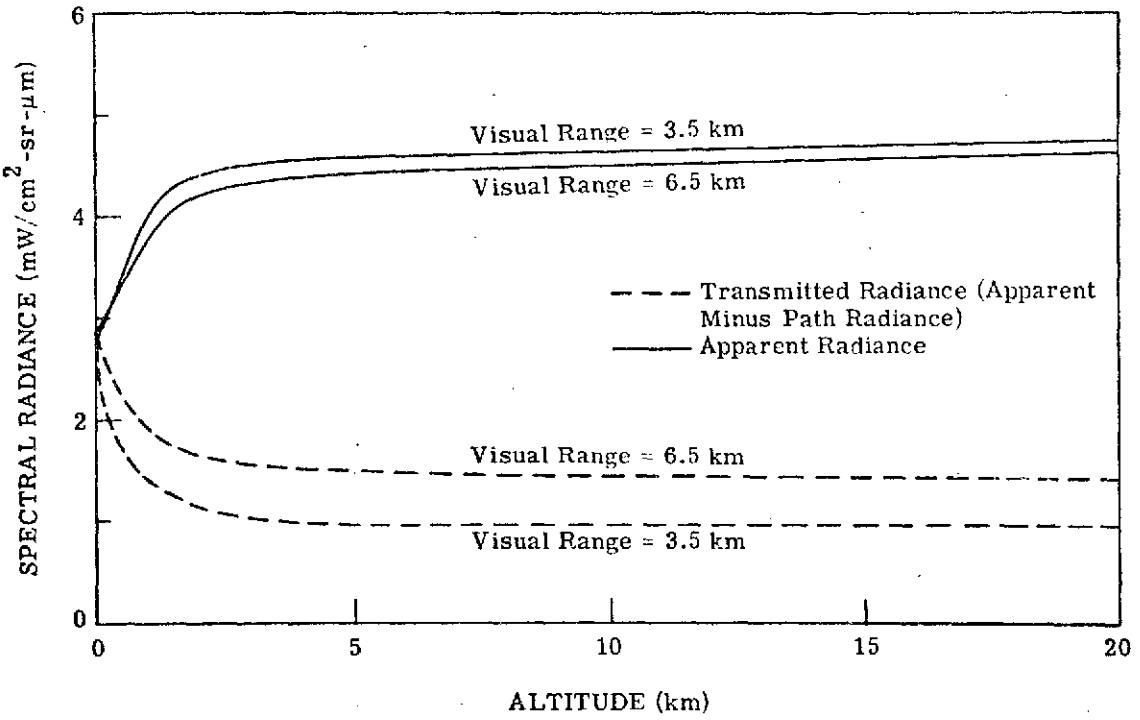

FIGURE 32. DEPENDENCE OF APPARENT AND TRANSMITTED TARGET SPECTRAL RADIANCES ON ALTITUDE FOR TWO VISUAL RANGES. Wavelength = 0.55 μm; background surface, green vegetation; target surface, ρ = 0.08; solar zenith angle = 45°; nadir scan angle = 0°; azimuthal angle = 0°.

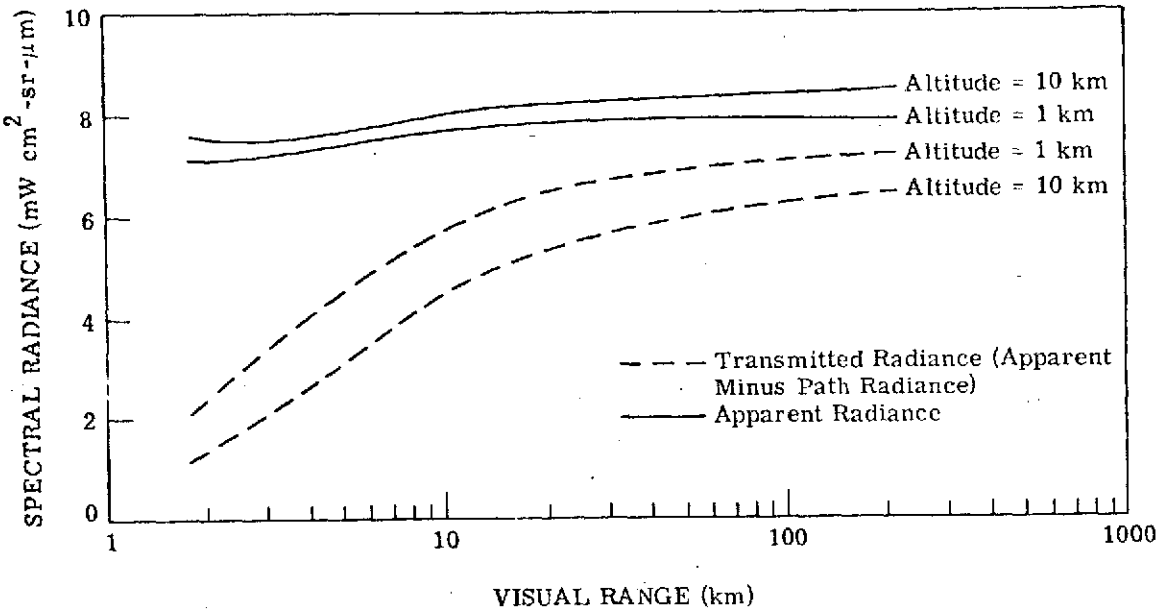

FIGURE 33. DEPENDENCE OF APPARENT AND TRANSMITTED BACKGROUND SPECTRAL RADIANCES ON VISUAL RANGE FOR TWO ALTITUDES. Wavelength = 0.55 μm; green vegetation surface; solar zenith angle = 30°; nadir scan angle = 0°; azimuthal angle = 0°.

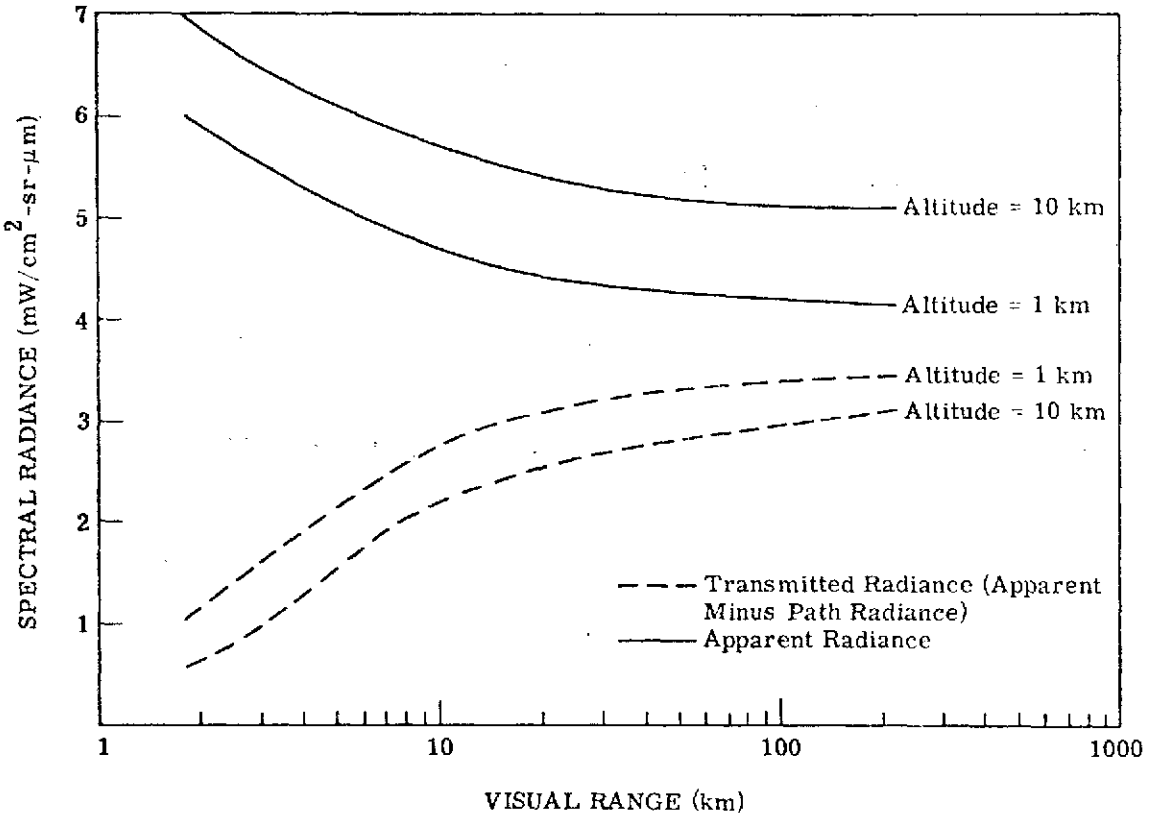

FIGURE 34. DEPENDENCE OF APPARENT AND TRANSMITTED TARGET SPECTRAL RADIANCES ON VISUAL RANGE FOR TWO ALTITUDES. Wavelength = 0.55 μm; background surface, green vegetation; target surface, ρ = 0.08; solar zenith angle = 30°; nadir scan angle = 0°; azimuthal angle = 0°.

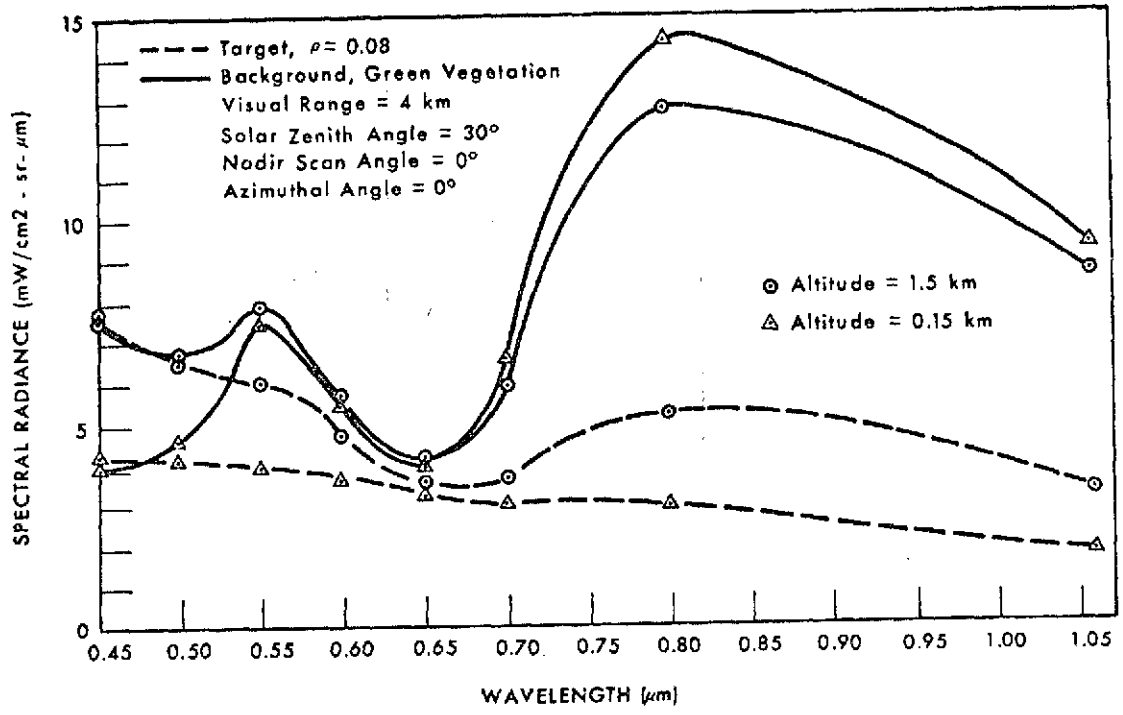

FIGURE 35. SPECTRAL RADIANCES AT DETECTOR FROM TARGET AND BACKGROUND FOR TWO ALTITUDES

Appendix V

PREPROCESSING TECHNIQUES TO REDUCE ATMOSPHERIC AND SENSOR VARIABILITY IN MULTISPECTRAL SCANNER DATA*

R. B. Crane

* Reprinted from Proceedings of the Seventh International Symposium on Remote Sensing of the Environment, Willow Run Laboratories, of the Institute of Science and Technology, The University of Michigan, Ann Arbor, 1971, pp. 1345-1355.

PREPROCESSING TECHNIQUES TO REDUCE ATMOSPHERIC AND SENSOR VARIABILITY IN MULTISPECTRAL SCANNER DATA

R. B. Crane

Willow Run Laboratories
Institute of Science and Technology
The University of Michigan
Ann Arbor, Michigan

ABSTRACT

Multispectral scanner data are potentially useful in a variety of remote sensing applications. Large-area surveys of earth resources carried out by automated recognition processing of these data are particularly important. However, the practical realization of such surveys is limited by a variability in the scanner signals that results in improper recognition of the data. This paper discusses ways by which some of this variability can be removed from the data by preprocessing with resultant improvements in recognition results.

1. INTRODUCTION

Errors in recognition maps may be caused by several types of variability in the signals received. A certain amount of random variation within each type of ground cover is inevitable. Maximum likelihood processing, outlined in Figure 1, has been designed to process such data and has successfully produced low error recognition maps.

Referring to Figure 1, the multispectral scanner records the signals from radiation reflected or emitted from the scene below in multiple channels, each channel corresponding to a frequency band in the ultra-violet, visible or infrared region of the spectrum. Measurements are made of the statistics of the data corresponding to training areas, where the ground cover is known a priori, from ground truth investigation. A likelihood decision rule based on these statistics is used to process all of the data from the scene and to produce a recognition map.

In this discussion, random variability within types of ground cover has been assumed to be defined by certain statistics which themselves are assumed not to vary. By systematic variation we mean the variation of these statistics themselves. There are a number of possible reasons for systematic variations, including the following: (1) The atmosphere that is present during scanning is not constant, but varies with both position and time. (2) All atmospheric effects in the data depend on the scan angle, the scanner altitude, and the amount and distribution of haze particles present, while some, in addition, depend on the sun position and the direction of scan. (3) The radiation collection and source geometries depend on sun position, scanner altitude, scan angle, direction of scan, and ground slope, as shown in Figure 2. (4) The scanner itself can introduce variance through system noise. Also, the gain of the scanner electronics is usually adjusted by the scanner operator to match the dynamic range of the received radiation and, therefore, is not kept constant for all of the data collection.

Thus, we see that there indeed can be both rapid fluctuations and slowly varying trends in the

The work reported in this paper was supported by NASA under Contract NAS9-9784.

data received from identical ground covers, and this variability has the effect of reducing recognition capability. There is more than one approach that can be taken in accounting for some of the variability found in multispectral scanner signals to improve recognition results. One can use many training areas that are representative of the varied conditions under which data are collected, but this has the disadvantage of more complex computers or more time-consuming recognition processing and requires a substantial amount of ground-truth information. One can add auxiliary inputs that provide a basis for estimating the amount by which the observation conditions (and, consequently, the signals) change and additionally, or alternatively, apply preprocessing transformations to the data before recognition processing.

For several years, personnel at The University of Michigan's Willow Run Laboratories have been using preprocessing as part of the data analysis and recognition functions performed on multispectral scanner data. The Michigan analog recognition processing equipment contains a multifunction preprocessor, and several digital preprocessing methods have been programmed and used in digital recognition operations. It has been possible, using preprocessing, to recognize ground cover in data sets for which recognition was not successful, or was more complicated, when the original data were used directly. Some of this work was described at the Sixth International Symposium on Remote Sensing of the Environment, [Ref 1], and other aspects of it are described in separate papers being presented at this Seventh Symposium [Refs 2 & 3].

The main objective of the current paper is to discuss a generalized correction scheme whose purpose is to remove systematic variations from multispectral scanner data. This method is an outgrowth of the several preprocessing methods that have been developed and used at Michigan. Another objective is to summarize and illustrate the use of the more successful of these other methods.

2. GENERALIZED CORRECTION

Consider the desirable features of an operational system to handle systematic variations in multispectral scanner data. First, an idealized processor would have an optimal likelihood decision rule that changed in synchronism with the data. However, the likelihood decision rule is not easy to instrument, and it is sufficient for many purposes to preprocess the data to remove systematic variations before deriving the likelihood functions. In this manner, the likelihood circuitry can be invariant. Second, the preprocessing should be defined and accomplished automatically, with few, if any, functions performed by a human operator. In fact, complete automation is desired for a single data set, corresponding to one overpass of the scanner. Third, there should be a small number of training areas used to determine the correction functions needed to transfer from data set to data set. Finally, it is desirable that the method not depend upon knowing the atmospheric and geometric states exactly because the fewer the number of auxiliary measurements required, the easier the collection and correction tasks are to instrument and accomplish.

In the development of the generalized correction, two basic assumptions are made concerning the data gathering process: (1) that the scene being scanned contains areas, such as agricultural fields, that can be assumed to contain uniform, and different, ground covers, and (2) that, ignoring the ever present noise, we can write the radiance signal received by any reflective channel of the scanner as:

$$L(\tau) = \rho E(\tau) T(\tau) + L_p(\tau) \tag{1a}$$

where:

- τ is a parameter denoting the condition of measurement (such as scan angle, distance along track, or altitude; see Section 3 for more discussion)
- ρ is a reflectance distribution function of the ground cover
- $E(\tau)$ is the irradiance impinging on the scene
- $T(\tau)$ is atmospheric attenuation between ground and scanner, and
- $L_p(\tau)$ is the path radiance observed by the scanner.

Equation (1a) can be written for a specific reference value of τ, say τ_o

$$L(\tau_o) = \rho E(\tau_o) T(\tau_o) + L_p(\tau_o) \tag{1b}$$

Noting that ρ is assumed independent of τ, it can be eliminated between the two equations, resulting in a linear relationship between $L(\tau_o)$ and $L(\tau)$, thus

$$L(\tau_o) = L(\tau)U(\tau) + V(\tau) \tag{2}$$

where $U(\tau,\tau_o)$ and $V(\tau,\tau_o)$ are functions of $E(\tau_o)$, $T(\tau_o)$, $L_p(\tau_o)$ and $E(\tau)$, $T(\tau)$, $L_p(\tau)$. The exact functional dependences of $U(\tau)$ and $V(\tau)$ on these quantities are unimportant since we intend to determine $U(\tau)$ and $V(\tau)$ empirically from the data itself. What is important is that $U(\tau)$ and $V(\tau)$ are independent of ρ.

An interpretation of Equation (2) is that the radiance measured under condition τ can be converted to the value that would have been measured under condition τ_o by using $U(\tau)$ and $V(\tau)$. The corrections functions $U(\tau)$ and $V(\tau)$ are to be determined directly from each data set by using signals received from areas having uniform ground covers. The observation of one material (i.e., a certain value of ρ) under condition τ and under condition τ_o provides a particular pair of values $L(\tau_o)$ and $L(\tau)$. Two such pairs of observations provides the data for a simultaneous solution of equations to determine $U(\tau)$ and $V(\tau)$. Ideally, many pairs of $L(\tau_o)$, $L(\tau)$ values will be obtained and will be used to determine $U(\tau)$ and $V(\tau)$ by a regression based on averages over the data. The averaging process reduces the effect of noise and minimizes the effect of irregularities in the reflectance properties of the materials used. Note that the identity of the ground cover in these areas need not be known, and that the correction functions apply to all surface materials.

Because the transformation uses the in-scene reference areas, it does not require a knowledge of the particular atmospheric state present. It removes the smooth variation introduced by the atmosphere, but does not remove the atmospheric effects at the reference condition. Processing is improved because the ground truth data will have the same reference atmosphere. Correction function to transfer from scene to scene will be determined by taking advantage of temporal and spatial continuity or by using a few areas known to be of the same composition and condition in pairs of scenes.

The procedure that has been followed in the development of a generalized correction can be summarized as follows:

(1) Assume a model for the remote sensing process along with constraints on the physical situation.

(2) Decide where the corrections are to occur, basically by modifying data (preprocessing) or modifying the decision rule.

(3) Relate the signal or processes at all values of τ to the signal at the reference condition. From this point on, the form of preprocessing or the form of modification of the decision rule is forced by the model and assumptions.

The physical model may be expanded and generalized to cover more cases, and this basic procedure will then be followed again. As an example, recall that in Equation (1), the reflectance function, ρ, is independent of the parameter, τ. If we consider τ to be the scan angle, this might mean that all surface materials must be diffuse reflectors in order for the transformation to be effective. However, it can be shown that the transformation has more general applicability. For example, if ρ is not independent of τ for all materials, but can be approximated by

$$\rho \approx \rho^* K_1(\tau) + K_2(\tau) \tag{3}$$

where $K_1(\tau)$ and $K_2(\tau)$ are independent of material and ρ^* is independent of θ, then the corrections based on the signal formulation, Equation (1) are still valid but the quantities in the equation become apparent rather than measurable. This means that, even if the reflectances of the materials depend on scan angle, the transformation will account for them as long as the dependence is the same or can be adequately approximated by the form of Equation (3).

As a third example, we can generalize the physical model to include the scattering of radiation from neighboring resolution elements into the line of sight. This has the effect of making the apparent color of each resolution element more like its neighbors.

The physical model can be represented by:

$$L(x,y,\tau) = \rho(x,y)E(\tau)T(\tau) + L_{p_o}(\tau) + \iint_{-\infty}^{\infty} E(\tau)T(\tau)\rho(x',y')H(x-x',y-y',\tau)\,dx'\,dy' \tag{4}$$

The term $L_{p_o}(\tau)$ is the part of the path radiance which arises from scattering of solar radiation from the atmosphere, independent of the reflections off of the ground cover. The double integral is the contribution from the neighboring resolution elements. The function $[\delta(x-x', y-y') + H(x-x', y-y')]$ can be regarded as a filter operating on ρET. The problem of defining an inverse filter which will recover the original shape of the function $\rho(x,y)$ is being studied. It has been found that the signal variation between two large fields contains enough information to define this inverse filter.

Note that near the middle of large fields there is no noticeable effect of the boundary. Mathematically this is expressed by setting $\rho(x', y')$ equal to a constant. Equation 4 then becomes

$$L(x,y,\tau) = \rho(x,y)E(\tau)T(\tau)\left(1 + \int\int_{-\infty}^{\infty} H(x-x', y-y',\tau)dx'dy'\right) + L_{p_o} \qquad (5)$$

This equation has the same form as Equation (1) (i.e., linear in ρ and ρ is independent of τ) so that the $U(\tau)$ and $V(\tau)$ correction could be calculated from data from just the middle of fields far from boundaries. The inverse filter can be designed so as to correct all values, including the values near boundaries, to that which would have been observed if the point had been in the middle of large fields. Once again, we have assumed a physical model, and solved for a formula which would allow us to convert all data to a reference condition; in this case, the chosen reference condition is the middle of large field.

3. USES OF GENERALIZED CORRECTION

In Figure 4 we outline the uses for the generalized correction method. The first use mentioned is to correct for the scan angle effect, where the statistics of the data are functions of the scan angle. This effect is especially noticable when the data is collected through a hazy atmosphere and the scanning plane includes the position of the sun. Without correction, this effect can make data virtually useless. In order to correct the data, we let the parameter τ correspond to the scan angle and τ_o to a reference angle, such as the angle when the scanner is pointed vertically downward.

If we let τ be the along-track distance, we are correcting the data for slowly varying atmospheric conditions. This is equivalent to expanding the scan angle correction into a two-dimensional problem, because if the atmosphere changes sufficiently to be measurable in the-along-track direction, the scan angle correction might be different and should be recomputed.

With scattered clouds present during data collection, the irradiance of the ground will differ in the sunlit and shadowed areas. Without the generalized correction separate training areas are needed for the two irradiance conditions, and the locations of these would not be known before data collection. Generalized correction provides a method of data processing with only one set of training areas. Note, that this is equivalent to expanding the scan angle correction to a two-dimensional problem, because the scan angle correction may be dependent on the presence or absence of clouds.

Similarly, the generalized correction provides a means of using the same training set, and hence the same processing, for data sets taken at different altitudes or on different days. The atmosphere will affect the data differently when taken at two different altitudes, simply because more of the atmosphere is in the transmission path at the higher altitude. Day to day atmospheric and illumination conditions cannot be expected to be constant. The use of the generalized correction to systematically tie together the data from day to day has much practical value, especially in large area surveys, which may continue day after day. In order to make the correction it is necessary, as a minimum, that there be an overlap region containing two different ground cover types. The particular ground covers do not have to be identified as to type. A single set of training areas may be taken scattered throughout the different days or all on one day.

The next extension past day to day corrections is the correction of all data to a common condition and the accumulation of this data into a data bank. Then possibly a minimum of two different ground covers may be identified in a new set of data, and used to relate the new data to the data bank. The signatures for all other types of ground covers may then be taken from the data bank.

4. RELATIONSHIP TO PAST UNIVERSITY OF MICHIGAN EXPERIENCE

The development of the generalized approach described above has been stimulated by the success of a number of preprocessing techniques used at the University of Michigan in recent years.

Each of these techniques was developed to respond to particular types of variation noted in particular sets of data. We group these techniques into inferential, predetermined, and adaptive categories, as shown in the table, Figure 5.

In the category inferential we include those types of preprocessing which require ancillary measurements to obtain some information about the conditions of measurement of the primary data. Usually some physical model would be used to establish a relationship between the ancillary measurements, the conditions of measurement and the corrections to be applied to the primary scanner data. Detailed physical models of radiation transfer in the atmosphere are described in Reference 6 and 7.

Examples of ancillary measurements which might be used to supplement the data are estimates of visual range, measurements of altitude of sensor aircraft, and measurements of temperature and humidity. One type of ancillary measurement that has been available for several years is the sun sensor on top of the University of Michigan aircraft. This sensor provides a measurement, in each spectral channel, of the downward irradiance at the altitude of the aircraft. It seems reasonable to assume, and indeed it has been shown from detailed modelling studies, that both the radiance reflected from the ground and the path radiance (radiation scattered into the observers line of sight), are proportional to the irradiance at the aircraft. Therefore, a reasonable normalization to pursue is to divide the signal in each channel by its associated sun sensor signal. This will return all signals to a reference illumination condition, at the altitude of the aircraft. Further discussion of the operation of the sun sensor with examples is given in Reference 4.

Certain types of preprocessing transformations may be used which operate only on the primary multispectral scanner data and which, once chosen, are applied to every data point in a definite, predefined way, independent of surrounding data points or variations in the conditions of measurement. All of the predetermined preprocessing transformations so far found to be useful involve more than one spectral channel. Generally, in using these transformations, one hopes to take advantage of the simularity of variations in adjacent spectral channels to partially remove the effects of variation in the conditions of measurement.

The specific predetermined preprocessing techniques which have been used are normalization by the adjacent channel:

$$x_i' = \frac{x_i}{x_{i+1}} \tag{6}$$

normalization of adjacent channel differences by adjacent channel sum,

$$x_i' = \frac{x_i - x_{i+1}}{x_i + x_{i+1}} \tag{7}$$

and normalization by the sum of all channels:

$$x_i' = \frac{x_i}{\sum x_i} \tag{8}$$

A detailed discussion of the rationals behind these techniques and examples of their use are given in References 1 and 4.

In the category of adaptive techniques we include all those techniques which utilize information obtained from a larger area than the individual resolution element. For example, subtraction of the darkest object is a technique which requires one to first of all explore the data to find the smallest signal values (i.e., to find the darkest object). This smallest value is then subtracted from every data point in the neighborhood. If the darkest object is indeed non-reflecting the signal subtracted is just the path radiance.

The first example of the generalized correction method described in section 3 (i.e., as given in equation 2) is of course an adaptive method in the above sense, since the functions $U(\tau)$ and $V(\tau)$ are empirically determined as regression coefficients from large areas of data. A successful example of a similar technique applied to scan angle as the variable condition of measurement

(i.e., $\tau \rightarrow \theta$, the scan angle) is given in Reference 3. Using several types of fields a multiplicative correction function $U(\theta)$ was established so that all the $L(\theta)$ observations could be returned to a reference condition, thus:

$$L(\theta_o) = L(\theta)U(\theta) \tag{9}$$

The function $U(\theta)$ was manually fitted to the data, leading to successful compensation for scan angle effects in the data without the necessity of an additive function, $V(\theta)$.

A peculiarity of the data set, upon which this correction was performed, was that the atmosphere was very clear and there were major variations of ground slope over the scene; and so the path radiance was assumed to be small, and the path transmission was nearly unity. The multiplica- correction therefore was probably compensating primarily for the geometry of illumination combined with variation in the slope of the ground.

5. SUMMARY

The recognition capability of the multispectral scanner remote sensor is degraded whenever changes in the data are induced by atmospheric, geometric, or scanner sensitivity effects. Various methods have been used to reduce these effects, with varying degree of success. As an outgrowth of these efforts, a generalized correction has been developed with features of several of the previous methods and is being adapted to an automatic data processing capability.

The generalized correction can start with any model of the sensing process, with the vector τ being used to describe any or all of the conditions of measurement, scan angle being one of these. The equation describing the sensing process can then be put in the form of a correction function which returns all signals to a reference condition, τ_o. The functions of τ which result, such as $U(\tau)$ $V(\tau)$ and $H(x,y,\tau)$, described in Section 2, are then determined empirically from the data using standard techniques of regression analysis. Thus, the generalized correction technique is really a systematic procedure for developing and applying preprocessing algorithms. It is hoped through this procedure to eliminate much of the manual and human analysis previously required for the successful application of preprocessing techniques.

REFERENCES

1. Kriegler, F., et.al., "Preprocessing Transformations and Their Effects on Multispectral Recognition", Proceedings of the Sixth International Symposium on Remote Sensing of Environment, Vol. 1, Oct. 69, p. 97-131.

2. Remote Sensing with Special Reference to Agriculture and Forestry, National Academy of Sciences, Washington, D.C., 1970 p. 391-396.

3. Smedes, H.M., Spencer, M.M., Thomson, F.J., "Preprocessing of Multispectral Data and Simulations of ERTS Data Channels to Make Computer Terrain Maps of a Yellowstone National Park Test Site", Seventh International Symposium on Remote Sensing of Environment, May 1971.

4. Nalepka, R.F., Investigations of Multispectral Discrimination Techniques, Report No. 2264-12-F, Willow Run Laboratories, U of M., Jan 1970, p. 13-23.

5. Investigations of Spectrum Matching Techniques for Remote Sensing in Agriculture, Final Report, Jan 1968 through Sep 1968, Dec 1968 Report No. 1674-10-F, WRL, U of M p. 21-27.

6. Malila, W.A., et.al., Studies of Spectral Discrimination, Report No. 031650-22-T, WRL, U of M May 1971, p. 27-45

7. Turner, R.E., et.al., "Importance of Atmospheric Scattering in Remote Sensing", Seventh International Symposium on Remote Sensing of Environment, May 1971.

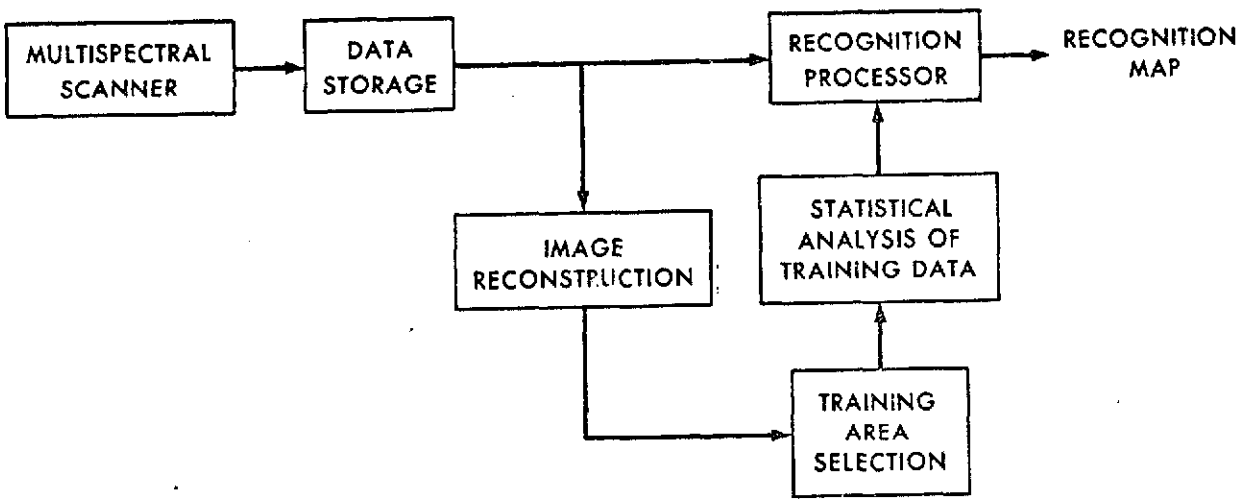

FIGURE 1. MULTISPECTRAL RECOGNITION

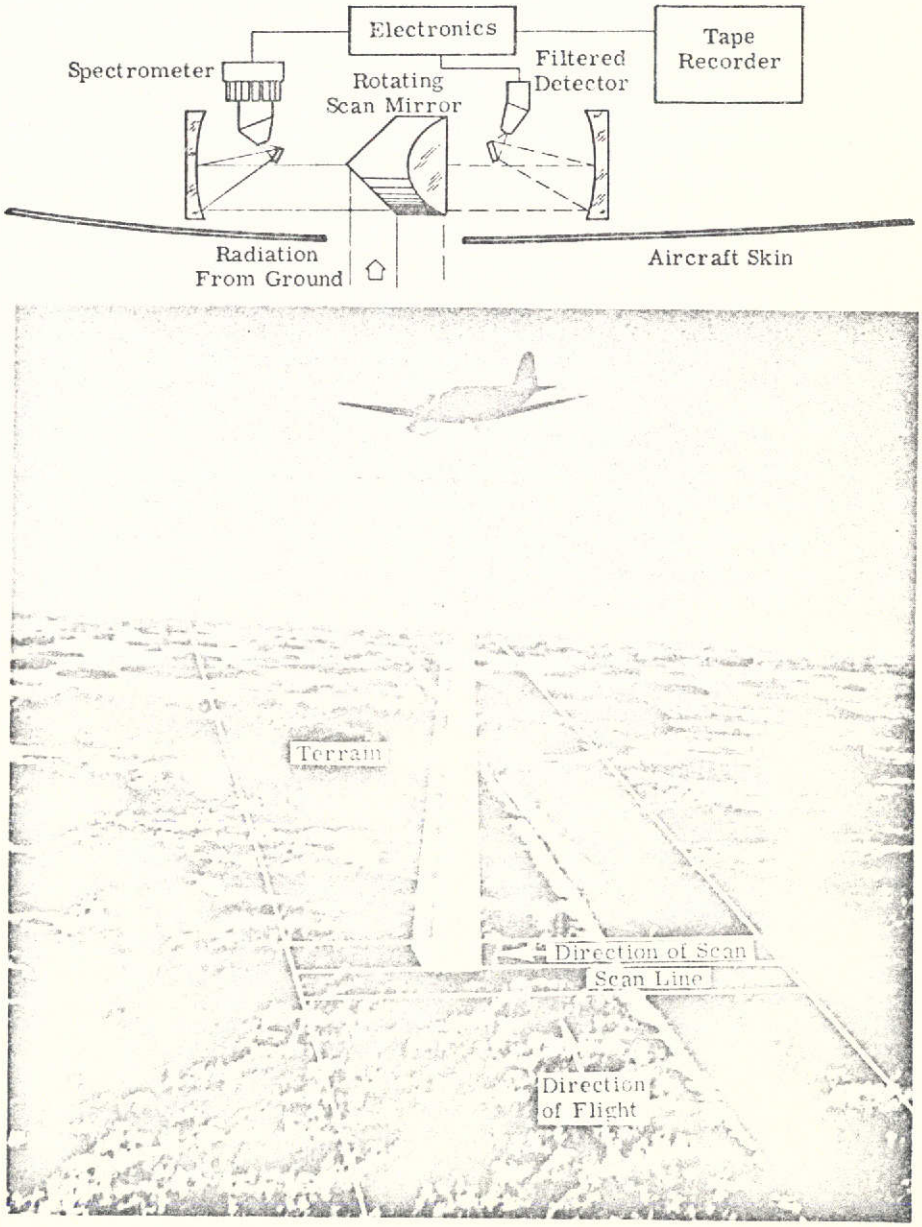

FIGURE 2. MULTISPECTRAL DATA COLLECTION OPERATIONS

$$L_i(\tau) = \rho_i E(\tau) T(\tau) + L_p(\tau)$$

$$L_i(x, y) = \rho(x, y) ET + L_p + ET \iint \rho(x', y') H(x - x', y - y')\, dx'\, dy'$$

FIGURE 3. ASSUMED PHYSICAL MODEL

$$L(\tau_0) = L(\tau)U(\tau) + V(\tau)$$

where

$L(\tau_0)$ = radiance at reference condition τ_0

τ = parameter denoting condition of observation

$U(\tau)$ and $V(\tau)$ = correction functions independent of materials

Useful in Correcting for:

--- Scan-Angle Effects

--- Illumination Changes Along Flight Line

--- Cloud Shadows

--- Altitude Effects

--- Day-to-Day Changes In Atmospheric and Illumination Conditions

--- Changes Required to Use Data Bank

FIGURE 4. GENERAL PREPROCESSING TRANSFORMATION

INFERENTIAL

- SUN SENSOR
- ATMOSPHERIC MODEL

PREDETERMINED

- RATIO OF ADJACENT CHANNELS
- RATIO OF DIFFERENCE TO SUM OF ADJACENT CHANNELS
- NORMALIZATION OF CHANNELS BY SUMS OF CHANNELS

ADAPTIVE

- CALIBRATION LAMP NORMALIZATION
- SUBTRACT DARKEST OBJECT
- MULTIPLICATIVE
- SUBTRACTIVE

FIGURE 5. USEFUL PREPROCESSING TRANSFORMATIONS

Appendix VI
LIST OF RELATED REPORTS

Miller, L. D., The Investigation of a Method for Remote Detection of Life on a Planet, Report No. 6590-4-F, Grant No. NsG 715, Willow Run Laboratories of the Institute of Science and Technology, The University of Michigan, Ann Arbor, November 1965.

George, D. and T. Limperis, Unusual Reconnaissance Concepts (Interim Report), Vol. II: Sources of Experimental Errors in Spectrophotometric Measurements, Report No. 5698-33-P(II), AFAL-TR-65-331, Willow Run Laboratories of the Institute of Science and Technology, The University of Michigan, Ann Arbor, January 1966, AD 481 796, RC019423.

Ulrich, J., Unusual Reconnaissance Concepts (Interim Report), Vol. III: A Bibliography of Recent Contributions on Electromagnetic and Acoustic Scattering, Report No. 5698-33-P(III), AFAL-TR-65-331, Willow Run Laboratories of the Institute of Science and Technology, The University of Michigan, Ann Arbor, January 1966, AD 481 817.

Lowe, D. and J. Braithwaite, "A Spectrum Matching Technique For Enhancing Image Contrast," J. of Appl. Opt., Vol. 5, No. 6, June 1966.

Target Signature Analysis Center: Data Compilation, Report No. 7850-2-B, Willow Run Laboratories of the Institute of Science and Technology, The University of Michigan, Ann Arbor, July 1966, AD 489 698.

Second Supplement: Report No. 8492-5-B, July 1967, AD 819 712.

Fifth Supplement: Report No. 8492-15-B, August 1968, AD 840 091.

Addendum: Report No. 8492-26-B, October 1968.

Seventh Supplement: Report No. 8492-35-B, January 1969, AD 856 343.

Tenth Supplement: Report No. 8492-49-B, July 1969, AD 864 957.

Braithwaite, J., Dispersive Multispectral Scanning: A Feasibility Study (Final Report), Report No. 7610-5-F, U.S.G.S., Department of Interior, Contract No. 14-08-001-10053, Willow Run Laboratories of the Institute of Science and Technology, The University of Michigan, Ann Arbor, September 1966.

Lowe, D. S., J. Braithwaite, and V. L. Larrowe, An Investigative Study of a Spectrum-Matching Imaging System (Final Report), Report No. 8201-1-F, Contract NAS 8-21000, Willow Run Laboratories of the Institute of Science and Technology, The University of Michigan, Ann Arbor, October 1966.

Holter, M., Sensing and Interpretation Techniques, Annals of the N. Y. Academy of Sciences, Vol. 140, Art. 1, December 1966.

Olson, C. E., Jr., Optical Sensing of Moisture Content in Fine Forest Fuels (Final Report), Report No. 8036-1-F, USDAW-1209-FS-66, Contract 13-220, Willow Run Laboratories of the Institute of Science and Technology, The University of Michigan, Ann Arbor, May 1967.

Olson, Charles, Jr., "Accuracy of Land Use Interpretation from Infrared Imagery in the 4.5 to 5.5 Micron Band," Annals of Ass. of Am. Geographers, Vol. 57, No. 2, June 1967.

Thomson, F., Multispectral Discrimination of Small Targets, Report No. 6400-135-T, Contract DA 28-043-AMC-00013(E), Willow Run Laboratories of the Institute of Science and Technology, The University of Michigan, Ann Arbor, December 1967, AD 389 761.

Horvath, R., Multispectral Survey of Arctic Regions, Report No. 1248-1-L, Contract NONR 3996(01), Willow Run Laboratories of the Institute of Science and Technology, The University of Michigan, Ann Arbor, January 1968, AD 671 779.

Ulrich, J. P., Metallic Reflection, Report No. 8492-21-T, Contract No. F33615-67-C-1293, Willow Run Laboratories of the Institute of Science and Technology, The University of Michigan, Ann Arbor, March 1968.

Paprocki, C. and R. Miller, Use of Image-Intensifiers For Real-Time Multispectral Viewing, Report No. 7919-26-T, Willow Run Laboratories of the Institute of Science and Technology, The University of Michigan, Ann Arbor, July 1968.

Braithwaite, J., Airborne Multispectral Sensing and Applications, Proc. of the Society of Photo-Optical Instrumentation Engineers, 13th Annual Technical Symposium, 19-23 August 1968.

Larsen, L. M. and P. G. Hasell, Jr., Calibration of an Airborne Multispectral Optical Sensor, Report No. 6400-137-T, Contract DA 28-043-AMC-00013(E), Willow Run Laboratories of the Institute of Science and Technology, The University of Michigan, Ann Arbor, September 1968, AD 842 419.

Ulrich, J. P., The Reflectance of Some Clean and Contaminated Military Paints, Report No. 8492-32-T, Contract F33615-67-C-1293, Willow Run Laboratories of the Institute of Science and Technology, The University of Michigan, Ann Arbor, September 1968.

Investigations of Spectrum-Matching Techniques for Remote Sensing in Agriculture, Report No. 1674-10-F, Contract No. 12-14-100-9503(20), Willow Run Laboratories of the Institute of Science and Technology, The University of Michigan, Ann Arbor, December 1968.

Horvath, R., J. Braithwaite and F. Polcyn, Effects of Atmospheric Path on Airborne Multispectral Sensors, Report No. 1674-5-T, NsG 715/23-05-071, Willow Run Laboratories of the Institute of Science and Technology, The University of Michigan, Ann Arbor, January 1969.

Polcyn, F. C. and R. A. Rollin, Remote Sensing Techniques for the Location and Measurement of Shallow-Water Features, Report No. 8973-10-P, Willow Run Laboratories of the Institute of Science and Technology, The University of Michigan, Ann Arbor, January 1969, AD 848 054.

Lowe, D. S. and J. G. Braithwaite, Study of Requirements to Calibrate Reconofax IV and RS-7 Infrared Scanners, Report No. 2122-8-X, Willow Run Laboratories of the Institute of Science and Technology, The University of Michigan, Ann Arbor, February 1969.

Hasell, P. G., Development of an Aerial Background Measurement System, Report No. 2134-8-F, Willow Run Laboratories of the Institute of Science and Technology, The University of Michigan, Ann Arbor, March 1969.

Bornemeier, D., R. Bennet and R. Horvath, Target Temperature Modeling, Report No. 1588-5-F, RADC TR 69-404, Willow Run Laboratories of the Institute of Science and Technology, The University of Michigan, Ann Arbor, December 1969.

Braithwaite, J. G., L. Larsen and E. Work, Further Infrared Systems Studies for the Earth Resources Program, Report No. 2122-4-F, Willow Run Laboratories of the Institute of Science and Technology, The University of Michigan, Ann Arbor, December 1969.

Higer, A. L., N. S. Thomson, F. J. Thomson and M. C. Kolipinski, Applications of Multispectral Remote Sensing Techniques to Hydrobiological Investigations in Everglades National Park, Report No. 2528-5-T, Willow Run Laboratories of the Institute of Science and Technology, The University of Michigan, Ann Arbor, January 1970.

Horvath, R., W. Morgan and R. Spellicy, Measurements Program for Oil-Slick Characteristics, Report No. 2766-7-F, Willow Run Laboratories of the Institute of Science and Technology, The University of Michigan, Ann Arbor, February 1970.

Thomson, F., Investigations of Multispectral Discrimination of the Earth Features, Report No. 2528-10-F, Willow Run Laboratories of the Institute of Science and Technology, The University of Michigan, Ann Arbor, April 1970.

Wagner, T., Automatic Processing and Analysis of Soils and Soil Conditions, Report No. 2760-2-F, Willow Run Laboratories of the Institute of Science and Technology, The University of Michigan, Ann Arbor, July 1970.

Burg, W. G. and W. L. Brown, A Study of Waterfowl Habitat in North Dakota Using Remote Sensing Techniques, Report No. 2771-7-F, Willow Run Laboratories of the Institute of Science and Technology, The University of Michigan, Ann Arbor, July 1970.

Bair, M. E., D. C. Cramer and S. R. Steward, A Gonioreflectometer Facility Using Coherent and Incoherent Sources, Report No. 1652-24-T, AFAL-TR-70-161, Willow Run Laboratories of the Institute of Science and Technology, The University of Michigan, Ann Arbor, August 1970, AD 874 434.

Anding, D. and R. Kauth, Atmospheric Effects on Infrared Multispectral Sensing of Seasurface Temperature from Space, Report No. 2676-4-P, Willow Run Laboratories of the Institute of Science and Technology, The University of Michigan, Ann Arbor, August 1970.

Analysis of Polarization and Thermal Properties of Targets and Backgrounds, Report No. 3221-11-P, Contract No. F33615-70-C-1123, Willow Run Laboratories of the Institute of Science and Technology, The University of Michigan, Ann Arbor, August 1970.

Braithwaite, J. and E. Work, Optical Transfer Techniques for Orbital Scanners, Report No. 3165-21-T, Willow Run Laboratories of the Institute of Science and Technology, The University of Michigan, Ann Arbor, March 1971.

Larsen, L., Detector Utilization in Line Scanners, Report No. 3165-29-T, Willow Run Laboratories of the Institute of Science and Technology, The University of Michigan, Ann Arbor, August 1971.

Kriegler F. and R. Marshall, A Prototype Hybrid Multispectral Processor (SPARC/H) with High Throughput Capability, Report No. 31650-23-T, Willow Run Laboratories of the Institute of Science and Technology, The University of Michigan, Ann Arbor, March 1971.

Marshall, R. E. and F. J. Kriegler, Data Display Requirements for a Multispectral Scanner Processor with High Throughput Capability, Report No. 3165-28-L, Willow Run Laboratories of the Institute of Science and Technology, The University of Michigan, Ann Arbor, July 1971.

Braithwaite, J. Calibration of Multispectral Scanners, Report No. 3165-27-L, Willow Run Laboratories of the Institute of Science and Technology, The University of Michigan, Ann Arbor, September 1970.

Malila, W. A., R. B. Crane, C. A. Omarzu, and R. E. Turner, Studies of Spectral Discrimination, Report No. 31650-22-T, Willow Run Laboratories of the Institute of Science and Technology, The University of Michigan, Ann Arbor, May 1971.

Nalepka, R., H. Horwitz, and N. S. Thomson, Investigations of Multispectral Sensing of Crops, Report No. 31650-30-T, Willow Run Laboratories of the Institute of Science and Technology, The University of Michigan, Ann Arbor, May 1971.

Brown, W., F. Polcyn, A. N. Sellman, and S. R. Stewart, Investigation of Shallow Water Features, Report No. 31650-31-T, Willow Run Laboratories of the Institute of Science and Technology, The University of Michigan, Ann Arbor, August 1971.

Leeman, V., D. Earing, R. Vincent, and S. Ladd, The NASA Earth Resources Spectral Information System: A Data Compilation, Report No. 31650-24-T, Willow Run Laboratories of the Institute of Science and Technology, The University of Michigan, Ann Arbor, May 1971.

Earing, D. and V. Leeman, NASA/MSC Earth Resources Spectral Information System Procedures Manual, Report No. 31650-32-T, Willow Run Laboratories of the Institute of Science and Technology of The University of Michigan, Ann Arbor, Printed 1971.

Vincent, R., Data Gaps in the NASA Earth Resources Spectral Information System, Report No. 31650-25-T, Willow Run Laboratories of the Institute of Science and Technology, The University of Michigan, Ann Arbor, March 1971.

Vincent, R., R. Horvath, F. Thomson, and E. Work, Remote Sensing Data Analysis Projects Associated with the NASA Earth Resources Spectral Information System, Report No. 31650-26-T, Willow Run Laboratories of the Institute of Science and Technology, The University of Michigan, Ann Arbor, April 1971.

Erickson, J. and F. Thomson, Investigations Related to Multispectral Imaging Systems for Remote Sensing, Report No. 31650-17-P, Willow Run Laboratories of the Institute of Science and Technology, The University of Michigan, Ann Arbor, September 1971.

Erickson, J., Investigations Related to Multispectral Imaging Systems — Final Report, Willow Run Laboratories of the Institute of Science and Technology, The University of Michigan, Ann Arbor, in preparation.

Leeman, V., R. Vincent, and S. Ladd, The NASA Earth Resources Spectral Information System: A Data Compilation First Supplement, Report No. 31650-69-T, Willow Run Laboratories of the Institute of Science and Technology, The University of Michigan, Ann Arbor, March 1972.

Leeman, V., NASA/MSC Earth Resources Spectral Information System Procedures Manual, Supplement, Report No. 31650-72-T, Willow Run Laboratories of the Institute of Science and Technology, The University of Michigan, Ann Arbor, September 1971.

Nalepka, R. F., H. Horwitz, and P. Hyde, Estimating Proportions of Objects from Multispectral Data, Report No. 31650-73-T, Willow Run Laboratories of the Institute of Science and Technology, The University of Michigan, Ann Arbor, March 1972.

Malila, W., R. Crane, and W. Richardson, Discrimination Techniques Employing Both Reflective and Thermal Multispectral Signals, Report No. 31650-75-T, Willow Run Laboratories of the Institute of Science and Technology, The University of Michigan, Ann Arbor, in publication.

Vincent, R., Rock-Type Discrimination from Ratio Images of the Pisgah Crater, California Test Site, Report No. 31650-77-T, Willow Run Laboratories of the Institute of Science and Technology, The University of Michigan, Ann Arbor, June 1972.

Vincent, R., G. Suits, J. Erickson, and H. Horwitz, Investigation of Theoretical Methods for the Optical Modeling of Agricultural Fields and Rough-Textured Rock and Mineral Surfaces, Report No. 31650-78-T, Willow Run Laboratories of the Institute of Science and Technology, The University of Michigan, Ann Arbor, June 1972.

REFERENCES

1. W. A. Malila, R. B. Crane, C. A. Omarzu, and R. E. Turner, "Studies of Spectral Discrimination," Report No. 31650-22-T, Willow Run Laboratories of the Institute of Science and Technology, The University of Michigan, Ann Arbor, 1971.
2. R. E. Turner, Course Notes, "Advanced Infrared Technology," The University of Michigan Engineering Summer Conferences, Ann Arbor, 1971.
3. H. Koschmieder, "Theorie der horizontalen Sichtweite," Beitr. Phys. freien Atm., Vol. 12, 1924, pp. 33-53, 171-181.
4. L. Elterman, "U.V., Visible and IR Attenuation for Altitudes to 50 km," 1968, Report No. AFCRL-68-0153, Air Force Cambridge Research Laboratories, Office of Aerospace Research, Bedford, Massachusetts, 1968.
5. D. Deirmendjian, Electromagnetic Scattering on Spherical Polydispersions, American Elsevier Publishing Company, Inc., New York, 1969.
6. A. I. Ivanov, Atmospheric Optics, ed. by N. B. Divari, Consultants Bureau, New York, 1969.
7. V. Leeman, D. Earing, R. K. Vincent, and S. Ladd, "The NASA Earth Resources Spectral Information System: A Data Compilation," NASA CR, 31650-24-T, 1971.
8. K. L. Coulson, J. V. Dave, and Z. Sekera, Tables Relating to Radiation Emerging from a Planetary Atmosphere with Rayleigh Scattering, University of California Press, Berkeley, 1960.
9. S. Chandrasekhar, Radiative Transfer, Dover Publications, New York, 1960.
10. G. H. Suits, "The Calculation of the Directional Reflectance of a Vegetative Canopy," Proc. of the Seventh Symposium on Remote Sensing of Environment, Willow Run Laboratories of the Institute of Science and Technology, The University of Michigan, Ann Arbor, 1971.
11. R. F. Nalepka, H. M. Horwitz, and N. S. Thomson, "Investigations of Multispectral Sensing of Crops," Report No. 31650-30-T, Willow Run Laboratories of the Institute of Science and Technology, The University of Michigan, Ann Arbor, 1971.
12. H. Cramer, The Elements of Probability Theory, John Wiley and Sons, Inc., New York, 1956, Chapter 15.
13. D. Anding, R. Kauth, and R. Turner, "Atmospheric Effects on Infrared Multispectral Sensing of Sea-Surface Temperature from Space," Report No. 2676-6-F, Willow Run Laboratories of the Institute of Science and Technology, The University of Michigan, Ann Arbor, 1970.
14. T. W. Mullikin, "The Complete Rayleigh Scattered Field Within a Homogeneous Plane-Parallel Atmosphere," Astrophysical J., Vol. 145, 1966.
15. R. Bellman and R. Kalaba, "On the Principle of Invariant Imbedding and Propagation Through Inhomogeneous Media," Proc. Nat. Acad. Sci., Vol. 42, 1956, pp. 629-632.
16. I. P. Grant and G. E. Hunt, "Discrete Space Theory of Radiative Transfer and its Application to Problems in Planetary Atmospheres," J. of Atmos. Sci., Vol. 26, No. 5, 1969, p. 963.

17. W. M. Porch, R. J. Charlson, and L. F. Radke, "Atmospheric Aerosol: Does a Background Level Exist?", Sci., Vol. 170, 1971, pp. 315-317.

18. S. I. Rasool and S. H. Schneider, "Atmospheric Carbon Dioxide and Aerosols: Effects of Large Increases in Global Climate," Sci., Vol. 173, 1971, pp. 138-141.

19. J. A. Stratton, Electromagnetic Theory, McGraw-Hill, New York, 1941.

20. H. C. van de Hulst, Light Scattering by Small Particles, John Wiley and Sons, Inc., New York, 1957.

21. M. Kerker, The Scattering of Light and Other Electromagnetic Radiation, Academic Press, 1969.

22. K. Bullrich, Advances in Geophysics, edited by H. E. Landsberg and J. van Mieghem, Vol. 10, 1964.

23. R. G. Fleagle and J. A. Businger, An Introduction to Atmospheric Physics, Academic Press, New York, 1963.

24. C. E. Junge, Air Chemistry and Radioactivity, Academic Press, New York, 1963.

25. N. Robinson, Solar Radiation, American Elsevier Publishing Company, Inc., New York, 1966.

26. L. Larmore and F. F. Hall, Jr., "Optics for the Airborne Observer," SPIE Journal, Vol. 9, No. 3, 1971, p. 87.

27. W. E. K. Middleton, Vision Through the Atmosphere, University of Toronto Press, 1952.

28. J. C. Johnson, Physical Meteorology, Chapman and Hall, Ltd., London, 1954.

29. W. A. Malila, "Multispectral Techniques for Image Enhancement and Discrimination," Photogrammetric Engineering, June 1968.

Page intentionally left blank

Earth Resources Laboratory, GS
Mississippi Test Facility
Bay St. Louis, Mississippi 39520
ATTN: Mr. R. O. Piland, Director (1)

U. S. Department of Interior
Geological Survey
GSA Building, Room 5213
Washington, D. C. 20242
ATTN: Mr. W. A. Fischer (1)

NASA Wallops
Wallops Station, Virginia 23337
ATTN: Mr. James Bettle (1)

Purdue University
Purdue Industrial Research Park
1200 Potter
West Lafayette, Indiana 47906
ATTN: Mr. David Landgrebe (1)